Hard Master, Soft Slave Haptic Teleoperation

Göran A. V. Christiansson

Hard Master, Soft Slave Haptic Teleoperation

Proefschrift

ter verkrijging van de graad van doctor
aan de Technische Universiteit Delft,
op gezag van de Rector Magnificus prof. dr. ir. J.T. Fokkema,
voorzitter van het College voor Promoties,
in het openbaar te verdedigen op vrijdag 12 oktober 2007 om 10:00 uur
door

Göran Anders Viking CHRISTIANSSON

Civilingenjör Teknisk Fysik, Chalmers University of Technology
geboren te Risinge, Östergötland, Zweden.

Dit proefschrift is goedgekeurd door de promotor:
Prof. Dr. F.C.T. van der Helm

Samenstelling promotiecommissie:
Rector Magnificus, voorzitter
Prof. Dr. F.C.T. van der Helm, promotor (Technische Universiteit Delft)
Prof. Dr. Ir. M. Steinbuch (Technische Universiteit Eindhoven)
Prof. Dr. Vincent Hayward (McGill University, Montreal, Canada)
Prof. Dr. Ir. P.A. Wieringa (Technische Universiteit Delft)
Prof. Dr. Ir. C.W. Scherer (Technische Universiteit Delft)
Dr. Ir. R.Q. van der Linde (Technische Universiteit Delft)
Ir. P. Lammertse (Moog-FCS, The Netherlands)

ISBN: 978-90-8559-307-2

Contents in brief

Contents

Symbols

Table 1: *List of Symbols (part one)*

	Symbol	*Meaning*
Forces	$F_x(t)$,$F_x(s)$	Force at point x [N], in the time domain and the Laplace domain
	F_h	Contact force between the human operator and master device
	$F_{\mathrm{h}^\star}$,$F_{\mathrm{h,ext}}$	Exogeneous operator force, active force
	F_e	Contact force between the slave device and the environment
	F_mc, F_sc	Controlled forces at the master and slave side
Velocities	$v_x(t)$,$V_x(s)$	Velocity at point x [m/s], in the time domain and the Laplace domain
	$v_\mathrm{h}(t)$,$V_\mathrm{h}(s)$	End-effector velocitiy of the hand-master device interaction point
	$v_\mathrm{e}(t)$,$V_\mathrm{e}(s)$, $V_\mathrm{st}(s)$	End-effector velocitiy, slave device tip
	$V_\mathrm{sb}(s)$	Base-velocity, for the soft slave device
Mechanical Components	m_x	Mass of component x, [kg]
	b_x	Damping of component x, [Ns/m]
	k_x	Stiffness of component x, [N/m]
	$Z_x(s)$	Impedance of component x Force(s)/Velocity(s) [Ns/m]
	$Y_x(s)$	Admittance of component x ($Z^{-1}(s)$) Velocity/Force [m/Ns]
	$Z_\mathrm{m}(s)$ (e.g. $m_\mathrm{m}\,s + b_\mathrm{m}$)	Mechanical impedance of the master device
	$Z_\mathrm{s}(s)$ (e.g. $m_\mathrm{s}\,s + b_\mathrm{s}$)	Impedance of a hard slave device
	$Z_\mathrm{s,ee}$,$Z_\mathrm{s,be}$,$Z_\mathrm{s,eb}$,$Z_\mathrm{s,bb}$	The four impedances of the soft slave device
	k_s, b_s	Intrinsic stiffness and damping of the soft slave compliance

Table 2: *List of Symbols (part two)*

	Symbol	*Meaning*
Operator/Environment	$Z_\mathrm{h}(s)$ (e.g. $m_\mathrm{h}\,s + b_\mathrm{h} + k_\mathrm{h}/s$)	Impedance of the human operator
	$Z_\mathrm{e}(s)$ (e.g. $b_\mathrm{e} + k_\mathrm{e}/s$)	Impedance of the environment
Linear Model	H(s)	The hybrid transfer function matrix
	$h_{ij}(s)$	H-matrix elements, h_{11}, h_{12}, h_{21}, h_{22}
	$r_{11}(s)$,...	Real part of $h_{11}(s)$ etc. (used for stability formulae.)
	Z, Y, G, B, C	Equivalent model notations
Controller	$C_i(s)$ (C_m,C_s,C_1-C_6)	Controller transfer functions Lawrence/Salcudean notation
	K,$k_{ij}(s)$	Controller transfer functions General MIMO notation
	K_p, K_d	Position, velocity gains elements of a simple PD-controller
	$Z_\mathrm{vm}(s)$	Virtual model impedance for FCS Virtual Model controller
Teleop. Behaviour	$Z_\mathrm{to}(H, Z_\mathrm{e}, s)$	Impedance presented by the master device
	$Z_\mathrm{te}(H, Z_\mathrm{h}, s)$	Impedance presented by the slave device
	Z_width	Impedance width, dynamic range
	T_error	Transparency Error, distortion
	P_i(P_1,P_2, ...)	Performance measure enumeration
	$\hat{m}_\mathrm{free}$, $\hat{b}_\mathrm{free}$, $\hat{k}_\mathrm{free}$	Master impedance approximation for slave in free air
	$\hat{m}_\mathrm{stiff}$, $\hat{b}_\mathrm{stiff}$, $\hat{k}_\mathrm{stiff}$	Master impedance approximation for slave in stiff contact

Part I

Introduction to Haptic Teleoperation

Chapter 1

Introduction

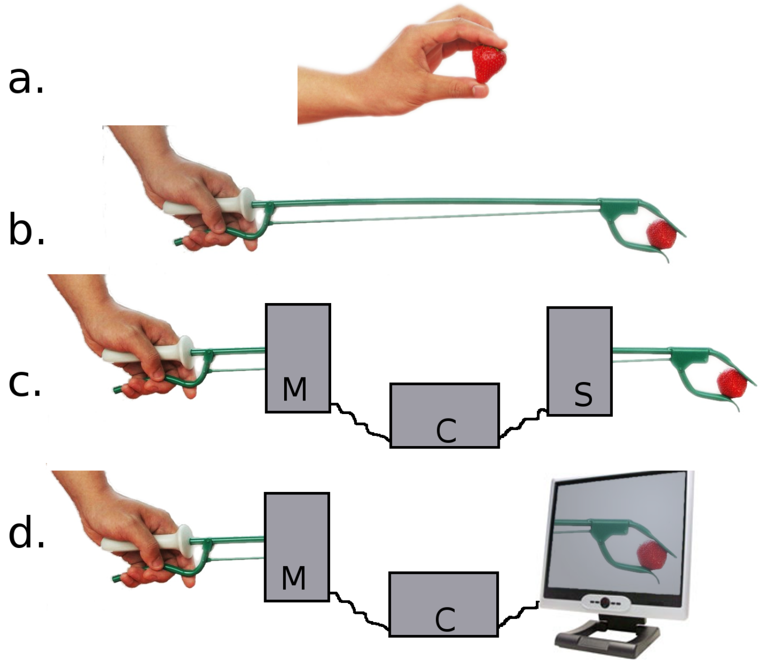

Figure 1.1: *Interaction and Manipulation: a. Direct physical interaction b. Indirect physical interaction c. Teleoperation d. Virtual reality interaction. M = master device, S = slave device, C = controller*

1.1 Background

We humans have a instinctive desire to touch, feel and explore the world using our hands and the sense of touch. Everyday we handle objects and instantly percieve the objects' weight, surface structure, stiffness and size. Object manipulation and material identification is a primal and essential task.

If it is not possible to manipulate an object directly with the bare hands (Fig. 1.1 a.), sometimes indirect interaction using a tool is appropriate (Fig. 1.1 b.). The tool-based interaction is called *teleoperation*, when the tool is divided into two parts, (Fig. 1.1 c.), connected by an electrical connection, called the controller. A *teleoperator* consists thus of an operator interface (*master device*) and a slave robot (*slave device*), connected via a *controller*. The human who holds onto the master device is called the *operator*, and the object that is manipulated is called the *environment*.

Teleoperation - to use a remotely controlled robotic tool to perform a task in a remote environment - has been used for 50 years in the nuclear industry (Burdea, 1996). Haptic teleoperation technology is currently used in nuclear research sites to manipulate hazardous materials, for deep-sea robotics, and to a limited extent for space operations. Teleoperation technology is also used in "drive-by-wire systems" for aircrafts and prototype cars, where the human control interface (e.g. the steering wheel) is electronically connected to a slave actuator (wheel-steering motor) (Kapaan et al., 2001; Pan et al., 2006).

One important class of teleoperators are those where the interaction forces from the slave side are communicated to the operator via the master, so that the operator can *feel* the remote object. This is called "haptic teleoperation", and is the main topic of this thesis.

A related technology is virtual reality interaction, shown in Fig. 1.1 d., where the slave robot and the environment are replaced by a computer model. This technology allows physical interaction with virtual objects. One example is the possibility to simulate the surfaces of a CAD-model to allow touching (feeling) a product before it is manufactured. Some of the methods developed in this thesis can also be applied for virtual reality haptic interaction, but the focus of the research is on teleoperation applications.

The haptic information, collected by sensors in the skin, muscles and joints, is important for a variety of tasks in everyday life. In numerous studies different sensoric pathways have been blocked using anasthesics and the loss of performance has been quantified (Johansson, 1996). This suggests that also for teleoperation, haptic information is beneficial. It has been shown that haptic feedback to the operator can improve the task performance in certain teleoperation tasks, e.g. tissue identification (Wagner et al., 2002; Kazi, 2001). However, it is still unknown *how good* this feedback must be to actually help the operator.

This chapter gives an overview of the history of haptic teleoperation, giving a background to the most important research areas in haptics today. One key issue is identified and chosen as the main goal of this thesis, and is reformulated as a number of research hypotheses. Finally, at the end of this chapter, the disposition of the whole thesis is presented.

1.2 History of Haptic Teleoperation

The earliest remote-controlled robotic tools were developed at the Argonne National Laboratory in the US in the 1950's, to manipulate radioactive objects. The laboratory developed tools for nuclear activities, both for civil and military use, and needed to extend the reach of the mechanical manipulators used thus far. The teleoperators developed from the 1950's until the 1970's had *kinematically identical* master and slave devices. The controllers were implemented as separate analog controllers for each joint of master and slave, with a one-to-one mapping of forces and angles. The requirement of kinematic similarity was an important restriction that made different master- and slave devices incompatible, which hindered widespread use.

In the 1970's, thanks to advances in digital computer control, *kinematically dissimilar* master-slave systems could be implemented, where communication between master and slave could be done in cartesian end-effector coordinates. This step of generalization made it possible to combine different master- and slave devices for different purposes. The teleoperation slave devices were sometimes used as autonomous manipulators at this time and were the de-facto predecessors to the modern industrial robot. In effect, the master device and the operator were replaced by a computer program with pre-programmed task trajectories. This is the way most industrial robots are still used today.

In Europe too, most research on teleoperation was done at the nuclear laboratories, notably at the Commissariat d'Energie Atomique outside Paris, where Jean Vertut developed both theory and experimental practice of teleoperation (Burdea, 1996). Some of the robots developed by Vertut in the 1970's are still in use today. In those days, haptic teleoperators were called "bilateral-", "force-reflecting-" and sometimes "force-feedback teleoperators".

In the 1970's and 1980's, the space industry made a technological leap, and at laboratories around the world teleoperators for orbital systems were developed. The most important issue of earth-space teleoperation is the communication link, which introduces significant time delay, and strong bandwidth limitations. The famous NASA Jet Propulsion Laboratory made impressive advances at the time, and Ken Salisbury, Blake Hannaford, Antal Bejczy and Paolo Fiorini laid the basis for modern teleoperation. The theoretical advances of the time were mainly the insights that teleoperators could be modelled as linear network systems (Hannaford, 1989b), which allowed more accurate predictions of performance and stability. The linear network modelling framework, often using the Hybrid matrix, is still the leading modelling paradigm. This is explained in detail in Chapter 2.

In the 1990's, the tremendous development of computer simulation and virtual reality emerged as a parallel track in the teleoperation research. It was now possible to interact with simulated objects using haptic master devices. The slave robot and the environment were simulated by a computer model of the physical objects, see Fig. 1.1 d. From being a very specialized niche product, haptic devices became prevalent, especially for computer games, but also for certain virtual reality CAD tasks and for surgical trainers (Massie and Salisbury, 1994). This allowed a significant price drop of haptic interfaces and increased ease of programming, which in turn attracted a much larger research community and application base. Now the psychomotorics of haptics could be investigated using haptic devices by psychologists and physiologists, and the multidiciplinary conference EuroHaptics was initiated. One important insight was that the operator perception of teleoperation was found to be similar to the concept of extended physiological proprioception developed for protheses by Doubler and Childress (Doubler and Childress, 1984). If the teleoperator is responsive enough, it will after training feel like a part of the body. The main advantage is that the cognitive load for the operator is vastly reduced, and certain manipulations can be performed almost subconciously.

The research on control of teleoperation systems was strongly influenced by the important results from the research on robust control (μ-analysis and robust controller synthesis) and passivity theory of this time.

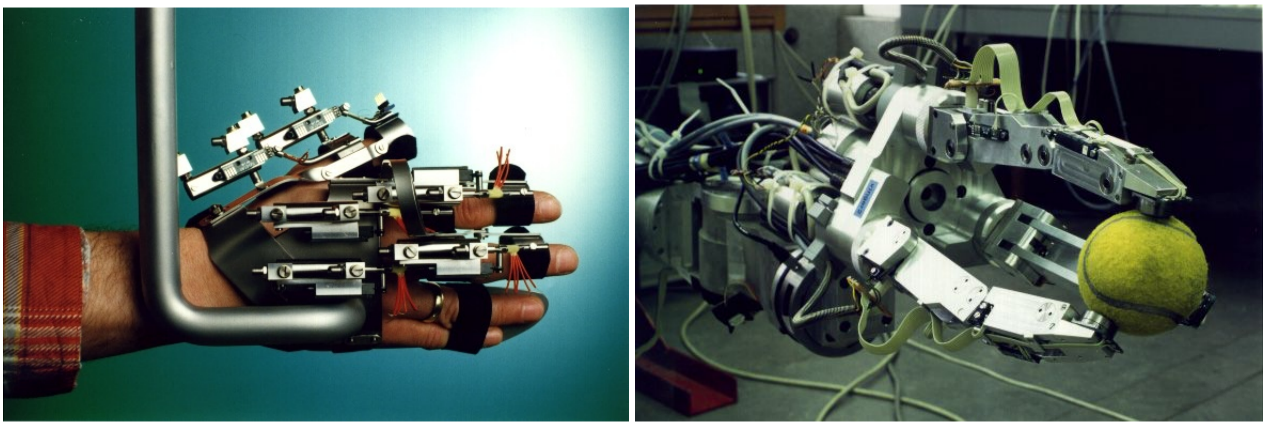

Figure 1.2: *The Teleman-18 teleoperator. The master device (top) is a lightweight exoskeleton device for three fingers, the slave robot (bottom) is a much stiffer and heavier device. (photo by Eric van Houten, adapted from (van der Ham, 1997))*

Delft University of Technology participated in a European haptic teleoperation project (TeleMan-18), and a teleoperated 3-fingered master-slave gripper was developed, see Fig. 1.2 (Stramigioli, 1998; van der Ham, 1997; Holweg, 1996). The teleoperator was designed for maintenance of nuclear plants and included a hand-exoskeleton for the master device to control the three robot fingers. Both master and slave device was actuated using electrohydraulic pistons. The main conclusion was that the high complexity of this implementation was a great obstacle to practical implementation. In the same project H_∞-robust control was also evaluated for a one degree-of-freedom medical teleoperator, with limited success (Lazeroms, 1999). It was possible to synthesize a controller using this optimization method, but the performance of this controller was subjectively qualified as less good than a hand-tuned controller. This suggests that the optimization criteria were not chosen to reflect the real requirements of the task. The difficulty in selecting an appropriate optimization criteria (or cost function J in robust control terms) is still a major hurdle for the implementation of modern control techniques.

In the 2000's, teleoperation took the step into the surgery theater. Two commercial systems, with roots in a military US-DARPA project, entered the market of surgical teleoperation, Intuitive Surgical's *daVinci* and Computer Motion's *Zeus*. In all these systems, there is only visual feedback, and no haptic feedback, so the surgeon can not feel what she is doing. Nevertheless, surgical operations are performed in more than hundred hospitals around the world using these systems, with remarkable success. There have even been a number of spectacular demonstrations in which a remote surgeon performed various surgical operation tasks at transatlantic distance (Marescaux et al., 2001). It is thus possible to perform a number of medical procedures *without* haptic feedback. Still, it is often suggested that haptic feedback would help to improve patient safety and to reduce the surgeon's mental workload (Zemiti et al., 2004; de Gersem, 2005). However, as mentioned earlier, it is not yet known *how good* the haptic feedback has to be to actually help the surgeon. This is a general problem for haptic teleoperation.

An important current development in the field is an increased interest in the human operator perception and the haptic communication channel. The traditional teleoperator development was strongly linked to industrial robot research, where high stiffness and high positional accuracy are the main control goals. However, the human perception is limited in many ways. For many stimuli we cannot distinguish differences below 10 percent of the current stimulus level (sometimes called the *Weber fraction*) (Gaydos, 1958). By using information about the human sensory system, it could be possible to reformulate the requirements for the teleoperator, especially for the master device, to allow better information transfer to the operator (Daniel and McAree, 1998; Tan et al., 1994; Howe, 1992). Likewise, the characteristics of the task dictate the optimal design of the slave robot.

Teleoperated tasks can be categorized along a floating scale from position-tasks at one extreme to force-tasks at the other extreme, see Fig. 1.3. Different tasks have different requirements; for some tasks the position

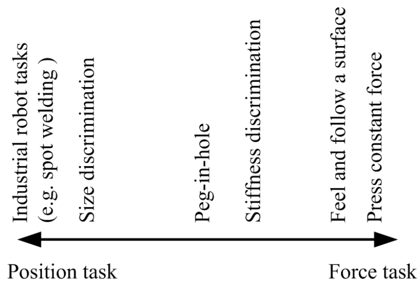

Figure 1.3: *Teleoperation task characterization: Position tasks at one extreme and force tasks at the other. Most real tasks are somewhere in between.*

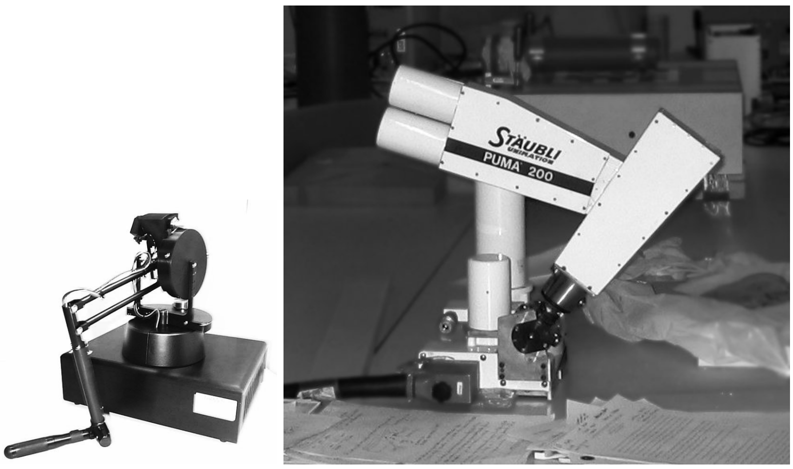

Figure 1.4: *A typical teleoperation setup. The master device (left) is lightweight and soft, the slave robot (right) is heavy and strong.*

feedback is important, and for others the force information dominates. This was already observed by Hogan (1985), who introduced the concept of impedance control for robotics, using an analogy with human motion control. It has also been shown that the human operator changes impedance based on the task (Abbink, 2006), being stiff for position tasks and soft for force tasks. This suggests that the requirements on the teleoperator (and the master and slave devices) are different for different tasks. Position tasks require accurate positioning capabilities and high stiffness of the slave robot. Force tasks, like feeling the texture of a surface, on the other hand require sensitive interaction and low stiffness.

1.3 Current Problems in Haptic Teleoperation

Even though the field has a long history of increasingly successful projects, there are still a number of problems, mainly related to the trade-off between performance and stability.

A common approach to teleoperation research is to purchase a commercially available haptic master device and connect it to an existing industrial robot and use control science to connect the two systems into a haptic teleoperator. In Fig. 1.4, a SensAble Phantom (SensAble Technologies Inc., Woburn, MA, USA, (SensAble, 2006)) is used as a master device and is connected to a Stäubli Puma (Stäubli GmbH, Beyreuth, Germany), which serves as the slave device.

Similar setups are used for nuclear waste handling (Daniel and McAree, 1998), underwater operations (Robotics, 2007) and has been suggested for surgery (Nagy et al., 2004), (de Gersem, 2005).

However, there are two fundamental problems in this kind of setup: contact instability for stiff environment objects and poor information transfer from the environment to the operator. The slave device (a traditional industrial robot) is strong, stiff and heavy, which works fine in free-air motion, but not so well in contact tasks. Industrial robots were designed and optimized for free-air movement and position control, i.e. position tasks (see Fig.1.3). Therefore, this kind of robots are very difficult to use for force control (An et al., 1988), which is often necessary in haptic teleoperation. The mechanical design is optimized for free-air movements and low position errors - a completely different set of criteria than for accurate force-tracking performance.

Another part of the problem is related to the momentum of the master and slave devices. Daniel and McAree showed that the impact force (dependent on the inertia of the device) can destabilize the system if the slave is heavier than the master (Daniel and McAree, 1998). They showed that the communicated force must be attenuated with a gain equal to the master/slave mass ratio (master mass/slave mass). The mass-ratio for the system in Fig. 1.4 is more than a one to thousand. It means that to deal with contact force transients in a stable way, the measured force is reduced to less than a thousandth before it is presented on the master device, to guarantee contact stability. It also means that non-transient (e.g. steady state) forces are practically imperceptible.

Furthermore, the sheer inertia of the slave robot makes it a poor transducer for surface structure information. Our fingertips move over surfaces and can easily follow surface structures and detect small variations and edges, thanks to the low inertia and the flexible contact. However, this is a very difficult task for a heavy robot.

Finally, the slender master device depicted in Fig. 1.4 is not very strong. The stiffness of this type of master device is quite low (<1 N/mm) and they have relatively low bandwidth (<30Hz). High frequency information and high-stiffness objects cannot be presented accurately to the operator. The combination of a strong slave and a weak master works good for movement in free air and contact with soft objects. However, in contact with stiff or brittle objects another approach is necessary.

Historically, the original master and slave manipulators were mechanically identical. However, over time, the slave robot has in general become stronger and stronger, and the master device, with a few notable exceptions, weaker and weaker. The main reason herefore is that each component has been optimized for certain criteria, separate from the requirements of the total teleoperator system.

1.4 Towards Hard Master, Soft Slave Teleoperation

During the last few years, research on haptic teleoperation has been intensified, searching for new solutions to the fundamental problems of teleoperation; the trade-off between stability, performance and complexity.

Many groups work on software solutions - how to tame a strong slave robot using clever control laws. One direction is to try to change the stiffness of the device via impedance control, using a force sensor mounted at the end-effector of the slave device. Based on the classic methods for robotic force control (An et al., 1988), the sensed force information is used to emulate a low-impedance system. The strong robot pretends that it is weak. This works very good for low frequencies, but at the moment of impact, the total inertia of the robot will always be felt. Furthermore, the sensitivity to high frequency surface structures and forces is still low. Another direction is to avoid using the end-effector force sensor for the master-slave communication and work with estimated forces, to avoid the destabilizing effect of the impact impulse (Park and Khatib, 2006; de Gersem, 2005). The main drawback of this approach is that the high frequency interaction forces are not detected at all.

A different approach to the whole problem is to zoom out and study the teleoperation system as a whole, and to look for relevant optimization criteria. By focussing on the *necessary information transfer between the operator and the environment* and the *sensomotoric capabilities* of the operator, the design requirements for the teleoperator components can be adjusted, to allow for a better total teleoperator performance.

One interesting observation is that while the sensoric input of the skin is sensitive above 100 Hz, the muscular system allows for only relatively *low frequency movements*. For precision manipulation the frequency is often around 1 Hz, and the movement velocities around 10 mm/s. The accuracy of the motion is around 1% of the moving range, and the force resolution around 10% of the current force level (Weber fraction). This is in stark contrast to the requirements of industrial robots, where movement speeds to 5 m/s are common

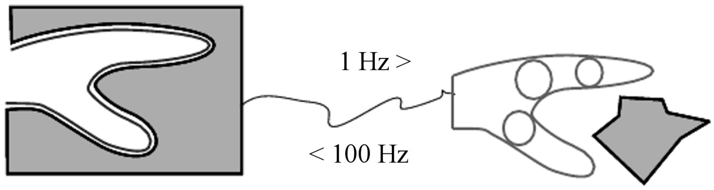

Figure 1.5: *The hard-master soft-slave teleoperator concept: Low frequency information from the human (left) and high frequency information back.*

and positioning repeatability of 0.01% of the workspace (typically 0.05 mm), and accelerations to $20\,\mathrm{m/s^2}$ (Robotics, 2006). Force accuracy of typical strain gauge force sensors is better than 0.1 %.

This means that the slave device - which is an extension to our body, and just has to follow our motion - does not have to move very fast, and probably not with as high position accuracy as a modern industrial robot. However, the slave device should be able to detect high frequency variations in the contact force, in order to communicate this to the master device and the human operator, see Fig. 1.5.

The observation that current industrial type slave robots are much "better" than necessary for certain requirements (e.g. much higher position accuracy and speed than needed) allows us to relax certain criteria and look for other mechatronic solutions. By allowing small position errors and lower position bandwidth, it is possible to achieve superior force control capabilities and to reduce the impedance presented at the tip of the slave device.

One actuation principle with these properties is called "Series Elastic Actuation" (Pratt et al., 2002). An intrinsic stiffness and damping realizes a local physical force-loop, and the measured positions control the actuator's motion. Furthermore, a large part of the device inertia is separated from the end-effector inertia by the compliant section, which reduces impact forces significantly. Both these effects would be beneficial for a teleoperation slave robot, because it could increase sensitivity at the endpoint and improve stability. Furthermore, by measuring and communicating the real tip position of the slave device, the master could present the size of the manipulated objects accurately.

To convey the sensed contact information from hard objects to the human operator, high bandwidth is necessary. It has been shown that high-frequency contact transients are important for discrimination of stiffness of the environment (LaMotte, 2000). It is therefore desireable to use a high-bandwidth, stiff master device that can represent stiff environments. Until now, only very few high-bandwidth, stiff master devices are available on the market: the "FCS Haptic Master" (v. d. Linde and Lammertse, 2003) (Moog FCS B.V., Nieuw-Vennep, Netherlands) and the "Omega" (ForceDimension, 2006) (Forcedimension SA., Lausanne, Switzerland).

We coined the term "Hard-Soft Haptic Teleoperation" to describe the use of a compliant slave robot and a hard master device. A lower slave stiffness seems to improve stability, but could also influence the perception of the remote environment, due to deformation of the soft component.. By measuring the deformation and deriving the true end-point position of the slave device it should be possible to achieve better stability with equal or better task performance compared with a hard-hard teleoperator. Hard-soft teleoperation seems well suited for teleoperation in stiff environments, typical for space operations, nuclear sites, assembly and certain medical procedures.

1.5 Goal and Approach

The goal of this thesis is to quantify the advantages of hard-soft teleoperation considering human capabilities, remote environment characteristics and task requirements. This leads to design guidelines that allow teleoperator designers to achieve a better trade-off between task performance, stability and complexity.

The first aspect to consider is the influence of device characteristics on human task performance. It is clear that a low-stiffness slave device will have lower position bandwidth and total teleoperator stiffness than a hard-hard teleoperator. However, it is not always the tool that limits the human task performance.

Human task performance is limited by both the teleoperator capabilities and the human perception. Im-

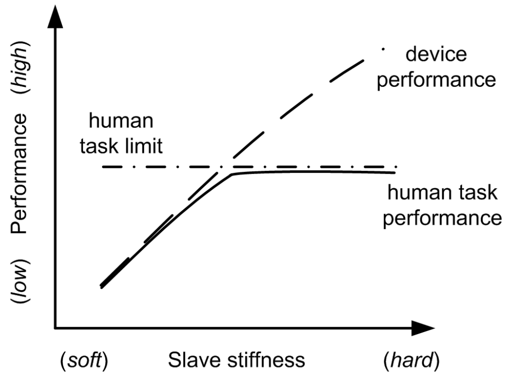

Figure 1.6: *Task related human performance. Above a certain limit, improvement of the device does not improve the human task performance. This level is different for each task.*

proving the teleoperator device performance often helps the operator and improves task performance, but only up to a certain level. When the teleoperator is "good enough", improvements of the device will not improve task performance. This is illustrated in Fig. 1.6, where the human upper limit is drawn as a dash-dotted line, in a conceptual diagram of some device performance measure, e.g. teleoperator stiffness. An example of this behaviour has been shown by O'Malley and Goldfarb (O'Malley and Goldfarb, 2004).

The relationship between device performance and human task performance is investigated for two fingergrip grasping tasks: size discrimination and stiffness discrimination. For this human factors experiment, a novel teleoperator "Hugin" for grasping tasks is developed, with adjustable intrinsic stiffness and damping for both master and slave. This teleoperator is described in detail in Chapters 3-4. The experimental task is to feel two objects and determine which is the largest or stiffest of the two, and performance is quantified as percentage correct guesses, all of which is explained in detail in Chapter 7. It is expected that human size and stiffness discrimination performance is reduced with lower teleoperator stiffness and increased teleoperator damping. The effect of using brackets around the fingers is also investigated, to quantify the relative loss of performance due to the reduction of the contact information into a one-dimensional signal. It is expected that there is a significant loss of performance due to this reduction of tactile information.

The second aspect to quantify is the improvement of contact stability in hard contact for the hard-soft teleoperator compared with a hard-hard teleoperator. Based on literature on force controlled industrial robots (Whitney, 1985), we expect a relationship similar to Fig. 1.7. Lower slave stiffness implies lower device performance (e.g. position control bandwidth and stiffness) and higher stability margins. The point is that any relaxation of requirements of the device performance allows a lower slave stiffness, which in turn would give better stability characteristics. The question here is, how much does the stability improve? This is theoretically and experimentally investigated using the 1-dof teleoperator "Hugin", in Chapter 5.

The final aspect of teleoperation in this thesis is the choice of which haptic cues to present to the human operator. For this part of the research, a novel planar hard-soft teleoperator is developed, with which remote assembly tasks can be performed. For this type of more complex assembly tasks, a combination of visual and haptic feedback is used. The soft slave device detects contact information over a wide frequency range, and the hard (high-frequency) master device can present haptic feedback over a wide band. The main question here is how high- and low-frequency haptic feedback influences task performance. For assembly tasks, the relevant task performance metrics are: task completion time and the magnitude of impact forces. It is expected that the addition of either high- or low-frequency feedback would improve performance, and especially a combination of both types of cues. It is also expected that the subjective workload would improve with haptic feedback, compared to without haptic feedback. A novel three degrees-of-freedom planar hard-soft teleoperator "Munin" is developed for this human factors experiment. The teleoperator is described in Chapter 6 and the experiments in Chapter 8.

Figure 1.7: *The slave stiffness trade-off between stability and performance: increasing slave stiffness improves device performance but reduces stability.*

1.6 Hypotheses

This research investigates the following hypotheses.

- **H1.** Reduced total teleoperator stiffness reduces human size and stiffness discrimination performance.
- **H2.** Increased total teleoperator damping reduces human size discrimination performance.
- **H3.** For size and stiffness discrimination tasks, a bracket or a loose thimble around the fingers gives worse performance compared with direct manipulation.
- **H4.** A hard-soft teleoperator has better contact stability and lower contact forces compared with a hard-hard teleoperator.
- **H5.** Low-frequency and high-frequency haptic feedback improves (reduces) impact forces in hard-object assembly tasks.
- **H6.** Low-frequency and high-frequency haptic feedback improves (reduces) task completion time in hard-object assembly tasks.
- **H7.** Low-frequency and high-frequency haptic feedback improves (reduces) subjective workload in hard-object assembly tasks.

These hypotheses are generally assumed to be true, but have hitherto not been tested experimentally.

1.7 Scope and Restrictions

In general, the term "haptic" relates to the whole sense of touch, including vibrations, temperature and pain. This is a very rich sense, which allows us to interact with the world in sophisticated and elaborated ways. Each finger tip has more than one thousand sensors, of many different types and sensitivity ranges. This research focusses on interaction using a one-dimensional force/velocity signal for each moving degree of freedom, sometimes called *kineasthetic teleoperation* or force-reflective teleoperation, in contrast to communicating the complete pixel-based tactile information. Kineasthetic teleoperation is equivalent to using a tool to probe the environment instead of interacting with bare hands. Clearly this restricts the information available to the operator, but surprisingly many tasks can be performed using a tool instead of with the bare hands. It is still an open question how much of the force information is collected by the sensors in the skin and how much is sensed by sensors located in the muscles and the sinews.

Finally, a large part of this research investigates pure haptic tasks, where no visual or audio information is present. It is clear that additional information from other channels strongly influences the perception and generally improves task performance (Tan et al., 1994). However, it is important to understand the limitations and possibilities of the haptic channel itself to design optimal teleoperation systems.

1.8 Disposition of the Thesis

This thesis is divided into three parts:

In **Part I**, the fundamental concepts of haptic teleoperation are explained in detail. It lays the ground for the second part of the thesis, where the main research contributions are presented.

In **Part II**, the two experimental teleoperation systems that were developed in this project are presented. The first system is a single-degree of freedom grasping teleoperator, and the second is a three-degrees of freedom planar teleoperator. Both teleoperators have attracted international interest for the innovative concept of hard-soft teleoperation.

In **Part III**, the quantification of human performance in relationship to device performance is addressed. A series of psychophysics experiments were performed to quantify human performance in two teleoperated grasping tasks. The first round of experiments investigates the influence of stiffness and damping on human task performance in object identification. The second experiment round studies hard-soft teleoperation for an assembly task.

Finally, in **Part IV** the experimental results are discussed and some conclusions from the whole project are drawn.

In the **Appendix**, the mathematical infrastructure of the project is described. First the open source package "The HapticAnalysis Package" is described in Appendix A. In Appendix B, a clarification of the "Wave variable formulation" in the Lawrence 4-Channel framework is presented, using this toolbox.

Many of the chapters were published in peer-reviewed conferences and submitted to scientific journals, which is indicated on the opening page of each chapter. I have chosen to keep the original texts verbatim in this thesis. However, over time my judgement has changed in some respects, and at a number of points in the text, a footnote indicates a rephrasing of the original statement.

For more information and material (measurement data, experimental software, analysis tools) please refer to the Delft Haptics Laboratory website:

`http://haptics.3me.tudelft.nl`

See also the HapticAnalysis Project site, for Free Software and open information:

`http://hapticanalysis.org`.

Chapter 2

Analysis and Control of Haptic Teleoperation

G.A.V. Christiansson
Originally published as an Open Source Textbook in the HapticAnalysis Project

2.1 Introduction

This chapter provides an in-depth introduction to modelling and analysis of haptic teleoperators, which is the basis for this thesis.

First, a modelling framework is chosen, in which all teleoperator components are modelled. Second, a number of control architectures are presented, e.g. Position-error control and the Lawrence 4-channel architecture. Third, device performance measures and stability criteria are introduced, e.g. bandwidths, Z-width and the passivity criterion. Finally, a case study of a real teleoperator is introduced, where the device performance measures and stability criteria are computed for four different controllers.

2.2 Teleoperator Modelling

A teleoperator is an interface that communicates forces and movements between the human operator and a remote environment. Therefore the core of the model is how forces and movements are transmitted through the teleoperator, from the operator to the environment and back. The dynamic relationship between movement and force is called "impedance". At every physical connection point, where motion can induce a reaction force, there is an impedance.

A model is necessary to answer questions like:

- Given a certain environment impedance, which impedance is presented by the master interface to the operator?
- What is the impedance presented to the operator at the master interface when the slave moves in free air?
- What is the force bandwidth from the environment to the operator?
- Is the teleoperator stable in contact with a certain environment?
- How does the stability robustness change with variation of a design parameter, e.g. slave stiffness?

These questions can be posed both for purely mechanical tools and for electromechanical teleoperators, and the same analysis tools can be used to study both kinds of systems.

In this presentation, all teleoperator components and controllers are modelled as *linear time-invariant* systems. This is the dominating modelling framework in the literature, and the linearized analysis gives usually sufficiently good results, even though many aspects of the system cannot be expressed accurately. The signals (F_h, F_e, V_h, V_e, etc.) are and components (Z_e, Z_m, etc.) are all defined in the Laplace domain, see also Fig. 2.1. Unless necessary for the explanation, the dependency on the Laplace variable s is omitted.

The signals used are the so called "power variables" effort (force) and flow (velocity), conform with the major part of the literature. This heritage comes from the linear network theory, and the idea is to use units that multiply into *power*, to simplify energy-based analysis (Raju et al., 1989). This leads to a definition of impedance as force over velocity in the frequency domain ($Z(s) = F(s)/V(s)$). Some researchers instead define the impedance as force over position (Aliaga et al., 2004). It may seem more natural to use position, as most real teleoperators do measure position, but as long as the analysis is linear and time invariant, and the signals are assumed to be noise free, the choice of position/velocity is irrelevant. It is therefore suggested to follow the more widespread use of velocity as the analysis variable.

In the presentation, teleoperators with one degree-of-freedom (dof) movement of the end-effector are considered. It means that the methods and formulae presented are useful for teleoperators where the end-effector degrees of freedom are decoupled, e.g. the UBC 3-dof setup (Sirouspour et al., 2000).

A teleoperator consists of several components, see Fig. 2.1. Each component is modelled separately, and then combined into one complete teleoperator model using the H-matrix notation. For stability analysis it is necessary to include the operator and environment impedance in the model, which is then called a Connected Teleoperator System (CTS).

In the subsequent sections, each component of the CTS is presented, then the complete teleoperator model is composed.

2.2.1 Operator Model

The operator is not part of the teleoperator itself. However, the operator is mechanically connected to the teleoperator, and therefore part of the connected teleoperator system (CTS). Due to this mechanical coupling, the operator influences the dynamics of the system, mainly regarding stability, see Section 2.5. The same is true for the environment, which will be elaborated in Section 2.2.5. The operator impedance (Z_h) is defined as the force response from a movement of the master device, see Fig.2.2.

Different operators hold with different strengths, and they have different masses. Furthermore, one person can change the grip forces and modulate his impedance in a wide range during operation, in general to

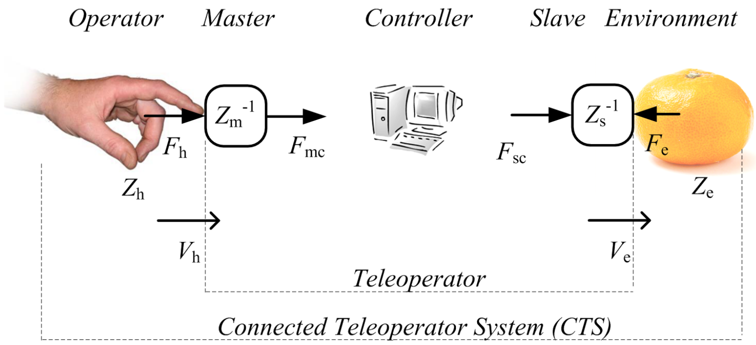

Figure 2.1: *The teleoperator (Master-Controller-Slave) is in contact with the operator (left) and the remote environment (right). The whole system is the Connected Teleoperation System.*

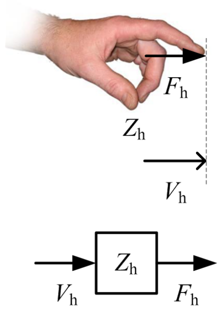

Figure 2.2: *The operator model (above) is modelled as an impedance block, where velocity of the contact point results in a force response (below).*

stabilize the complete system (de Vlugt et al., 2002). The operator also adjusts her performance based on the current task to improve performance, which makes this component task-dependent (Abbink, 2006).

Much can be said about this very interesting component in the total teleoperator system, but here, the discussion is kept short by observing that the operator model is mainly used in the stability analysis. Therefore the impedance of the operator can be approximated with a low-order model with parameters in a certain range, or expressed as a structured uncertainty.

Often, the operator is approximated as a time-invariant mass-spring-damper system, see eq. (2.1), and sometimes it is simplified to a single stiffness.

$$Z_h(s) = \frac{F_h}{V_h} = m_h\, s + b_h + \frac{k_h}{s} \tag{2.1}$$

The operator model can be seen as an impedance (Z_h) or an admittance (Z_h^{-1}), depending on the interconnection with the rest of the model. Numeric values for operator impedance for different interactions and grips are only available for certain poses of specific joints. Typically each device designer will have to measure the impedance of the operator. It is straightforward to get an approximate model with an identification experiment using a disturbance excitation, measuring the response and computing approximate values for the parameters of the model (m_h etc.) (Christiansson, 2004; Kern et al., 2006; Abbink, 2006).

For stability analysis it is necessary to know the minimum and maximum impedance of the operator. Therefore it is advised to perform an identification experiment of the operator while performing a few different tasks, to quantify the range of operator impedances the teleoperator will encounter during operation (Abbink, 2006). For marginally stable and unstable systems, humans generally adapt their reflexive feedback gains to add damping to try to stabilize the system. On the other hand, in the case of interaction with systems with large damping, human subjects tune their gains in the other direction, and even negative damping has been observed (de Vlugt et al., 2003). However, for practical purposes of designing haptic interfaces, it is usually enough to work with a lumped mass-spring-damper model as described above.

In addition to the mechanical response of the neuromuscular system of the operator, as indicated by the operator impedance (Z_h), the operator can also exert a voluntary force, sometimes called external operator force ($F_\mathrm{h,ext}$). This force is included in the control schemes in Section 2.3.

2.2.2 Master Device Models

The master device is the part of the teleoperator that the operator holds on to. The model comprises the main elements of the mechanics and actuation oof the master device, often including handles, transmissions and one or more electromotors. Often the master device is approximated with a simple mass-damper system (Lawrence, 1993; Hannaford, 1989b), see Fig. 2.3. Two forces act on the mechanical components of the master device, the human interaction force (F_h) and the controlled motor force (F_mc).

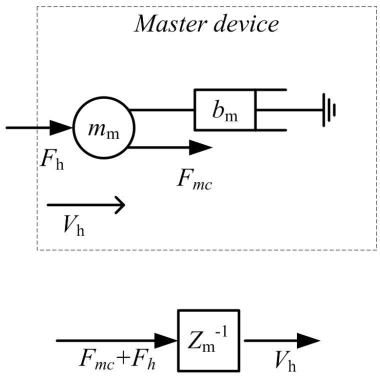

Figure 2.3: *Example of a master device model: Mechanical model (top) with m_m (inertia) and b_m (damping). Admittance model (bottom) where forces (F_h, F_mc) give a velocity response (V_h).*

The impedance of this simple device can be expressed in the Laplace form:

$$Z_\mathrm{m}(s) = \frac{F_\mathrm{h} + F_\mathrm{mc}}{V_\mathrm{h}} = m_\mathrm{m}\, s + b_\mathrm{m} \qquad (2.2)$$

Numerical values for the inertia (m_m) and the damping (b_m) are typically found by performing an identification experiment, like for the operator impedance. The inertia can sometimes be calculated quite accurately from the component masses and inertias, but the damping usually has to be measured in an identification experiment.

A single-mass model of the mechanics of the master device is only accurate up to the structural frequency of the mechanism, the first mode. For frequencies above the first eigenfrequency, a higher order model is necessary, e.g. the model developed by Kuchenbecker et al. to control the popular SensAble Phantom haptic master device (Kuchenbecker et al., 2006).

2.2.3 Controller Model

In this paper, the *controller* is a model of all electronics (sensors, amplifiers, transmission line, actuators, controller hardware and software) between the electromechanical master and the slave devices. Much of the literature on haptic teleoperation describes different “controller architectures” that describe different ways of connecting measured signals to controlled forces, and the whole Section 2.3 describes those in detail.

In general, the controller K is a multiple-input multiple-output (MIMO) component. A number of positions, velocities, accelerations and forces are measured and suitable actuation forces are calculated, see

Fig. 2.4. Remember that the analysis is done in the frequency domain, so the velocity signal includes all information about acceleration and position. Therefore, it is only necessary to include one of these signals in the model.

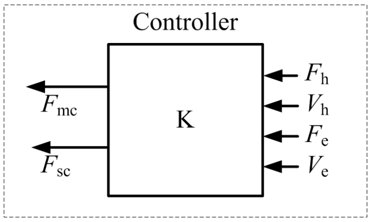

Figure 2.4: *A general MIMO block scheme of the teleoperation controller. A number of signals are measured and the actuator forces on the master and slave side (F_{mc}, F_{sc}) are controlled*

Assuming that the four signals (F_{h}, V_{h}, F_{e}, and V_{e}) are measured, the task of the control engineer is to choose controller transfer functions $k_{ij}(s)$ (k_{11}, k_{12}...) to optimize some performance function:

$$\begin{aligned} F_{\mathrm{mc}} &= k_{11}\,F_{\mathrm{h}} + k_{12}\,V_{\mathrm{h}} + k_{13}\,F_{\mathrm{e}} + k_{14}\,V_{\mathrm{e}} \\ F_{\mathrm{sc}} &= k_{21}\,F_{\mathrm{h}} + k_{22}\,V_{\mathrm{h}} + k_{23}\,F_{\mathrm{e}} + k_{24}\,V_{\mathrm{e}} \end{aligned} \tag{2.3}$$

In the literature there are a number of teleoperation control "architectures", which represent certain choices of the $k_{ij}(s)$ transfer functions, and will be explained in depth in Section 2.3. The optimization with respect to a certain performance function is however somewhat problematic. Not so much due to complicated algorithms as due to the fact that it is difficult to mathematically formulate a criterion that matches what we want to optimize for. In Section 2.4.1, a number of proposed performance measures are described.

2.2.4 Slave Device Model

The slave device is an electromechanical device just like the master device, so the same kind of model is used for this component, see Fig. 2.5. The slave impedance is often modelled as a mass-damper (Lawrence, 1993), or as a simple mass (m_{s}) (Sirouspour et al., 2000). This simple model is useful when the slave device is stiff, and a soft-slave model is introduced in Section 2.3.6 below and (Christiansson, 2004; Christiansson et al., 2006a).

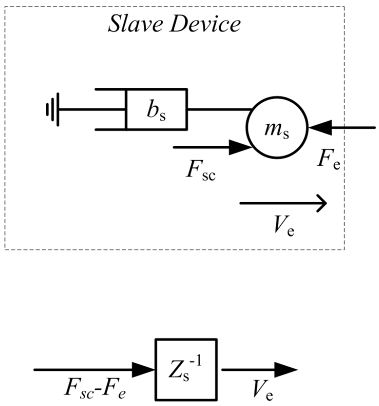

Figure 2.5: *Example of a slave device: Mechanical model (top) with inertia (m_{s}) and damping (b_{s}). Admittance block model (bottom) with input force and output velocity.*

The equations governing the movement of the slave are identical to those of the master device in this example with a single-mass model, see (2.4).

$$Z_{\mathrm{s}} = m_{\mathrm{s}}\, s + b_{\mathrm{s}} = \frac{F_{\mathrm{sc}} - F_{\mathrm{e}}}{V_{\mathrm{e}}} \tag{2.4}$$

Another part of the linear network legacy is the choice of the direction of the force F_{e}. In the illustration in Fig. 2.5 the environment force F_{e} is defined as the contact force pushing on the slave device - opposite the direction of the controlled motor force (F_{sc}), in contrast to the definition of the human force F_{h} in the model of the master device. This definition leads to that when F_{h} and F_{e} are equal, there is no movement. In the linear network theory of electricity, that is equivalent to the same voltage on both sides of the network, resulting in no current. Note that the force and motion at the operator interface (F_{h} and V_{h}) are in the same direction but at the environment side (F_{e} and V_{e}), they are opposite. Unfortunately, not all researchers use the same notation, which makes it difficult to compare formulae and results.

2.2.5 Environment Model

The environment is a part of the connected teleoperator system (CTS), like the operator. Therefore it is part of the closed loop system and influences stability. The environment is generally the most uncertain component in a teleoperation system. The variation in environment impedance can be large, especially when the slave can move in free air and suddenly come in contact with a stiff or heavy environment. A realistic model would contain this position-dependent impedance, but that is a nonlinear effect, even if it only contains linear components. For linear analysis, as in most of the literature, one specific value for the environment impedance has to be given, see Fig.2.6, often a stiffness (k_{e}), sometimes with a damper (b_{e}):

$$Z_{\mathrm{e}}(s) = k_{\mathrm{e}}/s + b_{\mathrm{e}} \tag{2.5}$$

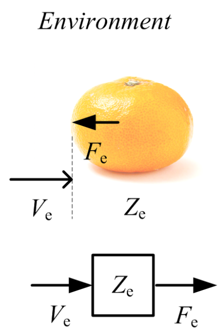

Figure 2.6: *Example of an environment model: Mechanical model (top). Impedance model (bottom) where velocity (V_{e}) gives a force response (F_{e}).*

In practice, it is useful to look at the extreme values, the minimum and maximum impedance gain functions that the environment will have, and test these for stability. For certain control architectures, like the Position Error controller (called PERR, PEB, position-position, explained in Section 2.3.2), the free-air stability is the most critical. For other schemes including force sensor measurements, like the Lawrence 4-Channel control (see Section 2.3.4), the highest environment impedance is limiting the stability.

Furthermore, an environment model is often used to quantify the performance of a teleoperator. The "transparency" or "fidelity" express how well the teleoperator can present a certain remote environment to the operator. The performance measures are elaborated in detail in Section 2.4.

2.2.6 Teleoperator Model - Input/Output Model

The component models of the master, the slave and the controller can be combined into one linear teleoperator model. This model describes everything that happens between the operator and the environment, in the form of transfer functions. The inputs and outputs of this model are then F_h, F_e, V_h and V_e. Any two can be chosen as input, and the other two becomes the output signals. The most popular representation is the *Hybrid Matrix Configuration* (Hannaford, 1989b), see Fig. 2.7, where master velocity V_h and slave force F_e are chosen as inputs:

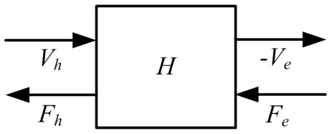

Figure 2.7: *The Hybrid Matrix Model: Master velocity (V_h) and slave contact force (F_e) are chosen as inputs, see* (2.6).

$$\begin{bmatrix} F_\mathrm{h} \\ -V_\mathrm{e} \end{bmatrix} = \begin{bmatrix} h_{11} & h_{12} \\ h_{21} & h_{22} \end{bmatrix} \begin{bmatrix} V_\mathrm{h} \\ F_\mathrm{e} \end{bmatrix} \tag{2.6}$$

The H-matrix elements h_{ij} are rational transfer functions, containing all the information about the device models and the controller: By combining equations (2.2), (2.4) and (2.3), the H-elements (h_{ij}) are calculated. (The tradition of chosing $-V_\mathrm{e}$ as the output signal comes from the electrical linear networks, where positive currents are going into the network.)

In Section 2.3, the H-matrix elements for some example teleoperation control architectures are calculated symbolically. In Section 2.6, a real teleoperation system is used to illustrate what it means in practice. The practice of certain researchers, e.g. Lazeroms (Lazeroms et al., 1997), and Flemmer (Flemmer et al., 1999) to publish the complete H-matrix of their teleoperator devices is encouraged, because it allows potential users to calculate any linear performance measure for any remote environment and any operator.

The H-matrix components h_{ij} can be interpreted as (Hannaford, 1989b):

$$H = \begin{bmatrix} \text{input impedance} & \text{force scale} \\ -\text{velocity scale} & \text{output admittance} \end{bmatrix} \tag{2.7}$$

The teleoperator model can be connected to the admittance of the operator (Z_h^{-1}) and the impedance of the environment (Z_e) to give a model of the connected teleoperator system (CTS), see Fig. 2.8, to compute closed-loop stability characteristics. Please note that the environment impedance Z_e is defined as the force response to velocity into the environment, but the velocity V_e has a different direction. Therefore a minus sign in the block model is necessary.

The hybrid model (2.6) is only one of six possible combinations of inputs and outputs of the four variables F_h, F_e, V_h and V_e. The second most popular choice is the *impedance matrix notation* (Z-matrix-notation) with V_h and V_e as inputs and F_h and F_e as outputs (Raju et al., 1989) [1].

Two other forms are the inverses of the above two notations: *admittance matrix* $Y\,(= Z^{-1})$ and the *alternate hybrid matrix* $G\,(= H^{-1})$. Furthermore, for analytical purposes, sometimes two models of less physical meaning are used, where both force and velocity on the same side of the system are used as inputs: the *chain matrix* C (F_h and V_h are inputs), and its inverse, the *alternate chain matrix* B. We owe the names of these linear network models from the domain of Electrical Engineering, where these models have been used for a long time (Feldtkeller, 1937).

[1] NB. The hybrid matrix has V_h and F_e as inputs. In certain papers, e.g. (Lawrence, 1993), the alternate chain matrix (with F_e and V_e as inputs) is used with the letter H, to much confusion. Please use B for that matrix.

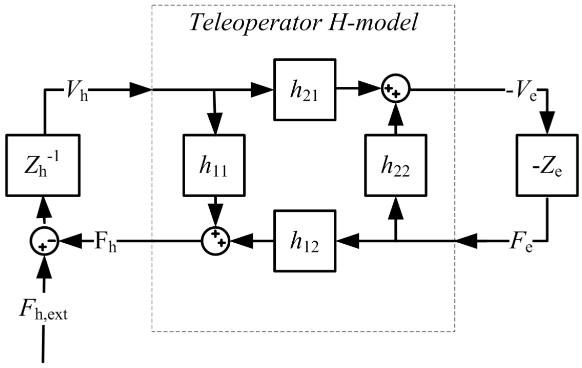

Figure 2.8: *Connected Teleoperation System: The operator (Z_h), the teleoperator (H-matrix elements), and the environment (Z_e). The active (exogeneous) force from the operator is shown as $F_{h,ext}$.*

2.3 Control Architectures

There has been numerous control architectures proposed for haptic teleoperation through the years. The "controller" is in this context the combined system of sensors, signal conditioning, control algorithm and communication channel. This section provides an overview of the most popular control architectures and shows how to calculate a teleoperator model (H-matrix) symbolically for each of them.

Every controller has a set of adjustable parameters (gains), and the control objective is usually to maximize some measure of the performance while keeping the system stable. The performance of the teleoperator, as well as the stability, can be expressed using the H-matrix. By combining the controller equations with the equations describing the master and slave devices, the H-matrix elements are explicitly computed.

First a generalized MIMO scheme is presented, and then some selected control architectures from the literature are shown to be specializations thereof. All controllers are expressed using the K-matrix form, which allows numerical comparison between the controllers. Many controllers can also be expressed in the popular Lawrence/Salcudean 4-channel scheme
(Lawrence, 1993; Hashtrudi-Zaad and Salcudean, 2002), which is also a special case of the generalized MIMO scheme. The control scheme diagrams are shown for each of the controllers described, both in a classic form and as special cases of the Lawrence/ Salcudean 4-channel scheme. The reason herefore is to also allow visual comparison of the various "control architectures" proposed in literature

The controllers presented here have in common that all measured signals are used for control. Some of the controllers proposed in the literature are controllers where one or more of the signals is only used on one side (e.g. measured master force is only used on the master side and not sent to the slave side). Those controllers can be seen as special cases of the controllers here, with one or more gains fixed zero. However, the author thinks that it is wise to use as much information as possible for control, and that throwing away measured signals is a waste.

Time delay, while important for e.g. space teleoperation applications, is not explicitly written in any of the formulae below, but can be introduced as part of the control-transfer functions, as a factor ($e^{-s\,T}$).

Another point worth stressing is that the models presented in this sections are used for analysis, not implementation. A real implementation may communicate both position, velocity and accelleration measurements, all of which are represented by the velocity signal ($V(s)$) in the analytical model.

2.3.1 Generalized MIMO Controller

The most general linear controller is a set of transfer functions from all possible measured signals to all actuated outputs. This can be expressed as choosing transfer functions $k_{ij}(s)$, in equation (2.3), here repeated:

$$\begin{aligned} F_{\mathrm{mc}} &= k_{11}\,F_{\mathrm{h}} + k_{12}\,V_{\mathrm{h}} + k_{13}\,F_{\mathrm{e}} + k_{14}\,V_{\mathrm{e}} \\ F_{\mathrm{sc}} &= k_{21}\,F_{\mathrm{h}} + k_{22}\,V_{\mathrm{h}} + k_{23}\,F_{\mathrm{e}} + k_{24}\,V_{\mathrm{e}} \end{aligned} \tag{2.8}$$

Each transfer function $k_{ij}(s)$ can have any order, and is often a P-controller (single gain) or a PI-controller (gain + integrator with gain). However, any transfer function is possible.

Combining the MIMO controller equations (2.8) with the impedance models of master and slave devices (Z_m and Z_s), the hybrid matrix elements can be computed by straightforward linear algebra:

$$\begin{aligned} h_{11} &= \frac{(Z_\mathrm{m} - k_{12})\ Z_\mathrm{s} - k_{24}\, Z_\mathrm{m} + k_{12}\, k_{24} - k_{14}\, k_{22}}{(k_{11}+1)\ Z_\mathrm{s} + (-k_{11}-1)\ k_{24} + k_{14}\, k_{21}} \\ h_{12} &= -\frac{k_{13}\, Z_\mathrm{s} - k_{13}\, k_{24} + k_{14}\, k_{23} - k_{14}}{(k_{11}+1)\ Z_\mathrm{s} + (-k_{11}-1)\ k_{24} + k_{14}\, k_{21}} \\ h_{21} &= -\frac{k_{21}\, Z_\mathrm{m} + (k_{11}+1)\ k_{22} - k_{12}\, k_{21}}{(k_{11}+1)\ Z_\mathrm{s} + (-k_{11}-1)\ k_{24} + k_{14}\, k_{21}} \\ h_{22} &= -\frac{(k_{11}+1)\ k_{23} - k_{13}\, k_{21} - k_{11} - 1}{(k_{11}+1)\ Z_\mathrm{s} + (-k_{11}-1)\ k_{24} + k_{14}\, k_{21}} \end{aligned} \tag{2.9}$$

These expressions are useful because they can express the resulting H-matrix for any linear controller implemented on the Z_m and Z_s devices. It is all a matter of choosing the transfer functions of the k_{ij}-elements, which will be explained below.

Even though the expressions are quite large, some interesting things can be observed in the hybrid matrix model (2.9). First, the free-air impedance part of the model (h_{11}) depends on both master and slave device impedances (Z_m and Z_s). Furthermore, the master impedance (Z_m) is part of expressions h_{11} and h_{21}, but the slave impedance (Z_s) is part of all four expressions. This is an artefact due to the asymmetric nature of the hybrid matrix model, by choosing one force and one velocity as input, and the other two as outputs.

One advantage of modelling the controller as a separate block is that the step is small to use tools from multivariable control (e.g. μ-analysis and synthesis). One way to draw the general control scheme is shown in Fig. 2.9. Note, however, that the hybrid model does only model the teleoperator and does not include the operator (Z_h) or the environment (Z_e).

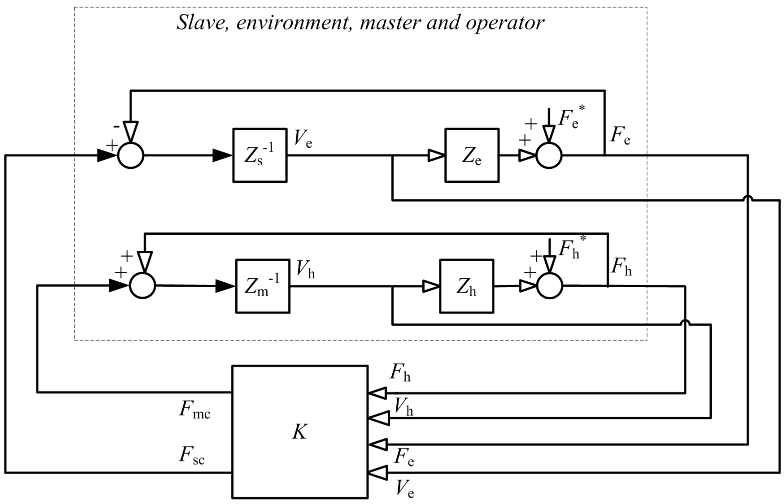

Figure 2.9: *Generalized MIMO controller, as part of the connected teleoperator system (CTS)*

2.3.2 Position Error Control

The first documented controller used for haptic teleoperation is the *Position Error Controller*, (also called position-position control, position-exchange control and bilateral position control) (Aliaga et al., 2004). The idea is that the position of the two devices are measured, and the controller strives to make this position error small. There are two position servos, one for the master and one for the slave where each one gets the reference position from the current value of the other. In this analysis, velocity signals are used, so position is integrated velocity, which in the Laplace domain is expressed as $(1/s)$. A control scheme for the position error controller is depicted in Fig. 2.11. The servo gain K_p can be seen as a servo stiffness [N/m]. (Sometimes, an additional servo damper is used, e.g. by implementing a classic PD-controller seen from position.)

The layout of the control scheme can also be drawn in the style of Lawrence and Salcudean (Lawrence, 1993), (Salcudean and Stocco, 2000), see Fig. 2.11. In the figure, the physical forces and velocities are marked with hollow arrows and the controlled signals with filled arrows, follwing the notation of Goldfarb (Fite et al., 2001).

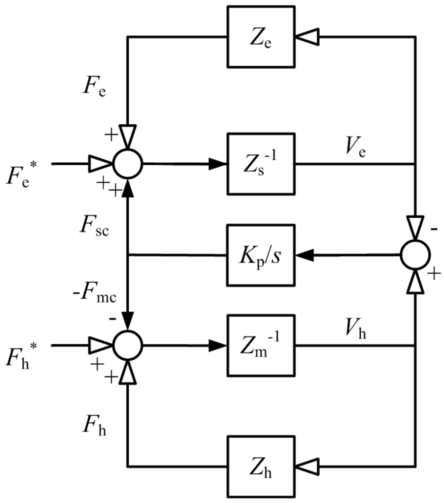

Figure 2.10: *Position Error Control - as it is usually presented. The difference in position (integrated velocity) is fed back with a position gain K_p, identical for master and slave. ($F_{\mathrm{h}^\star}$ and $F_{\mathrm{e}^\star}$ are active forces from operator and environment)*

Even more useful is to express this controller in the generalized MIMO framework using the transfer functions k_{ij}, from Section 2.2.3 above. The controller motor forces F_mc and F_sc depend on the integrated velocity (V_h/s) and a position gain or stiffness (K_p). No forces are measured, so the gain for the contact forces $(F_\mathrm{h}$ and $F_\mathrm{e})$ is zero:

$$\begin{gathered}\begin{cases} F_\mathrm{mc} = 0\,F_\mathrm{h} - K_\mathrm{p}/s\,V_\mathrm{h} + 0\,F_\mathrm{e} + K_\mathrm{p}/s\,V_\mathrm{e} \\ F_\mathrm{sc} = 0\,F_\mathrm{h} + K_\mathrm{p}/s\,V_\mathrm{h} + 0\,F_\mathrm{e} - K_\mathrm{p}/s\,V_\mathrm{e} \end{cases} \\ \Rightarrow K(s) = \begin{bmatrix} 0 & -K_\mathrm{p}/s & 0 & K_\mathrm{p}/s \\ 0 & K_\mathrm{p}/s & 0 & -K_\mathrm{p}/s \end{bmatrix}\end{gathered} \tag{2.10}$$

When combining this controller equation with the master and slave impedances (Z_m and Z_s) we get a H-matrix:

$$H(s) = \begin{bmatrix} \frac{(sZ_\mathrm{m}(s)+K_\mathrm{p})Z_\mathrm{s}(s)+K_\mathrm{p}Z_\mathrm{m}(s)}{sZ_\mathrm{s}(s)+K_\mathrm{p}} & \frac{K_\mathrm{p}}{sZ_\mathrm{s}(s)+K_\mathrm{p}} \\ -\frac{K_\mathrm{p}}{sZ_\mathrm{s}(s)+K_\mathrm{p}} & \frac{s}{sZ_\mathrm{s}(s)+K_\mathrm{p}} \end{bmatrix} \tag{2.11}$$

2.3.3 Position-Force Control

The classic Position-Force Control architecture is in essence that the operator gives position commands, and the slave measures forces that are subsequently presented to the operator (Aliaga et al., 2004). A schematic of this control architecture is shown in Fig. 2.12.

A typical characteristic of this controller is that there is only one local feedback loop. This is one reason for the stability problems of this architecture. The controller can be expressed in the MIMO framework:

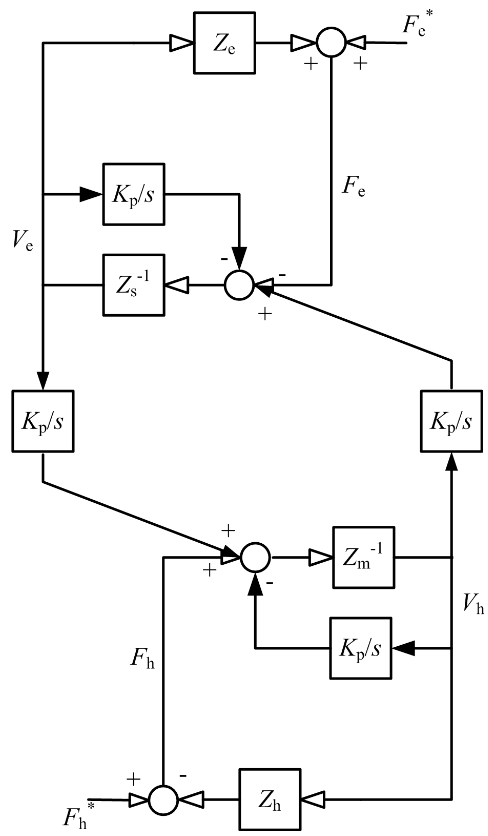

Figure 2.11: *Position Error Control - in the Lawrence/Salcudean framework. Note that the subtraction of positions is done after the multiplication with the servo stiffness K_p/s.*

$$\begin{cases} F_\mathrm{mc} = 0\,F_\mathrm{h} + 0\,V_\mathrm{h} + K_\mathrm{f}\,F_\mathrm{e} + 0\,V_\mathrm{e} \\ F_\mathrm{sc} = 0\,F_\mathrm{h} + K_\mathrm{p}/s\,V_\mathrm{h} + 0\,F_\mathrm{e} + K_\mathrm{p}/s\,V_\mathrm{e} \end{cases}$$
$$\Rightarrow K(s) = \begin{bmatrix} 0 & 0 & K_\mathrm{f} & 0 \\ 0 & K_\mathrm{p}/s & 0 & -K_\mathrm{p}/s \end{bmatrix} \tag{2.12}$$

Now that the H-elements are expressed as functions of both the position and force gains (K_p,K_f) and master and slave device impedances (Z_m and Z_s):

$$H(s) = \begin{bmatrix} Z_\mathrm{m}(s) & -K_\mathrm{f} \\ -\frac{K_\mathrm{p}}{s\,Z_\mathrm{s}(s) + K_\mathrm{p}} & \frac{s}{s\,Z_\mathrm{s}(s)+K_\mathrm{p}} \end{bmatrix} \tag{2.13}$$

This classic Position-Force-scheme does not make use of all measured information for control purposes; the force is measured at the slave, but only used for the control of the master, and the master and slave position/velocity measurements are only used at the slave side. This is one of the problems with this control architecture, and can be seen in (2.12) as the three zero transfer functions k_{12}, k_{14} and k_{23}. By restricting these three transfer functions to the constant value zero, the search space for optimal controllers is greatly, and unnecessarily, reduced. This is the main reason for the poor performance/stability characteristics of this controller architecture. Many of the proposed control architectures for teleoperation unfortunately suffer from this deficiency, that measured information is not used for control.

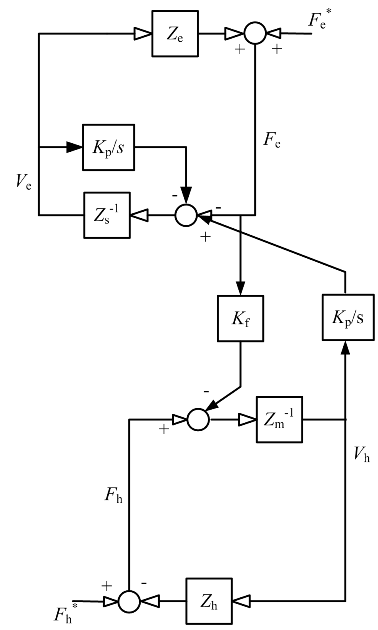

Figure 2.12: *Position-Force Control: The master measures the hand position, and the slave measures the interaction force which is subsequently presented to the operator. Note the long 8-shaped loop.*

2.3.4 4-Channel Control

A milestone in the development of control architectures for haptic teleoperation was the generic control scheme suggested by Lawrence (Lawrence, 1993). He showed the advantage of communicating both forces and positions/velocities between master and slave, and called this "4-channel control", denoting the four analysis variables ($F_{\rm h}$, $V_{\rm h}$, $F_{\rm e}$, $V_{\rm e}$). Salcudean, Hashtrudi-Zaad and Zhu developed the ideas further to encompass local force-feedback to improve the stability/performance trade-off (Zhu and Salcudean, 1995),(Hashtrudi-Zaad and Salcudean, 2002), shown in Fig. 2.13.

In the Lawrence/Salcudean framework, the controller is often defined as eight independent blocks (C_1 to C_6, plus $C_{\rm m}$ and $C_{\rm s}$). These eight blocks correspond directly to the eight k_{ij} blocks from the generalized MIMO notation:

$$\begin{aligned}
&\begin{cases} F_{\rm mc} = k_{11}\, F_{\rm h} + k_{12}\, V_{\rm h} + k_{13}\, F_{\rm e} + k_{14}\, V_{\rm e} \\ F_{\rm sc} = k_{21}\, F_{\rm h} + k_{22}\, V_{\rm h} + k_{23}\, F_{\rm e} + k_{24}\, V_{\rm e} \end{cases} \\
&\begin{cases} F_{\rm mc} = C_6\, F_{\rm h} - C_{\rm m}\, V_{\rm h} - C_2\, F_{\rm e} - C_4\, V_{\rm e} \\ F_{\rm sc} = C_3\, F_{\rm h} + C_1\, V_{\rm h} - C_5\, F_{\rm e} - C_{\rm s}\, V_{\rm e} \end{cases} \\
&\Rightarrow K = \begin{bmatrix} C_5 & -C_{\rm m} & -C_2 & -C_4 \\ C_3 & C_1 & -C_6 & -C_{\rm s} \end{bmatrix}
\end{aligned} \tag{2.14}$$

Lawrence also suggested a certain choice of the controller transfer functions (C_i) to "optimize" for a certain device performance function that he called *transparency*. Transparency and other performance measures are explained in detail in Section 2.4.1. The optimization is actually a recipe where certain transfer functions are assumed to be known ($C_{\rm m}$, $C_{\rm s}$), some are identity or zero, and the others are expressed as function of the model parameters. The force gains are all chosen scalar, being 0 or 1, and the velocity functions are chosen to be PI-controllers. (In reality implemented as PD-controllers for position.) In practice the recipe works well, even though not all mechanical dynamics (especially inertia) can be compensated. Lawrence also showed how to adapt the scheme to compensate for communication time delay (Lawrence, 1993).

The hybrid matrix for a teleoperator with the Lawrence 4-channel controller can be expressed as:

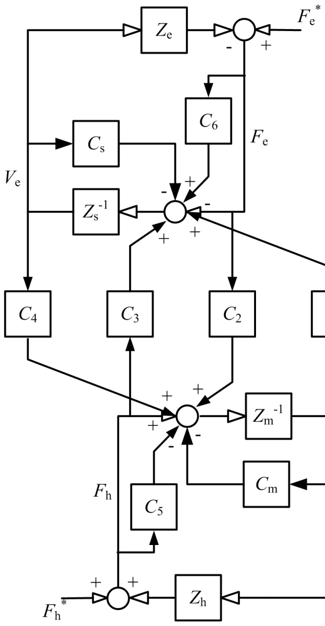

Figure 2.13: *Lawrence 4-Channel Controller, adapted from (Lawrence, 1993)*

$$H(s) = \begin{bmatrix} \frac{(Z_m+C_m)\,Z_s+C_s\,Z_m+C_m\,C_s+C_1\,C_4}{(C_6+1)\,Z_s+(C_6+1)\,C_s-C_3\,C_4} & \frac{C_2\,Z_s+C_2\,C_s-C_4\,C_5-C_4}{(C_6+1)\,Z_s+(C_6+1)\,C_s-C_3\,C_4} \\ -\frac{C_3\,Z_m+C_3\,C_m+C_1\,C_6+C_1}{(C_6+1)\,Z_s+(C_6+1)\,C_s-C_3\,C_4} & \frac{(C_5+1)\,C_6+C_5-C_2\,C_3+1}{(C_6+1)\,Z_s+(C_6+1)\,C_s-C_3\,C_4} \end{bmatrix} \tag{2.15}$$

2.3.5 FCS-Virtual Model control

Some interesting work on teleoperation was done at the company Fokker Space BV, The Netherlands, in the 1980's (since 2006 the company is called Moog-FCS BV). They presented a control scheme where the master and slave devices together represent a virtual object (Lam and de Vries, 1981). The control scheme can be drawn in many ways, the most common one is based on their patent application drawings, see Fig. 2.14.

The basic idea is that the contact forces (on master and slave) are measured and assumed to act on a virtual object, modelled as an impedance (Z_{vm}). The forces generate thus a virtual movement, which is used as the reference velocity and position for the master and slave device. The velocity servo K_v is often, but not necessarily, identical for master and slave. The important thing is to achieve convergence of the states at master and slave. Typically, the virtual model is a pure mass or a mass-damper system ($Z_{vm}(s) = m_v\,s + b_v$). In essence, the controller tries to change the impedance of the device (nonlinear, heavy, high friction) into a well-defined, pleasant impedance, usually with lower mass and lower damping. This works well up to the bandwidth of the velocity controller, so at high frequencies, the real inertia dominates. In the field of robotics control, this is sometimes called a "model reference controller". Moog-FCS calls the control scheme "admittance control".

The FCS Haptic Master (Moog-FCS, Nieuw Vennep, The Netherlands) uses this control scheme, and the master and slave device inertias ($<$ 10 kg) is reduced to around 1 kg. With additional accelleration measurement, this can be improved to 0.1 kg, but then the contact stability is somewhat reduced.

The Virtual model control scheme can also be expressed in the Lawrence/Salcudean framework, see Fig. 2.15, or using the MIMO-notation, see (2.16), which helps to understand its pros and cons.

The virtual model controller can be expressed using the MIMO-notation:

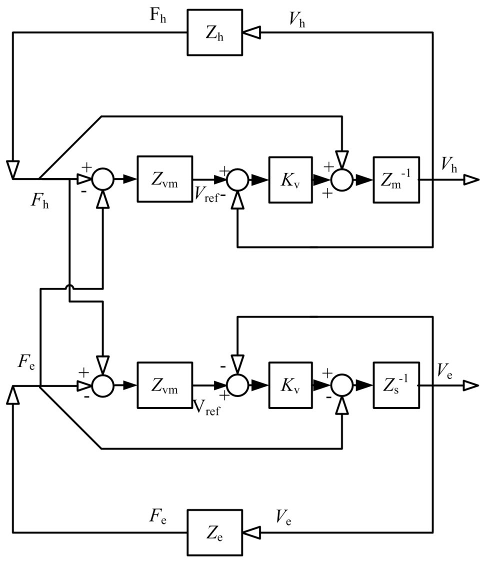

Figure 2.14: *Virtual Model Control (FCS Admittance Control), as it is usually presented. The two external forces (F_h,F_e) are measured and in the controller they act on a virtual object with impedance Z_vm, and a reference velocity V_ref for the endpoint is calculated. K_v is a velocity servo controller*

$$\begin{aligned} &\begin{cases} F_\mathrm{mc} = \frac{K_\mathrm{v}}{Z_\mathrm{vm}} F_\mathrm{h} - K_\mathrm{v}\, V_\mathrm{h} - \frac{K_\mathrm{v}}{Z_\mathrm{vm}} F_\mathrm{e} + 0\, V_\mathrm{e} \\ F_\mathrm{sc} = \frac{K_\mathrm{v}}{Z_\mathrm{vm}} F_\mathrm{h} + 0\, V_\mathrm{h} - \frac{K_\mathrm{v}}{Z_\mathrm{vm}} F_\mathrm{e} - Kv\, V_\mathrm{e} \end{cases} \\ \Rightarrow K = &\begin{bmatrix} \frac{K_\mathrm{v}}{Z_\mathrm{vm}} & -K_\mathrm{v} & -\frac{K_\mathrm{v}}{Z_\mathrm{vm}} & 0 \\ \frac{K_\mathrm{v}}{Z_\mathrm{vm}} & 0 & -\frac{K_\mathrm{v}}{Z_\mathrm{vm}} & -Kv \end{bmatrix} \end{aligned} \tag{2.16}$$

There are two important differences, compared with the classic Lawrence/Salcudean 4-channel scheme: First, there are two zeros in the controller, for the use of measured position/velocity in the original scheme. In practice, small gains are used to avoid drift, which is illustrated in Figure 2.15. Second, there is an addition of an integration term for the force loop. The mass in the virtual model is effectively an integrating term in the controller. This move from P-control to PI-control of the measured forces is very interesting. Integration of force over time gives the transferred momentum or impulse at the contact point, arguably the most fundamental physical entitiy in describing motion and impact. For all physical impacts, there is a conservation of momentum. The I-control on the force can be used to emulate impulse balance, or similar momentum for master and slave. The FCS Virtual Model Control scheme is so far the only scheme in the literature that uses integrated force.

The hybrid matrix for the Virtual model control can be expressed as:

$$H = \begin{bmatrix} \frac{(Z_\mathrm{m}+K_\mathrm{v})\, Z_\mathrm{vm}}{Z_\mathrm{vm}+K_\mathrm{v}} & \frac{K_\mathrm{v}}{Z_\mathrm{vm}+K_\mathrm{v}} \\ -\frac{K_\mathrm{v}\, Z_\mathrm{m}+K_\mathrm{v}^2}{(Z_\mathrm{s}+K_\mathrm{v})\, Z_\mathrm{vm}+K_\mathrm{v}\, Z_\mathrm{s}+K_\mathrm{v}^2} & \frac{Z_\mathrm{vm}+2\, K_\mathrm{v}}{(Z_\mathrm{s}+K_\mathrm{v})\, Z_\mathrm{vm}+K_\mathrm{v}\, Z_\mathrm{s}+K_\mathrm{v}^2} \end{bmatrix} \tag{2.17}$$

Note that the velocity information from "the other side" is not used in the basic Virtual Model scheme. The consequence thereof is that velocity errors add up to low frequency position drift, and it is usually compensated by adding a small position feedback term to the velocity feedback. That can be seen as a superposition of the simple Position Error scheme on top of the model presented here, also shown with parentheses in Fig. 2.14.

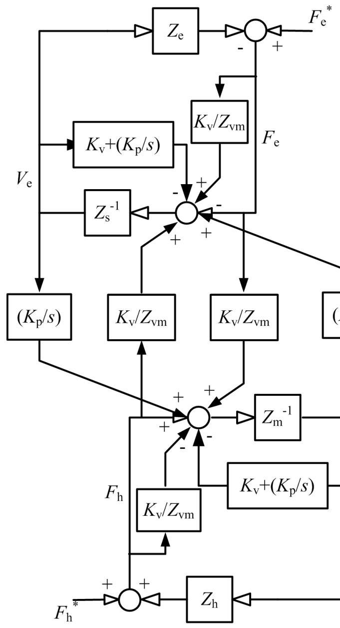

Figure 2.15: *Virtual Model Control (FCS Admittance Control), in the Lawrence/Salcudean framework. The additional position-error gains are given in parentheses (K_p/s).*

2.3.6 5-Channel Soft Slave Controller

The controllers presented above assume that both master and slave devices are rigid bodies, modelled as a single mass or a mass-damper system. However, for many applications it can be advantageous to use a soft slave device, see (Christiansson et al., 2006a). In this case, the slave device consists of two interconnected masses, see Fig. 2.16.

It is easy to extend the generalized MIMO control scheme to allow for additional measured signals. In this case we add an additional controller component for the base velocity (V_sb). The K-matrix gets one more column, with k_{15} and k_{25}:

$$\begin{aligned} F_\mathrm{mc} &= k_{11}\, F_\mathrm{h} + k_{12}\, V_\mathrm{h} + k_{13}\, F_\mathrm{e} + k_{14}\, V_\mathrm{e} + k_{15}\, V_\mathrm{sb} \\ F_\mathrm{sc} &= k_{21}\, F_\mathrm{h} + k_{22}\, V_\mathrm{h} + k_{23}\, F_\mathrm{e} + k_{24}\, V_\mathrm{e} + k_{25}\, V_\mathrm{sb} \end{aligned} \tag{2.18}$$

The generalized H-matrix becomes slightly larger due to the additional parameters (*not shown*).

Some day, it will be possible to choose the control gains using some optimization method, but for now the selection is often done by a recipe method, based on the Lawrence 4C-recipe. As a starting point for a 5C controller, a 4C-controller can be taken, where the position/velocity information sent to the master from the slave can be a combination of the tip-position and base-position. Ideally, only the tip-position should be used (k_{14}), because this is the position of the object that is encountered, and that is precisely what the operator wants to feel. However, for real implementations, there is sometimes a need to also use information from the base velocity (V_sb, and k_{15}), especially when moving in free air. This is yet another example of the trade-off between performance in free air and contact, which will be further elaborated in the subsequent Section.

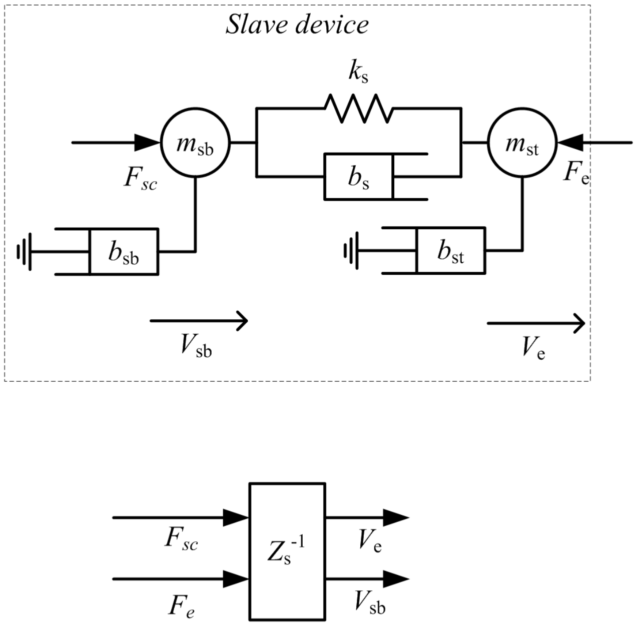

Figure 2.16: *A soft slave device: Mechanical model (top) shows the two masses, which have distinct velocities (V_{sb}, V_e). Block model (below) shows the two input forces and the two output velocities.*

2.4 Performance

How good is a teleoperator? And how can I make it better?

That is a simple but complex question. It all depends on what we want to use it for. It has often been suggested that the teleoperator should present the environment forces without distortion, so that the operator can feel exactly how the environment feels like. Using a metaphor from visual transmission, the teleoperator should be "transparent". However, there is always some influence on the percieved forces and impedances, just like a mechanical tool also influences the perception of the operator, being a mechanical filter, amplifying some frequencies and attenuating other.

Therefore the best performance criteria are defined from how well an operator can use it to perform the task it is built for, see e.g. (Yokokohji et al., 2003). It is possible to quantify the task performance of a device from human factors experiments with existing devices, but this is a slow and time-consuming procedure. Furthermore this kind of studies are only possible to do after a design is realized, so this is only useful for existing teleoperators. The use of human testing to quantify performance of force-controlled machines is the standard procedure in the domain of motion platform flight simulators (Mulder et al., 2005).

Currently, most teleoperator designers use measurable device performance measures as optimization criteria, like force bandwidth and position error, (Lazeroms et al., 1997). This section describes the most important and widely used device performance measures in the literature. All these performance measures can be computed from the linear model of the teleoperator described in Section 2.2. The performance measures are enumerated as P_1, P_2, etc. and expressed as function of the H-matrix elements. In Section 2.6 on page 42, all these performance measures are computed for a real teleoperator.

Each of these performance measures describe a certain characteristic of the device, and typically, the designer wants to optimize for many conflicting goals: light weight, stiff, fast, strong and stable. The first attempt to quantify a combination of performance criteria was done by Yokokohji and Yoshikawa (1994) and they proposed a weighted mean of the force and velocity tracking errors. However, their definition assumes that the operator and environment impedances are known.

One important open questions in teleoperation research today is: Which information is most important for each specific task? Or, more technically, how shall the "integrated performance function" combine the various device performance measures to accurately quantify the usefulness of a teleoperator for a certain task?

Modern control science is focussed on optimization. It is generally assumed that the "integrated performance function" is known, and then any of a variety of methods can be used (H_∞, LQG, LPV, etc.). There are papers showing that these methods can synthesize stable controllers for teleoperators (Lazeroms, 1999). The problem is that so far no one has been able to synthesize a controller that achieves as good a trade-off between performance and stability as a hand tuned controller. This is in spite of the fact that humans are very poor in general at finding optima for multidimensional functions, here represented by the numerous controller gains in a typical controller architecture.

One essential step to finding a good integrated performance function is to understand both the human control engineer, and how he/she tunes the gains, as well as the perceptual and sensoric capabilities of the human operator. A short passage below introduces the human performance demands and the psychophysics of haptics teleoperation.

A prerequisite for performance is stability. In the subsequent Section 2.5 some popular stability criteria based on the linear model are presented.

2.4.1 Device Performance Measures

The Connected Teleoperator System (CTS) is a kind of bi-directional transmission line of information between the operator and the environment. The quality of a teleoperator depends on how information is communicated, i.e. how forces and velocities, and the related impedances, are transferred. The various device performance measures presented here all describe different aspects of the quality of the teleoperator.

Some important device characteristics cannot be described by a linear model, most notably saturations, e.g. maximum actuation force. These aspects have to be considered separately, and that is outside the scope of this text.

The most common performance measures (bandwidths, transparency, maximum stiffness etc.) are all functions of the linear model of the system. The rest of this section describes the most important device performance measures, expressed as functions of the linear model, the H-matrix.

Tracking Errors

The most straightforward way of assessing the quality is to compare the movements and forces of the master and the slave. The velocity and force tracking errors were also the first measures used to quantify teleoperator performance (Pawluk and Ellis, 1991), (Yokokohji and Yoshikawa, 1994).

The tracking errors must be computed for both directions, both from master-to-slave and from slave-to-master, because these can be quite different. Velocity tracking is calculated when the other device moves in free air ($F_\mathrm{e} = 0$ for master-to-slave tracking and $F_\mathrm{h} = 0$ for slave-to-master tracking). Force tracking is calculated when the other device is in contact with a hard object ($V_\mathrm{e} = 0$ for master-to-slave tracking and $V_\mathrm{h} = 0$ for slave-to-master tracking). Both values are taken relative to the nominal velocity or force.

The use of the maximum error (ΔV) over the all frequencies (ω) of the task was introduced by Pawluk (Pawluk and Ellis, 1991). However, by focussing on the gain of the frequency function, the important effects of phase lag is left unquantified using this performance measure. The choice to use the maximal value over the frequency range is quite arbitrary, and represents an ∞-norm of the error. Other alternatives could be average error (1-norm) or "error energy" (2-norm).

First we look at the velocity tracking, from master-to-slave and then from slave-to-master (matrix $G = H^{-1}$):

$$\begin{aligned} P_1 &= \max \left|\Delta V_\mathrm{rel}(s)\right|_{F_\mathrm{e}=0} = \max \left|\frac{V_\mathrm{h} - V_\mathrm{e}}{V_\mathrm{h}}\right|_{F_\mathrm{e}=0} = \max_\omega \left|1 - h_{21}(j\,\omega)\right| \\ P_2 &= \max \left|\Delta V_\mathrm{rel}(s)\right|_{F_\mathrm{h}=0} = \max \left|\frac{V_\mathrm{e} - V_\mathrm{h}}{V_\mathrm{e}}\right|_{F_\mathrm{h}=0} = \max_\omega \left|1 + g_{12}(j\,\omega)\right| \\ &\text{where } g_{12} = -\frac{h_{12}}{h_{11}\,h_{22} - h_{21}\,h_{12}} \end{aligned} \tag{2.19}$$

These velocity tracking formulae can also be used to calculate position tracking (or *drift* as it was called by Arcara et al. (Arcara and Melchiorri, 2002)) - with an integration ($1/s$) added to the basic formulae.

Likewise, for the force tracking error from slave-to-master and master-to-slave:

$$
\begin{aligned}
P_3 &= \max |\Delta F_{\text{rel}}(s)|_{V_{\text{h}}=0} = \max \left| \frac{F_{\text{h}} - F_{\text{e}}}{F_{\text{e}}} \right|_{V_{\text{h}}=0} = \max_{\omega} |h_{12}(j\,\omega) - 1| \\
P_4 &= \max |\Delta F_{\text{rel}}(s)|_{V_{\text{e}}=0} = \max \left| \frac{F_{\text{h}} - F_{\text{e}}}{F_{\text{h}}} \right|_{V_{\text{e}}=0} = \max_{\omega} |1 - g_{21}(j\,\omega)| \\
&\text{where } g_{21} = -\frac{h_{21}}{h_{11}\,h_{22} - h_{21}\,h_{12}}
\end{aligned}
\tag{2.20}
$$

Bandwidths

Bandwidth is related to the information transfer between the operator and the remote environment. The requirements for information transfer from master to slave differ considerably from the requirements from slave to master (Lawrence, 1993), (Kato and Hirose, 2000). The human operator gives force and movement commands with relatively low frequency content, on the order of 0-10 Hz, whereas the contact information at the slave side often contains frequencies up to 1000 Hz in stiff environments.

It is usually stated that the bandwidth should be as high as possible, and often a lower bound is given (Burdea, 1996). Less often it is stated which bandwidth is meant (Fischer et al., 1990). Each of the four transfer functions $h_{ij}(s)$ between forces and velocities has its own bandwidth. This corresponds to velocity bandwidths from master to slave ($\omega_{\text{v,ms}}$), slave to master ($\omega_{\text{v,sm}}$), and force bandwidths from master to slave ($\omega_{\text{F,ms}}$) and slave to master ($\omega_{\text{F,sm}}$). These four performance measures are here denoted P_5-P_8.

The velocity bandwidth is closely related to the tracking error, so it is calculated from a similar transfer function. The bandwidth is defined as the frequency where the signal drops to 3 dB ($\frac{1}{\sqrt{2}}$) below the low frequency gain, and can be calculated by solving an equation like (2.21). The velocity bandwidth from master to slave (P_5=$\omega_{\text{v,ms}}$) is the solution to:

$$
|1 - h_{21}(j\omega_{\text{v,ms}})| = \frac{1}{\sqrt{2}} |1 - h_{21}(0)| \tag{2.21}
$$

The velocity bandwidth from slave to master (P_6= $\omega_{\text{v,sm}}$) is the solution to:

$$
\begin{aligned}
&|1 + g_{12}(j\omega_{\text{v,sm}})| = \frac{1}{\sqrt{2}} |1 + g_{12}(0)| \\
&\text{where } g_{12} = -\frac{h_{12}}{h_{11}\,h_{22} - h_{21}\,h_{12}}
\end{aligned}
\tag{2.22}
$$

The force bandwidth from slave to master (P_7= $\omega_{\text{F,sm}}$) is similarly connected to the force tracking error, and it is calculated in the same way, as the solution to (2.23).

$$
|h_{12}(j\omega_{\text{F,sm}}) - 1| = \frac{1}{\sqrt{2}} |h_{12}(0) - 1| \tag{2.23}
$$

The force bandwidth from master to slave (P_8= $\omega_{\text{F,ms}}$) is similarly computed:

$$
\begin{aligned}
&|1 - g_{21}(j\omega_{\text{F,sm}})| = \frac{1}{\sqrt{2}} |1 - g_{21}(0)| \\
&\text{where } g_{21} = -\frac{h_{21}}{h_{11}\,h_{22} - h_{21}\,h_{12}}
\end{aligned}
\tag{2.24}
$$

Just as for the tracking error, the bandwidth performance measure has no information about delays or phase lag, which is a reason for caution. Two systems with the same bandwidth and different phase lag can behave quite differently!

Scaling Product

Scaling defines how forces and velocities are magnified between the master and the slave. The force scaling and the velocity scaling are easily calculated from the H-matrix (2.7), and their product is called the *scaling product*. As Lawrence (Lawrence, 1993) points out, the scaling product is often assumed to be identity - also for micromanipulation. However, by choosing a scaling product of less than unity, the remote environment is less accurately represented while stability can be improved thanks to artificial energy loss (Lazeroms et al., 1997), (Kazi, 2001), (Kumar et al., 2000). Therefore, the product of the scaling factors can be seen as a performance measure, with a nominal value of one.

The scaling product is a product of frequency functions, so it also depends on the frequency. Here we choose the low-frequency limit value, representing the steady-state scale:

$$P_9 = \text{scalingproduct} = \lim_{s \to 0} |\, h_{12}(s)\, h_{21}(s)\,| \tag{2.25}$$

Transmitted Impedance

The operator will never feel exacly the same impedance at the master device as the real environment. The teleoperator always influences the impedance to a certain extent. Using the H-matrix model, the transmitted impedance of the environment through the teleoperator to the operator ($Z_{\text{to}}(s)$) can be computed (when exogeneous environment force $F_{\text{e}^\star}$ is zero):

$$Z_{\text{to}} = \left.\frac{F_{\text{h}}}{V_{\text{h}}}\right|_{F_{\text{e}^\star}=0} = \frac{h_{11} \,+\, (h_{11}\, h_{22} \,-\, h_{12}\, h_{21})\; Z_{\text{e}}}{1 \,+\, h_{22}\, Z_{\text{e}}} \tag{2.26}$$

This expression is very important, and is the key to all performance measures that quantify how the environment impedance is distorted in the transmission to the operator. The impedance felt at the master side is a function of the teleoperation device parameters (h_{ij}) and the environment impedance (Z_{e}). Remember that the H-matrix components h_{ij} depend both on the device hardware and the controller gains chosen.

In free air, the environment impedance $Z_{\text{e}}(s)$ is zero, so the expression simplifies to (note that $Z_{\text{to,free}}$ and h_{11} are transfer functions). This is the impedance present at the master device when the slave device moves in free air.

$$Z_{\text{to,free}} = h_{11} \tag{2.27}$$

The *Free air inertia* and *Free air damping* are sometimes used as performance measures (Chang et al., 1999; Arcara and Melchiorri, 2002). These performance measures can be seen as a the parameters of a mass-damper approximation of the free-air impedance at the master device ($Z_{\text{to,free}}$=h_{11}), see (2.28). These measures represent the minimum gain impedance of the teleoperator.

The free air inertia ($\hat{m}_{\text{free}}$=P_{10}) and free air damping ($\hat{b}_{\text{free}}$ = P_{11}) essentially define how "light" the teleoperator moves in free air, and it is often claimed that these should be as low as possible (Hannaford, 1989b; Yokokohji and Yoshikawa, 1994). Usually, the free air stiffness ($\hat{k}_{\text{free}}$ = P_{12}) is very low or zero (unless a workspace-centering-spring has been implemented, like in some joysticks). The approximation can be written as:

$$\begin{aligned} & Z_{\text{to,free}}(s) \approx \hat{m}_{\text{free}}\, s + \hat{b}_{\text{free}} + \hat{k}_{\text{free}}/s \\ & \Rightarrow \begin{cases} P_{10} = \hat{m}_{\text{free}} \\ P_{11} = \hat{b}_{\text{free}} \\ P_{12} = \hat{k}_{\text{free}} \end{cases} \end{aligned} \tag{2.28}$$

The same type of approximation can be done for the highest possible impedance transmitted to the operator: when the slave is in contact with a very stiff environment. Let the environment impedance Z_{e} go to infinity at all frequencies and equation (2.26) simplifies to:

$$Z_{\text{to,stiff}} = \frac{h_{11}\, h_{22} \;-\; h_{12}\, h_{21}}{h_{22}} \tag{2.29}$$

$$\begin{aligned} &Z_{\text{to,stiff}}(s) \approx \hat{m}_{\text{stiff}}\, s + \hat{b}_{\text{stiff}} + \hat{k}_{\text{stiff}}/s \\ &\Rightarrow \begin{cases} P_{13} = \hat{m}_{\text{stiff}} \\ P_{14} = \hat{b}_{\text{stiff}} \\ P_{15} = \hat{k}_{\text{stiff}} \end{cases} \end{aligned} \tag{2.30}$$

The most popular of these performance measures is the *stiff contact stiffness* ($\hat{k}_{\text{stiff}}$=P_{15}), which quantifies the maximum stiffness that the master device can present. The fitting of the three-term model should be done over a frequency range relevant to the application in question. For most tasks a range of 0.1-10 Hz can be chosen.

Another important aspect of the transmitted impedance of a teleoperator is the impedance transmitted to the environment. This impedance (Z_{te}) was introduced by Hashtrudi-Zaad and Salcudean and is unfortunately often ignored (Hashtrudi-Zaad and Salcudean, 2002). Z_{te} represents the impedance of the tip of the slave device, which to some extent depends on the impedance of the human operator that holds on to the master. It is possible to express the different aspects of this impedance analog to how the master impedance was expressed above (when exogeneous human force $F_{\text{h}^\star}$ is zero):

$$Z_{\text{te}} = \left.\frac{F_{\text{e}}}{-V_{\text{e}}}\right|_{F_{\text{h}^\star}=0} = \frac{h_{11} \;+\; Z_{\text{h}}}{(h_{11}\, h_{22} \;-\; h_{12}\, h_{21}) \;+\; h_{22}\, Z_{\text{h}}} \tag{2.31}$$

The transmitted slave impedance (Z_{te}) quantifies how stiff/heavy the slave device is at the tip, which is crucial when studying contact dynamics in contact with the environment. In case both the environment and the transmitted slave device impedance are stiff, the interaction time scale is very short and there is a large risk for contact instability.

Dynamic range

The dynamic range of a teleoperation system quantifies the range of impedances that the master can present to the operator, for all different environments (Colgate and Brown, 1994). This is sometimes called the *Z-width*. The impedance at the master side is calculated for the two situations of the slave moving in free air ($Z_{\text{to,free}}$) and in hard contact with a stiff wall ($Z_{\text{to,stiff}}$), like in (2.26). The integrated difference between the absolute values of the two impedances is the *Z-width* of the teleoperator:

$$P_{16} = Z_{\text{width}} = \frac{1}{\omega_1 - \omega_0} \int_{\omega_0}^{\omega_1} ||\log Z_{\text{to,stiff}}(j\,\omega)| - |\log Z_{\text{to,free}}(j\,\omega)||d\omega \tag{2.32}$$

In Fig. 2.17 the Z-width is plotted for a simplified mass-spring-damper model. To calculate the "area", the relevant frequency range for the task must be chosen, and here the choice is: $\omega \in [1\,100]$ rad/s. These frequencies cover the frequencies where the bilateral position/force communication is the most important for the teleoperated tasks.

For a small Z-width, it is difficult to distinguish between different environments, because all environments are presented to the operator with very similar impedances. The larger the Z-width, the richer the information presented to the operator can be. The Z-width can be increased in many ways, e.g. by increasing the teleoperator stiff contact stiffness ($\hat{k}_{\text{stiff}}$) or by reducing the free air damping ($\hat{b}_{\text{free}}$), see Fig. 2.18.

Transparency

Another popular performance measure is the *Transparency Error*, introduced by Lawrence (Lawrence, 1993). It is a quantification of the transmission distortion, and is often assumed that the transparency error should be

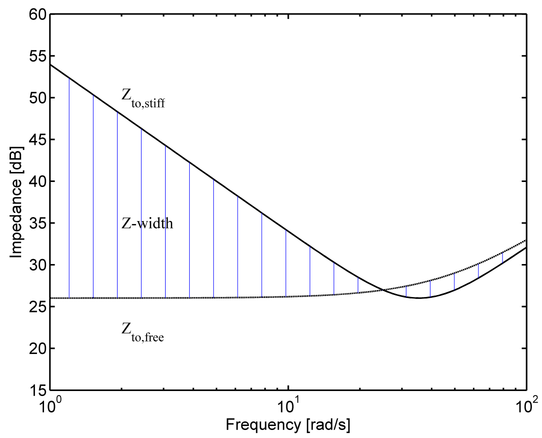

Figure 2.17: *The Z-width is a measure of the area between the free air impedance ($Z_{\mathrm{to,free}}$) and stiff contact impedance ($Z_{\mathrm{to,stiff}}$) that a teleoperator can present at the master side. Note that the curves may cross around the eigenfrequency for this model.*

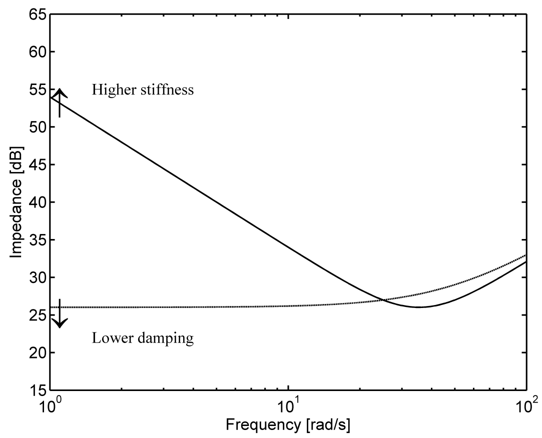

Figure 2.18: *The Z-width (the area between the curves) is improved by increasing the teleoperator stiff contact stiffness ($\hat{k}_{\mathrm{stiff}}$) or by reducing the teleoperator free air damping ($\hat{b}_{\mathrm{free}}$)*

as small as possible. For any given environment impedance (Z_{e}) it is possible to calculate how it is presented at the master side (Z_{to}), see (2.26). The transparency error is a measure of how much these two impedances differ, in gain and in phase. In the original paper, Lawrence compared with only one environment impedance, which was an important limitation. Here the transparency error is quantified by comparing the transmitted impedance with the real impedance for a set of typical environments ($Z_{\mathrm{e,k}}$) (Pintelon and Schoukens, 2001):

$$P_{17} = T_{\mathrm{error}} = \frac{1}{n} \sum_{Z_{\mathrm{e,k}}}^{n} \frac{1}{\omega_1 - \omega_0} \int_{\omega_0}^{\omega_1} || \log(Z_{\mathrm{e,k}}(j\,\omega))| - |\log(Z_{\mathrm{to,k}}(j\,\omega)|| \, d\omega \tag{2.33}$$

The transparency is generally improved (transparency error is reduced) with increased teleoperator stiffness and reduced damping, because a larger range of impedances can then be presented to the operator.

All these seventeen performance measures describe some aspect of the characteristics of a teleoperator. However, they are arguably not all independent. An important item for future research is to understand

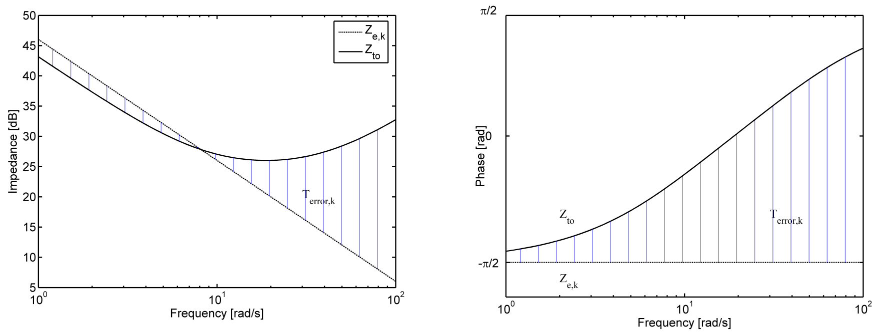

Figure 2.19: *The* Transparency error *(T_{error}) is the area between one environment impedance (Z_{e}) and the transmitted impedance (Z_{to}). The error is calculated both in the gain and in the phase, for a set of environment impedances ($Z_{\mathrm{e,k}}$).*

which of these performance measures are the most important ones. Probably a handful can be found to be independent, in the sense that they describe unique features of teleoperators, that can vary independently from each others. This set of core performance measures will be the basis for device design and controller optimization.

2.4.2 Human Performance

The most important aspect of how good or bad a teleoperator really is, is whether or not the operator can do something useful with it. Therefore, both the device characteristics (as described above) and the human perception and motoric capabilities are relevant.

There is a tremendous literature describing the human perception and the human neuromuscular system for direct manipulation of objects. However, regarding virtual and teleoperated tasks, much less research has been done, and there are still many open questions. It is largely unknown how a the properties of a mechanical filter (a mechanical tool or a teleoperator) influences the human perception and task performance. It is often claimed that e.g. higher teleoperator stiffness is better, but very few quantitative studies have been performed.

One interesting study on haptic interaction with virtual objects was performed by O'Malley and Goldfarb (O'Malley and Goldfarb, 2004). They reduced the performance (device stiffness, maximum force) of a haptic master device and measured the influence on human task performance. They found that human subjects could perform some tasks very well also with "low" device performance, to a certain level. At the Delft Haptics Laboratory we performed an extension to their study with a teleoperated grasp task, where we found similar results (Christiansson et al., 2006b).

However, there is still much research needed to quantify how human task performance depends on device performance in teleoperation.

2.5 Stability

Stability is necessary for useful and safe operation of teleoperation. Typical underlying reasons for instability in teleoperation systems are communication time delay, sampling time delay, and too high control gains in some part of the system. The most straightforward way to guarantee stability is to dissipate the energy in the system using physical dampers and to reduce the feedback gains, which of course lead to lower performance, as quantified in the criteria presented in Section 2.4. For teleoperation design, the crux is to ensure enough stability robustness against realistic disturbances, with as low reduction of performance as possible.

This section describes how to analyze stability, based on the linear teleoperator model presented in Section 2.2. For reference, the illustration in Fig. 2.8 on page 20 is repeated in Fig. 2.20. The stability analysis methods used in this presentation are based on classic control theory, and can essentially only tell whether or not a system is stable. There are also modern tools, like μ-analysis, that also quantify the stability robustness against structured uncertainties.

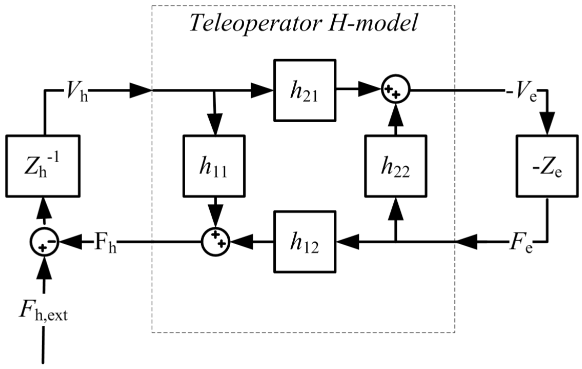

Figure 2.20: *The complete teleoperation model with the operator (Z_h), the teleoperator (h_{ij}), and the environment (Z_e). Note the closed loops through the operator and the environment.*

To analyse the stability of teleoperation systems, a definition of stability is needed, and many have been proposed. One concept of stability is *bounded input-bounded output (BIBO) stability*. A system is said to have BIBO stability if every bounded input results in bounded outputs regardless of what goes on inside the system (Franklin et al., 1994). In general, if a linear time invariant continuous-time system has any pole on the imaginary axis or in the right half-plane (RHP), the system will not be BIBO-stable. Conversely, if every pole is in the left half-plane (LHP), then the system will be BIBO-stable. Another concept of stability, from Lyapunov, is that the output and all the internal variables never become unbounded and go to zero as time goes to infinity for sufficiently small initial conditions. This will happen if all the poles of the system are strictly in the LHP. This is called *asymptotic internal stability*. The stability concept which will be adhered to in this paper is from (Skogestad and Postlethwaite, 1996), saying:

Definition 2.1 *A system is (internally) stable if none of its components contain hidden unstable modes and the injection of bounded external signals at any place in the system result in bounded output signals measured anywhere in the system.*

It should be noted that for linear systems the difference between the stability concepts has no practical importance. For more information on the stability and the feedback control of dynamic systems see e.g. (Franklin et al., 1994) and (Skogestad and Postlethwaite, 1996).

The block diagram of the connected teleoperation system presented in Fig. 2.20 shows that the feedback loops of the system include both the environment and the human operator. The stability of the whole system does therefore depend on both the teleoperator, and the impedances of the human operator (Z_h) and the environment (Z_e). However, often the numerical values of these impedances are not known.

A first set of stability measures (Section 2.5.1) can be used when the impedances Z_h and Z_e are known. A second set of stability measures (Section 2.5.2) can be used when the impedances Z_h and Z_e are not known exactly, but it is known that they fulfil some requirement, e.g. passivity. The second set is a stricter requirement for the teleoperator, because it guarantees that the teleoperator is stable in contact with a larger range of impedances.

2.5.1 Stability Analysis with Known Operator and Environment

In this section the stability of the connected teleoperation system will be analysed assuming the operator and environment impedances (Z_{h} and Z_{e}) are known. First, we note that the teleoperation system is represented as a negative feedback system. The block diagram of the hybrid matrix model, shown in Fig. 2.20, is used to calculate the open- and closed loop transfer functions. The interconnected systems matrix can be computed using a linear fractional transformation. Following Hannaford (Hannaford, 1989b) the loop is opened at the V_{h}-signal and the corresponding open loop tranfer function $L(s)$ is computed.

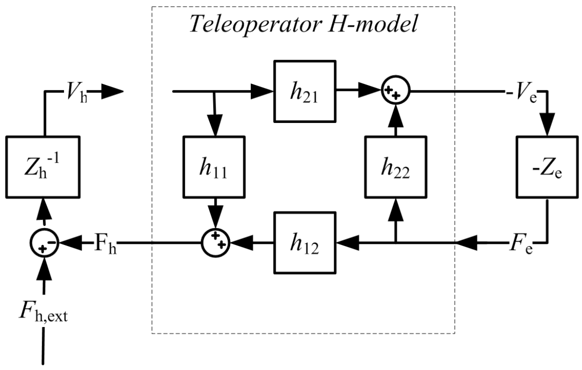

Figure 2.21: *Open loop model for the Connected Teleoperator System, open at the V_{h} signal. The open loop model is here called $L(s)$*

$$L(s) = \frac{(h_{11}h_{22} - h_{12}h_{21})\, Z_{\mathrm{e}} + h_{11}}{(h_{22}Z_{\mathrm{e}} + 1)\, Z_{\mathrm{h}}} \tag{2.34}$$

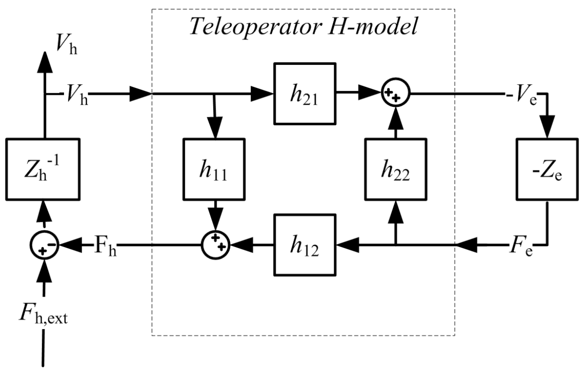

Figure 2.22: *Closed loop model for the Connected Teleoperator System, here seen from $F_{\mathrm{h,ext}}$ to the V_{h} signal.*

The closed loop function can be calculated, as e.g. the transfer function from exogeneous force ($F_{\mathrm{h,ext}}$) to hand velocity[2] (V_{h}), see Fig.2.22. The denominator of this closed-loop transfer function is used in the subsequent stability formulae.

[2]Another choice of input/output signals would give the another numerator, but the same denominator of the closed-loop function, which defines the stability properties.

$$\frac{V_{\mathrm{h}}}{F_{\mathrm{h,ext}}} = \frac{L(s)}{L(s)-1} = \frac{h_{22}Z_{\mathrm{e}}+1}{\left(h_{22}Z_{\mathrm{e}}+1\right)Z_{\mathrm{h}} + \left(h_{11}h_{22}-h_{12}h_{21}\right)Z_{\mathrm{e}} + h_{11}} \tag{2.35}$$

Root Locus

The root-locus method shows how changes in the system's feedback characteristics and other parameters influence the closed loop pole locations. Using this technique the locus of the closed loop pole locations in the s-plane is plotted as one design parameter varies. This graph is called a "root locus", see the example in Fig. 2.23.

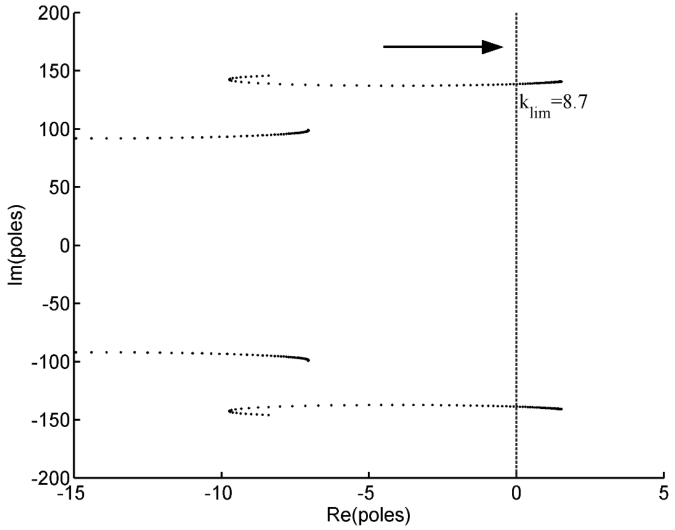

Figure 2.23: *Example of a root-locus plot for a soft-slave teleoperator with increasing slave stiffness k_{s}. Above a certain stiffness value, (k_{s}=8.7 N/mm), two poles move into the right half plane, and the system is unstable. Adapted from (Christiansson and v. d. Helm, 2007).*

The denominator of the closed loop function derived in (2.35) above is used to generate the root locus of a teleoperation system, for various design parameters, both controller gains and mechanical component parameters. If one or more of the poles move into the right half plane, the system becomes unstable. For details about the method see e.g. (Franklin et al., 1994). Root locus techniques are used by e.g. (Daniel and McAree, 1998) and (Love and Book, 2004).

The advantages of the root locus method are:

- Information about pole locations and hence about the system's behaviour[3] is directly available.
- The stability conditions are not conservative.

Disadvantages are:

- Stability conditions can only be given as a function of one variable at a time.

Nyquist Stability

The Nyquist stability concept uses the open loop representation from Figure 2.21. The open loop transfer function is plotted as a polar function of frequency. The Nyquist stability criterion is given as follows (Skogestad and Postlethwaite, 1996):

[3]Note: the behaviour is only well-defined when the system is stable, so this is only true for the part of the root-locus lying in the left half plane.

Definition 2.2 *Let P_{ol} denote the number of open-loop unstable poles in $L(s)$. The closed-loop system with loop transfer function $L(s)$ and negative feedback is stable if and only if the Nyquist plot of* $\det(1 + L(s))$

1. *makes P_{ol} anti-clockwise encirclements of the point -1 and*
2. *does not pass through the point -1.*

The Nyquist plot is usually used for two purposes; to determine if the system is stable or not and if it is stable, to quantify the stability margins.

For teleoperation systems, only the stable-or-not question can be answered with the Nyquiest method, but the stability margins can not be computed this way. The teleoperation system open loop function $L(s)$ as expressed in (2.34) is not of the form GK with G the system and K the controller, so gain and phase margins have only a limited value. In particular, the gain and phase margins will have different values depending on where the loop is opened. This is a drawback of this classical method, and can only be addressed by using modern tools like μ-analysis (Skogestad and Postlethwaite, 1996).

If one bears this in mind, the Nyquist stability can still be useful for stability analysis of teleoperation systems, see e.g. (Lawrence, 1993), (Zhu and Salcudean, 1995), (Fite et al., 2001), (Tafazoli et al., 2002) and (Fite et al., 2004).

The advantage of the Nyquist diagram is:

- The stability conditions are not conservative.

Disadvantages are:

- Phase and gain margins have only a limited value.

2.5.2 Stability Analysis with Unknown Operator and Environment

If the operator and environment impedances Z_h and Z_e are unknown, there are still a few useful methods available. With the restriction that both Z_h and Z_e are passive (see Section 2.5.2) the stability of the teleoperator system can be analysed. The operator and the environment can not in practive assume any passive impedance, so these stability conditions are more conservative than when the impedances are known.

Absolute Stability

Absolute or unconditional stability means that the system is stable for all possible passive (see Section 2.5.2) operators and environments. The necessary and sufficient conditions for absolute stability can be expressed in terms of the H-elements and the real part thereof (r_{11}=real(h_{11})) (Haykin, 1970). These conditions constitute *Llewellyn's criterion for absolute stability*:

1. $h_{11}(s)$ and $h_{22}(s)$ have no poles in the right half plane
2. Any poles of $h_{11}(s)$ and $h_{22}(s)$ on the imaginary axis are single with real and positive residues
3. For all real values of ω

$$\begin{array}{l} r_{11}(j\,\omega) \;\; \geq \;\; 0 \\ r_{22}(j\,\omega) \;\; \geq \;\; 0 \\ 2r_{11}r_{22} - r_{12}r_{21} - |h_{12}h_{21}| \geq 0 \end{array} \tag{2.36}$$

If any of the conditions is not satisfied, the network is potentially unstable, i.e. there exist some combinations of operator and environment for which the system is unstable.

The last of conditions 3 can also be rewritten (Hashtrudi-Zaad and Salcudean, 2001) as:

$$\eta = -\cos(\angle(h_{12}h_{21})) + 2\frac{r_{11}r_{22}}{|h_{12}h_{21}|} \geq 1 \qquad \forall\omega \tag{2.37}$$

The parameter η is called the *network stability parameter*. The system is stable for $\eta \geq 1$. It is interesting to notice that with a perfectly transparent teleoperator, with identical forces and velocities at master and slave side, $\eta = 1$. This means that *the perfect transparent teleoperator is marginally stable*. This is another illustration of the classic trade-off between stability and performance.

Absolute stability is used by e.g. (Hashtrudi-Zaad and Salcudean, 2001), (Adams and Hannaford, 2002) and (c. Cho and Park, 2004).

The advantage of using absolute stability is:

- Models of the human operator and environment are not needed.

Disadvantages are:

- The stability conditions can be conservative.
- The network stability parameter η is the only quantitative measure available.

Passivity

Passivity is a very powerful concept, and is increasingly used in control of teleoperation systems (Hannaford et al., 2002),citepRYU2004. The idea behind passivity can be loosely expressed that if each component loses energy over time, the components together will also lose energy, and therefore be stable. For theoretical background, please refer to (der Schaft, 2000).

The necessary and sufficient conditions for passivity of the teleoperator in terms of the hybrid matrix elements h_{ij} are the *Raisbeck's passivity criterion* (Haykin, 1970) (r_{11} =real(h_{11}), I_{11} =im(h_{11}),):

1. No h_{ij} has poles in the right half plane
2. Any poles of the h_{ij}-elements $h_{11}, h_{12}, h_{21}, h_{22}$ on the imaginary axis are single. The residues $d_{11}, d_{12}, d_{21}, d_{22}$ of h_{ij}(s) at these poles satisfy the following conditions:

$$\begin{aligned} d_{11} &\geq 0 \\ d_{22} &\geq 0 \\ d_{11}d_{22} - d_{12}d_{21} &\geq 0 \quad \text{with } d_{21} = \bar{d_{12}} \end{aligned}$$

3. The real (r_{11} etc.) and imaginary parts (I_{11}) of the h_{ij}-elements satisfy the following conditions for all ω:

$$\begin{aligned} &r_{11} \geq 0 \\ &r_{22} \geq 0 \\ &4r_{11}r_{22} - (r_{12} + r_{21})^2 - (I_{12} - I_{21})^2 \geq 0 \end{aligned} \tag{2.38}$$

Passivity can also be expressed using scattering theory. The hybrid matrix model is transformed into the scattering domain, and expressed using the matrix function S (Haykin, 1970), sometimes called the "scattering operator":

$$F(s) - V(s) = S(s)(F(s) + V(s)) \tag{2.39}$$

with $F(s)$ and $V(s)$ being the Laplace transform of the time domain signals. In terms of the H-matrix, the scattering matrix can be written as (Anderson and Spong, 1989):

$$S(s) = \begin{bmatrix} 1 & 0 \\ 0 & -1 \end{bmatrix} (H(s) - I)(H(s) + I)^{-1} \tag{2.40}$$

The advantage of the scattering formulation of the model is that energy flow is easily expressed. The passivity criterion changes to:

Definition 2.3 *The system is passive if and only if:* $||S(j\,\omega)|| \leq 1 \quad \forall \omega$

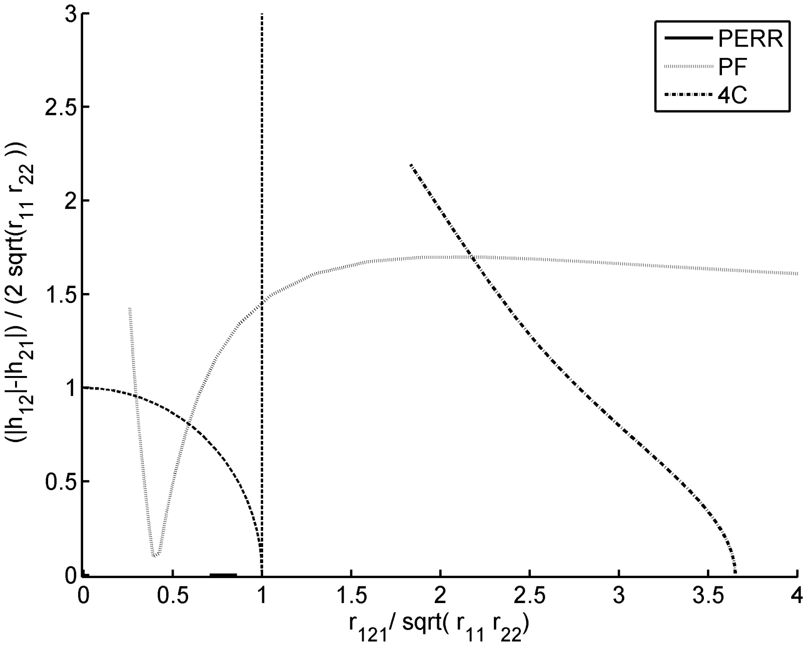

Figure 2.24: *Stability-activity diagram for three controllers implemented in the same teleoperator. The PERR curve is small, close to the x-axis, completely inside the "Passive" region. The PF curve is partly and the 4C is completely in the "potentially unstable" region.*

This is a mathematically very convenient criterion, and is increasingly popular. The "wave variable notation" is related to the scattering transformation and this may explain why there is an increased interest in "wave variable" control (Niemeyer and Slotine, 2004).

Passivity is slightly more conservative than absolute stability, and the perfectly transparerent teleoperator lies on the overlapping part. The relationship between these criteria will be further illustrated in Section 2.5.3 below. Passivity is used by e.g. (Anderson and Spong, 1989), (Lawrence, 1993), (Yokokohji and Yoshikawa, 1994), (Colgate et al., 1995), (Colgate and Schenkel, 1996), (Ryu et al., 2004) and (Diolaiti et al., 2005).

The advantages of using passivity are:

- Models of the human operator and environment are not needed.
- The criterion is also applicable to nonlinear systems.
- The scattering form of the model leads to a very elegant characterisation

Disadvantages are:

- The stability conditions are conservative. Even more than the absolute stability criterion in Section 2.5.2.

2.5.3 The Stability-Activity Diagram

The criteria for absolute stability and passivity can be illustrated in a graphical form called the "Stability-Activity Diagram"(Haykin, 1970), shown in Fig. 2.24. A comparison of the absolute stability conditions (2.36) with the passivity conditions (2.38) indicates that the essential difference lies in the last of conditions 3. For absolute stability this condition can be rewritten as:

$$\frac{r_{121}}{\sqrt{r_{11}r_{22}}} \leq 1 \tag{2.41}$$

where r_{121} is the real part of $\sqrt{h_{12}h_{21}}$ and r_{ij}(s) are the real parts of the corresponding h_{ij}(s). For passivity the last condition can be manipulated in the form:

$$\frac{r_{121}^2}{r_{11}r_{22}} + \frac{(|h_{12}| - |h_{21}|)^2}{4r_{11}r_{22}} \leq 1 \tag{2.42}$$

In the *stability-activity diagram* of Fig. 2.24 the conditions are represented by plotting $||h_{12}|-|h_{21}||/2\sqrt{r_{11}r_{22}}$ against $r_{121}/\sqrt{r_{11}r_{22}}$.

Each teleoperator H-matrix is a function of $s = j\,\omega$, which means that for each value of ω, a point will be drawn in the diagram. By letting ω go from 0 to ∞, a parametric curve will be plotted. If the curve is completely inside the "Passive" region, the teleoperator is passive at all frequencies. Equivalently, the curve must be completely inside the "Absolutely Stable" region to be absolutely stable. If any part of the curve lies to the right of the vertical dashed line in the diagram, it means that the teleoperator is "Potentially Unstable". That means that there exists some combination of environment and operator impedance that renders the teleoperator unstable.

In Fig. 2.24 the hybrid matrices from three teleoperator implementations are compared. In the same teleoperator hardware, three controllers were implemented, (from the case study in Section 2.6) and for each, the corresponding activity-curve is plotted. We can see that the PERR controller is completely within the passive region, difficult to see, close to (actually on) the y-axis. The PF controller curve starts in the absolutely passive region, but moves out at higher frequencies. The 4C controller is in the potentially unstable region at all frequencies.

2.6 A Case Study

This section describes a numerical case study, to illustrate the different controllers presented above in Section 2.3. For each of the controllers, the numerical values of the performance measures introduced in Section 2.4 are computed. The controllers are implemented on the teleoperator *Hugin*, see Fig. 2.25, developed at the Delft Haptics Laboratory (Fritz et al., 2004; Christiansson, 2004; Christiansson et al., 2006b). It is a one-degree-of-freedom teleoperator with a slave device with adjustable stiffness and damping, explined below in Section 2.6.1. For most of the cases presented here, the slave stiffness will be set to the maximum value of 200 N/mm, and for one case (5C-control) the slave stiffness is set to 1.2 N/mm.

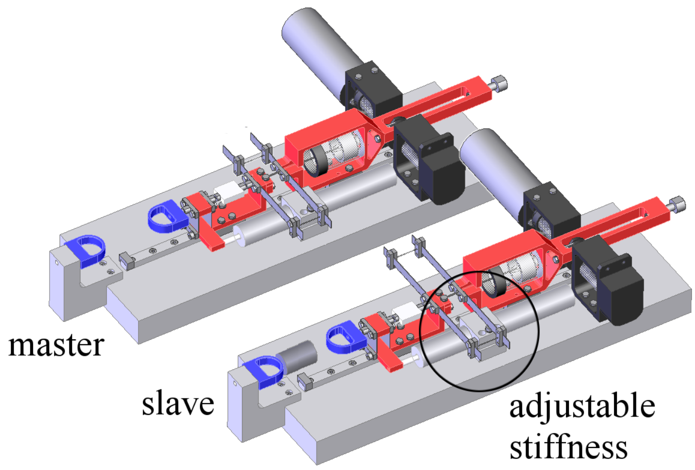

Figure 2.25: *The haptic teleoperator Hugin used in the numerical examples. The slave device has adjustable intrinsic stiffness (k_s) and damping (b_s).*

For each of the controllers, the H-matrix model is calculated. Using this model, performance and stability measures can be calculated. The control gains are optimized using hand-tuning to get a reasonable balance of stability and performance.

2.6.1 Mechanical Model

The mechanical models are the ones introduced in Section 2.2. The master is a simple mass-damper models as shown in Fig. 2.26. The adjustable compliance of the slave device is set to “stiff” for three of the controllers, so a mass-damper model is appropriate. For one controller, the slave device is in “soft” mode, which is best modelled with the soft slave mechanical model. Both models are shown in Fig.2.27.

The numerical values are presented in Table 2.1. The real parameters were identified using a time-domain parametric identification technique, explained in detail in (Christiansson, 2004). The mass and stiffness parameters have low variation between calibrations, whereas the damping varies quite a lot depending on the pre-tension in the cable that transforms the rotary motor action into linear motion which gives a pre-load to a linear guide. The dampings given here are typical values.

2.6.2 Position Error Controller

The true classic of all teleoperation controllers is the position-error controller, and it is the simplest one. The position error controller is hand tuned to K_p= 10.000 N/m and no controlled damping.

The H-matrix expression was derived in (2.11), and can be computed with the numerical values of the components:

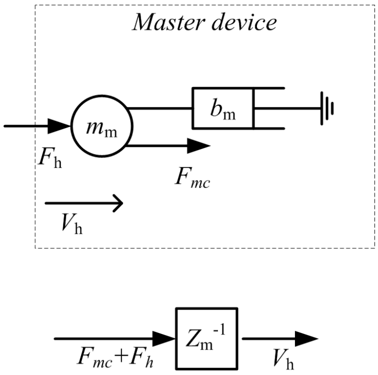

Figure 2.26: *Mechanical model for the master device of the case study, repeated from Figures Fig. 2.3.*

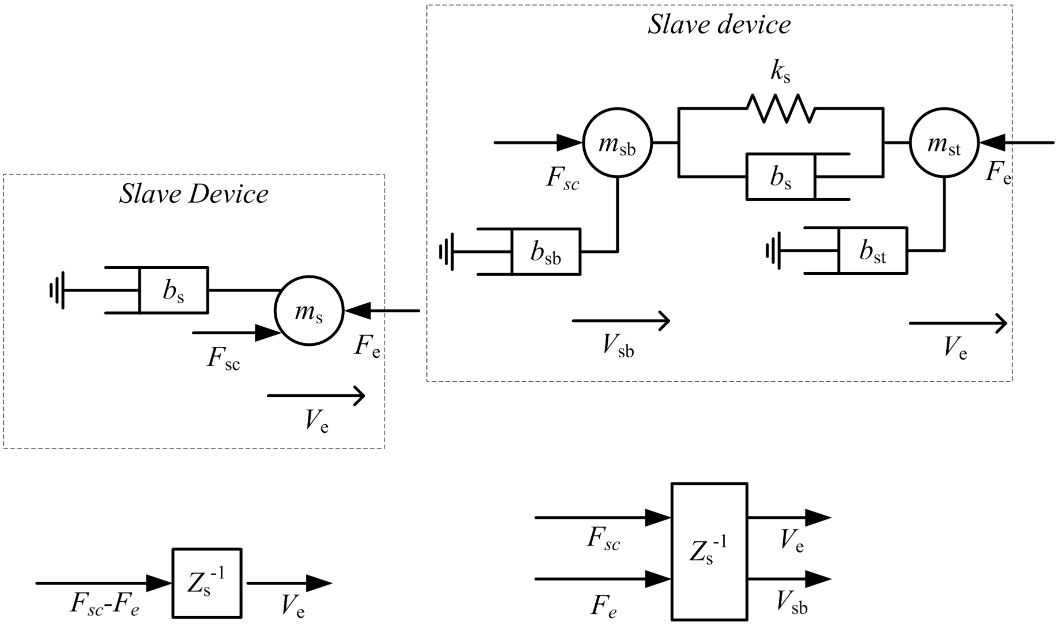

Figure 2.27: *Models for the slave device of the case study. Hard slave (above) and soft slave (below), repeated from Figures Fig. 2.5 and Fig. 2.16.*

$$
\begin{aligned}
H(s) &= \begin{bmatrix} \frac{s\,Z_\mathrm{m}}{s-K_\mathrm{p}} & -\frac{K_\mathrm{p}}{s-K_\mathrm{p}} \\ -\frac{K_\mathrm{p}\,Z_\mathrm{m}}{(s-K_\mathrm{p})\,Z_\mathrm{s}} & \frac{s}{(s-K_\mathrm{p})\,Z_\mathrm{s}} \end{bmatrix} \\
&= \begin{bmatrix} \frac{0.16s^3+4s^2+8025s+10000}{0.4s^2+5s+10000} & \frac{10000}{0.4s^2+5s+10000} \\ -\frac{10000}{0.4s^2+5s+10000} & \frac{s}{0.4s^2+5s+10000} \end{bmatrix}
\end{aligned} \tag{2.43}
$$

For this H-matrix the performance measures can be calculated, and are shown in Table 2.2.

A few of these performance numbers are interesting. First of all, two numbers are not computed: the slave-to-master velocity and force bandwidths ($P_6$and P_7) do not exist. This is due to an artefact of the H-matrix notation, and that this model is a simplification of the real teleoperator.

Second, a number of performance measures reflect the fact that this model is equivalent to a physical mass-spring-mass-damper model, as no time-delay has been modelled. The free-air mass (P_{10}) is slightly

Table 2.1: *Numerical Parameter Values*

	Parameter	*Value*
master	$m_{\rm m}$*(mass)*	0.40 kg $\pm 1\%$
	$b_{\rm m}$	5.0 Ns/m *(damping)* $\pm 10\%$
slave	$m_{\rm s}$*(total mass)*	0.40 kg $\pm 1\%$
	$m_{\rm s,b}$*(base mass)*	0.30kg $\pm 1\%$
	$b_{\rm sb}$*(base damping)*	4.0 Ns/m $\pm 10\%$
	$m_{\rm s,t}$*(tip mass)*	0.10 kg $\pm 1\%$
	$b_{\rm st}$*(tip damping)*	1.0 Ns/m $\pm 10\%$
	$k_{\rm s}$*(intrinsic stiffness)*	1.0 10^3 N/m $\pm 5\%$
	$b_{\rm s}$*(intrinsic damping)*	5.0 Ns/m $\pm 10\%$
operator	$Z_{\rm op}$*(stiffness and damping)*	500 N/m + 10.0 Ns/m
environment	$Z_{\rm e}$*(stiffness)*	100000 N/m

Table 2.2: *Numerical Performance Values for the PERR Controller*

	Performance Measure	*Value*
P1	MS velocity tracking	2.7
P2	SM velocity tracking	0.67
P3	SM force tracking	0.67
P4	MS force tracking	0.67
P5	MS velocity bandwidth	188
P6	SM velocity bandwidth	Inf
P7	SM force bandwidth	188
P8	MS force bandwidth	Inf
P9	Scaling product	2.8
P10	Free air m	0.93
P11	Free air b	10.5
P12	Free air k	0.0137
P13	Stiff contact m	0.40
P14	Stiff contact b	5
P15	Stiff contact k	10000
P16	Transparency	29
P17	Zwidth	80

larger than the total mass of the two devices, which also applies to the damping (P_{11}). The maximum stiffness felt at the master side (P15) is essentially identical to the controlled position feedback gain ($K_{\rm p}$).

2.6.3 Position-Force Control

Another simple controller is the position-force controller, introduced in Section 2.3.3. This controller is hand tuned to $K_{\rm p}$= 1000 N/m, $K_{\rm f}$= 0.8. The H-matrix expression is repeated from (2.13):

$$H(s) = \begin{bmatrix} Z_{\rm m} & -K_{\rm f} \\ -\frac{K_{\rm p}}{s\,Z_{\rm s}+K_{\rm p}} & \frac{s}{s\,Z_{\rm s}+K_{\rm p}} \end{bmatrix} = \begin{bmatrix} 0.4\,s+5 & -\frac{1000}{0.4\,s^2+5\,s+1000} \\ -0.8 & \frac{s}{0.4\,s^2+5\,s+1000} \end{bmatrix} \tag{2.44}$$

This H-matrix is used to compute the performance measures for this system, see Table 2.3.

Table 2.3: *Numerical Performance Values for the PF Controller*

	Performance Measure	*Value*
P1	MS velocity tracking	4.4
P2	SM velocity tracking	1.50
P3	SM force tracking	1.80
P4	MS force tracking	2.2
P5	MS velocity bandwidth	59
P6	SM velocity bandwidth	Inf
P7	SM force bandwidth	Inf
P8	MS force bandwidth	46
P9	Scaling product	3.2
P10	Free air m	0.40
P11	Free air b	5
P12	Free air k	0.00
P13	Stiff contact m	0.40
P14	Stiff contact b	5
P15	Stiff contact k	800
P16	Transparency	53
P17	Zwidth	50

The most interesting aspect of the position-force-controller is that the dynamics of the slave are not felt at the master side. This can be seen e.g. in the free-air mass (P_{10}) and the stiff-contact mass (P_{13}), which are identical to the master device mass.

2.6.4 Lawrence 4-Channel

The 4-channel controller, introduced in Section 2.3.4, is tuned according to the recipe described in (Lawrence, 1993):

$$\begin{aligned}
C_\mathrm{m} &= 2500/s + 2 \\
C_\mathrm{s} &= 2500/s + 2 \\
C_1 &= -C_\mathrm{s} - b_\mathrm{s} = -(2500/s + 2 + 5) \\
C_2 &= 0.99 \\
C_3 &= 0.99 \\
C_4 &= C_\mathrm{m} + b_\mathrm{m} = 2500/s + 2 + 5 \\
C_5 &= 0 \\
C_6 &= 0
\end{aligned} \tag{2.45}$$

This is equivalent to a local PD-loop for position around master and slave (C_m and C_s), and a (almost) unity communication of measured forces (C_2 and C_3). The master and slave dampings are fed forward in C_1 and C_4.

$$H(s) = \begin{bmatrix} \frac{(Z_\mathrm{m}+C_\mathrm{m})\,Z_\mathrm{s}+C_\mathrm{s}\,Z_\mathrm{m}+C_\mathrm{m}\,C_\mathrm{s}+C_1\,C_4}{(C_6+1)\,Z_\mathrm{s}+(C_6+1)\,C_\mathrm{s}-C_3\,C_4} & \frac{C_2\,Z_\mathrm{s}+C_2\,C_\mathrm{s}-C_4\,C_5-C_4}{(C_6+1)\,Z_\mathrm{s}+(C_6+1)\,C_\mathrm{s}-C_3\,C_4} \\ -\frac{C_3\,Z_\mathrm{m}+C_3\,C_\mathrm{m}+C_1\,C_6+C_1}{(C_6+1)\,Z_\mathrm{s}+(C_6+1)\,C_\mathrm{s}-C_3\,C_4} & \frac{(C_5+1)\,C_6+C_5-C_2\,C_3+1}{(C_6+1)\,Z_\mathrm{s}+(C_6+1)\,C_\mathrm{s}-C_3\,C_4} \end{bmatrix} \tag{2.46}$$

The performance measures are computed, see Table 2.4.

Table 2.4: *Numerical Performance Values for the 4C Controller*

	Performance Measure	*Value*
P1	MS velocity tracking	2
P2	SM velocity tracking	0.75
P3	SM force tracking	0.0188
P4	MS force tracking	0.030
P5	MS velocity bandwidth	Inf
P6	SM velocity bandwidth	Inf
P7	SM force bandwidth	Inf
P8	MS force bandwidth	Inf
P9	Scaling product	1
P10	Free air m	0.35
P11	Free air b	5.4
P12	Free air k	0.0038
P13	Stiff contact m	20
P14	Stiff contact b	450
P15	Stiff contact k	250000
P16	Transparency	6.5
P17	Zwidth	157

2.6.5 5-Channel Soft Slave Control

The 5-channel soft-slave control architecture is an extension of the Lawrence/Salcudean 4-channel scheme. It is explained in more detail in Section 2.3.6 and (Christiansson and v. d. Helm, 2007). The slave position/velocity information used for control of the master device and in the local feedback loop is a combination of tip velocity (V_{e}, k_{14}) and the slave base velocity (V_{sb}, k_{14}).

Ideally, only the tip velocity should be used, because this reflects the position of the object touched, and that is what the operator wants to feel. However, in the real slave device implementation used in this example, there is unfortunately significant friction between the tip of the slave and a linear guide. This causes an annoying stick-slip effect when moving the slave device in free air, and this is reduced by also using the base velocity. In the formulae below, the factor 0.5 is introduced. The disadvantage of this is that the stiffness transmitted to the operator (in Z_{to}) will always be a little lower. With a better design with the tip truly moving in free air, this can be avoided.

$$
\begin{aligned}
k_{11} &= 0 \\
k_{12} &= -2500/s - 2 \\
k_{13} &= 1 \\
k_{14} &= 0.5(2500/s + 2 + 5) \\
k_{15} &= 0.5(2500/s + 2 + 5) \\
k_{21} &= 0.99 \\
k_{22} &= -2500/s - 2 - 5 \\
k_{23} &= 0 \\
k_{24} &= 0.5(2500/s + 2) \\
k_{25} &= 0.5(2500/s + 2)
\end{aligned} \tag{2.47}
$$

This is equivalent to the Lawrence controller above, but using two different velocity measurements from the slave. The performance measures for this system are shown in Table 2.5.

Table 2.5: *Numerical Performance Values for the 5C Controller*

	Performance Measure	*Value*
P1	MS velocity tracking	4.1
P2	SM velocity tracking	1.85
P3	SM force tracking	0.030
P4	MS force tracking	0.030
P5	MS velocity bandwidth	87
P6	SM velocity bandwidth	170
P7	SM force bandwidth	Inf
P8	MS force bandwidth	Inf
P9	Scaling product	3.4
P10	Free air m	0.38
P11	Free air b	10.2
P12	Free air k	0.022
P13	Stiff contact m	20
P14	Stiff contact b	450
P15	Stiff contact k	250000
P16	Transparency	7.9
P17	Zwidth	148

2.6.6 Overview of Performance and Stability

Now an exhaustive numerical exercise has been performed to quantify various aspects of the information transfer through the teleoperator. However, it is not always clear which information the operator needs to perform each specific task. Therefore it is very difficult to make any judgement regarding which of the four control architecture is the "best", in the sense of giving optimal support to the operator while performing a certain operation. To get a deeper understanding of which performance measures are relevant for each task, human factors experiments are necessary.

In the following comparison, it is assumed that the lower the distortion on the signal, the better for the task. To facilitate comparison, all performance measures are repeated in Table 2.6. First of all, the global performance measures *Transparency Error* (P_{16}, lower is better) and *Z-width* (P_{17}, higher is better) are interesting: The two simpler schemes (position-error and position-force) perform much worse than the more sophisticated (4C and 5C schemes).

The same pattern is seen for the stiff contact impedance (P_{13}-P_{15}) and the force tracking error and bandwidth (P_3,P_4,P_7,P_8). However, for the free-air performance (P_{10}-P_{12}) and the velocity tracking error and bandwidth (P_1,P_2,P_5,P_6) there is no clear difference. This is because the addition of the force-channels are not used in free air, because the force-sensors only measure interaction forces during contact.

For all the performance metrics, the 4C controller has better values than the 5C-controller. This seems to indicate that the 4C controller is superior. However, the advantage of the 5C controller lies in improved contact stability, which is not captured by the rough yes-no stability measures presented here. A more detailed study of the stability robustness is necessary to reveal the strength of the 5C scheme.

For all teleperators, the three stability measures (passivity, absolute stability and closed loop stability) are also computed. The closed-loop stability is computed for an environment being a constant stiffness of 100 N/mm, ($Z_\mathrm{e} = 100000/s$) and an operator which is a stiffness-damper ($Z_\mathrm{h} = 500/s + 10$).

The only controller that is stable according to all three criteria, i.e. in contact with any environment, is the position-error controller.

Table 2.6: *Numerical Performance Values for all four Controllers*

	Measure	*PERR*	*PF*	*4C*	*5C*
P1	MS velocity tracking	2.7	4.4	2	4.1
P2	SM velocity tracking	0.67	1.50	0.75	1.85
P3	SM force tracking	0.67	1.80	0.0188	0.030
P4	MS force tracking	0.67	2.2	0.030	0.030
P5	MS velocity bandwidth	188	59	Inf	87
P6	SM velocity bandwidth	Inf	Inf	Inf	170
P7	SM force bandwidth	188	Inf	Inf	Inf
P8	MS force bandwidth	Inf	46	Inf	Inf
P9	Scaling product	2.8	3.2	1	3.4
P10	Free air m	0.93	0.40	0.35	0.38
P11	Free air b	10.5	5	5.4	10.2
P12	Free air k	0.0137	0.00	0.0038	0.022
P13	Stiff contact m	0.40	0.40	20	20
P14	Stiff contact b	5	5	450	450
P15	Stiff contact k	10000	800	250000	250000
P16	Transparency	29	53	6.5	7.9
P17	Zwidth	80	50	157	148

Table 2.7: *Stability Values (stable = 1, potentially unstable = 0)*

Measure	*PERR*	*PF*	*4C*	*5C*
stabname = Passivity Passivity	1	0	0	0
stabname = Absolute Stability Absolute Stability	1	0	0	0
stabname = Closed Loop Stability Closed Loop Stability	1	1	1	1

2.7 Conclusions

Haptic teleoperation is an exciting field, and it contains numerous interesting challenges. A number of popular control architectures, performance measures and stability formulae have been presented using a uniform general notation. The analysis is based on a linear model of the teleoperator in the Hybrid matrix (H) notation.

As a case study, numerical performance measures are computed for an experimental teleoperation system, for four different controllers. This gives some insight in the quantitative differences between the control architectures.

Hopefully, this overview of the analysis of teleoperators will lead to new methods for structured control synthesis. All the analysis and the computations were done with the open-source “HapticAnalysis Package” (`www.hapticanalysis.org`).

Appendix 1 - H, G, Y, Z, C, B-matrix conversions

The H-matrix notation is one of six different, mathematically equivalent, representations of a linear network. In this Section, the different linear network matrices are related to each other. For alternative Lawrence/Salcudean diagrams, see (Hashtrudi-Zaad and Salcudean, 2002).

Z = Impedance Matrix:

$$\begin{bmatrix} F_\mathrm{h} \\ F_\mathrm{e} \end{bmatrix} = \begin{bmatrix} z_{11} & z_{12} \\ z_{21} & z_{22} \end{bmatrix} \begin{bmatrix} V_\mathrm{h} \\ V_\mathrm{e} \end{bmatrix} \tag{2.48}$$

$Y =$ Admittance Matrix $= Z^{-1}$:

$$\begin{bmatrix} V_\mathrm{h} \\ V_\mathrm{e} \end{bmatrix} = \begin{bmatrix} y_{11} & y_{12} \\ y_{21} & y_{22} \end{bmatrix} \begin{bmatrix} F_\mathrm{h} \\ F_\mathrm{e} \end{bmatrix} \tag{2.49}$$

$H =$ Hybrid Matrix:

$$\begin{bmatrix} F_\mathrm{h} \\ -V_\mathrm{e} \end{bmatrix} = \begin{bmatrix} h_{11} & h_{12} \\ h_{21} & h_{22} \end{bmatrix} \begin{bmatrix} V_\mathrm{h} \\ F_\mathrm{e} \end{bmatrix} \tag{2.50}$$

$G =$ Alternate Hybrid Matrix $= H^{-1}$:

$$\begin{bmatrix} V_\mathrm{h} \\ F_\mathrm{e} \end{bmatrix} = \begin{bmatrix} g_{11} & g_{12} \\ g_{21} & g_{22} \end{bmatrix} \begin{bmatrix} F_\mathrm{h} \\ -V_\mathrm{e} \end{bmatrix} \tag{2.51}$$

$C =$ Chain Matrix:

$$\begin{bmatrix} F_\mathrm{h} \\ V_\mathrm{h} \end{bmatrix} = \begin{bmatrix} c_{11} & c_{12} \\ c_{21} & c_{22} \end{bmatrix} \begin{bmatrix} F_\mathrm{e} \\ V_\mathrm{e} \end{bmatrix} \tag{2.52}$$

$B =$ Alternate Chain Matrix $= C^{-1}$:

$$\begin{bmatrix} F_\mathrm{e} \\ V_\mathrm{e} \end{bmatrix} = \begin{bmatrix} b_{11} & b_{12} \\ b_{21} & b_{22} \end{bmatrix} \begin{bmatrix} F_\mathrm{h} \\ V_\mathrm{h} \end{bmatrix} \tag{2.53}$$

Conversion between Z and C

$$\begin{array}{ll} z_{11} = \frac{c_{11}}{c_{21}} & z_{21} = \frac{1}{c_{21}} \\ z_{12} = -\frac{c_{11}c_{22}-c_{12}c_{21}}{c_{21}} & z_{22} = -\frac{c_{22}}{c_{21}} \end{array} \tag{2.54}$$

$$\begin{array}{ll} c_{11} = \frac{z_{11}}{z_{21}} & c_{21} = \frac{1}{z_{21}} \\ c_{12} = -\frac{z_{11}z_{22}-z_{12}z_{21}}{z_{21}} & c_{22} = -\frac{z_{22}}{z_{21}} \end{array} \tag{2.55}$$

Conversion between H and C

$$\begin{array}{ll} c_{12} = -\frac{h_{11}}{h_{21}} & c_{22} = -\frac{1}{h_{21}} \\ c_{11} = -\frac{h_{11}h_{22}-h_{12}h_{21}}{h_{21}} & c_{21} = -\frac{h_{22}}{h_{21}} \end{array} \tag{2.56}$$

$$\begin{array}{ll} h_{11} = \frac{c_{12}}{c_{22}} & h_{21} = -\frac{1}{c_{22}} \\ h_{12} = \frac{c_{11}c_{22}-c_{12}c_{21}}{c_{22}} & h_{22} = \frac{c_{21}}{c_{22}} \end{array} \tag{2.57}$$

$$\begin{array}{ll} h_{11} = \frac{z_{11}z_{22}-z_{12}z_{21}}{z_{22}} & h_{21} = \frac{z_{21}}{z_{22}} \\ h_{12} = \frac{z_{12}}{z_{22}} & h_{22} = -\frac{1}{z_{22}} \end{array} \tag{2.58}$$

$$\begin{array}{ll} z_{11} = \frac{h_{11}h_{22}-h_{12}h_{21}}{h_{22}} & z_{21} = -\frac{h_{21}}{h_{22}} \\ z_{12} = -\frac{h_{12}}{h_{22}} & z_{22} = -\frac{1}{h_{22}} \end{array} \tag{2.59}$$

$$\begin{array}{ll} b_{11} = \frac{1}{h_{12}} & b_{21} = -\frac{h_{22}}{h_{12}} \\ b_{12} = -\frac{h_{11}}{h_{12}} & b_{22} = \frac{h_{11}h_{22}-h_{12}h_{21}}{h_{12}} \end{array} \tag{2.60}$$

$$\begin{array}{ll} h_{11} = \frac{1}{y_{11}} & h_{21} = -\frac{y_{21}}{y_{11}} \\ h_{12} = -\frac{y_{12}}{y_{11}} & h_{22} = -\frac{y_{11}y_{22}-y_{12}y_{21}}{y_{11}} \end{array} \tag{2.61}$$

$$\begin{array}{ll} y_{12} = -\frac{h_{12}}{h_{11}} & y_{22} = -\frac{h_{11}h_{22}-h_{12}h_{21}}{h_{11}} \\ y_{11} = \frac{1}{h_{11}} & y_{21} = -\frac{h_{21}}{h_{11}} \end{array} \tag{2.62}$$

Part II

Realizations

Chapter 3

Haptic Gripper with Adjustable Inherent Passive Properties

E.C. Fritz, G.A.V. Christiansson, R.Q. van der Linde
Proceedings of Eurohaptics 2004, München, Germany

This paper describes the design and implementation of an experimental teleoperation setup with adjustable inherent properties for both the master and the slave interface. With this setup certain aspects of biological inspired teleoperation can be explored. The system consists of two identical 1 degree of freedom devices with structural stiffness adjustable between 0.2 and 100 N/mm and a relative damping adjustable between 0 and 1.

3.1 Introduction

Teleoperators with haptic feedback gain in popularity, from underwater operations (Sayers et al., 1996) and nuclear inspection robots (Holweg, 1996) to nanomanipulators (Grange et al., 2001) and surgery stations(Kazi, 2001).

The current design of teleoperator slave robots is focused on precise sensors, stiff structures and fast controllers. This approach results in high haptic performance (v. d. Linde and Lammertse, 2003), but makes the system sensitive, potentially dangerous and expensive. Moreover this results in high frequency instability in contact with hard environments. To achieve stability in contact with a wide range of impedances, controller-simulated damping and stiffness are introduced, either with constant damping (Bardorfer, 2000), a passivity observer/controller (Hannaford et al., 2002), or by adapting the closed loop dynamics (Ryu and Kwon, 2001).

An alternative design is found in biological systems. The slenderness and stability of a human arm stands in a bright contrast to industrial robots. The two most important differences in the constitution of a robotic arm and a human arm are the control principles and the actuator properties.

There have been numerous studies that show that it is possible to make robotic machines that function in a similar way as the biological systems, e.g. *biorobotic* machines (Wu and Chang, 1995). It has been suggested that biorobotic manipulators can achieve higher performance than traditional robots for certain tasks (Hannaford et al., 1995). Our research intends to investigate to which extent these methods can improve teleoperation.

This paper describes an experimental setup for 1-degree of freedom (dof) teleoperation where the biorobotic principles can be implemented, tested and evaluated. Preliminary results suggest that contact stability can be improved thanks to the inherent mechanical properties, even with a very simple controller.

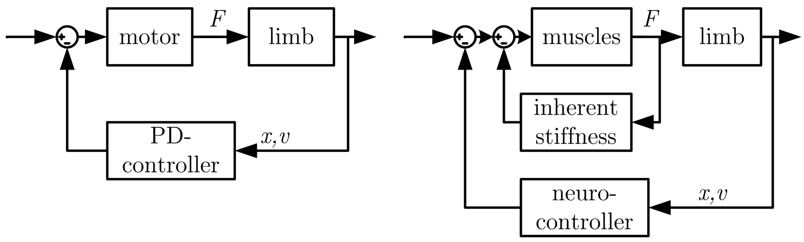

Figure 3.1: *Traditional robot motion controller (*left*) and a biological motion controller (*right*)*

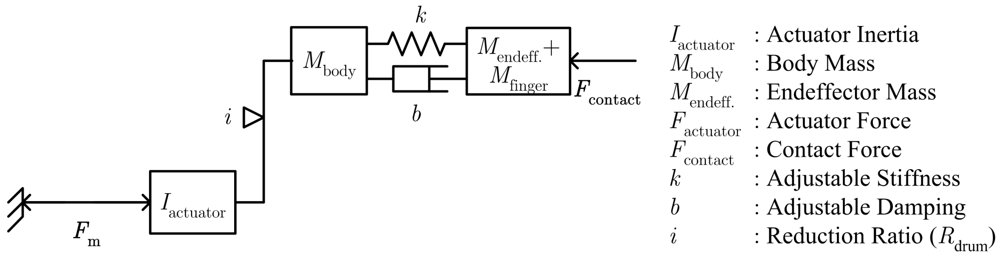

Figure 3.2: *Schematic overview of the experimental setup. The stiffness and damping between the actuator and the endeffector are adjustable*

3.2 Biorobotics for Teleoperation

A teleoperation system can be seen as an extension of the human body. The interface with the operator - the master - should reproduce the characteristics of the remote environment. The remote slave robot on the other hand represents the operator's hand. The difference in stiffness for the master and the slave introduces a hard-soft asymmetry which has important implications for the dynamics of the system. We believe that a sensitive and stable system can be achieved using the biorobotic principles for control and actuation.

The control principles used in a biological system is based on a completely mechanical, thus fast, inner loop and a slow outer neural feedback loop with an effective bandwidth of 1-10 Hz, see Fig. 3.1. This neural control loop is much slower than a robotic controller, which typically has a bandwidth of 1-10 kHz. The biological neuro-controllers are furthermore nonlinear, in contrast to the common linear robotic PD controllers.

The actuator systems found in biological systems, muscles and tendons, have characteristic inherent mechanical stiffness and damping (de Vlugt et al., 2002). The most popular actuator for robotics, the electric motor, has very different inherent properties, but is easy to control thanks to the linear current/torque relationship.

3.3 Design Requirements

To explore the influence of intrinsic properties of haptic hardware, it shall be possible to adjust the stiffness and damping between the end effector and the actuator, see Fig. 3.2 for a schematic overview of the experimental setup.

Two setups are built to form a teleoperation system. The focus of our research is grasping of small objects between the index finger and the thumb, which dictates ranges of motion and force. The required range of motion is set to 50 mm. As mentioned in (Burdea, 1996) the maximum force humans can apply with the index finger for short periods of time is about 50 N. Tests showed that significant levels of discomfort are encountered after only 10 minutes at grasp levels of only 25% of the maximum force. Based on this information a continuous force of 10 N, and a peak of at least 50 N are required for the setup.

In (Tan et al., 1994) tests were performed to determine the minimum stiffness required to simulate a rigid

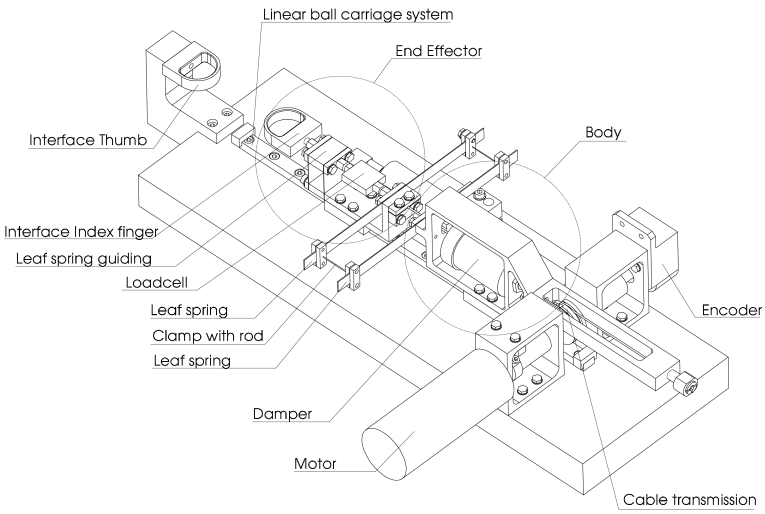

Figure 3.3: *The experimental setup with the body and endeffector supported by a linear circular ball carriage system. The leaf springs with the clamps provide for a connection with adjustable stiffness. The adjustable damper is integrated in the body. A cable transmission links the motor to the body*

object. The researchers found a human stiffness threshold between 15.3 N/mm and 41.5 N/mm. With the setup configured as a master interface, the stiffness setting must be adjusted above this limit. With the setup configured as a slave interface, it shall be possible to adjust a value closer to the human finger stiffness. The required stiffness range for the adjustable spring is generously set to 1-100 N/mm. For each setting the relative damping must be adjustable between 0 and 1.

The interface shall be suitable for an many different control schemes, including impedance control. Therefore the inertia and friction must be minimized to assure backdrivability. A good haptic sensation also requires minimal play and vibrations in the system.

In the setup the actuator position, endeffector position and the contact force have to be measured. For human-centered performance the resolution of the force sensor must be at least 0.1 N (Burdea, 1996). For position measurements the accuracy requirement is set to 0.03 mm.

3.4 Experimental Setup

The components that are used for the experimental setup are specified in the Appendix. The endeffector and the body are supported by a linear circular ball carriage system. Although some friction is present in this system, air bearings were avoided because of complexity, build in volume and dependency on clean air supply. The stiffness and damping are realized using a leaf spring construction and an adjustable air damper, see Fig.3.3.

The actuator chosen is a brushed DC motor, since considerable experience is present in the control of this element. Later in the program other actuators will be evaluated in the same experimental setup. To provide for a smooth transmission for conversion of the motor torque to a force vector, a cable transmission is used. The drum radius (R_{drum}) at which maximum acceleration is achieved, the inertial match, is calculated using (3.1).

$$R_{\mathrm{drum}} = \sqrt{\frac{I_{\mathrm{motor}}}{M_{\mathrm{body}} + M_{\mathrm{endeffector}}}} \tag{3.1}$$

Considering the stroke of 50 mm, a non-helix windup of the cable is possible in the cable transmission, when the radius of the drum is at least 10 mm. To provide for 10 N of continuous force a motor torque of at

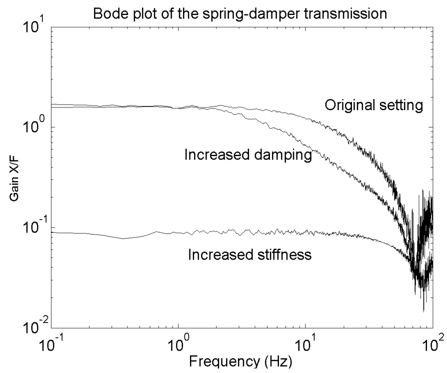

Figure 3.4: *The adjustable stiffness and damping are measured using multisine frequency identification. With increased damping, the Bode plot breakpoint moves left, to lower frequencies. Increasing the stiffness gives a smaller low-frequency gain. This way the human hand capabilities can be matched*

least 0.1 Nm is necessary. Given the formula for the inertial match (3.1) and the motor chosen (see Appendix), the maximum acceleration can be achieved at a drum radius of 6 mm. The choice for a radius of 10 mm, to avoid a more complex construction, reduces the maximum acceleration from 47 to 40 m/s^2, and this reduction is accepted.

To avoid torques on the linear ball carriage, two leaf spring constructions in a symmetrical configuration are used for the connection of the body and endeffector. Changing the position of the clamps adjusts the stiffness. To avoid high friction levels caused by misalignments, a thin rod is used in the clamps. To adjust the relative damping between 0 and 1 for each stiffness setting, the damping coefficient needs to be adjustable between 0 and 0.163 Ns/mm. A low friction adjustable pneumatic dashpot is used for this purpose. A point of attention in the use of pneumatic damping is the compressibility of air, wich appears as an additional stiffness between the body and the endeffector.

The selected force sensor is a small s-beam load cell provided with strain gauges. To protect the load cell from loads other than the axial to be measured, a leaf spring guiding is used. For accurate measurements the load cell is calibrated in combination with the guiding. For measurement of the endeffector position, an LVDT is integrated, and an encoder measures the rotation of the motor which gives the position of the body.

For the control a PC/104 computer with the Matlab Simulink xPCtarget environment is used. A 12 bit IO card is used for sensor readouts and for analog output to the linear amplifier that drives the motors.

3.5 Preliminary Results

Measurements showed that the force sensor has a resolution of 0.05 N, thus it meets the requirement. Also the position measurements are accurate enough; Both the LVDT and the 2048 step encoder meet the 0.03 mm target. Quasi-static measurements showed that the stiffness is adjustable between 0.2 N/mm and 100 N/mm. The damping coefficient of the damper is adjustable from 0.002 Ns/mm to well above the required 0.163 Ns/mm. The friction in the system is found to be between 0.35 and 0.6 N.

For each stiffness and damper setting the dynamic response of the system is determined with a crested multisine frequency response identification method. In Fig. 3.4 an example of the response for three different settings is given.

3.6 Conclusions and Future Work

A teleoperation system was built with adjustable stiffness and damping in both the master and slave. Future research shall focus on the possibilities of teleoperation systems with a stiff master and a soft slave. The flexible platform allows evaluation of actuators, sensors and control algorithms.

Component	*Supplier type*
Motor	MAXON RE35 30V
Encoder	Hewlett Packard HEDS-5540 I12
LVDT	Schaevitz 2000 LCIT
Loadcell + conditioning	FUTEK L2357+JM-2A
Linear Amplifier	Aerotech BL-10-40-B
Adjustable damper	Airpot 2K240
Linear guiding	THK RSH 9
Computer	Diamond Prometheus PC104
I/O Card	Diamond-MM-AT
Platform	xPC Target 2.0, Mathworks

Chapter 4

Measuring Asymmetric Haptic Teleoperation Device Properties

G.A.V. Christiansson

Proceedings of IEEE Systems, Man and Cybernetics, 2004, pp. 2454-2458, The Hague, Netherlands

Asymmetric haptic teleoperation - with a stiff master device and a compliant slave device - offers new possibilities to solve the contact instability problem. The prolonged timescale of the build-up of contact forces allows for stable teleoperation in contact also with stiff environments, which has been shown in force controlled robotics. This very principle can be applied to haptic teleoperation. When developing teleoperator devices with adjustable stiffness and damping, there arises a need to quickly and accurately determine the momentary compliance of the device. This paper describes a way to apply modern system identification methods to automatically identify various dynamic properties of teleoperation master and slave devices offline. The main focus is on linear parametric identification, and the extension to nonlinear models is briefly explained, along with an example of identification measurements of the human operator.

Table 4.1: *Symbols used in the models*

Symbol	*Meaning*
M_x	Mass of component x
k_x	Stiffness of component x
b_x	Viscous damping of component x
F_m, F_s	Contact forces at master and slave
v_m, v_s	End-effector velocities, master and slave
H	The hybrid transfer function matrix

4.1 Introduction

Robotic telemanipulation systems where the operator can feel a representation of the forces from the remote environment is called a *haptic teleoperator*, or a *force reflecting master-slave system*. The operator holds onto the master device and the slave device is operating in a remote environment. The last ten years we have seen a steady growth in the applications for haptic teleoperation, both in surgery (Kazi, 2001), underwater operations (Sayers et al., 1996) and nuclear inspection (Holweg, 1996).

One of the main problems of haptic teleoperation is to guarantee stability, especially in contact with stiff environments. The stability of the teleoperator system depends namely not only on the device itself, but also on the remote environment and the operator. Some teleoperation devices work well in e.g. soft tissue but fail in contact with bone. The main reason for the contact stability problem is that the contact dynamics on the master side and the slave side often are different. The time-scale of the interaction between the operator hand and the master device is often magnitudes larger than the contact between the slave robot and the environment.

There has been numerous attempts to tackle this problem, including either with passivity observer/controller (Hannaford et al., 2002), or by advanced adaptive control to achieve *similar closed loop dynamics* (Ryu and Kwon, 2001).

An alternative approach is to design a compliant slave robot, which operates in the remote environment. The inherent stiffness and damping in the device works as a mechanical filter and reduces the stability problems considerably. The advantage over e.g. adaptive control is reduced complexity, cost and reliability.

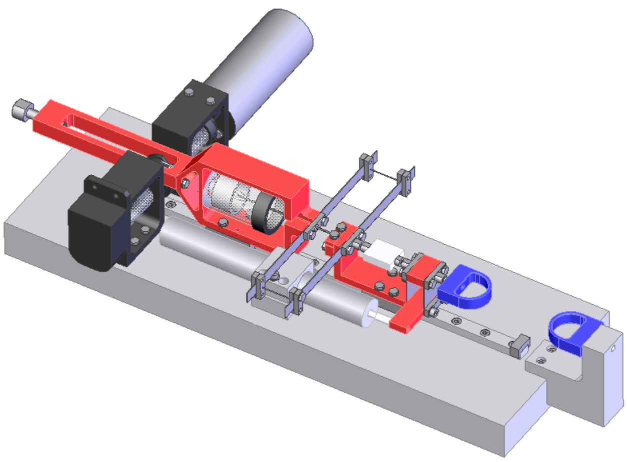

Figure 4.1: *A model of the compliant slave device. The leaf spring and the dashpot are used to adjust the contact compliance. The master device looks the same*

To investigate the optimal combination of stiffness and damping for each specific task, we designed and built a 1-dof experimental setup, see (Fritz et al., 2004) and Fig. 4.1 with adjustable stiffness and damping. The device is designed to allow two-fingered precision grasps.

Our goal is to optimize the design of the teleoperator, taking the human operator capabilities and shortcomings into account. Therefore we need to measure human task performance for a number of tasks with different settings of the inherent stiffness and damping. To be able to quantify the exact influence of the device parameters, an accurate model of the system is necessary, which leads us to the issue of repeated off-line identification, which is the focus of this paper. Each time the settings of the mechanical compliance are altered, the identification procedure must be re-run, so it is of high importance that it is an automated procedure.

4.2 Identification and Models

This section describes the purpose of the models, the mechanical models, the identification procedure and concludes with two possible extensions of the methods.

4.2.1 Purpose and Range

Analysis of teleoperation systems is based on a number of performance measures, most of which are defined using linear properties of the model (bandwidths, transparency etc.). Another purpose is to perform robust controller design using e.g. LQR or H_∞-design, which also are based in the linear domain. Therefore a linear model is chosen, but the possibilities to extend the identification procedures into the nonlinear domain are important for future alternative control methods.

As only a linear model is necessary, it is possible to do a *frequency based identification*, where input and output signals are transformed using a Fourier transform, for a good example see (de Vlugt et al., 2003). However, in this paper a time-domain identification is chosen because it offers a simple extension to nonlinear identification.

It has been shown that knowledge about the components improves the convergence properties of the identification method (Lindskog and Sjöberg, 1995), (Sjoberg, 2000). As the mechanical design of our device is well known, the structure of the model is also easy to determine, and a number of parameters remain to be identified.

The model must be accurate in the typical working range of the device, which depends on the task at hand. The device presented in this paper is intended for telemanipulation and remote precision tasks, see Fig. 4.2, which give the following range of frequencies, movement and forces during typical operation:

- Movement range: $\pm$ 20 mm
- Frequency range: 0.1-10 Hz
- Force range: $\pm$ 5 N

The frequency range of operation is limited to 10 Hz for the force commands from the operator to the slave robot due to the low-frequency characteristics of the human muscles. The contact information from the remote environment on the other hand contains information of higher frequency.

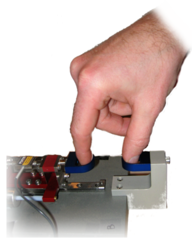

Figure 4.2: *The operator hand in position for the precision grip. The thumb is in contact with a grounding and the index finger is in contact with the end-effector of the device*

4.2.2 Mechanical Models of the Devices

Mechanical models of the master and the slave devices are presented in Fig. 4.3.

The master device is the classical haptic device model (Lawrence, 1993), (Lee and Lee, 1993), (Zhu et al., 1999) and (Carignan and Cleary, 2000). The slave model on the contrary is much more complex due to the adjustable compliance (a kind of series elastic actuation (Zinn et al., 2002)).

Some of the properties of the models are easy to measure, e.g. the masses can be accurately determined using a scale. However, to get an accurate value of the dampers, it is necessary to perform a system identification procedure with a well-chosen input signal.

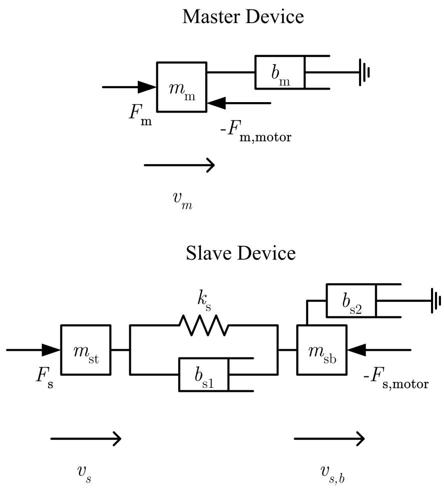

Figure 4.3: *A mechanical model of the master device (top) and slave device (bottom) of the teleoperation setup. The symbols introduced in this image represent linear model properties, and are all identified using the procedure presented below*

4.2.3 Signals

System identification is based on comparison of input and output signals from a system and from a simulated version of the system.

We can accurately enough measure the base position, the tip position and the contact force, and control the motor current, which gives us enough flexibility to measure all device properties using the device itself.

The input signal used in the identification procedures is a crested multisine signal (de Vlugt et al., 2003), with an equal amount of all frequencies in the spectrum to study (0.1-50 Hz). All signals are sampled at 1 kHz at 12 bits using a calibrated IO card.

4.2.4 Measurements

The master device model is simple to identify, as it is only one parameter to determine. However, the slave parameters are determined in a series of measurements, to improve the accuracy of the identification. The smaller the dimensionality of the search space, the faster the iteration converges, and the less crosstalk between the parameters. First the base of the device - only the motor and the moving base ($m_{\mathrm{s,b}}$, b_{s2}) - is identified, followed by a measurement of the complete friction. Finally the compliant part is identified with the end-effector clamped. This last measurement is done each time the adjustable compliance is changed.

4.2.5 Identification Procedure

The goal of the identification is to find a mathematical model that gives the same output as the real measured output for the same input. It is a kind of optimization problem, where the fit function depends on the values of the model parameters, and the goal is to find the optimal set of model parameters. An initial guess of the values is used to start the search for the optimum. In this paper a line search method (Matlab `lsqnonlin`, (Mathworks, 2003)) is used using the Levenberg-Marquardt algorithm to find the optimal fit. The model is described as a Simulink model, in which the parameters are adjusted in each iteration step. The initial values for the optimization process are chosen from experience and preliminary measurements.

To quantify how good a certain model is we use *Variance Accounted For* (VAF) (4.1), usually expressed as a percentage. A perfect fit is thus 100 %.

$$\mathrm{VAF} = 1 - \frac{\|y_{\mathrm{measured}} - y_{\mathrm{simulated}}\|_2}{\|y_{\mathrm{measured}} - y_{\mathrm{mean}}\|_2} \tag{4.1}$$

To avoid overfitting, two time segments are used, one for fitting and one for validation. The identified model parameters, along with standard deviation and VAF values are presented in Section 3 below.

4.2.6 Extension 1 - The Operator

It is possible to identify the dynamic impedance of the operator using the same procedure as is used to identify the hardware devices. The most important aspect of the operator impedance is the influence on stability. Often the human operator works as a damper or a stabilizer (Burdea, 1996), but sometimes the operator can be locally unstable when manipulating a strongly damped system.

The parametric model chosen was presented by Lawrence (Lawrence and Chapel, 1994) and is shown in Fig. 4.4.

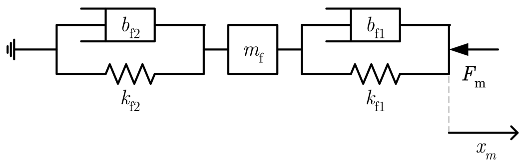

Figure 4.4: *Identification model of the operator finger, adapted from Lawrence (Lawrence and Chapel, 1994)*

In the experimental setup used in this paper, the end-effector position and the contact force are measured with high resolution, which allows impedance measurement of the external load. The operator gets a task to hold the device with a constant force and the grip gets perturbed by a multisine signal. The resulting force/displacement data is used to estimate the dynamic impedance[1].

However, the operator dynamics depend on the muscle tension and the grip, so it will change in a wide range during operation, so a precise value is neither possible to measure nor necessary for analysis. Nevertheless it is good to chart the boundaries of operation and estimate minimal and maximal values, both regarding damping, stiffness and mass.

The external environment can also be measured in a similar fashion.

4.2.7 Extension 2 - Nonlinear Parametric Models

The most important unmodelled nonlinearity in the models presented is the Coulomb friction - a constant force opposing the direction of movement. It is straightforward to include this force in the model and perform exactly the same identification procedure above, and get a separation of the damping into the linear viscous damping coefficient and the nonlinear Coulomb friction force, see Fig. 4.5

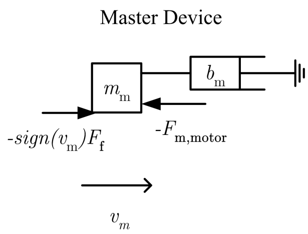

Figure 4.5: *Identification model of the master with a Coulomb friction component*

[1]The operator impedance depends on the task at hand. Here, the task was to press with a constant force of 4 N, which is a typical force while feeling the size or stiffness of an object, without moving it.

4.3 Results

The results of the identification procedures are presented in this section, with six measurements performed for each parameter. In the tables below, the average value is given (± the standard deviation).

Hardware Measurements: (VAF 80±5 %)

$$\begin{aligned} m_{\mathrm{m}} &= 0.376 \pm 0.0005\,kg \\ m_{\mathrm{s,b}} &= 0.242 \pm 0.0005\,kg \\ m_{\mathrm{s,t}} &= 0.111 \pm 0.0005\,kg \\ b_{\mathrm{m}} &= 4.48 \pm 0.03\,Ns/m \\ b_{\mathrm{s2}} &= 11.0 \pm 0.08\,Ns/m \\ b_{\mathrm{s1}} &= 1.108 \pm 0.011\,Ns/m \\ k_{\mathrm{s}} &= 7139 \pm 3.5\,N/m \end{aligned} \tag{4.2}$$

The adjustable parameters k_{s} and b_{s1} can assume a wide range of values, see (Fritz et al., 2004), but the other parameters remain constant.

4.3.1 Extension 1 - Operator

These measurements were made with disturbances around a static grip force of 3 N: (VAF 60%) Standard deviation is not calculated, but the values vary about ±30%.

$$\begin{aligned} m_{\mathrm{f}} &= 0.010\,kg \\ b_{\mathrm{f1}} &= 10\,Ns/m \\ k_{\mathrm{f1}} &= 430\,N/m \\ b_{\mathrm{f2}} &= 10\,Ns/m \\ k_{\mathrm{f2}} &= 430\,N/m \end{aligned} \tag{4.3}$$

4.3.2 Extension 2 - Nonlinear Model of the Friction

Using the model with separate viscous damping and Coulomb friction: (VAF 95%)

$$\begin{aligned} b_{\mathrm{m}} &= 0.721 \pm 0.006\,Ns/m \\ F_{\mathrm{f}} &= 0.445 \pm 0.003\,Ns/m \end{aligned} \tag{4.4}$$

4.4 Discussion and Future Work

The measurements of the hardware devices is straightforward and gives adequate values for analysis and controller synthesis. The standard deviation is low (0.1-2), which show that also this method is reliable. For each new setting of the adjustable slave compliance a new measurement can easily be performed.

For the setting in this measurement, we can calculate the linear model of the whole teleoperator, the so called H-matrix (Raju et al., 1989) with four transfer functions. We can compare the ideal value in (4.5) with a Bode plot of the measured H-matrix of the teleoperator with a simple P-controller in Fig. 4.6

$$H = \begin{bmatrix} 0 & 1 \\ -1 & 0 \end{bmatrix} \tag{4.5}$$

The extensions of the identification method allow some interesting reflections. The measurements of the operator finger give a less good fit, due to the variations of the muscle tone during the measurement and unmodelled reflexive behaviour. Nevertheless, these approximate values give an indication to the range of stiffnesses and dampings present in this grip. It also became clear that the stiffnesses k_{f1} and k_{f2}, as well as the dampings b_{f1} and b_{f2} can be modelled as identical without loss of precision for this type of grasps.

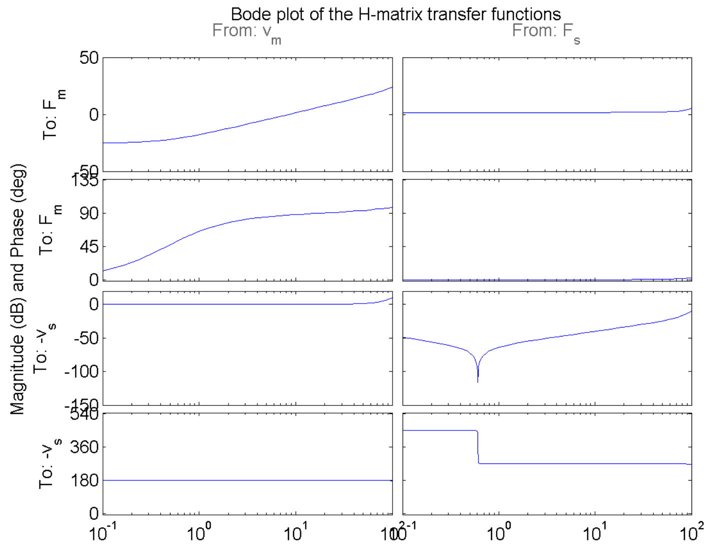

Figure 4.6: *Bode diagram of the H-matrix components. Note that the h_{12} and h_{21} are very close to ideal up to 100 rad/s. The slave impedance has a small low-frequency resonance dip, but because the absolute value is so low, it will not be noticed*

The identification of the master with a nonlinear friction component in the model gives a better fit than the linear model, which indicates that this model is more accurate. If a linear model is necessary for subsequent analysis, it is sometimes more useful to have a less accurate linear model than an accurate nonlinear one. Nevertheless, it is due to raise the question of the applicability of the linear performance measures commonly used to quantify teleoperator performance.

Future work includes measurements of performance measures and investigations of the relationship with human task performance. We believe that the controller parameters and the adjustable inherent stiffness and damping can be chosen optimal for each specific task, and this will be investigated in detail in the rest of this project.

4.5 Conclusions

As presented in this paper, time-domain identification of a parametrized model is a useful method to acquire an accurate model of asymmetric devices, as well as of the human operator. This method can be used by all developers of compliant slave devices, and the extensions can be used for measuring the human operator and for estimation of the remote environment.

Chapter 5

The Low-Stiffness Teleoperator Slave - a Trade-off between Stability and Performance

G.A.V. Christiansson, F.C.T. van der Helm
International Journal of Robotics Research, Vol. 26, No. 3, pp. 287-299 (2007)
(parts) Proceedings of Eurohaptics Conference, 2006, Paris, France

Stability is essential for teleoperation and a prerequisite for performance. This paper analyzes the the stability/performance trade-off of a teleoperator where the slave device has a built-in passive intrinsic stiffness. Stability is quantified as time delay robustness *and performance is expressed using* teleoperator damping *and* teleoperator stiffness*, the boundaries of the Colgate* Z-width.

Two classic control schemes, Position Error *and* Lawrence 4-Channel*, are used along with a novel* 5-Channel *scheme where the slave stiffness deflection is measured, and compensated for, to improve the performance.*

The teleoperator system was theoretically analyzed using a linear model and the findings were experimentally validated on a 1-degree of freedom teleoperation setup.

It was found that:

- *A lower slave stiffness improves stability for all three teleoperator architectures*
- *The stability boundary of the three controllers is similar*
- *The performance of the controllers is increasing from:* (poor) *Position Error, 4-Channel to* (excellent) *5-Channel*
- *A classical linear analysis method can accurately predict the stability characteristics of the teleoperator system*

Therefore it is can be concluded that a compliant slave device offers a stability advantage for a range of teleoperation situations and that the loss of performance can be partly compensated.

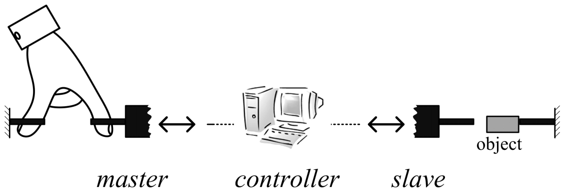

Figure 5.1: *Components of a teleoperator system: The operator holds the master device (left), which is coupled via the controller to the slave device (right). The interaction information (forces/movements) is communicated both ways in a haptic teleoperator.*

5.1 Introduction

Master-slave manipulators (*teleoperators*) are used in a variety of tasks, ranging from underwater operations to nuclear maintenance (Karlsson, 2004). *Haptic* teleoperators (sometimes called *bilateral* or *force-feedback teleoperators*) allow the human operator to feel some of the interaction forces between the slave robot and the remote environment.

The components of a teleoperator system are presented in Fig. 5.1. The operator communicates both position/velocity and force with the system by holding onto a haptic master device, and the controller relays this information to the slave, which interacts with the remote environment. The contact information is communicated back to the operator and presented as forces and movements in the haptic master handle. In other words, the channel used for input (the interaction with the master device) is also used for output, which can cause interesting stability problems.

Even though force-reflecting teleoperators have been in use for more than 50 years (Burdea, 1996), a number of problems remain to be solved.

One of the key questions is how to balance the trade-off between stability, performance and complexity in the mechatronic design. A tremendous amount of research has been done to improve the controller, but so far the mechanical design has received somewhat less attention. This paper analyzes this trade-off by assessing the stability and performance characteristics of three controllers with increasing complexity. The method proposed in this paper is illustrated with a specific device parameter (slave stiffness) but can be applied for any design parameter.

Stability is essential for teleoperators and instabilities can occur for many different reasons. The most prominent instability is the contact instability, with the slave in contact with a hard environment (Colgate and Hogan, 1989). It is sometimes called "hammering", and the symptom is that the slave device enters a limit cycle with intermittent contact with the environment. This is a well known problem in force controlled robotics, and many solutions have been proposed. Whitney presented an early overview of the stability issues of force control (Whitney, 1985), which was further elaborated by Hogan (Hogan, 1988) and Qian (Qian, 1993). All methods proposed include some kind of low-pass filter; sometimes using an active low-pass filter or active impedance control, and sometimes as a mechanical filter, like a "remote center compliance" or low-stiffness force sensor.

More recently, adaptive methods have been shown to provide for stable interaction with stiff environments, e.g. the adaptive impedance force control by Jung et al. (Jung et al., 2004). It is probable that adaptive methods would enhance the stability of haptic teleoperation, but at the cost of a variation on the impedance transmission characteristics of the teleoperator. It would be difficult for the operator to distinguish between impedance variations due to the environment and variations due to the adaptation of the controller. Therefore, adaptive control methods have been excluded from this study, and the focus is on a passive stiffness incorporated in the slave device.

A passive stiffness in the slave device does also influence the operator's perception of the remote environment, and reduce teleoperator performance, but in a consistent way. It has been shown (Christiansson et al., 2006b) that total teleoperator stiffness is important for e.g. stiffness discrimination, where the teleoperator stiffness must be larger than the objects you want to feel, but the requirements can be set much lower for e.g. size discrimination. In general, manipulation tasks often require a higher teleoperator stiffness than pure sensing.

By adding complexity in the form of an extra sensor, the deflection of the slave stiffness can be measured and compensated. Thereby, the total teleoperator stiffness can be enhanced and the human performance improved.

Another way to address the high frequency performance of the teleoperator by incorporating an accellerometer in the slave device has been pursued by Howe et al. (Howe, 1992) and more recently Kuchenbecker et al. (Kuchenbecker et al., 2006). This is also only meaningful if the slave device is relatively compliant, so that the effective end tip mass is low and the acceleration matches the high frequency contact forces.

The trade-off between teleoperator performance and complexity has been illustrated for some controllers in an excellent overview by Aliaga et al. (Aliaga et al., 2004). This paper extends their work with a stability analysis and a method to incorporate mechatronic design.

5.1.1 Problem Statement

In brief, this paper presents the details of the trade-off between stability, performance and complexity.

The main questions in this research are:

- In which way does *slave device stiffness* influence stability?
- How do the three controllers compare?
- How does the *slave stiffness* influence performance?
- How well can the slave stiffness deflection be compensated?
- Is a linear model adequate for analysis of stability and performance of teleoperator systems?

5.1.2 Approach

Stability and performance for a teleoperator is theoretically analyzed using a linear model of the teleoperator. The classic *Hybrid matrix* notation is used (Hannaford, 1989b), both for stability and performance analysis.

The two main dependent parameters that are used in the analysis are:

- Slave device stiffness
- Type of controller

The results from the theoretical analysis are then experimentally validated on a real teleoperator.

In the subsequent sections a teleoperator model is developed, stability and performance measures presented and the experimental setup is described. Finally results from the theoretical analysis and the measurements are analyzed.

5.2 Method

A theoretical model is used to calculate theoretical values for the stability and performance, and an experimental setup is used to validate the findings.

5.2.1 Theoretical Analysis

Teleoperator Model

This section describes the mathematical model of the teleoperator used in the analysis. A linear *hybrid matrix* model of the whole teleoperator system is generated by combining models of the separate components. Each component is introduced and the complete model is presented in Section 5.2.1.

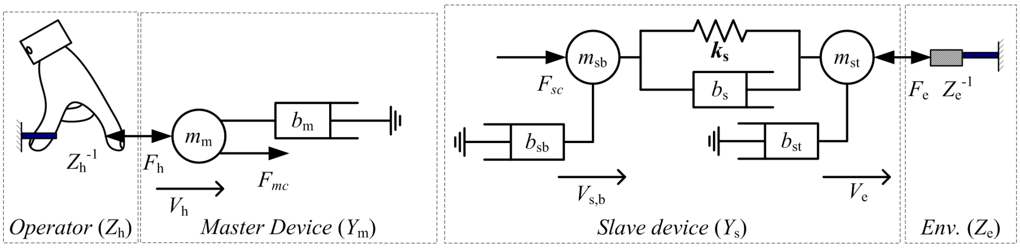

Figure 5.2: *Mechanical models of the components in the experimental teleoperator setup: The human operator and master (left), connected via the controller to the slave device and environment (right). The passive slave stiffness k_s is the main parameter in this study.*

Master and Slave Devices

The mechanical models for the teleoperator components are shown in Fig. 5.2, and a sketch of the realization is shown in Fig. 5.7.

The device models are expressed as admittances, the inverse of impedance, following the notation of Lawrence (Lawrence, 1993) and Hashtrudi-Zaad (Hashtrudi-Zaad and Salcudean, 2001). The master device admittance (Y_m):

$$Y_\mathrm{m} = Z_\mathrm{m}^{-1} = \frac{1}{m_\mathrm{m}\, s \, + \, b_\mathrm{m}} \tag{5.1}$$

The slave device has two masses, due to the passive compliant coupling in the slave device, which gives a 2x2 transfer function from forces to velocities (for Y_s):

$$\begin{bmatrix} v_\mathrm{e} \\ v_\mathrm{sb} \end{bmatrix} = \begin{bmatrix} Y_\mathrm{s,ee} & Y_\mathrm{s,be} \\ Y_\mathrm{s,eb} & Y_\mathrm{s,bb} \end{bmatrix} \begin{bmatrix} F_\mathrm{e} \\ F_\mathrm{sc} \end{bmatrix} \tag{5.2}$$

Detailed expressions of $Y_\mathrm{s,ee}$ etc. expressed in the mechanical components can be found in Appendix 5.5. The numerical values for the components can be found in Appendix 5.5.

Operator Model

The operator is here modelled as a linear time-invariant stiffness-damper system. This model is often used (see e.g. (Lawrence, 1993), (Raju et al., 1989), (Aliaga et al., 2004)), but not without controversy. It is clear that human operators modulate the intrinsic stiffness and damping depending on the task and the dynamics of the haptic device, sometimes into an active component, see (de Vlugt et al., 2002). However, the transition from stable motion to undampable instability is so short ($< 0.1\,\mathrm{s}$), that the change of human impedance during this period is negligible. Therefore a static model is sufficient for the purposes of this paper:

$$Z_\mathrm{h} = k_\mathrm{finger}/s + b_\mathrm{finger} \tag{5.3}$$

This model was identified during nominal grasping movement, using a time domain identification procedure, explained in (Christiansson, 2004).

For some teleoperation systems, the operator mass plays an important role for stability, due to the significant phase loss. However, in this fingertip grasping task, the finger mass (around 10 g) is negligible compared with the moving mass of the master device (almost 400g).

Environment Model

The environment for these experiments is modelled a pure stiffness, see (5.4). That is actually equivalent to a fixated slave device. In the experiments, a unilateral constraint was used (contact with a stiff object), which is a nonlinear effect, and impossible to model using this linear method. However, it has been argued (Lawrence, 1993) that the nonlinear transition is not the real cause of the instability, but that it can be traced to unstable or poorly damped linear dynamics. It is still an open question if the same transition point between stable and unstable modes can be found in a linear model with the same stiffness. Therefore it is

$$Z_{\mathrm{e}} = k_{\mathrm{e}}/s \tag{5.4}$$

The two operation modes that are emulated in the stability analysis, the free air movement and stiff contact mode are represented as a very small and a very large stiffness. For numerical values, see Section 5.5.

Controller Model

The controller is modelled using a generalized MIMO model, see Fig. 5.3:

$$K = \begin{bmatrix} k_{11}(\mathrm{s}) & k_{12}(\mathrm{s}) & k_{13}(\mathrm{s}) & k_{14}(\mathrm{s}) & k_{15}(\mathrm{s}) \\ k_{21}(\mathrm{s}) & k_{22}(\mathrm{s}) & k_{23}(\mathrm{s}) & k_{24}(\mathrm{s}) & k_{25}(\mathrm{s}) \end{bmatrix} \tag{5.5}$$

By choosing the transfer functions ($k_{ij}(s)$) to specific values, any controller architecture can be implemented.

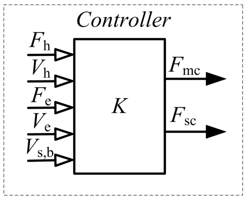

Figure 5.3: *A MIMO model for a general 1-dof teleoperation controller. The measured signals are forces and velocities at the master and slave (right), and the controlled output is the motor forces (left).*

In this paper three different controllers are used: a Position-Error controller (PERR), a Lawrence 4-Channel controller (4C) and a novel 5-Channel controller (5C), where also the deformation information is used to present more accurate information to the operator.

The three controller matrices are therefore:

$$\begin{aligned} K_{\mathrm{PERR}} &= \begin{bmatrix} 0 & -K_{\mathrm{p}}/s & 0 & K_{\mathrm{p}}/s & 0 \\ 0 & K_{\mathrm{p}}/s & 0 & -K_{\mathrm{p}}/s & 0 \end{bmatrix} \\ K_{4\mathrm{C}} &= \begin{bmatrix} C_6 & -C_{\mathrm{m}} & -C_2 & -C_4 & 0 \\ C_3 & C_1 & -C_5 & -C_{\mathrm{s}} & 0 \end{bmatrix} \\ K_{5\mathrm{C}} &= \begin{bmatrix} C_6 & -C_{\mathrm{m}} & -C_2 & -C_4/2 & -C_4/2 \\ C_3 & C_1 & -C_5 & -C_{\mathrm{s}}/2 & -C_{\mathrm{s}}/2 \end{bmatrix} \end{aligned} \tag{5.6}$$

The three controllers were tuned to be stable in the range of 2-3 ms time delay for the highest slave stiffness (k_{s} =105 N/mm), and the same controller gains were used throughout the experiment. The numerical values for the controller gains can be found in Appendix 5.5.

The 5-Channel controller here uses two position measurements plus the force measurement, which may seem superfluous. In practice, the advantage of using both measurements is to better accommodate for the free air/contact phases.

It is worth noting that controller optimization is difficult in haptic teleoperation, as it is still largely unclear which information is most important to the human operator for each specific task. Without a well-defined, relevant, performance measure, modern controller synthesis methods cannot be used, and we have to revert to semi-manual tuning.

Each controller architecture has its pros and cons, and the three architectures presented here are of increasing complexity and cost.

The time delay is introduced in the transfer functions from the master measurements to the slave control, and from slave to master, to emulate communication delay.

Complete Closed-loop Model

By combining the component models, a complete system model is acquired, see Fig. 5.4.

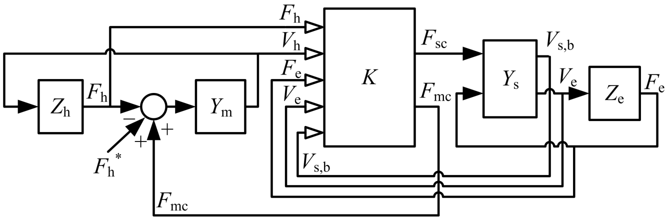

Figure 5.4: *A complete model of the system components: Operator (Z_h), master (Y_m), controller (K), slave (Y_s), environment (Z_e).*

This model can be converted into the well known *hybrid matrix model* (Hannaford, 1989a),(Hashtrudi-Zaad and Salcudean, 2002) by linear transformations, and in Appendix 5.5 complete formulae can be found.

The hybrid matrix model is a 2x2 matrix of transfer functions and can be illustrated as in Fig. 5.5. It is often used to express device performance characteristics and stability properties of a teleoperation system. The two important parameters for the stability analysis below, the *slave stiffness* (k_s) and the *time delay* (T_d) in

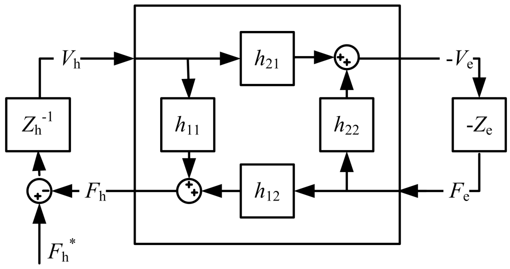

Figure 5.5: *The total system consists of the human operator (Z_h), the teleoperator (H-matrix) and the remote environment (Z_e)*

the communication are embedded inside the H-matrix elements.

Stability

Stability is analyzed using the *root locus method*, from classical control engineering (de Vegte, 1990). There has been other methods proposed, ranging from passivity (Anderson and Spong, 1989) to absolute stability (Hashtrudi-Zaad and Salcudean, 2002).

The root-locus method studies the position of the closed-loop system poles, as a function of a system parameter. Often a control gain is varied, but in this paper the parameters that are studied are time delay and slave device stiffness. In this paper the analysis is done in the continuous time frequency domain, which gives the criterion for stability that the closed-loop poles must be on the left half-plane (negative real part).

The complete model, as presented in Fig. 5.5, is a set of linear SISO blocks, for this one-degree-of-freedom system. Therefore we can select any input and output signal and calculate the closed-loop gain, which gives the closed loop system poles. However, it is not meaningful to calculate a phase- or gain margin, because the system is not on "GK"-form (de Vegte, 1990).

The closed-loop transfer function from $F_\mathrm{h}^\star$ to V_h is:

$$G(s) = \frac{V_\mathrm{h}}{F_\mathrm{h}^\star} = \frac{1 + h_{22} Z_\mathrm{e}}{(1 + Z_\mathrm{e} h_{22})(Z_\mathrm{h} + h_{11}) - h_{12}\, h_{21}\, Z_\mathrm{e}} \tag{5.7}$$

The denominator of the rational transfer function $G(s)$ is the characteristic equation of the system, the roots whereof are the closed-loop poles. By varying the parameters in the model, it is possible to calculate $G(s)$ for each value, and see how the closed-loop poles move in a *Root-Locus diagram*. When a pole moves into the right half-plane (positive real part), the system becomes unstable. The two operating modes (free air and stiff contact) are represented using one very low and one very high value of the environment stiffness (Z_{env}), see Section 5.5.

The main factor influencing the stability in this paper is the slave device stiffness, k_{s}. The stability analysis formula can only give a yes/no answer, so in order to get a more quantitative measure, we also use the additional component *time delay* (T_{d}). The time delay between master and slave is increased in small steps and the maximum allowed time delay before instability occurs is used as a quantitative measure for the stability of the system. For the root locus analysis, the time delay is implemented as a first order Taylor approximation. The same procedure is done for each controller architecture (PERR/4C/5C), to illustrate the trend - how the stability is influenced by the slave stiffness.

Performance

The performance for each of the controller is measured for two reasons. First, the theoretical prediction is compared with the experimental result. Second, the three controller architectures are quantitatively compared with each other.

The two performance measures used in this paper are *teleoperator stiffness* and *teleoperator damping*. The teleoperator stiffness is defined as the maximum stiffness that the master device can present to the operator, i.e. how a very stiff environment feels. The teleoperator damping is the resistance to movement in free air. The teleoperator stiffness and damping are effectively the upper and lower boundaries of the *Z-width*, as proposed by Colgate (Colgate and Brown, 1994). An illustration of the Z-width is shown in Fig. 5.6.

The teleoperator stiffness and damping are chosen because they illustrate some of the most important characteristics of the teleoperator and because the choice of controller is of influence.

The theoretical calculation of the teleoperator stiffness and damping are based on the H-matrix formulation. The impedance that the operator feels at the master side (the transmitted impedance Z_{to}) can for any environment (Z_{e}), see eq. (5.8) (Aliaga et al., 2004). Using this formula it is straightforward to calculate how the master feels when the slave moves in free air ($Z_{\mathrm{e}} = 0$) and in contact with a very stiff environment ($Z_{\mathrm{e}} = \infty$):

$$\begin{aligned}\frac{F_{\mathrm{h}}}{V_{\mathrm{h}}} = Z_{\mathrm{to}}(s) &= \frac{h_{11} + (h_{11}h_{22} - h_{12}h_{21})Z_{\mathrm{e}}}{1 + h_{22}Z_{\mathrm{e}}} \\ Z_{\mathrm{to,stiff}}(s) &= \frac{h_{11}h_{22} - h_{12}h_{21}}{h_{22}} \\ Z_{\mathrm{to,free}}(s) &= h_{11}\end{aligned} \tag{5.8}$$

The *teleoperator stiffness* is the low-frequency asymptote of the stiff contact impedance ($Z_{\mathrm{to,stiff}}$). The *teleoperator damping* is the dominant low-frequency component of the free air impedance ($Z_{\mathrm{to,free}}$):

$$\begin{aligned}\hat{k} &= \lim_{s\to 0} s\, Z_{\mathrm{to,stiff}}(s) = \lim_{s\to 0} \frac{s\,(h_{11}(s)h_{22}(s) - h_{12}(s)h_{21}(s))}{h_{22}(s)} \\ \hat{b} &= \lim_{s\to 0} Z_{\mathrm{to,free}}(s) = \lim_{s\to 0} h_{11}(s)\end{aligned} \tag{5.9}$$

Ideally, for identical forces and velocities at master and slave side, the transmitted impedance Z_{to} would be identical to the real remote environment Z_{e} (Hannaford, 1989b), but there will always be some distortion. In contact with a very stiff object, we would like to feel a high value of the impedance ($Z_{\mathrm{to,stiff}}$), which is realized e.g. if h_{22} is small. In free air the operator feels $Z_{\mathrm{to,free}} = h_{11}$, which includes all damping in the system, and it should be small to allow free motion. For a small Z-width, it is difficult to distinguish different environments, because everything feels very similar. The larger the Z-width, the richer the information presented to the operator can be.

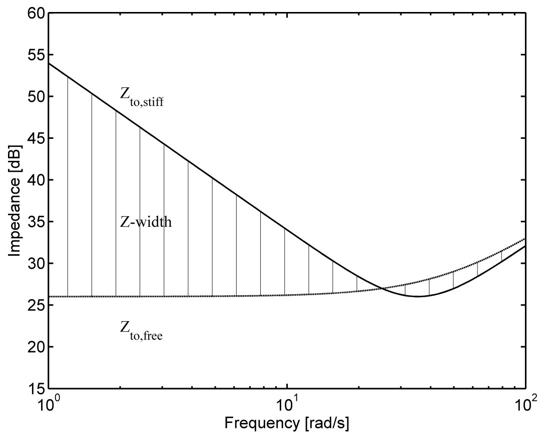

Figure 5.6: *The Z-width is a measure of the area between the free air impedance ($Z_{\mathrm{to,free}}$) and stiff wall impedance ($Z_{\mathrm{to,stiff}}$) that a teleoperator can transmit to the master side. Figure adapted from (Colgate and Brown, 1994).*

5.2.2 Experimental Stability and Performance

Experimental Apparatus

The teleoperation system used in this study is a custom-made teleoperator for two-finger grasps, using a fixed thumb and a moving fore-finger, see Fig. 5.7. To illustrate the size of the system, a photo of an operator using the teleoperator is presented in Fig. 5.8.

The master and slave devices are in principle identical, the only difference is that the slave device has an adjustable compliant section. The stiffness can be adjusted using a leaf spring from 0.1 to 100 N/mm and the damping using a dashpot from 1 to 200 Ns/m. The actuation is achieved using two Maxon RE35 motors of 90W (Maxon, Sachseln, Switzerland) and a pulley-wire transmission to get a linear motion. The total moving mass is less than 400 g on the master and slave devices, including the rotary inertia of the motors. The achievable maximum teleoperator stiffness using a 4C controller has been measured to 35 N/mm, with a damping of less than 1 N/ms, and a friction level of 0.1 N. The measurement accuracy is 0.03 mm for position and 0.05 N for force. The teleoperator is explained in detail in (Fritz et al., 2004).

The purpose of the system is to allow accurate object discrimination in a teleoperated setting - i.e. the operator should be able to feel differences in object size and stiffness on a distance.

The experiment was designed to test stability in the most critical modes of the system - the free air mode and the stiff contact mode.

The master device was moved in free air and brought into contact with a stiff object where a force of around 4 N was applied - a typical force for object identification in a two-finger grasp.

The slave device adjustable stiffness (k_{s}) was manually adjusted to three different values for the experiments: 1.2±3%, 7.2±2% and 105±15% N/mm.

Controller Tuning

The controllers (PERR/4C/5C) were implemented using Matlab Simulink (Mathworks, Natick, USA) on a dSpace 1102 DSP (dSPACE GmbH, Paderborn, Germany) controller at a 1 kHz sampling rate. The minimum time delay between master and slave in the system was therefore 1.5 ms (1 ms measurement interval and 0.5 ms due to the zero-order hold of the analog output).

In the experiments, the time delay between master and slave was increased in steps of 1 ms until instability occurred. The last stable setting - the maximum allowed time delay for a certain slave stiffness - was taken as the robustness measure, and is presented in the subsequent section.

Except for the varying time delay, the three controllers (PERR/4C/5C) were kept constant during the whole experiment, with values from described below in Appendix 5.5.

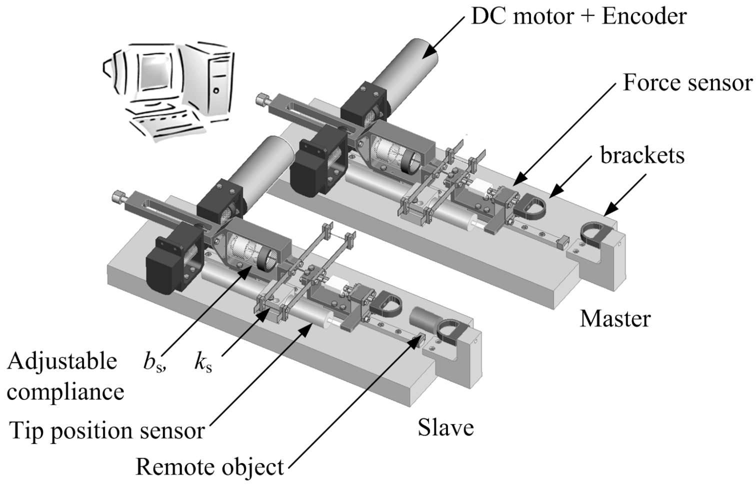

Figure 5.7: *The haptic teleoperator used in the experiments. The slave device has an adjustable mechanical stiffness (k_s) which influences stability and performance.*

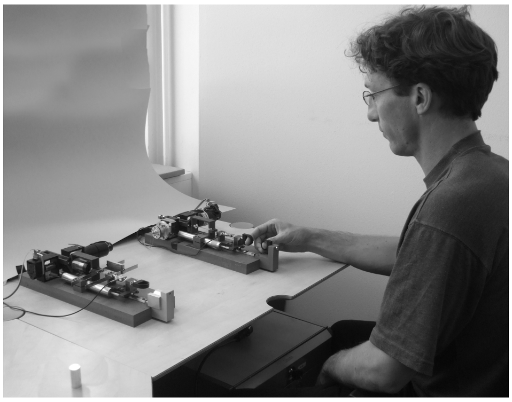

Figure 5.8: *The haptic teleoperator in operation. The operator has his hand in the master device (right) in a comfortable position. Time delay is artificially added by the controller.*

Instability Detection

Different kinds of instabilities can occur in a teleoperation system.

Free air-instabilities are generally out-of-phase movements of coupled masses, e.g. master and slave. The masses move towards each other and apart, in an oscillatory growing way. This is most common for position-based controllers, where the controller acts as a spring between master and slave. However, it can also happen in the flexible elements of the devices.

Contact instability is often seen as "induced by force-sensors" (Qian, 1993), often for the slave device in contact with a stiff environment. It often has a characteristic hammering effect at the master or the slave side.

All these effects are measured as separate conditions in the real-time program, and the program stops the execution whenever an instability occurs and reports what happened. By testing the three controllers under a set of conditions, (varying slave stiffness k_s and increasing time delay T_d) the experimental stability boundary can be found. Each condition is repeated three times to get an estimate of variance.

As a result we get the maximum allowed time delay before instability occurs for each of the controllers and for each slave stiffness.

Performance Measurement

The experimental measurement of the teleoperator stiffness and teleoperator damping is done during the same grasping task as is used for the stability evaluation. The operator moves the device in free air and then presses on a rigid object with a nominal force of 4 N.

The contact force (F_h) and the position (x_h) are logged for free air and stiff contact and used separately. Each set of forces/positions is used as input and output to fit a parametric mass-spring-damper admittance model using a nonlinear least squares model. In this way, a best fit is found on the teleoperator damping from the free air movement, and a fit of the teleoperator stiffness from the constrained motion. The identification is done in the time domain in contradiction to the frequency based measurement method of Aliaga et al. (Aliaga et al., 2004). The reason is that the excitation signal from the human operator has a limited frequency content in this kind of task, so the time-based identification method gives better estimates.

5.3 Results

5.3.1 Slave Stiffness and Stability

The theoretical allowed time delay is plotted along with the experimentally measured allowed time delay in Fig. 5.9. The curves denote the theoretical time delay robustness and the markers show the experimentally measured values. The curves delimit an upper bound of the allowed time delay and the experimental values are indeed below the line for all controllers.

For all measurements, the difference between the experiment and the theory is within the 1 ms measurement resolution.

The key observation is that for all three controllers, the allowed time delay before instability occurs is largest for the lower-stiffness settings. In other words, a lower slave stiffness improves stability.

Furthermore, we can observe that there is only a small difference between the three controllers (PERR/4C/5C). For these specific controller gains, all three controllers have comparable time delay robustness.

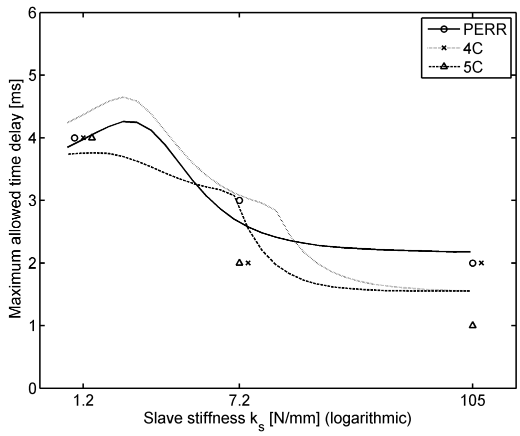

Figure 5.9: *Theoretical (curves) and experimental (markers) time delay robustness (T_d) for different slave stiffness (k_s), for the three control architectures. There is a clear trend towards higher stability robustness for lower slave stiffness.*

Another way to illustrate the stability improvement is to study the effect on the root-locus for a system with a given time delay and to increase the slave stiffness. A Position Error controller with time delay of 3 ms is illustrated in Fig. 5.10.

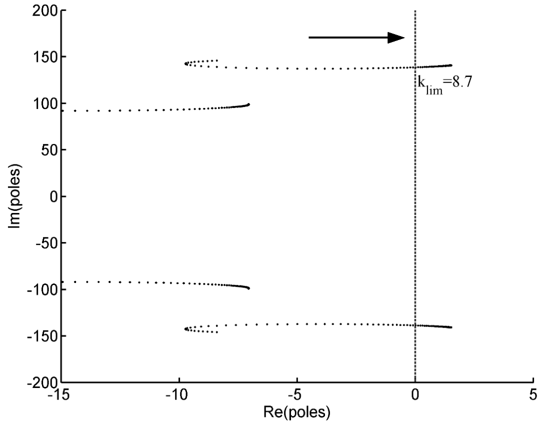

Figure 5.10: *Root-locus diagram for a Position-Error controller with 3 ms time delay. The slave stiffness increases from k_s=1.2 N/mm to 105 N/mm. The stability limit is reached for k_s=8.7 N/mm, at the frequency of 140 rad/s.*

5.3.2 Instabilitites Inspected

There are two major classes of instabilities in the teleoperation system, free air instability and stiff contact instability.

The free air instability occurs when a small position error between the master and slave is amplified with an out-of-phase movement. In Fig.5.11 a PERR controller with a time delay of 5 ms is moved in free air. A small position error (due to sensor noise or friction) induces an exponential increase in the sinusoid amplitude.

The frequency of the oscillation is around 20 Hz and the growth of the position error from indistinguishable to 15 mm occurs in 0.3 s. This quick transition is faster than the reaction time of an operator, so there is no possibility to damp out this oscillation by a reactive action.

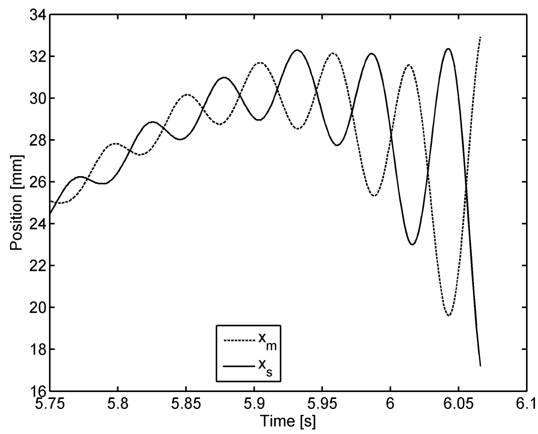

Figure 5.11: *Example of a free-air instability (PERR for a time delay of 5 ms). The position of the master and slave is plotted and the out-of-phase movement is illustrative.*

It is also interesting to notice that the frequency of the oscillation is similar to the prediction from the theoretical value that can be deduced from the root-locus diagram in Fig. 5.10. The pole is crossing the imaginary axis at about 140i, which corresponds to an eigenfrequency of 140 rad/s $\approx$ 22 Hz. This is very close to the frequency observed in the free-air oscillation.

The other type of instability is the contact instability, see Fig.5.12. A 4C controller with a time delay of 4 ms is moved into contact with a stiff object.

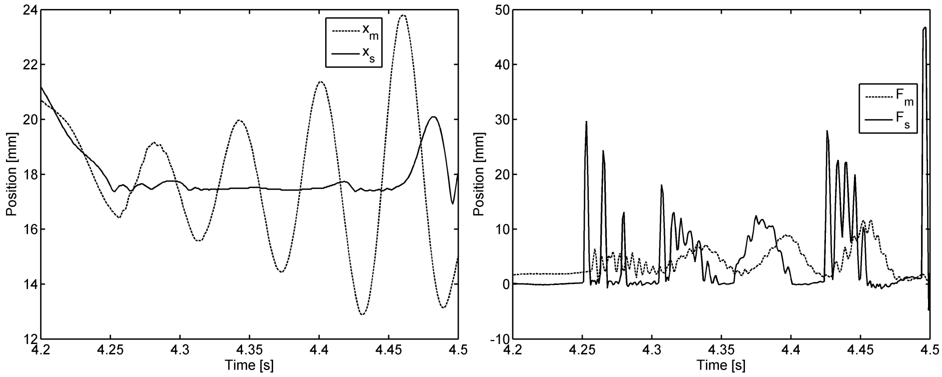

Figure 5.12: *Example of a contact instability (4C for a time delay of 4 ms). The slave moves in free air and contacts the object at $x = 17.5$ mm. The position of the master and slave is plotted (left) along with the forces of master and slave (right).*

The slave device comes in contacts the environment at ($x = 17.5$ mm) and starts a hammering movement with increasing amplitude. The master device follows a more sinusoid trajectory, also with increasing amplitude. The effect of the hammering is most illustrative in the force plot.

The linear analysis method used in this paper can only predict the transition from stable mode to unstable mode, but not how the slave device moves once the instability occurs.

5.3.3 Performance Comparison

The performance of the three controllers is expressed using teleoperator stiffness and damping - a low-order approximation of the complete characteristics. This section describes how the teleoperator stiffness ($\hat{k}$) depends on the choice of controller and slave stiffness (k_s) and how the teleoperator damping ($\hat{b}$) depends on the choice of controller and the time delay.

The teleoperator stiffness is greatly influenced by the slave stiffness in all three controllers used, see Fig.5.13. However, some important phenomena can be distinguished. First of all, there is a significant difference between the three controllers. The PERR controller is remarkably worse than the 4C and 5C controllers, which is consistent with the experimental study by Aliaga et al.(Aliaga et al., 2004). Second, the 5C controller performs better than the 4C for the two lower stiffnesses tested in the experiment. The teleoperator stiffness is almost twice as large for the 5C compared with the 4C controller.

There is a deviation between the experimental data and the theoretical prediction for the stiffest setting for the 4C and 5C controllers. This is due to the small movement of the master device. The device stiffness is 105 N/mm, which gives a movement of only 40 μm, which is in the order of the total play of the master and slave devices, and only ten times the measurement accuracy. Therefore the experimental value of the stiffness is lower.

The influence of time delay on the teleoperator stiffness is negligeable (*not shown*), as the stiffness is the low-frequency asymptotic behaviour of the impedance function. However, the influence on the damping is more noticable, see Fig.5.14. The teleoperator damping is presented for a slave stiffness of 7.2 N/mm and for increasing time delay. The damping increases for higher time delay both for the theoretical model and the experiment.

However, this is somewhat contradictory to how the device feels. As the time delay increases, the phase margin shrinks and the device gets closer and closer to instability. Therefore it feels as if the damping actually *decreases*. The reason for this contradiction is that the simple mass-spring-damper model becomes less and less accurate for increasing time delay. In effect, the higher-order effects include negative damping that work destabilizing.

Regarding the validity of the measurement, the spread in the measured damping is much larger than the spread in the stiffness, (cf. Figs. 5.13 and 5.14). This is mainly due to the inaccuracy in the measurements. The

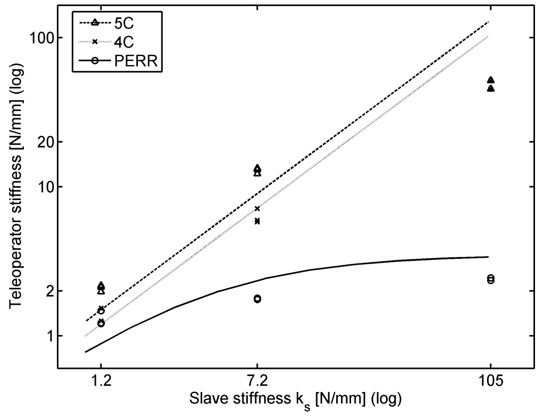

Figure 5.13: *The theoretical and experimental values for the teleoperator stiffness for the three controllers and increasing slave stiffness (k_s). Time delay is 1 ms.*

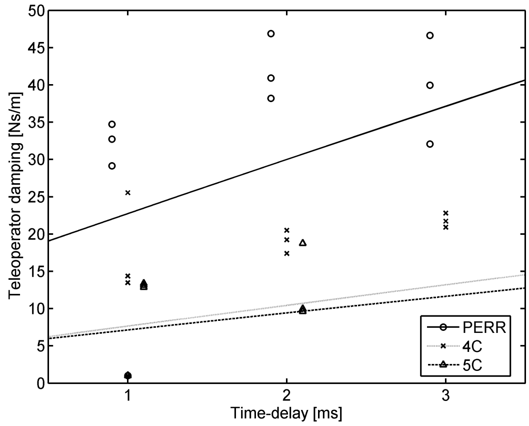

Figure 5.14: *The theoretical and experimental values for the teleoperator damping for the three controllers and increasing time delay (T_d). The slave stiffness (k_s) is 7.2 N/mm. There are no experimental values for the 5C controller for the three second case because that configuration was unstable.*

velocity is not measured, only estimated from the position measurements, which introduces a larger variation in velocity-dependent parameters in the identification procedure. Furthermore, the theoretical model was identified using a wide-band multisine excitation signal and here the excitation signal was the operator movement, which is of a smaller frequency spectrum.

The influence of slave stiffness on the teleoperator damping is negligeable (*not shown*), as the slave stiffness is only active in contact mode and the damping is measured in the free air.

5.4 Discussion

A comparison between the theoretical and experimental stability in Fig. 5.9 allows a number of interesting observations:

First of all, the experimental results do accurately validate the model, as it can reproduce the main characteristics of the stability for the teleoperation system, for a wide range of controllers and working conditions. Therefore we can conclude that the linear analysis method is useful for the analysis of haptic teleoperation systems.

Second, there is an non-smooth transition in the curves for the 4C and 5C controllers, around the middle stiffness, which is related to the transition between two failure modes. There is also a maximum around 2 N/mm on the stability curves in Fig. 5.9, which implies that there is an optimal stiffness for the 4C and 5C controllers.

The quantitative stability improvement is a factor two for the range of slave stiffnesses tested, and it is similar for all three controllers on this experimental setup. That difference is significant, but may for some applications be insufficient. It is of course possible to use the low-stiffness slave, as proposed in this paper, in combination with another time delay compensation method to achieve even larger robustness.

The influence on performance from the slave stiffness is most striking for the *teleoperator stiffness*. The dramatic influence on the teleoperator stiffness, as shown in Fig. 5.13, is to be expected because the slave stiffness is in series with the environment stiffness.

This is a clear illustration of the stability/performance trade-off. The lower the stiffness, the better the stability - at the expense of the performance (expressed using the teleoperator stiffness).

However, part of the performance loss can be compensated. By using the deflection information, as in the 5C controller, it is possible to compensate for part of this stiffness and to present it to the operator twice as stiff as with the uncompensated 4C controller.

The influence of slave stiffness on the *teleoperator damping* is insignificant. The teleoperator damping is somewhat influenced by the time delay, and thereby the controllers can also be compared for a set of working conditions. However, for increasing time delays, the simple mass-spring-damper model becomes inaccurate so the meaning of these values is questionable.

Finally, the three controller architectures with increasing complexity can be compared. The stability characteristics is quite similar for all controllers. On the other hand, both for *teleoperator stiffness* and *teleoperator damping*, there is a clear distinction of performance.

The simple PERR controller performs the worst, outperformed by the more complex 4C controller. The most complex 5C controller even better, even though the difference in performance compared with the 4C controller is quite small. The novel deflection compensation mechanism in the 5C controller in this paper is relatively primitive and future research can strive to find a better way to use this information.

5.5 Conclusions

The main focus of this research is the trade-off between stability, performance and complexity. A novel mechanical design of the slave device, the compliant section with the slave stiffness (k_s), is evaluated for influence on stability and performance, for three controllers of increasing complexity.

The main conclusion from this research is:

- A lower slave stiffness improves stability for all three teleoperator architectures
- The stability boundary of the three controllers is similar
- A lower slave stiffness reduces performance in terms of *teleoperator stiffness*, but does not affect *teleoperator damping*
- The performance of the controllers is increasing from: (poor) Position Error, 4-Channel to (excellent) 5-Channel
- The novel 5-Channel scheme allows for a better tradeoff between stability and performance, at the cost of one additional position sensor
- A classical linear analysis method can accurately predict the stability and performance characteristics of the teleoperator system

Appendix - Device components

The teleoperator master and slave device components were identified using multisine identification of a linear model in the time domain. For specific components (motors, sensors etc.), see (Fritz et al., 2004).

Numerical values for the mechanical components are given as mean value and standard deviation of the estimate:

Table 5.1: *Numerical values of system components*

Component	*Value*
m_{m}	0.376±0.0005 kg
b_{m}	4.48±0.03 Ns/m
$m_{\mathrm{s,b}}$	0.242±0.0005 kg
$m_{\mathrm{s,t}}$	0.111±0.0005 kg
b_{sb}	4.0±0.1 Ns/m
b_{st}	1.2±0.08 Ns/m
b_{s}	25.1±0.3 Ns/m
k_{s}	1.2 ±3%, 7.2±2%, 105±15% N/mm

Detailed Models

This section presents detailed models of the soft slave admittance, and the complete expression for the H-matrix.

Slave Admittance

The slave admittance is a fourth order dynamical system for a compliant slave system, see (5.2). Expressed in mechanical model terms, the admittance component are:

$$
\begin{aligned}
&Y_{\mathrm{s,ee}} = \frac{V_{\mathrm{e}}}{F_{\mathrm{e}}} = \\
&-\frac{m_{\mathrm{s,b}} s^2 + (b_{\mathrm{sb}} + b_{\mathrm{s}})\, s + k_{\mathrm{s}}}{m_{\mathrm{s,b}} m_{\mathrm{s,t}} s^3 + ((b_{\mathrm{sb}} + b_{\mathrm{s}})\, m_{\mathrm{s,t}} + (b_{\mathrm{st}} + b_{\mathrm{s}})\, m_{\mathrm{s,b}})\, s^2 + (k_{\mathrm{s}} m_{\mathrm{s,t}} + k_{\mathrm{s}} m_{\mathrm{s,b}} + (b_{\mathrm{sb}} + b_{\mathrm{s}})\, b_{\mathrm{st}} + b_{\mathrm{s}} b_{\mathrm{sb}})\, s + (b_{\mathrm{st}} + b_{\mathrm{sb}})\, k_{\mathrm{s}}} \\
&Y_{\mathrm{s,be}} = \frac{V_{\mathrm{e}}}{F_{\mathrm{sc}}} = \\
&\frac{b_{\mathrm{s}} s + k_{\mathrm{s}}}{m_{\mathrm{s,b}} m_{\mathrm{s,t}} s^3 + ((b_{\mathrm{sb}} + b_{\mathrm{s}})\, m_{\mathrm{s,t}} + (b_{\mathrm{st}} + b_{\mathrm{s}})\, m_{\mathrm{s,b}})\, s^2 + (k_{\mathrm{s}} m_{\mathrm{s,t}} + k_{\mathrm{s}} m_{\mathrm{s,b}} + (b_{\mathrm{sb}} + b_{\mathrm{s}})\, b_{\mathrm{st}} + b_{\mathrm{s}} b_{\mathrm{sb}})\, s + (b_{\mathrm{st}} + b_{\mathrm{sb}})\, k_{\mathrm{s}}} \\
&Y_{\mathrm{s,be}} = \frac{V_{\mathrm{sb}}}{F_{\mathrm{e}}} = \\
&\frac{b_{\mathrm{s}} s + k_{\mathrm{s}}}{m_{\mathrm{s,b}} m_{\mathrm{s,t}} s^3 + ((b_{\mathrm{sb}} + b_{\mathrm{s}})\, m_{\mathrm{s,t}} + (b_{\mathrm{st}} + b_{\mathrm{s}})\, m_{\mathrm{s,b}})\, s^2 + (k_{\mathrm{s}} m_{\mathrm{s,t}} + k_{\mathrm{s}} m_{\mathrm{s,b}} + (b_{\mathrm{sb}} + b_{\mathrm{s}})\, b_{\mathrm{st}} + b_{\mathrm{s}} b_{\mathrm{sb}})\, s + (b_{\mathrm{st}} + b_{\mathrm{sb}})\, k_{\mathrm{s}}} \\
&Y_{\mathrm{s,bb}} = \frac{V_{\mathrm{sb}}}{F_{\mathrm{sc}}} = \\
&\frac{m_{\mathrm{s,t}} s^2 + (b_{\mathrm{st}} + b_{\mathrm{s}})\, s + k_{\mathrm{s}}}{m_{\mathrm{s,b}} m_{\mathrm{s,t}} s^3 + ((b_{\mathrm{sb}} + b_{\mathrm{s}})\, m_{\mathrm{s,t}} + (b_{\mathrm{st}} + b_{\mathrm{s}})\, m_{\mathrm{s,b}})\, s^2 + (k_{\mathrm{s}} m_{\mathrm{s,t}} + k_{\mathrm{s}} m_{\mathrm{s,b}} + (b_{\mathrm{sb}} + b_{\mathrm{s}})\, b_{\mathrm{st}} + b_{\mathrm{s}} b_{\mathrm{sb}})\, s + (b_{\mathrm{st}} + b_{\mathrm{sb}})\, k_{\mathrm{s}}}
\end{aligned}
\tag{5.10}
$$

Complete Hybrid Matrix for a Hard-Soft Teleoperator

The Hybrid matrix, expressed using the admittances of the devices ($Y_{\mathrm{m}}(s)$ and $Y_{\mathrm{s}}(s)$) and the controller transfer functions ($k_{ij}(s)$):

$$
\begin{aligned}
h_{11} &= \\
&-\frac{\left(Y_{\mathrm{m}}Y_{\mathrm{s,be}}k_{12}-Y_{\mathrm{s,be}}\right)k_{25}+\left(Y_{\mathrm{m}}Y_{\mathrm{s,bb}}k_{12}-Y_{\mathrm{s,bb}}\right)k_{24}+\left(-Y_{\mathrm{m}}Y_{\mathrm{s,be}}k_{15}-Y_{\mathrm{m}}Y_{\mathrm{s,bb}}k_{14}\right)k_{22}-Y_{\mathrm{m}}k_{12}+1}{\left(Y_{\mathrm{m}}Y_{\mathrm{s,be}}k_{11}+Y_{\mathrm{m}}Y_{\mathrm{s,be}}\right)k_{25}+\left(Y_{\mathrm{m}}Y_{\mathrm{s,bb}}k_{11}+Y_{\mathrm{m}}Y_{\mathrm{s,bb}}\right)k_{24}+\left(-Y_{\mathrm{m}}Y_{\mathrm{s,be}}k_{15}-Y_{\mathrm{m}}Y_{\mathrm{s,bb}}k_{14}\right)k_{21}-Y_{\mathrm{m}}k_{11}-Y_{\mathrm{m}}} \\
h_{12} &= \\
&\frac{\left(\left(Y_{\mathrm{s,bb}}Y_{\mathrm{s,ee}}-Y_{\mathrm{s,be}}Y_{\mathrm{s,eb}}\right)k_{14}-Y_{\mathrm{s,be}}k_{13}\right)k_{25}+\left(\left(Y_{\mathrm{s,be}}Y_{\mathrm{s,eb}}-Y_{\mathrm{s,bb}}Y_{\mathrm{s,ee}}\right)k_{15}-Y_{\mathrm{s,bb}}k_{13}\right)k_{24}+\left(Y_{\mathrm{s,be}}k_{15}+Y_{\mathrm{s,bb}}k_{14}\right)k_{23}+Y_{\mathrm{s,ee}}k_{15}+Y_{\mathrm{s,eb}}k_{14}+k_{13}}{\left(Y_{\mathrm{s,be}}k_{11}+Y_{\mathrm{s,be}}\right)k_{25}+\left(Y_{\mathrm{s,bb}}k_{11}+Y_{\mathrm{s,bb}}\right)k_{24}+\left(-Y_{\mathrm{s,be}}k_{15}-Y_{\mathrm{s,bb}}k_{14}\right)k_{21}-k_{11}-1} \\
h_{21} &= \\
&\frac{\left(Y_{\mathrm{m}}Y_{\mathrm{s,be}}k_{11}+Y_{\mathrm{m}}Y_{\mathrm{s,be}}\right)k_{22}+\left(Y_{\mathrm{s,be}}-Y_{\mathrm{m}}Y_{\mathrm{s,be}}k_{12}\right)k_{21}}{\left(Y_{\mathrm{m}}Y_{\mathrm{s,be}}k_{11}+Y_{\mathrm{m}}Y_{\mathrm{s,be}}\right)k_{25}+\left(Y_{\mathrm{m}}Y_{\mathrm{s,bb}}k_{11}+Y_{\mathrm{m}}Y_{\mathrm{s,bb}}\right)k_{24}+\left(-Y_{\mathrm{m}}Y_{\mathrm{s,be}}k_{15}-Y_{\mathrm{m}}Y_{\mathrm{s,bb}}k_{14}\right)k_{21}-Y_{\mathrm{m}}k_{11}-Y_{\mathrm{m}}} \\
h_{22} &= \\
&-\frac{\left(\left(Y_{\mathrm{s,bb}}Y_{\mathrm{s,ee}}-Y_{\mathrm{s,be}}Y_{\mathrm{s,eb}}\right)k_{11}+Y_{\mathrm{s,bb}}Y_{\mathrm{s,ee}}-Y_{\mathrm{s,be}}Y_{\mathrm{s,eb}}\right)k_{24}+\left(-Y_{\mathrm{s,be}}k_{11}-Y_{\mathrm{s,be}}\right)k_{23}+\left(\left(Y_{\mathrm{s,be}}Y_{\mathrm{s,eb}}-Y_{\mathrm{s,bb}}Y_{\mathrm{s,ee}}\right)k_{14}+Y_{\mathrm{s,be}}k_{13}\right)k_{21}-Y_{\mathrm{s,ee}}k_{11}-Y_{\mathrm{s,ee}}}{\left(Y_{\mathrm{s,be}}k_{11}+Y_{\mathrm{s,be}}\right)k_{25}+\left(Y_{\mathrm{s,bb}}k_{11}+Y_{\mathrm{s,bb}}\right)k_{24}+\left(-Y_{\mathrm{s,be}}k_{15}-Y_{\mathrm{s,bb}}k_{14}\right)k_{21}-k_{11}-1}
\end{aligned}
\tag{5.11}
$$

Position Error Controller (PERR)

The position error controller is one of the classical controllers in teleoperation. It is cheap to implement, as there is no need for force sensors. The position feedback gain was chosen to be 2500 N/m, so the K-matrix became:

$$K = \begin{bmatrix} 0 & -(\frac{2500}{s}) & 0 & \frac{2500}{s}\,e^{-T_{\mathrm{d}}s} & 0 \\ \\ 0 & \frac{2500}{s}\,e^{-T_{\mathrm{d}}s} & 0 & -\frac{2500}{s} & 0 \end{bmatrix} \tag{5.12}$$

In the theoretical analysis the time delay was approximated with a first order Taylor expansion ($e^{-T_{\mathrm{d}}s} \approx 1 - sT_{\mathrm{d}}$).

Lawrence 4-Channel (4C) Controller

The 4-Channel controller gains were selected according to the "Transparency Optimization" method presented in (Lawrence, 1993): (There is a direct relationship between the Lawrence/Salcudean notation and the K-matrix notation)

$$\begin{aligned} K &= \begin{bmatrix} k_{11} & k_{12} & k_{13} & k_{14} & k_{15} \\ k_{21} & k_{22} & k_{23} & k_{24} & k_{25} \end{bmatrix} \\ &= \begin{bmatrix} C_6 & -C_{\mathrm{m}} & -C_2 & -C_4 & 0 \\ C_3 & C_1 & -C_5 & -C_{\mathrm{s}} & 0 \end{bmatrix} \\ &= \begin{bmatrix} 0 & -(2+\frac{2500}{s}) & -1\,e^{-T_{\mathrm{d}}s} & (7+\frac{2500}{s})\,e^{-T_{\mathrm{d}}s} & 0 \\ \\ 1\,e^{-T_{\mathrm{d}}s} & (7+\frac{2500}{s})\,e^{-T_{\mathrm{d}}s} & 0 & -(2+\frac{2500}{s}) & 0 \end{bmatrix} \end{aligned} \tag{5.13}$$

5-Channel (5C) Controller

The gains were selected according to the method presented by Lawrence, (Lawrence, 1993), and a weight-factor that selected a part of the velocity information from the slave base and the tip. For these experiments, the weight factor was chosen to be 0.5.

$$K = \begin{bmatrix} 0 & -(2+\frac{2500}{s}) & -1\,e^{-T_{\mathrm{d}}s} & 0.5\,(7+\frac{2500}{s})\,e^{-T_{\mathrm{d}}s} & 0.5\,(7+\frac{2500}{s})\,e^{-T_{\mathrm{d}}s} \\ \\ 1\,e^{-T_{\mathrm{d}}s} & (7+\frac{2500}{s})\,e^{-T_{\mathrm{d}}s} & 0 & -(2+\frac{2500}{s})\,0.5 & -(2+\frac{2500}{s})\,0.5 \end{bmatrix} \tag{5.14}$$

This gain selection is conservative and well-balanced. It allows somewhat higher teleoperator stiffness, at the cost of one extra sensor and slightly lower stability robustness.

Chapter 6

A novel 3-DOF Planar Haptic Teleoperation System

G.A.V. Christiansson
Proceedings of IEEE WorldHaptics Conference 2007, pp. 361-366, Tsukuba, Japan

A novel planar 3-degree of freedom (dof) haptic teleoperator based on the "hard-soft" principle is presented. The mechatronic concept of using a stiff master and a compliant slave has previously been shown to improve haptic teleoperation performance in 1-dof teleoperation, and the concept can now be experimentally verified for more realistic tasks.

The master device consists of a stiff double-rhomb force-redundant parallel robot and the slave device is a serial robot with flexible joints.

Identification experiments show that the teleoperation setup can achieve high stiffness (>1.5 N/mm) for the master side and low stiffness on the slave side (0.100 N/mm).

6.1 Introduction

It is difficult to optimize the design of teleoperators, both regarding the controller and the mechanical realization. In the early days, optimization was done mainly based on classic performance criteria for robots, e.g. high stiffness and accurate positioning. The last few years, a number of studies have looked into the perceptual side of the design criteria: Which information is most important for the operator to complete a certain task?

One of the main insights in the sensomotorics of manipulation is that humans move with relatively low frequencies (often < 1 Hz) but that our sensoric system is sensitive in much higher frequencies (up to 1000 Hz) (Daniel and McAree, 1998). One example of task where high frequency information is important is tool interaction with hard environments (LaMotte, 2000). It can therefore be useful to have low bandwidth capabilities in the forwards channel from the human operator to the environment and much higher bandwidth in the feedback channel.

This can be achieved in many different ways. One path, followed by Kuchenbecker et al. (Kuchenbecker et al., 2006) consists of using identical mechanics on master and slave and of adding an accellerometer at the slave. The contact information is used in a feedforward path to the master device.

Another path is to look into the complete mechatronic model and also change the mechanical design of the master and slave devices (Christiansson et al., 2006a; Christiansson and v. d. Helm, 2007). It was shown that a hard-soft teleoperator achieves high performance with appealing stability characteristics in contact with stiff environments. Furthermore, the use of a compliant section in the slave device reduces impact forces because the end-effector inertia is decoupled from the significantly larger inertia of the linkage and motor system. This is an important factor for application in sensitive environments.

The concept of using a stiff master device and a compliant slave device should also be validated in other tasks, of higher dimensionality. This paper presents the design of a 3-dof planar haptic teleoperator for interaction with a stiff environment.

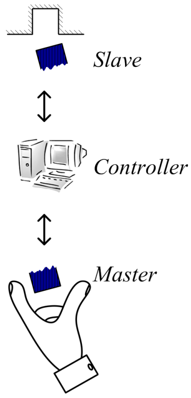

Figure 6.1: *Teleoperator task illustration: The teleoperator allows remote assembly tasks, e.g. peg-in-hole.*

6.2 Design Requirements

The teleoperator will be used in experimental studies of planar 3-dof tasks such as assembly, peg-in-hole and contour following.

6.2.1 Task Requirements

The teleoperator will be used for precision assembly tasks. This type of precision tasks are preferrably performed with the arm in a resting position and the operator working with his wrists and hands. The nominal workspace of the device is therefore chosen to be a square with ± 50 mm in x- and y- directions, with an allowed rotation of $\pm 45°$. This choice for workspace size is similar to the workspace of the Phantom Omni (SensAble, 2006), the ForceDimension Omega (ForceDimension, 2006) and the Sirouspour/Salcudean Double Pantograph (Sirouspour et al., 2000).

This type of precision tasks are performed with relatively small speeds (<50 mm/s) and voluntary movement with frequencies up to 1 Hz (Christiansson et al., 2006b). The contact with a stiff object, on the other hand, generates interesting information up to hundreds of hertz, so a higher master force bandwidth is necessary, preferrably exceeding 100 Hz.

6.2.2 Hard-Soft Requirements

The hard-soft concept of haptic teleoperation is based on a high-stiffness master device, which can accurately represent a stiff environment, and a slave robot that represents the human operator, which in this context is relatively soft.

We choose a minimum master stiffness of: 1 N/mm, enough to provide the illusion of a solid object as long as other modalities are consistent. A corresponding maximum slave stiffness, that can represent the stiffness of the human hand is chosen to be of 0.1 N/mm.

6.2.3 Perceptual Requirements

The psychophysics of haptics for precision tasks gives additional requirements and possibilities. For example, the requirements on absolute static error in force and position can be relatively low, in the order of a few %, because it will not be noticed (Gaydos, 1958). However, the sensitivity for small relative errors must be higher, in the order of the tolerances of the task or in the tens of microns.

Based on our experiments on 1-dof grasping tasks (Christiansson et al., 2006b) we chose the same positioning accuracy of at least 30 micrometers in x- and y-direction, which is equivalent to 10 mrad in ϕ-direction.

6.2.4 Derived Requirements

Based on experience from precision tasks (Christiansson et al., 2006b), we can estimate the necessary end-point forces and accelerations necessary. The typical fingertip forces during manipulation is around 4 N, for a majority of users, even though it has been observed that certain subjects use forces as small as 1 N and others use higher forces even exceeding 10 N. Therefore the choice is to allow peak forces up to 15 N, and static forces to 7.5 N.

6.3 Design

The design of the teleoperator system consists of a trade-off between versatility, complexity and cost. We have chosen for standard industrial components wherever possible, to keep the cost at a reasonable level, and allow straightforward technology transfer from lab to applications.

6.3.1 Master Device

The design requirements for the master device - of high stiffness and high force bandwidth - lead to a parallel kinematic design. The main advantage of a parallel design is that high stiffness can be achieved with a relatively low moving mass, with the flip side that the device itself occupies a large volume compared to the workspace. For most applications that is not a problem. We chose to look into the design of the Salcudean "double-pantograph" design introduced in (Sirouspour et al., 2000; Salcudean and Stocco, 2000).

The original design had to be changed to allow for higher end-point forces. We chose for a capstan-transmission using 17 strand steel wire between the motors and the base links, with a transmission ratio of 1:6. Gears were avoided due to problems with backlash and vibrations.

The kinematic optimization of the mechanical structure in Fig. 6.2 was done using the method of Global Isotropy Index (GII) introduced by Salcudean and Stocco (Salcudean and Stocco, 2000). The idea is to look at the variation of the eigenvectors of the Jacobian matrix (from q_1, q_2 to x, y) throughout the workspace. It is equivalent to striving for manipulability ellipsoids that are as "spherical" as possible. The base length (L_1) and first link length (L_2) are optimized for a given constant second link length ($L_3 = 0.12m$).

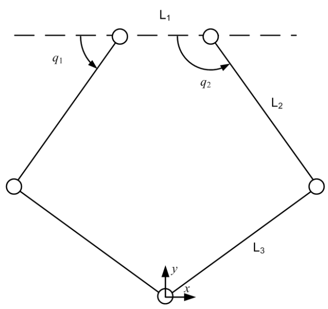

Figure 6.2: *One of the two master "pantographs". The second link length ($L_3 = 0.12m$) is held constant, and the kinematics optimization parameters are the base length (L_1) and first link length (L_2).*

An image of the search space is shown in Fig. 6.3, where we look for a global optimum, marked with an 'x' (*lower right*). For the practical implementation, the distance between the joints in the base, the base length L_1 is restricted to positive values to avoid crossing arms, which gives another optimum, marked with a 'o' (*center*). This optimum is a design where the all four base joints coincide ($L_1 = 0$), and all link lengths are identical. This is the design we chose.

It is worth noting that the GII function is almost identical in a band running from upper-left to lower-right part of the graph. The upper-left alternative is the short-base pentagonical form chosen by Salcudean, where the first link must be somewhat shorter than the second link. One advantage of the identical-link approach is that both the forwards and inverse kinematic transformations are significantly easier to express on closed form. The link to connect the two pantographs and the end-effector was chosen to have a joint-separation length of 20 mm, to allow for the necessary precision in rotation.

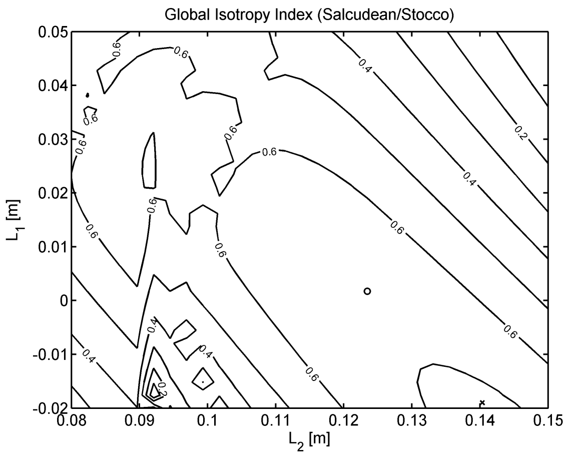

Figure 6.3: *Isotropy Index for two design parameters - base joint distance (L_1) and first link length (L_2), for a constant second link ($L_3 = 0.12m$).*

To allow for the maximum force and acceleration, while keeping the motor inertia balanced with load, both the motor constant and the maxiumum allowed current is important. Early on in the design phase we decided to work with a force sensor at the end-effector of the master device. The main advantage is that friction and damping can be easily compensated, and also inertia to some extent.

There are four actuators for three dof of motion, which means that there are theoretically infintely many combinations of motor torques that would give the same net force at the end effector - force redundancy resolution. Many schemes have been proposed to choose the forces in an optimal way, ranging from power minimization, internal force minimization (Dasgupta and Mruthyunjaya, 1998), or to control a certain pre-loading force in the end-effector linkage (Muller, 2005). We chose to minimize the internal force in the end-effector linkage using a static transformation similar to the jacobian pseudo-inverse method used by Salcudean et al. (Sirouspour et al., 2000).

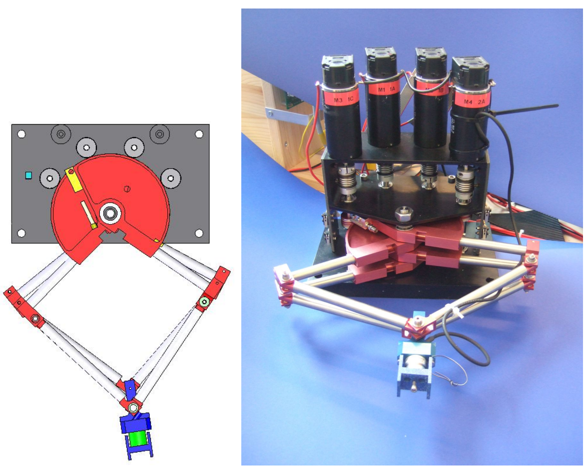

Figure 6.4: *The High Stiffness Master Device: A double-rhomb parallel robot with force redundancy, drawing (left) and realization (right).*

6.3.2 Slave Device

The requirements for the slave device leads to flexible link and flexible joint robots. We chose for a flexible-joint robot, because it was easier to measure joint angles and joint deflection than link deflection. The complete design is a three-link serial robot with flexible joints, shown in Fig. 6.5.

The actuators are all positioned in the base of the robot, and connected to each joint via a compliant transmission. The first base joint is driven directly via a leaf spring, and the second joint via a four-bar linkage and a second leaf spring. The third joint is driven via cables over the other two joints, with wire springs in series.

All in all it means that the positioning bandwidth is within the bounds, and the moving mass at the end-effector can be kept at a minimum to reduce impact forces and enhance sensitivity.

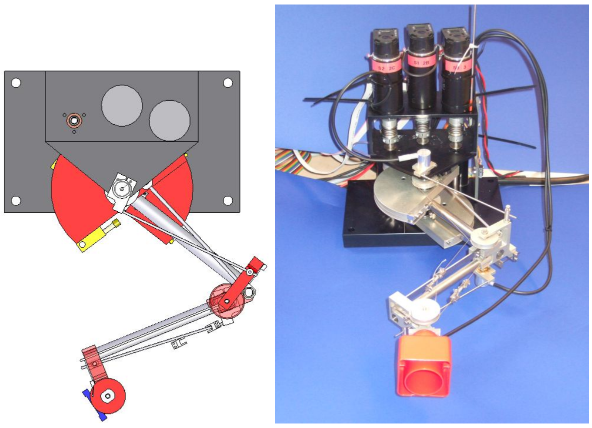

Figure 6.5: *The Soft Slave Device: A serial planar robot with intrinsic compliance, drawing (left) and realization (right).*

The slave device is an example of 3-dof *series elastic actuation* (Pratt et al., 2002).

6.3.3 Controller

The controller design is based on a two-layer structure. At the master and slave side, there is an inner loop that linearizes the kinematics and decouples the dynamics in the three degrees of freedom. Outside this loop, a bilateral cartesian controller is placed, which communicates both force and position setpoints to the master and the slave.

The balance between force and position control is different for master and slave. The master device stiffly replicates the end-effector movement of the slave and therefore the emphasis is on the position control. The slave on the other hand is mainly force controlled, to follow the human intended force. To be robust to variations in the environment impedance, from free air to stiff contact, that is not enough, and there is also some force feedback to the master, as well as some position feedback to the slave.

For the preliminary measurements presented in this paper, a quasistatic approach has been taken, where the bilateral controller is formulated in cartesian space and a static transformation from control torque to motor torques is used at both master and slave side.

The master side controller is presented in Fig. 6.6. The static force redundancy resolution function minimizes the internal force in the crank-link segment, by sharing the forces and torques equally on the two rhombs, similar to the method of the Jacobian pseudoinverse (Hashtrudi-Zaad and Salcudean, 2002).

The slave side controller is shown in Fig. 6.7. The joint deflection is $x_{s,\gamma}$ is used to estimate the joint torques (Pratt et al., 2002), and is used to estimate the contact forces F_{e}.

The two cartesian controllers are shown together as one block in Fig. 6.8.

The first preliminary controllers implemented are a simple position-error controller, where the position and velocity difference between master and slave is used to generate the control effort, and a version of the Lawrence 4-Channel Controller (Lawrence, 1993).

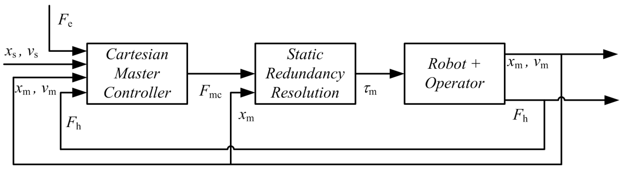

Figure 6.6: *The principal control structure for the master device. A static transformation is used to convert from controlled forces in cartesian space to joint torques.*

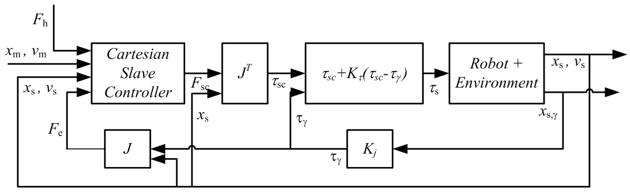

Figure 6.7: *Control structure for the slave. The joint deflection $x_{s,\gamma}$ is used to estimate joint torque and is used in an inner torque-servo loop.*

6.4 Realization

The master and slave devices were produced in the Delft University Central Workshop, in aluminum and stainless steel, and assembled in the Delft Haptics Laboratory. The master and slave devices are shown in Fig. 6.4 and Fig. 6.5.

The master device implementation involved a number of interesting trade-offs, including the choice of transmission ratio, end-effector crank length to balance force and torque needs and cost/benefit for the accuracy of each sensor. The position sensors used in the master device are incremental rotary encoders on the motor shaft, and a force sensor mounted on the end-effector.

To achieve a positional accuracy of 0.03 mm, the rotary encoders have a resolution of 4000 ticks/revolution, which can be attained with the standard Agilent HEDL-5500 optical encoder.

The force sensor chosen is a ATI Nano 17-SI 12, which allows for accurate force and torque measurement up to 12 N and 0.12 Nm. The limitation of the force and torque resolution (0.01 N and 0.0005 Nm - equivalent to only 11 bits) is probably due to the six single-ended analog inputs of the AD card used. The specifications state one bit less noise if connected to a double-ended analog input. Unfortunately, the sensor we got had a different cable connection than in the specification, which increased the end-effector crank length with 50%.

The controller was implemented on a standard Compaq Pentium III PC, using the Mathworks xPCTarget realtime operating system (Mathworks, Natick, MA, USA). The achievable controller servo rate was 1 kHz, limited by the xPCTarget operating system. Higher update rates have been reported from using e.g. the open source alternative RTAI Linux, and we are currently investigating whether or not to switch to this platform.

The controllers for the master and slave systems are currently implemented in a single computer, because the distance between master and slave is short, as in many applications. The interfacing to the computer is done with one Quanser Q8 card (Quanser Inc. Markham, On., Canada) and one NI PCI6601 encoder card (National Instruments, Austin, TX, USA). However, the single-ended analog inputs of the Quanser card may be a limitation for the accuracy of the force measurements. The motors on the master and two of the slave motors are driven with Aerotech BL-20 linear amplifiers (Aerotech Inc. Pittsburg, PA, USA). The motor for the tip joint of the slave is driven with a Maxon LSC linear amplifier (Maxon Gmbh, Switzerland). All motors, on both master and slave are of the type Maxon RE35, 90W DC brushed motor.

The mechanical design of the slave device was somewhat more complex, to combine the concept of series-elastic actuaction while positioning the motors in the fixed base, and we wanted to have easily-replacable spring elements.

The slave device sensorization consists of six optical encoders which measures the motor angles and the absolute angles at the joints. The position sensors chosen for the slave are optical encoders. On the motor

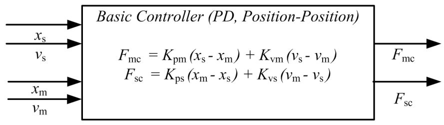

Figure 6.8: *Example Controller: A position-error controller. The controller position and velocity gains are higher on the master than slave side to allow hard-soft teleoperation.*

shaft we could use identical Agilent encoders as the master device. The sensor on the joints that measure the deflected rotation, the resolution must be higher with the same factor as the capstan transmission ratio. Here, ScanCon 2MC-H5000 encoders were chosen which give 20000 ticks per revolution. A relative end-point position resolution of less than 35 μm and $0.01\mathrm{deg}$ in the whole nominal workspace was thereby achieved.

The deflection in the flexible joints is also measured with this resolution, and the relative force resolution is therefore 0.04 N/m at the endpoint. However, the coulomb friction amount to a maximum of 0.1 N, which is the effective absolute limit of force resolution at the slave side.

6.5 Preliminary Results

The main result of this paper is the realization of the teleoperator, and the main design goals were met.

Achieved stand-alone master stiffness is 1.6 N/mm for both x- and y- directions, and 1.5 Nm/rad for the rotation. In the y-direction, the maximum static force is 18 N, which is more than enough. However, the maximum force in the x-direction is only 4.5 N, which is too low.

The underlying reason is that the design of the end-effector crank has two big problems. First of all, the grip is far from the rotation center between the joints, which creates a strong coupling between the x- and the ϕ- degrees of freedom. The leverage of the crank generates a significant torque for relatively low forces in the x-direction, which causes the drive system to saturate. Therefore the maximum force in the x-direction is lower lower than the requirements. A second problem with the crank is the short distance between the joints, which gives a too poor rotary resolution. Both these problems can be addressed with the redesign of one single mechanical component, e.g. like the Salcudean version (Salcudean and Stocco, 2000).

We found that optimizing the kinematics by looking at the isotropy alone is not the whole story. Isotropy gets better with longer arms, because the relative joint movement gets smaller. However, this is counteracted by a higher absolute value of the Jacobian, which results in lower position accuracy for the same sensor. Furthermore, it also means that the total moving inertia is higher. We suggest that an *extended GII-function* also should include a quantification of these effects.

The dynamics of the master and slave devices was identified using a parametric model fit, using a multisine excitation signal, for the method see (Christiansson, 2004). For the master, the end-effector inertia was identified to $260{\pm}10$ g in x- and y- directions and $0.025gm^2$ in the ϕ-direction. The slave device intrinsic stiffness does effectively decouple the end-effector mass (50 g) from the motor and capstan mass (230 g), in the radial direction. The inertia is lower in the other directions, and with a quite large variation over the workspace.

We also have an extra sensor available in addition to what has been presented above: an accellerometer on the tip of the slave device, which captures the interaction information accurately. The next step will be to include this information in the force signal presented by the master device to the operator. We believe that the for high frequency contact information, the acceleration of the slave is most relevant to present to the operator, and for low frequencies the force. The soft-slave configuration is in effect a low-frequency force sensor, with a decoupled low-mass end-effector that easily picks up high-frequency oscillations. This way, the hard-soft approach can be combined with ”high frequency acceleration matching” (Kuchenbecker et al., 2006).

6.6 Conclusion

A novel teleoperator experimental setup has been developed with a parallel redundant master device, and a flexible-joint serial slave device. The concept of hard-master and soft-slave is hereby extended to three dimensions.

Part III

Human Performance vs. Machine Performance

Chapter 7

Size and Stiffness Discrimination in Teleoperation

G.A.V. Christiansson, R.Q. van der Linde, F.C.T. van der Helm
(in press) IEEE Transactions on Robotics

Human task performance in teleoperation depends on many factors related to the teleoperation system. A haptic teleoperation system must transmit at least as much information to the operator as he/she needs to perform a given task.

Two typical teleoperated grasp tasks — size and stiffness discrimination — were studied to investigate how an improvement of device performance influences the human capabilities. The device characteristics that were altered were: teleoperator stiffness (size and stiffness discrimination) and teleoperator damping (size discrimination only).

It was found that there was no significant influence *from teleoperator stiffness (0.15-32 N/mm) on size discrimination. There was* no significant influence *from teleoperator stiffness (0.15-1.20 N/mm) on stiffness discrimination (object stiffnesses 0.21-1.81 N/mm). There was* no significant influence *from teleoperator damping (1-15 Ns/m) on size discrimination.*

Furthermore, when comparing teleoperated performance with direct interaction using bare hands or with the fingers in a bracket, it was found that:

- *teleoperated performance with reduced stiffness is equally good as bare hand performance for the size discrimination task;*
- *teleoperation with very low damping improves size discrimination performance compared to using the bare hands;*
- *teleoperated operation with low stiffness is less good for stiffness discrimination compared with bare hands or brackets.*

Therefore, a teleoperator for size discrimination in grasping tasks which allows performance equal to using bare hands can be designed with a very low stiffness.

Table 7.1: *List of Symbols*

Symbol	*Meaning*
F_{h}	Contact force, human hand - master
F_{e}	Contact force, slave - environment
$V_{\mathrm{h}}, V_{\mathrm{e}}$	End-effector velocities, master/slave
$H, h_{ij}(s)$	The hybrid transfer function matrix - a linear model of a teleoperator
Z_{h}	Impedance of the human operator
Z_{e}	Impedance of the environment
k_{e}	Stiffness of the object to feel
Z_{to}	Impedance that the operator feels at the master device. Function of Z_{e}.
$Z_{\mathrm{to,stiff}}$	Master device impedance for $Z_{\mathrm{e}} = \infty$
$Z_{\mathrm{to,free}}$	Master device impedance for $Z_{\mathrm{e}} = 0$
$\hat{k}$	Teleoperator stiffness - the maximum stiffness felt at the master side
$\hat{b}$	Teleoperator damping - the damping felt at the master side in free air motion
$\hat{m}$	Teleoperator mass - the inertia felt at the master side in free air motion
Z_{width}	Impedance Width - a teleoperator performance measure
T_{error}	Transparency Error - another performance measure

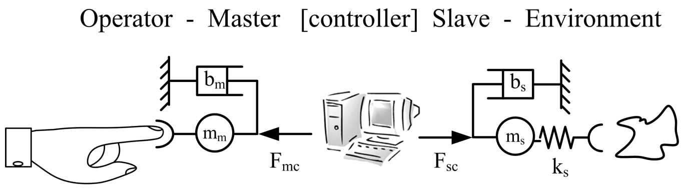

Figure 7.1: *A general teleoperator system. The operator touches the master device and probes the remote environment with the slave device*

7.1 Introduction

Teleoperation tools allow manipulation on a distance and are currently used in dangerous environments (nuclear sites, underwater operations) and in restricted confinements (surgery, micromanipulation) (Karlsson, 2004). There is also a drive to create new systems for e.g. space support operations (BLUETHMANN et al., 2003).

In Fig. 7.1, an example teleoperation system is shown. *Haptic* teleoperators allow the operator to feel forces from the remote environment, which has been shown to be advantageous for some surgical tasks (Kazi, 2001). However, it is still unclear how accurate the haptic feedback must be in order to help the operator to perform the remote task well.

Haptic teleoperation systems are often complex and too expensive for many applications, partly due to the high cost of precision sensors and high quality actuation. To allow wider application of teleoperation technology it is necessary to investigate what the minimum requirements are for acceptable performance of remote tasks.

Often the design goals are expressed in the form of how an "ideal teleoperator" (Hannaford, 1989b) would perform, with equal contact forces ($F_{\mathrm{h}} = F_{\mathrm{e}}$) and equal movements ($V_{\mathrm{h}} = V_{\mathrm{e}}$) of master and slave during contact tasks. Teleoperator performance measures express how well this ideal is followed, see (Hayward and

Astley, 1996), (Christiansson, 2005), (Yokokohji and Yoshikawa, 1994), (Lawrence, 1993). It is usually assumed that the closer the device comes to the ”ideal performance”, the better the operator can perform a remote task. However, it has been shown (Semere et al., 2004) that elimination of part of the haptic information in some teleoperated tasks still allows for remarkably good performance.

An intriguing study by O’Malley and Goldfarb (O’Malley and Goldfarb, 2004) investigated how human size discrimination performance in a virtual reality stylus task was influenced by the object stiffness. They found that human subjects performed surprisingly well also with a lower stiffness of the object. They found a limit of the stiffness at 0.4 N/mm, below which the performance dropped.

One of the critical tasks in telemanipulation is object identification by *grasping*. Haptic object identification is in real life done as a combination of exploratory procedures to detect temperature variations, surface structures and to feel kineasthetic force/position information. We assume that kineasthetic object identification is mainly done using a combination of stiffness and size discrimination.

Maybe the results of O’Malley and Goldfarb also extends to grasping tasks, where forces are perpendicular to the finger pad surface. Some evidence suggests that the performance would be worse: According to LaMotte, who studied tool interaction for stiffness discrimination (LaMotte, 2000), the performance in that task was better for a stylus grip than with a grasping movement.

In a virtual reality study, McKnight et al. (McKnight et al., 2004) quantified size discrimination performance for precision finger grasps using a relatively low object stiffness of approximately 1 N/mm. They found a task performance that was similar to bare hands performance, which suggests a similar effect as was shown by O’Malley and Goldfarb. The question is still: how low can the stiffness be and still allow full size discrimination capabilities?

Another important question relates to the loss of contact information due to thimbles or brackets compared with using the bare hands. Bicchi et al. showed (Bicchi et al., 2000) that the fingertip contact area gives important clues for object identification, and that performance was significantly better with bare hands than in contact with a flat surface.

One aspect that is more pronounced in teleoperation than in virtual reality is the presence of damping, often introduced to stabilize for time-delays (Niemeyer and Slotine, 2004). In one study on mechanical gripper tools (laparascopic forceps) (Heijnsdijk et al., 2004), it was found that additional friction does help the operator in some tasks and not in others. For e.g. a constant force task, the performance was improved by adding friction, but in a force sensing task, friction was detrimental. If damping influences performance, how much damping is acceptable before it reduces size discrimination performance?

Furthermore, the aspect of stiffness discrimination is directly influenced by a reduced teleoperator stiffness, because the stiffness of the object to probe comes in series with the teleoperator.

In order to acquire accurate and relevant design requirements for a teleoperator for *grasping tasks* it is therefore necessary to quantify the influence of device performance on human task performance. A set of specific questions can be formulated:

- In which way does teleoperator *stiffness* influence human *size discrimination*?
- In which way does teleoperator *damping* influence *size discrimination*?
- In which way does teleoperator *stiffness* influence human *stiffness discrimination*?
- How does teleoperated performance compare with bare hands performance and with indirect manipulation with the fingers in a bracket?

7.2 Teleoperator Model and Performance

To perform the experiments, a teleoperator with adjustable stiffness and damping is necessary. Part of the adjustable stiffness is done in the hardware using a physical spring, but most of the variation is achieved through using different control gains.

In this section a general model of the teleoperator and the controller is described (with a more detailed account in Appendix) which allows for analysis of the device performance measures.

To illustrate the relationship between the studied human task performance and measurable device performance, two widely accepted performance measures are used: the *Transparency*, introduced by Lawrence

(Lawrence, 1993) and the *Z-width*, introduced by Colgate and Brown (Colgate and Brown, 1994). Both these values can be calculated from a linear model of the teleoperator system.

7.2.1 Mathematical Model

The teleoperator of Fig. 7.1 consists of the mechanical master and slave devices and a controller. The block model is an adaptation of the Lawrence/Salcudean 4-channel scheme (Lawrence, 1993). It allows for a detailed linear model of master and slave devices, along with a very flexible way to define the controller.

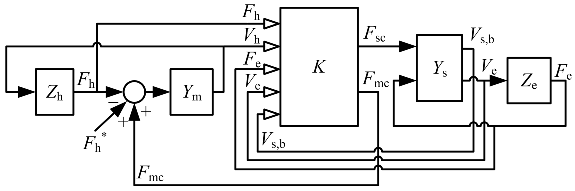

Figure 7.2: *A block model of the complete teleoperation system. The controller is a 5-in 2-out linear MIMO controller.*

For further analysis, the classic H-matrix model (Hannaford, 1989b) is used. The transformation from the component model above into the H-matrix model is explained in detail in Appendix. The H-matrix model is a 2x2 matrix of transfer functions and can be drawn using linear blocks as in Fig. 7.3.

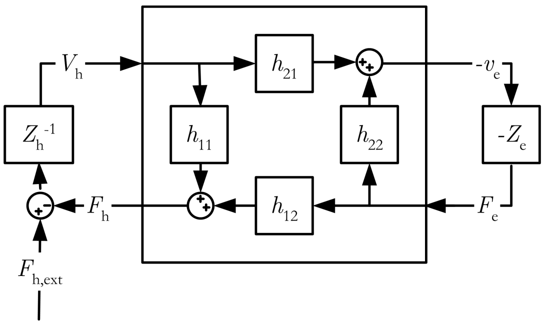

Figure 7.3: *The H-matrix model. The teleoperator is modelled in the classic Hybrid model notation.*

The Hybrid matrix elements ($h_{ij}(s)$) are calculated from the mechanical models of the master and slave devices along with a linear model of the controller. Each necessary teleoperator stiffness and damping can be achieved by changing the control gains or adjusting the mechanical structure.

The human operator and the environment are modelled as linear time-invariant systems. The operator (*not used in this study*) as an admittance (Z_{h}^{-1}) and the environment as an impedance (Z_{e}). Impedances are in this context defined as transfer functions from force to velocity (e.g. a mass-spring-damper model is modelled as: $m\,s + b + k/s$).

The impedance that the operator feels at the master side (the transmitted impedance Z_{to}) can by simple block-scheme reduction operations be expressed in the H-matrix components for any environment (Z_{e}), see eq. (7.1) (Aliaga et al., 2004). Using this formula it is straightforward to calculate how the master feels when the slave moves in free air ($Z_{\mathrm{e}} = 0$) and in contact with a stiff environment ($Z_{\mathrm{e}} = \infty$):

$$
\begin{aligned}
\frac{F_{\mathrm{h}}}{V_{\mathrm{h}}} &= Z_{\mathrm{to}}(s) = \frac{h_{11} + (h_{11}h_{22} - h_{12}h_{21})Z_{\mathrm{e}}}{1 + h_{22}Z_{\mathrm{e}}} \quad (\Longrightarrow Z_{\mathrm{e}}) \\
Z_{\mathrm{to,stiff}}(s) &= \frac{h_{11}h_{22} - h_{12}h_{21}}{h_{22}} \quad (\Longrightarrow \infty) \\
Z_{\mathrm{to,free}}(s) &= h_{11} \quad (\Longrightarrow 0)
\end{aligned}
\tag{7.1}
$$

The transfer characteristics of the teleoperation system, from the remote environment to the operator, can be approximated with a simplified model (Yokokohji and Yoshikawa, 1994), see Fig. 7.4.

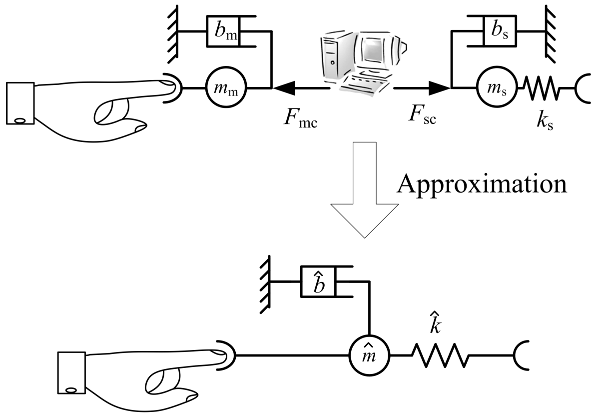

Figure 7.4: *A simplified model of a teleoperator (below) shows the main characteristics of the teleoperator - as a mass-spring-damper.*

The global "feel" of the teleoperator can be approximated to a *teleoperator mass* ($\hat{m}$), *teleoperator stiffness* ($\hat{k}$) and *teleoperator damping* ($\hat{b}$). These simplified characteristics are useful to describe the most important behaviour of a system, and are used in this paper to denote the experimental conditions below.

7.2.2 Z-width and Transparency

The impedance width - the Z-width - of a teleoperation system quantifies the range of stiffnesses that the master can present to the operator, for all different environments (Colgate and Brown, 1994). The impedance at the master side is calculated for the two situations of the slave moving in free air ($Z_{\text{to,free}}$) and in hard contact with a stiff wall ($Z_{\text{to,stiff}}$), like in (7.1). The integrated difference between the absolute values of the two impedances is the *Z-width* of the teleoperator:

$$Z_{\text{width}} = \int_{\omega_0}^{\omega_1} |\log |Z_{\text{to,stiff}}(j\,\omega)| - \log |Z_{\text{to,free}}(j\,\omega)||\, d\omega \tag{7.2}$$

For a small Z-width, it is difficult to distinguish different environments, because everything feels very similar. The larger the Z-width, the richer the information presented to the operator can be. The Z-width can be increased in many ways. In this paper two common ways are presented: either by increasing the teleoperator stiffness or by reducing damping, see Fig. 7.5.

The other quantitative device performance measure used here is the *Transparency Error*. It is a quantification of the transmission distortion, and should be as small as possible. For any given environment impedance it is possible to calculate how it is presented at the master side, see (7.1), and to see how big the difference is. Transparency as a performance measure was introduced by Lawrence (Lawrence, 1992), as a strive for equal gain and equal phase, and a variation was presented by Cavusoglu et al. (Cavusoglu et al., 2001). Here we propose a quantification of the transparency error by calculating the difference in both gain and phase between the transmitted impedance and the real impedance, for a set of typical environments ($Z_{\text{e,k}}$) (Pintelon and Schoukens, 2001):

$$T_{\text{error}} = \frac{1}{n} \sum_{Z_{\text{e,k}}}^{n} \int_{\omega_0}^{\omega_1} |\log(Z_{\text{e,k}}(j\,\omega)) - \log(Z_{\text{to}}(j\,\omega)|^2\, d\omega \tag{7.3}$$

It is possible to weight the phase and the gain error differently depending on the task at hand. Static tasks are phase-independent, but more dynamic actions require an in-phase behaviour. The transparency error is reduced with increased teleoperator stiffness and reduced damping.

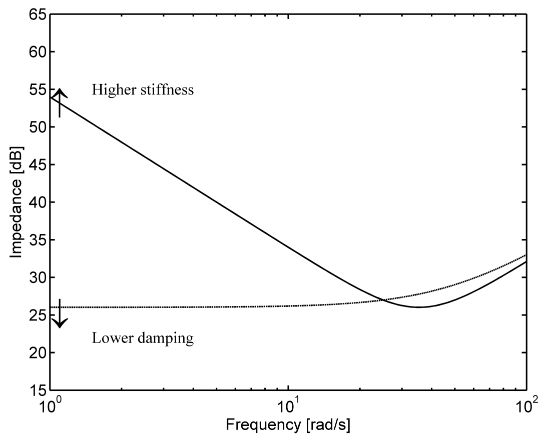

Figure 7.5: *The Z-width of the teleoperator. The Z-width is improved by increasing the teleoperator stiffness ($\hat{k}$) or by reducing the teleoperator damping ($\hat{b}$)*

In this paper, the typical environments $Z_{\mathrm{e,k}}$ are chosen to be: $1000/s$ and $1 + 100000/s$, representing a pure spring of 1 N/mm and a very stiff spring-damper system with a spring of 100 N/mm and a damper of 1 Ns/m. Those are good typical representations of the objects touched in the study.

7.3 Method and Materials

7.3.1 Experimental Procedure

Three human factors experiments were performed to study the relationship between human performance and the teleoperator settings:

- A: Size discrimination vs. teleoperator stiffness
- B: Size discrimination vs. teleoperator damping
- C: Stiffness discrimination vs. teleoperator stiffness

The subjects performed the experiments after a brief familiarization with the experimental apparatus and the task. The number of experiments for each subject was chosen so that each experiment session should take a little more than one hour. The rationale is that anything that cannot be detected within one hour of intense use is of limited importance for device builders.

For each experiment (A-C), naive subjects without haptic teleoperation experience were recruited. The experiments were performed with the dominant hand. All experiments were done with a screen blocking visual feedback both from the teleoperation system and from the operator's hand, both in the teleoperation conditions and the reference conditions. Some unwanted acoustic feedback was present in the experiment, although most of the sound drowned in the noise from the linear amplifier ventilation system. The experimental setup is shown in Fig. 7.8.

The experiments consisted of a series of paired stimuli, first a reference, than an unknown object, in a two-way forced-choice test. The subjects would feel the reference object for 3 s, then the unknown object for 3 s and then communicate their choice by pressing one of two buttons.

The result criterion for the human performance during the tasks is *percentage correct responses*. This percentage varies from 50% (random guessing) for indistinguishable differences to 100%, when the subjects do answer correctly every time. The resolution of this percentage is limited by the number of repetitions for each condition.

To allow comparison with experiments on human bare hand perception and to better understand stiffness-dependent performance, two reference conditions were included: bare hands and brackets. The *bare hands* condition means that the teleoperator is not used at all. The object is placed on a rail, touching the thumb of the subject, and the forefinger moves in free air until contact is made. The *brackets condition* means that the master device of the teleoperator is used. The object is placed against the thumb bracket and the forefinger moves the master device until contact is made. The difference is that the forefinger also feels the base friction and inertia and furthermore that there is a mechanical boundary between the object and the finger. The conditions are explained in Fig. 7.6.

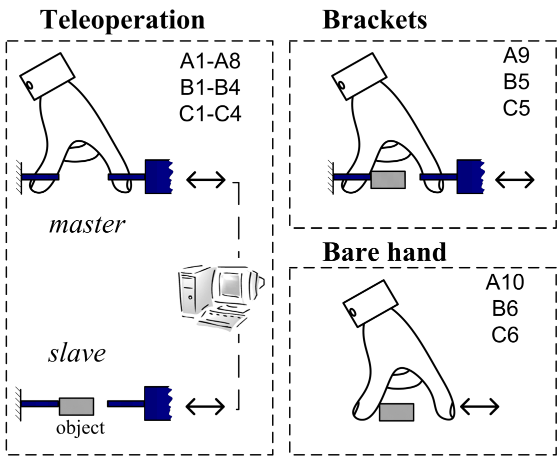

Figure 7.6: *The teleoperation settings (*A1-A8, B1-B4, C1-C4*) are compared with performance with the brackets in the master device only (*A9, B5, C5*) and with bare hands (*A10, B6, C6*). The gray rectangle in the figure is the object to feel the size/stiffness of*

The main factor (human task performance vs teleoperator setting) was analyzed using a one-way ANOVA (Analysis of variances) of the average performance for each subject and each setting, normalized to bare hands performance.

The second factor of the experiment - the comparison between bare hands, brackets and teleoperation, was tested using paired T-tests.

The bare hand performance is well researched, see e.g. (Gaydos, 1958), but it was unknown how much the performance would degrade when using brackets around the fingertips. Thimbles are often used, but Howe has shown (Howe, 1992) that the base load on the mechanoreceptors can reduce the performance in certain contact tasks. Therefore the brackets were spacious enough to avoid unnecessary pressure on the fingerpads.

In addition to the main factor of each experiment (stiffness/damping), a secondary factor (difference in stimulus strength) was also used for validation purposes. ANOVA was used to detect differences between the stimuli.

7.3.2 Experimental Apparatus

A custom made one-degree-of-freedom gripper tool, for thumb-forefinger grasps, see Fig. 7.7 was used in the experiments, (Fritz et al., 2004). On the master side, the thumb was positioned in a fixed bracket and the forefinger in a moving bracket. The slave device has an adjustable compliant section, where slave stiffness (k_{s}) could be tuned. Furthermore, the controller is programmable to allow for different teleoperator stiffnesses and dampings, while keeping the rest of the dynamics constant. The total teleoperator stiffness ($\hat{k}$) depends partly on the slave device stiffness (k_{s}) but also to a large extent on the controller gains, which can be seen in the formulae for the h_{ij}-elements in Appendix.

The controllers in Experiments A and C were enhanced *4-Channel Controllers* (Lawrence, 1993) (Hashtrudi-Zaad and Salcudean, 2002), with an additional fifth channel for the extra position information of the slave

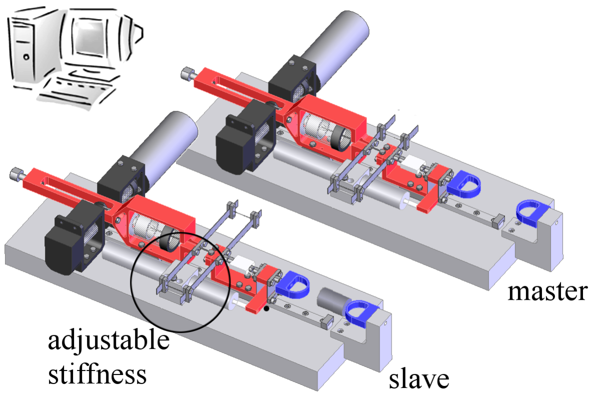

Figure 7.7: *The experimental setup used in the experiments. It is a single degree of freedom haptic teleoperation device with adjustable mechanical stiffness on the slave (k_s)*

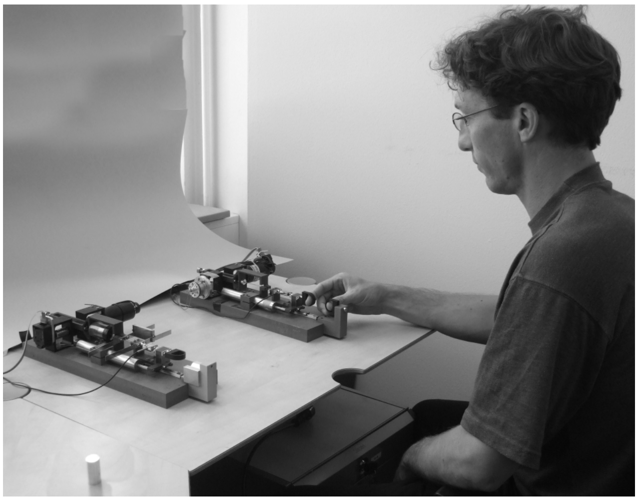

Figure 7.8: *The experimental setup with a subject holding the master device. Between the subject and the teleoperator a screen (not shown) was placed to occlude the view both of the master, the slave and the operator's hand.*

deformation. The damping variation in Experiment B was achieved using a *Virtual Model Controller*, sometimes called *Model following controller* or an *Admittance Controller* (Lam and de Vries, 1981). The controllers were implemented using Matlab Simulink (Mathworks, Natick, Ma.), on a dsp-based controller, dSpace 1102 (dSpace Gmbh, Paderborn, Germany) at a 1 kHz update rate.

For each experimental condition, the total stiffness and damping was measured at the master side six times to get a mean value and standard deviation. These values are presented in the tables below describing the teleoperation settings. In all experiments, the teleoperator mass was 0.40 kg±5%.

7.3.3 Experiment A - Size Discrimination vs. Teleop. Stiffness

The size discrimination experiment with varying teleoperator stiffness was done with six paid subjects; university students age: 22-26, one female, five male.

Main Factor: Teleoperator Stiffness

The main factor in the experiment is the teleoperator stiffness, which was varied according to Table 7.2, ranging from 0.15 N/mm to 32 N/mm. The range was chosen to go well beyond typical teleoperator stiffnesses (Flemmer et al., 1999),(Aliaga et al., 2004), both lower and higher. To get this wide range of total stiffnesses, two different slave stiffnesses were used and a number of different controllers. For setting A6 and A8, the slave stiffness set to the highest possible (100 N/mm), limited by the structural stiffness of the device. For the other settings (A1-A5 and A7), the slave stiffness was set to the minimal stiffness (1.12 N/mm $\pm 4\%$). The controller gains used are shown in Appendix.

The quantitative performance measures are calculated for each of the settings. The *Transparency Error* and the Z-width are shown along with the total device stiffnesses in Table 7.2 below. For illustration the Z-width is plotted in Fig. 7.9.

Table 7.2: *Experiment* A*: Teleoperator Stiffnesses*

Setting	*Teleoperator Stiffness* [N/mm] $\pm 6\%$	*Z-width* $\pm 5\%$	T_{error} $\pm 5\%$
A1	0.15	33.1	80.4
A2	0.30	42.7	72.2
A3	0.60	53.2	63.5
A4	1.10	63.8	55.2
A5	1.20	64.6	54.7
A6	2.50	77.1	45.4
A7	7.50	95.8	31.5
A8	32.0	126	17.5
A9	brackets	n/a	n/a
A10	bare hands	n/a	n/a

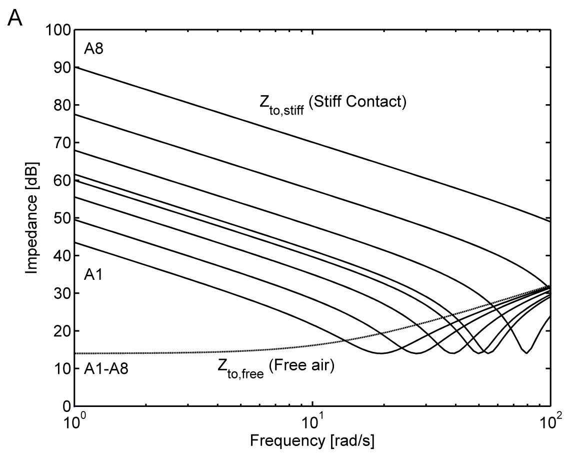

Figure 7.9: *Theoretical Z-width variation of Experiment* A*: The lower boundary - free air damping - is relatively constant, but the upper boundary varies significantly. The Z-width (area) increases almost three times from* A1 *to* A8

Secondary Factor: Object Size Difference

For each stiffness setting a number of different object pairs were presented to the subjects in a random order. The test paradigm followed that of Dietze (Dietze, 1961): The subject first feels a reference object, then an object with unknown size and afterwards indicates if the unknown object is bigger or smaller than the reference.

All subjects performed the experiment with their dominant hand, and used their non-dominant hand to indicate their choice by pressing one of two buttons (*bigger* or *smaller*).

To reproduce the settings of Dietze (Dietze, 1961) aluminum rods of different lengths were used, according to Table 7.3. The length indicated is the total length between the finger pads, so when the brackets or the teleoperator were used, all objects presented were 5 mm shorter to compensate for the material thickness. No objects with the same size were presented.

Table 7.3: *Experiment* A,B*: Object pairs for size discrimination*

Object pair	*Reference* [mm] $\pm 0.5\%$	*Unknown object* [mm] $\pm 0.5\%$
1	30	27
2	30	28
3	30	29
4	30	31
5	30	32
6	30	33

Each object pair was repeated three times for each of the settings, which resulted in total of 18 tests per setting, and total 180 tests per subject. The result of the three tests with each object-pair was averaged into a correctness percentage, representing the size discrimination performance for the given combination of stiffness and object pair.

7.3.4 Experiment B - Size Discrimination vs. Teleop. Damping

The size discrimination experiment with varying teleoperator stiffness was done with 10 paid subjects, all university students, age: 22-30 years, five female, five male. The subjects got 18 object-pairs per setting in random order, totalling 108 pairs, during the 65 minute session.

Main factor: Teleoperator Damping

The main factor to investigate was the damping in the teleoperator. An admittance controller (virtual model controller (Lam and de Vries, 1981)) with constant mass and varying damping was implemented, with damping in the range from 15 Ns/m to 1.0 Ns/m. For each setting, the theoretical Z-width and Transparency Error was calculated, see Table 7.4. The Z-width is also illustrated in Fig. 7.10.

Table 7.4: *Experiment B: Teleoperator Damping*

Setting	*Teleoperator Damping* [Ns/m] $\pm 8\%$	*Z-width* $\pm 5\%$	T_{error} $\pm 5\%$
B1	15	56.3	40.8
B2	10	62.5	41.5
B3	5	71.5	42.5
B4	1	83.9	43.3
B5	brackets	n/a	n/a
B6	bare hands	n/a	n/a

The values of the damping were chosen to be smaller and larger than the residual damping in Experiment A (around 5 Ns/m). The typical movement speeds during these tasks is 50-100 mm/s, which gives a reactive

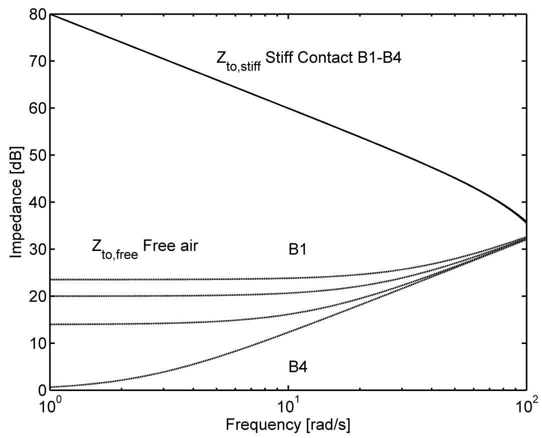

Figure 7.10: *Theoretical Z-width improvement of Experiment* B*: The lower boundary - free air damping - decreases significantly and the upper boundary is kept constant. The Z-width increases with about 50%*

force of around 1 N at the highest damping. This is a significant force at the fingertip and it could mask the force-change at the moment of impact, which can reduce human size discrimination perception.

Secondary Factor: Object Size Difference

The objects used to determine the size discrimination performance were the same as in Experiment A.

7.3.5 Experiment C - Stiffness Discrimination vs. Teleop. Stiffness

The third experiment of teleoperator stiffness and stiffness discrimination performance was done with eleven paid subjects, university students and employees, age: 23 - 33 years, two females, nine males.

Main Factor: Teleoperator Stiffness

The four stiffness settings C1-C4 are identical with the settings A1, A2, A3 and A5, see Table 7.2 and Table 7.5. The mechanical stiffness of the slave device (k_s) was held constant at 1.12 N/mm and the variation was purely generated by different controller gains.

Table 7.5: *Experiment* C*: Teleoperator Stiffnesses*

Setting	*Teleoperator Stiffness* $\hat{k}$[N/mm] ±6%	*Z-width* ±5%	T_{error} ±5%
C1	0.15	33.1	80.4
C2	0.30	42.7	72.2
C3	0.60	53.2	63.5
C4	1.20	64.6	54.7
C5	brackets	n/a	n/a
C6	bare hands	n/a	n/a

Because the stiffness settings are identical with settings A1-A5, the increase in the Z-width and Transparency is the same as above.

Secondary Factor: Object Stiffness Difference

The stiffness discrimination task was similar to the size discrimination tasks. The subjects would first feel a reference stiffness, then an unknown stiffness (k_e), see Fig. 7.11. Afterwards the subject would decide if the unknown stiffness was *stiffer* or *softer* than the reference.

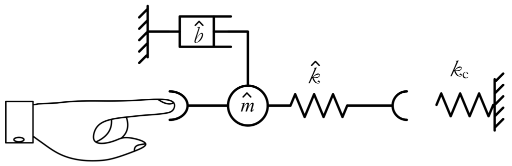

Figure 7.11: *Experiment* C*: Objects with different stiffness (k_e) are probed using the teleoperator. The teleoperator stiffness ($\hat{k}$) was varied for the conditions* C1-C4

The total stiffness transmitted to the operator can be seen as the serial connection of the two stiffnesses:

$$k_{to} = \frac{\hat{k}\, k_e}{\hat{k} + k_e} \tag{7.4}$$

It was expected that the subjects could feel a stiffness difference as long as the total projected stiffness difference was larger than 10%, which was measured to be the just noticable difference by Tan et al. (Tan et al., 1995).

Therefore the experiment was divided into two parts, with two reference objects, see Table 7.6. One reference is in the softer range (C_{low}) and one in the harder range (C_{high}) of the teleoperator stiffness.

Table 7.6: *Experiment* C*: Object pairs for stiffness discrimination*

Group	*Object pair*	*Reference* k_e[N/mm] $\pm 3\%$	*Unknown object* k_e[N/mm] $\pm 3\%$
C_{low}	1	0.35	0.21
	2	0.35	0.27
	3	0.35	0.40
	4	0.35	0.49
C_{high}	5	1.20	0.88
	6	1.20	1.08
	7	1.20	1.41
	8	1.20	1.81

The objects used were custom made springs with the same length (30 mm), but with different number of turns and different wire thickness to give the different stiffnesses.

The total transmitted stiffness (k_{to}) for each of the settings is shown in Fig. 7.12, along with the 10% JND line. It is expected that the C_{high}-settings are difficult for the subjects to detect, but that the C_{low}-settings are quite easy. That would mean that the design requirements for a teleoperator for stiffness discrimination has to be approximately twice as stiff as the object to touch for correct identification. However, the influence from the mass of the teleoperator has not yet been taken into account.

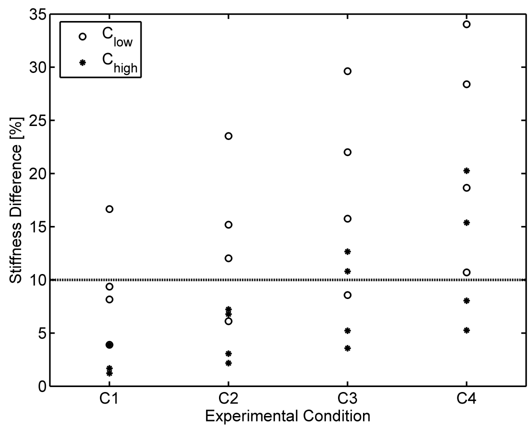

Figure 7.12: *Percieved stiffness difference for the different settings in Experiment* C*. The dotted line denotes the JND limit, so settings above this line are expected to be percieved.*

7.4 Results

7.4.1 Experiment A - Size Discrimination vs. Stiffness

Main factor: Teleoperator Stiffness

The size discrimination performance for the eight teleoperator stiffness settings and the references is presented in Fig. 7.13. The performance is measured as a percentage of correct size discrimination tests averaged over all objects. The boxplot variation is due to the variation among the subjects.

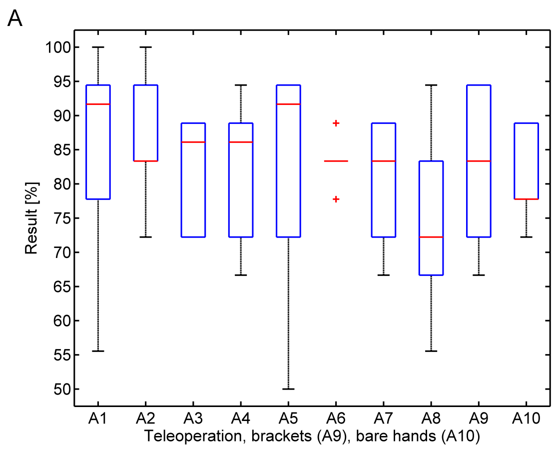

Figure 7.13: *Size discrimination performance for stiffness setting (*A1-A8*), and reference conditions brackets (*A9*) and bare hands (*A10*). There was no significant difference between the conditions*

Contrary to the theoretical prediction, *there is no significant improvement of performance* when stiffness is increased from very low (0.15 N/mm) to very high (32 N/mm).

Furthermore, the subjects perform the task in teleoperation (A1-A8) with just as good results as with the reference conditions using brackets (A9) and bare hands (A10). There was no significant difference between teleoperation, bare hands or brackets.

Secondary factor: Object Size

The variation of size discrimination performance due to size difference was highly significant (F[2,15]=16.87, $p < 0.001$). It early became apparent that the ± 1 mm difference was quite difficult to detect, whereas the larger differences were much easier, see Fig. 7.14.

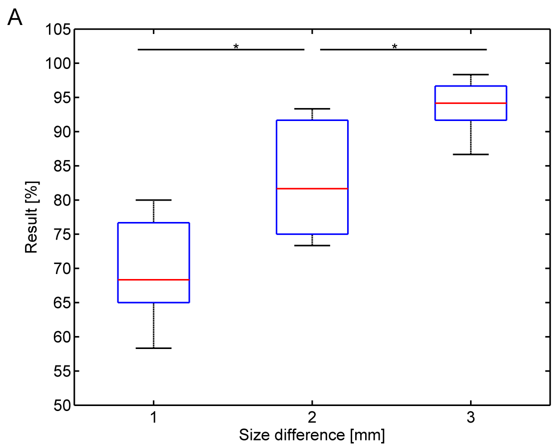

Figure 7.14: *Size discrimination performance related to the absolute size differences in experiment* A*. There was a significant difference in size discrimination performance,* $p < 0.01$

7.4.2 Experiment B - Size Discrimination vs. Damping

Main factor: Teleoperator Damping

The second experiment studied the influence of lowered damping on performance. In Fig. 7.15, a boxplot shows the results for the four teleoperation settings (B1-B4) and the reference conditions.

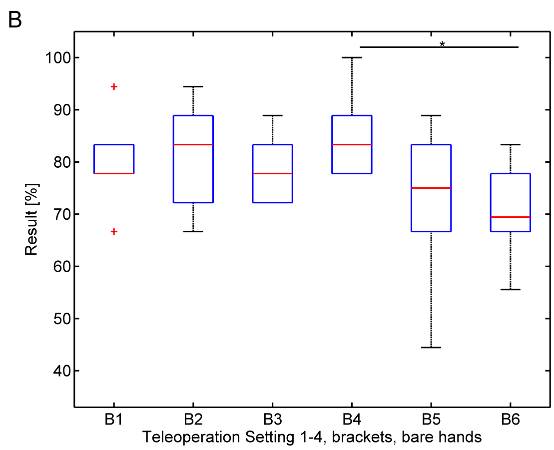

Figure 7.15: *Size discrimination performance for the damping conditions. There was a significant difference* ($p = 0.014$) *between the condition with the least damping (B4) and the bare hand condition, (marked with a line and a '*').*

There was no significant difference between the four teleoperated settings. The teleoperation performance was surprisingly significantly better than the bare hands performance ($t_{18,0.025}$=2.93, p=0.009). A post-hoc test of an anova of all settings, see Fig. 7.15, revealed that there was a significant difference between the setting with the least damping (B4) and the bare hands condition.($p = 0.014$).

This is surprising, since the teleoperator system acts as a mass between the operator's hand and the object to feel. Apparently this distortion of the contact information (the low-pass filter of the mass) helps the subject to extract the most important information needed for this size discrimination task.

There was also here no significant difference between the bare hands performance and the brackets.

Secondary Factor: Object Size

The variation attributed to the object size was even more prominent (F[2,27]=54.36, $p < 0.001$) than in Experiment A, see Fig. 7.16.

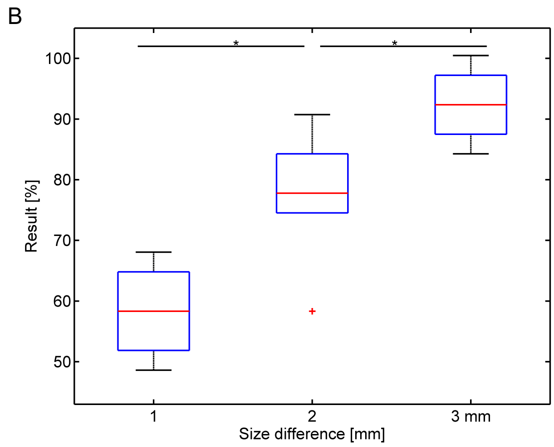

Figure 7.16: *Human performance related to absolute size difference in experiment* B. *There was a significant difference in size discrimination performance*, $p < 0.001$

7.4.3 Experiment C - Stiffness Discrimination vs. Stiffness

Main factor: Teleoperator Stiffness

The third experiment studied the influence of teleoperator stiffness on stiffness discrimination, for two different reference stiffnesses (C_{low} and C_{high}). For each set of objects, the six conditions were presented, and the task performance results are shown in Fig. 7.17 and Fig. 7.18 below.

There is no significant difference between the four teleoperation settings in C_{low}. There is however a significant difference both between teleoperation vs. bare hands ($t_{20,0.025}$=-2.88, p=0.009) and teleoperation vs. brackets ($t_{20,0.025}$=-4.83, $p < 0.001$).

For the harder reference object, there is no significant difference between the four teleoperation settings. There is still a significant difference both between teleoperation vs. bare hands ($t_{20,0.025}$=-3.52, p=0.002) and teleoperation vs. brackets ($t_{20,0.025}$=-4.25, p=0.000).

Secondary Factor: Object Stiffness

Also in the case of stiffness discrimination, the variance attributed to the real object-variation was much larger than the variance due to the different settings, see Fig. 7.19. The difference in human performance was highly significant (F[1,20]=16.28, p=0.001), for both C_{low} and C_{high}.

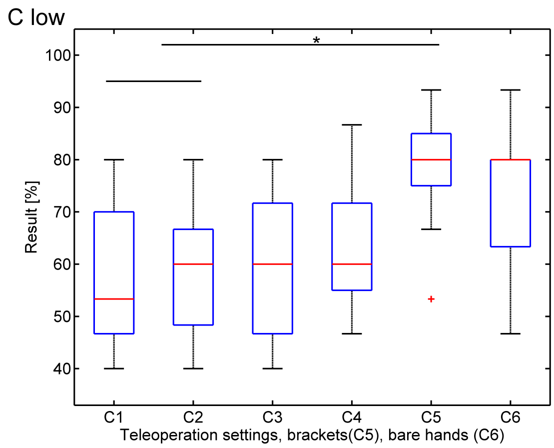

Figure 7.17: *Experiment C_{low}: Stiffness discrimination performance teleoperator stiffness conditions* C1-C4 *and references. There was a highly significant difference between the teleoperation conditions and the reference conditions*

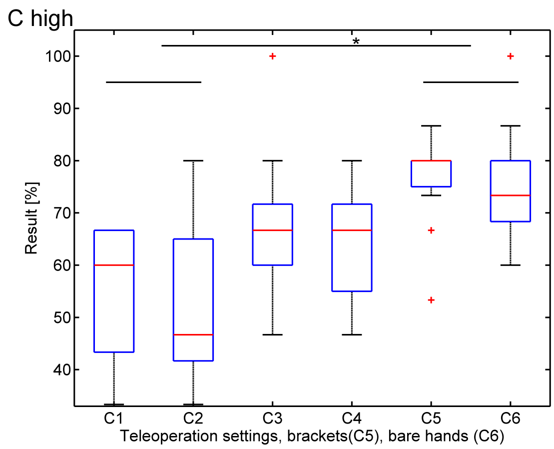

Figure 7.18: *Experiment C_{high}: Stiffness discrimination performance teleoperator stiffness conditions* C1-C4 *and references. There was a highly significant difference between teleoperation performance and the bracket condition*

7.4.4 Human Performance vs. Device Performance

To conclude the section of experiment results, a link can be given between the device performance measures used and the human task performance. For each of the settings in the three experiments, the average human task performance is calculated and plotted against the device perfomance measures: for the Z-width, see Fig. 7.20 and the Transparency Error in Fig. 7.21.

In these figures, it can be seen that the predicted positive influence of device quality on human task performance is not always present. For Experiment A - size discrimination with increased teleoperator stiffness - the performance apparently decreases slightly for ”improved quality”. For Experiment B - size discrimination with reduced teleoperator damping there is a clear improvement, especially related to the Z-width. The Transparency Error is almost constant during this experiment, so the trend here is less certain. Finally for the stiffness discrimination in Experiment C, there seems to be a positive influence from the both an increased Z-width and a reduced Transparency Error.

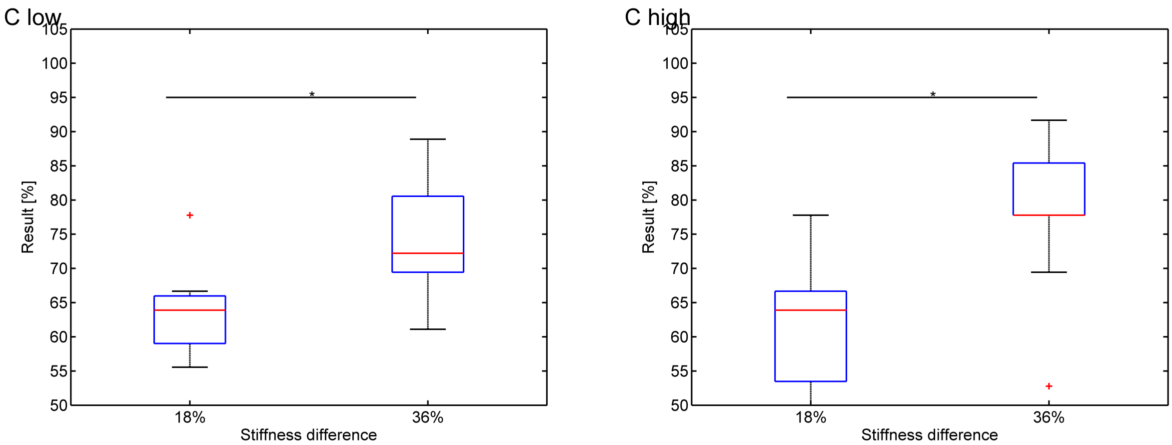

Figure 7.19: *Human performance related to relative stiffness difference in experiment* C*. There was a significant difference in stiffness discrimination performance,* $p = 0.001$

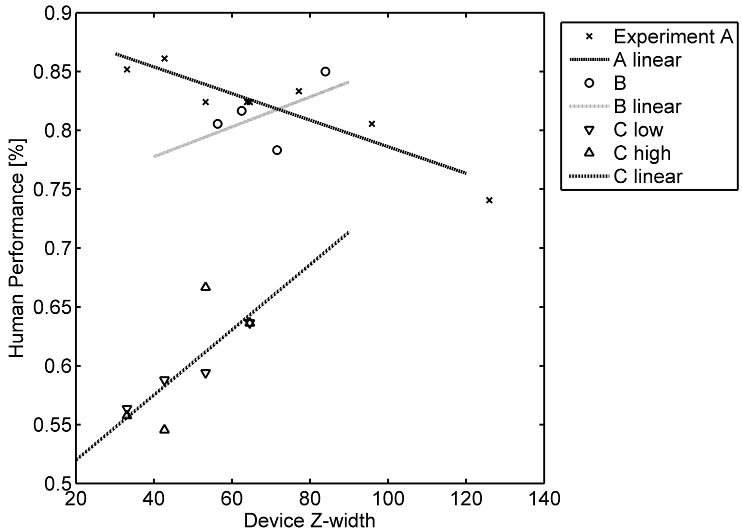

Figure 7.20: *Average task performance vs. Z-width of the teleoperator for all the settings in Experiment* A*,* B *and* C*. According to current theory, the human task performance should increase with increased Z-width.*

7.5 Discussion

Teleoperated size discrimination of objects was easier than was expected. With a low stiffness device, or with considerable damping, the performance was equal to that of direct manipulation with bare hands. This confirms and extends the findings of O'Malley and Goldfarb (O'Malley and Goldfarb, 2004). However, the expected threshold around 0.4 N/mm below which the performance would deteriorate was not found. Apparently the size discrimination is better in the grasp task is than in the stylus task. Human performance is high down at least to the lower bound used in this experiment - a stiffness of 0.15 N/mm.

This suggests that it is possible to design very simple and probably very cheap teleoperation systems for size discrimination tasks. Of course, a low-stiffness system has other disadvantages, such as a low eigenfrequency and difficulty to apply high forces.

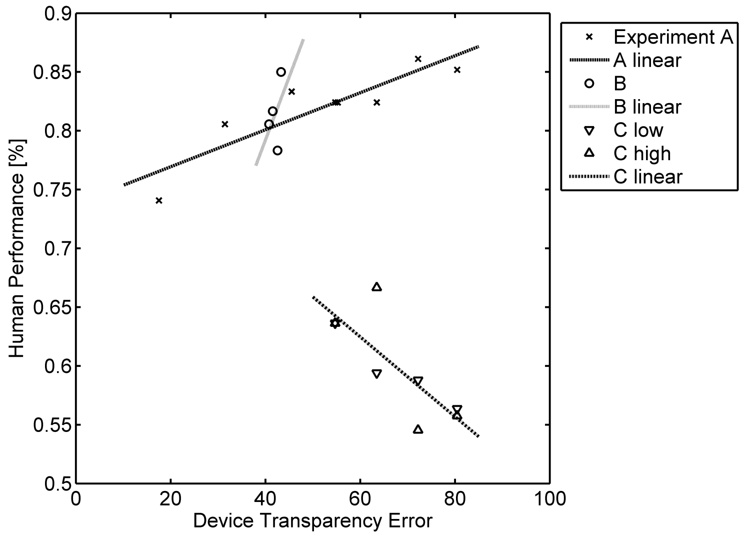

Figure 7.21: *Average task performance vs. Transparency Error of the teleoperator. According to current theory, the human task performance should decrease with increased transparency error.*

There was also no measurable difference between the performance in the settings using mechanical stiffness or controlled stiffness to achieve a certain total teleoperator stiffness. That means that the teleoperator designer has a choice where to put the stiffness in the system - either physical or controlled.

Another striking finding of this study is that a setting with very low damping and high stiffness, the size discrimination performance was even better than with bare hands. The mechanical filter of the teleoperator - a mass of 0.4 kg and virtually no damping - apparently helps the sensoric system for the subjects to perform this task.

The teleoperated stiffness discrimination was more difficult than expected. The subjects had considerable difficulty to distinguish the differences in stiffness, at stiffness differences well above the 10% level suggested by Tan et al. (Tan et al., 1995). Presumably, the mass of the teleoperator and possibly the damping influences the performance in such a way that teleoperated performance is significantly lower than using bare hands.

As seen in Section II, all the device performance measures in the literature are based on the assumption that the ideal transfer of force and velocity signals is the best support a human operator can have. Apparently that is not always the case. Sometimes we humans can profit from "imperfections" in the device that filter out certain parts of the information stream. In other domains of human support systems, e.g. hearing aids, frequency based filters are used to amplify selected parts of the information stream. Similar methods could probably be applied in the field of haptics and teleoperation.

Both size and stiffness of an object are physically static — independent of the speed of movement. However, the human senses work poorly at low frequencies, so people tend to sense these properties "dynamically", see Fig. 7.22, from Experiment A of size discrimination. We observe that the subjects press on the object with a time-varying force to sense the size of the object. A frequency analysis of the forces both at the master side (F_h) and the slave side (F_s) reveals that the most energy is concentrated slightly below 2 Hz (about 10 rad/s). Based on this observation it can be concluded that the important frequencies in the closed loop interaction are centered around this frequency. Higher frequencies are also interesting, especially to detect transitions, e.g. free-air to contact, in the communication from slave to master, see e.g. (Kato and Hirose, 2000). However, in this study the contact information seems less important than the relatively low frequency information extracted from pressing on the object instead of tapping.

Another interesting aspect of the variation between subjects is that the force applied varied with one order of magnitude.

It is now clear that for some, but not all tasks, a low stiffness device works equally well as a classical stiff

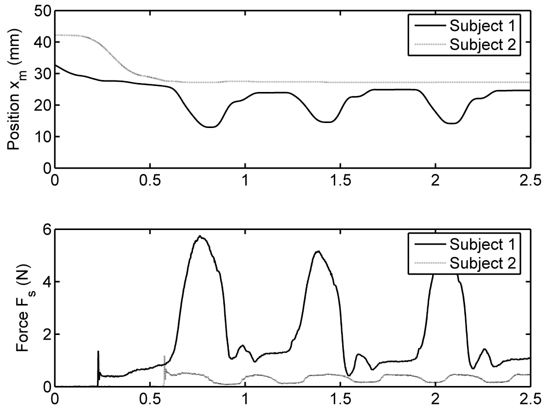

Figure 7.22: *Example of sensing strategies during the size discrimination experiment A: Subject 1 presses consistently harder than Subject 2. Both use "dynamic sensing" in this physically static task*

teleoperator. Therefore new designs can be envisioned, where e.g. a compliant slave device is used in contact with a brittle environment for gentle interaction. Especially interesting is the extension to more degrees of freedom, like peg-in-hole tasks and other assembly operations.

7.6 Conclusions

It was found that teleoperated performance in size discrimination is equally good over a large range of teleoperator stiffnesses (0.15-32 N/mm) and teleoperator dampings (1-15Ns/m). There was also no significant difference in stiffness discrimination performance using a teleoperator with varying stiffness (0.15-1.2 N/mm) to feel stiffnesses in the range of (0.21-1.81 N/mm).

Furthermore, when comparing teleoperated performance with direct interaction using bare hands or with the fingers in a bracket, it was found that:

- Teleoperation with low stiffness is equally good as bare hand performance for the size discrimination task.
- Teleoperation with very low damping improves the size discrimination performance compared to using the bare hands.
- Teleoperated operation with reduced stiffness is less good than bare hands for stiffness discrimination.

To conclude, the minimum design requirements for a stiffness discrimination teleoperator allows for a very low teleoperator stiffness, but higher stiffness is necessary for accurate stiffness discriminiation.

Detailed Models

A general model of the teleoperation system, based on mechanical components and controller gains is shown in Fig. 7.2. This Appendix shows the inside of the system boxes and how the mechanical components and controller gains combine into the calculation of the Hybrid Matrix Model elements - $h_{ij}(s)$.

First of all, the mechanical models of master and slave are shown in Fig. 7.23. Then numerical values are given for all components and the slave admittance and Hybrid matrix transfer functions are calculated. Finally, the exact controllers used in the experiments are shown in Table 7.8-7.9.

The teleoperator master and slave device components were identified using multisine identification of a linear model in the time domain. Numerical values for the components are given with mean value and standard deviation in Table 7.7:

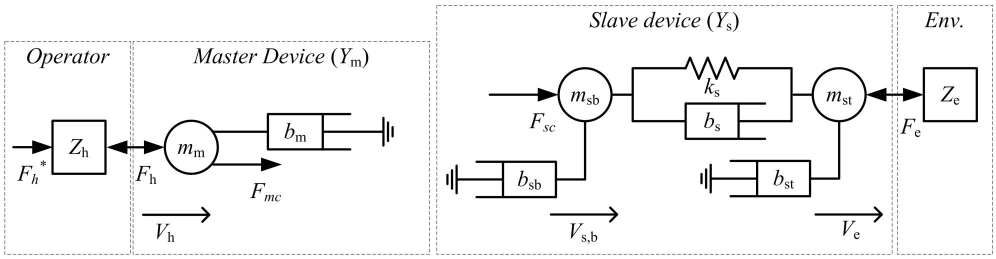

Figure 7.23: *Mechanical component models of master and slave devices*

Table 7.7: *Numerical values of system components*

	Component	*Value*
Z_m	m_m	0.376±0.0005 kg
	b_m	4.48±0.03 Ns/m
Z_s	$m_{s,b}$	0.242±0.0005 kg
	$m_{s,t}$	0.111±0.0005 kg
	b_{sb}	4.0±0.1 Ns/m
	b_{st}	1.2±0.08 Ns/m
	b_s	15.1±0.3 Ns/m
	k_s	1120±3%, 105000±15% N/m

Slave Admittance

The slave admittance is a fourth order dynamical system for a compliant slave system. Expressed in mechanical model terms, the admittance component are:

$$
\begin{aligned}
Y_{\mathrm{s,ee}} &= \frac{V_{\mathrm{e}}}{F_{\mathrm{e}}} = \\
&-\frac{m_{\mathrm{s,b}}s^2+\left(b_{\mathrm{sb}}+b_{\mathrm{s}}\right)s+k_{\mathrm{s}}}{m_{\mathrm{s,b}}m_{\mathrm{s,t}}s^3+\left(\left(b_{\mathrm{sb}}+b_{\mathrm{s}}\right)m_{\mathrm{s,t}}+\left(b_{\mathrm{st}}+b_{\mathrm{s}}\right)m_{\mathrm{s,b}}\right)s^2+\left(k_{\mathrm{s}}m_{\mathrm{s,t}}+k_{\mathrm{s}}m_{\mathrm{s,b}}+\left(b_{\mathrm{sb}}+b_{\mathrm{s}}\right)b_{\mathrm{st}}+b_{\mathrm{s}}b_{\mathrm{sb}}\right)s+\left(b_{\mathrm{st}}+b_{\mathrm{sb}}\right)k_{\mathrm{s}}} \\
Y_{\mathrm{s,be}} &= \frac{V_{\mathrm{e}}}{F_{\mathrm{sc}}} = \\
&\frac{b_{\mathrm{s}}s+k_{\mathrm{s}}}{m_{\mathrm{s,b}}m_{\mathrm{s,t}}s^3+\left(\left(b_{\mathrm{sb}}+b_{\mathrm{s}}\right)m_{\mathrm{s,t}}+\left(b_{\mathrm{st}}+b_{\mathrm{s}}\right)m_{\mathrm{s,b}}\right)s^2+\left(k_{\mathrm{s}}m_{\mathrm{s,t}}+k_{\mathrm{s}}m_{\mathrm{s,b}}+\left(b_{\mathrm{sb}}+b_{\mathrm{s}}\right)b_{\mathrm{st}}+b_{\mathrm{s}}b_{\mathrm{sb}}\right)s+\left(b_{\mathrm{st}}+b_{\mathrm{sb}}\right)k_{\mathrm{s}}} \\
Y_{\mathrm{s,be}} &= \frac{V_{\mathrm{sb}}}{F_{\mathrm{e}}} = \\
&\frac{b_{\mathrm{s}}s+k_{\mathrm{s}}}{m_{\mathrm{s,b}}m_{\mathrm{s,t}}s^3+\left(\left(b_{\mathrm{sb}}+b_{\mathrm{s}}\right)m_{\mathrm{s,t}}+\left(b_{\mathrm{st}}+b_{\mathrm{s}}\right)m_{\mathrm{s,b}}\right)s^2+\left(k_{\mathrm{s}}m_{\mathrm{s,t}}+k_{\mathrm{s}}m_{\mathrm{s,b}}+\left(b_{\mathrm{sb}}+b_{\mathrm{s}}\right)b_{\mathrm{st}}+b_{\mathrm{s}}b_{\mathrm{sb}}\right)s+\left(b_{\mathrm{st}}+b_{\mathrm{sb}}\right)k_{\mathrm{s}}} \\
Y_{\mathrm{s,bb}} &= \frac{V_{\mathrm{sb}}}{F_{\mathrm{sc}}} = \\
&\frac{m_{\mathrm{s,t}}s^2+\left(b_{\mathrm{st}}+b_{\mathrm{s}}\right)s+k_{\mathrm{s}}}{m_{\mathrm{s,b}}m_{\mathrm{s,t}}s^3+\left(\left(b_{\mathrm{sb}}+b_{\mathrm{s}}\right)m_{\mathrm{s,t}}+\left(b_{\mathrm{st}}+b_{\mathrm{s}}\right)m_{\mathrm{s,b}}\right)s^2+\left(k_{\mathrm{s}}m_{\mathrm{s,t}}+k_{\mathrm{s}}m_{\mathrm{s,b}}+\left(b_{\mathrm{sb}}+b_{\mathrm{s}}\right)b_{\mathrm{st}}+b_{\mathrm{s}}b_{\mathrm{sb}}\right)s+\left(b_{\mathrm{st}}+b_{\mathrm{sb}}\right)k_{\mathrm{s}}}
\end{aligned}
\tag{7.5}
$$

Complete Hybrid Matrix for a Hard-Soft Teleoperator

The Hybrid matrix, expressed using the admittances of the devices ($Y_\mathrm{m}(s)$ and $Y_\mathrm{s}(s)$) and the generalized controller transfer functions ($k_{ij}(s)$):

$$
\begin{aligned}
h_{11} &= \\
&-\frac{\left(Y_\mathrm{m} Y_{\mathrm{s,be}} k_{12} - Y_{\mathrm{s,be}}\right) k_{25} + \left(Y_\mathrm{m} Y_{\mathrm{s,bb}} k_{12} - Y_{\mathrm{s,bb}}\right) k_{24} + \left(-Y_\mathrm{m} Y_{\mathrm{s,be}} k_{15} - Y_\mathrm{m} Y_{\mathrm{s,bb}} k_{14}\right) k_{22} - Y_\mathrm{m} k_{12} + 1}{\left(Y_\mathrm{m} Y_{\mathrm{s,be}} k_{11} + Y_\mathrm{m} Y_{\mathrm{s,be}}\right) k_{25} + \left(Y_\mathrm{m} Y_{\mathrm{s,bb}} k_{11} + Y_\mathrm{m} Y_{\mathrm{s,bb}}\right) k_{24} + \left(-Y_\mathrm{m} Y_{\mathrm{s,be}} k_{15} - Y_\mathrm{m} Y_{\mathrm{s,bb}} k_{14}\right) k_{21} - Y_\mathrm{m} k_{11} - Y_\mathrm{m}} \\
h_{12} &= \\
&\frac{\left(\left(Y_{\mathrm{s,bb}} Y_{\mathrm{s,ee}} - Y_{\mathrm{s,be}} Y_{\mathrm{s,eb}}\right) k_{14} - Y_{\mathrm{s,be}} k_{13}\right) k_{25} + \left(\left(Y_{\mathrm{s,be}} Y_{\mathrm{s,eb}} - Y_{\mathrm{s,bb}} Y_{\mathrm{s,ee}}\right) k_{15} - Y_{\mathrm{s,bb}} k_{13}\right) k_{24} + \left(Y_{\mathrm{s,be}} k_{15} + Y_{\mathrm{s,bb}} k_{14}\right) k_{23} + Y_{\mathrm{s,ee}} k_{15} + Y_{\mathrm{s,eb}} k_{14} + k_{13}}{\left(Y_{\mathrm{s,be}} k_{11} + Y_{\mathrm{s,be}}\right) k_{25} + \left(Y_{\mathrm{s,bb}} k_{11} + Y_{\mathrm{s,bb}}\right) k_{24} + \left(-Y_{\mathrm{s,be}} k_{15} - Y_{\mathrm{s,bb}} k_{14}\right) k_{21} - k_{11} - 1} \\
h_{21} &= \\
&\frac{\left(Y_\mathrm{m} Y_{\mathrm{s,be}} k_{11} + Y_\mathrm{m} Y_{\mathrm{s,be}}\right) k_{22} + \left(Y_{\mathrm{s,be}} - Y_\mathrm{m} Y_{\mathrm{s,be}} k_{12}\right) k_{21}}{\left(Y_\mathrm{m} Y_{\mathrm{s,be}} k_{11} + Y_\mathrm{m} Y_{\mathrm{s,be}}\right) k_{25} + \left(Y_\mathrm{m} Y_{\mathrm{s,bb}} k_{11} + Y_\mathrm{m} Y_{\mathrm{s,bb}}\right) k_{24} + \left(-Y_\mathrm{m} Y_{\mathrm{s,be}} k_{15} - Y_\mathrm{m} Y_{\mathrm{s,bb}} k_{14}\right) k_{21} - Y_\mathrm{m} k_{11} - Y_\mathrm{m}} \\
h_{22} &= \\
&\frac{\left(\left(Y_{\mathrm{s,bb}} Y_{\mathrm{s,ee}} - Y_{\mathrm{s,be}} Y_{\mathrm{s,eb}}\right) k_{11} + Y_{\mathrm{s,bb}} Y_{\mathrm{s,ee}} - Y_{\mathrm{s,be}} Y_{\mathrm{s,eb}}\right) k_{24} + \left(-Y_{\mathrm{s,be}} k_{11} - Y_{\mathrm{s,be}}\right) k_{23} + \left(\left(Y_{\mathrm{s,be}} Y_{\mathrm{s,eb}} - Y_{\mathrm{s,bb}} Y_{\mathrm{s,ee}}\right) k_{14} + Y_{\mathrm{s,be}} k_{13}\right) k_{21} - Y_{\mathrm{s,ee}} k_{11} - Y_{\mathrm{s,ee}}}{-\left(Y_{\mathrm{s,be}} k_{11} + Y_{\mathrm{s,be}}\right) k_{25} - \left(Y_{\mathrm{s,bb}} k_{11} + Y_{\mathrm{s,bb}}\right) k_{24} - \left(-Y_{\mathrm{s,be}} k_{15} - Y_{\mathrm{s,bb}} k_{14}\right) k_{21} + k_{11} + 1}
\end{aligned}
\tag{7.6}
$$

Extended Lawrence 5-Channel (5C)

The teleoperator used in Experiments A and C were based on the 4-channel controller by (Lawrence, 1993). The values of the k_{ij}(s)-functions for Experiments A and C are shown in Tables 7.8- 7.9.

$$K = \begin{bmatrix} k_{11} & k_{12} & k_{13} & k_{14} & k_{15} \\ k_{21} & k_{22} & k_{23} & k_{24} & k_{25} \end{bmatrix} \tag{7.7}$$

Table 7.8: *Controller Gains and* k_s *in Experiment* A

Setting	k_{11} k_{21}	k_{12} k_{22}	k_{13} k_{23}	k_{14} k_{24}	k_{15} k_{25}	k_s [N/mm]
A1	0.95	0-500/s	-0.10	5+400/s	1+100/s	1.120
	0.10	3+500/s	0.00	-6-500/s	0	
A2	0.80	0-1000/s	-0.50	5+800/s	1+200/s	1.120
	0.50	3+1000/s	0.00	-6-1000/s	0	
A3	0.00	0-1500/s	-1.00	5+1200/s	1+300/s	1.120
	1.00	3+1500/s	0.00	-6-1500/s	0	
A4	0.00	0-2000/s	-0.90	5+2000/s	0	1.120
	0.90	2+2000/s	0.00	-5-2000/s	0	
A5	0.00	0-1000/s	-1.00	1+200/s	5+800/s	1.120
	1.00	3+1000/s	0.00	-6-1000/s	0	
A6	0.00	0-2000/s	-0.90	5+2000/s	0	100.000
	0.90	2+2000/s	0.00	-5-2000/s	0	
A7	0.00	0-3000/s	-1.00	4+1500/s	4+1500/s	1.120
	1.00	3+3000/s	0.00	-7-3000/s	0	
A8	0.00	0-3000/s	-1.00	4+1500/s	4+1500/s	100.000
	1.00	3+3000/s	0.00	-7-3000/s	0	

Table 7.9: *Controller Gains and* k_s *in Experiment* C

Setting	k_{11} k_{21}	k_{12} k_{22}	k_{13} k_{23}	k_{14} k_{24}	k_{15} k_{25}	k_s [N/mm]
C1	0.95	0-500/s	-0.10	5+400/s	1+100/s	1.120
	0.10	3+500/s	0.00	-6-500/s	0	
C2	0.80	0-1000/s	-0.50	5+800/s	1+200/s	1.120
	0.50	3+1000/s	0.00	-6-1000/s	0	
C3	0.00	0-1500/s	-1.00	5+1200/s	1+300/s	1.120
	1.00	3+1500/s	0.00	-6-1500/s	0	
C4	0.00	0-1000/s	-1.00	1+200/s	5+800/s	1.120
	1.00	3+1000/s	0.00	-6-1000/s	0	

Virtual Model Control

This controller for the experiment B is a model following controller, based on an outer force loop and an inner velocity/position loop. The values of the k_{ij}-functions are shown in Table 7.10 .

$$K = \begin{bmatrix} k_{11} & k_{12} & k_{13} & k_{14} & k_{15} \\ k_{21} & k_{22} & k_{23} & k_{24} & k_{25} \end{bmatrix} \tag{7.8}$$

Table 7.10: *Controller Gains and k_s in Experiment* B

Setting	k_{11} k_{21}	k_{12} k_{22}	k_{13} k_{23}	k_{14} k_{24}	k_{15} k_{25}	k_s [N/mm]
B1	$\frac{15}{1.0+0.50\,s}$	-15-5000/s	$\frac{15}{1.0-0.50\,s}$	0+2500/s	0+2500/s	100.000
	$\frac{15}{1.0+0.50\,s}$	0+5000/s	$\frac{15}{1.0-0.50\,s}$	-15-2500/s	0-2500/s	
B2	$\frac{15}{5.0+0.50\,s}$	-15-5000/s	$\frac{15}{-5.0-0.50\,s}$	0+2500/s	0+2500/s	100.000
	$\frac{15}{5.0+0.50\,s}$	0+5000/s	$\frac{15}{-5.0-0.50\,s}$	-15-2500/s	0-2500/s	
B3	$\frac{15}{10.0+0.50\,s}$	-15-5000/s	$\frac{15}{-10.0-0.50\,s}$	0+2500/s	0+2500/s	100.000
	$\frac{15}{10.0+0.50\,s}$	0+5000/s	$\frac{15}{-10.0-0.50\,s}$	-15-2500/s	0-2500/s	
B4	$\frac{15}{15.0+0.50\,s}$	-15-5000/s	$\frac{15}{-15.0-0.50\,s}$	0+2500/s	0+2500/s	100.000
	$\frac{15}{15.0+0.50\,s}$	0+5000/s	$\frac{15}{-15.0-0.50\,s}$	-15-2500/s	0-2500/s	

Chapter 8

An Experimental Study of Operator Cues in a Teleoperated Assembly Task

G. A. V. Christiansson
submitted to ASME Journal of Manufacturing Science and Engineering

*Haptic feedback is known to improve teleoperation task performance for a number of tasks, and one important question is which haptic cues are most important for each specific task. This research quantifies human performance in an assembly task for two types of haptic cues; low-frequency force feedback and high-frequency force feedback. A human subjects study was performed with those two main factors: (*F1*) low-frequency force feedback on/off, (*F2*) high-frequency force (acceleration) feedback on/off. The results show that the low-frequency haptic feedback (*F1*) improves (reduces) impact forces, but does not influence low-frequency contact forces or task completion time. The high-frequency information (*F2*) did not improve task performance at all, but did reduce the mental load of the teleoperator, but only in combination with low-frequency feedback (*F1*).*

8.1 Introduction

Teleoperated assembly has a number of interesting challenges. Mating of components and peg-in-hole subtasks are essentially force-controlled tasks with hard contact with the environment, which is a considerable challenge to conventional teleoperation architectures.

One promising way to achieve stable force control with low impact forces is to use series-elastic actuation for the slave robot. It has been shown that a soft slave robot improves contact stability (Christiansson et al., 2006b), and it was found (Christiansson et al., 2006a) that there is a range of allowable slave stiffnesses, where the human task performance is equal to the stiff slave case, at least for simple object identification tasks. Furthermore, it has been shown that for certain single-degree-of-freedom material identification task (LaMotte, 2000; Kuchenbecker et al., 2006), high-frequency information improves human performance in teleoperation. This is consistent with neurological studies where different sensoric systems were blocked, and human performance subsequently deteriorated in a number of tasks (Johansson, 1996).

This paper evaluates the relative importance of the classic low-frequency force-feedback information and the high-frequency contact information. This is implemented in a hard-master soft-slave haptic teleoperator, where both high- and low-frequency information is sensed by the slave and can be accurately reproduced at the master side to the operator. The teleoperator used in this study is shown in Fig.8.1, and explained in in Section 8.2.3, see also (Christiansson and Fritz, 2007).

The feedback modalities are evaluated in a human factors study, where subjects perform a Lego assembly task. This "Toy problem" is the first proposed benchmark task for teleoperator performance quantification (Yokokohji et al., 2003).

In Section 8.2, the experimental method and the conditions are elaborated. In Section 8.3 the results are presented and further discussed in Section 8.4. The main conclusions of the paper are condensed in 8.5.

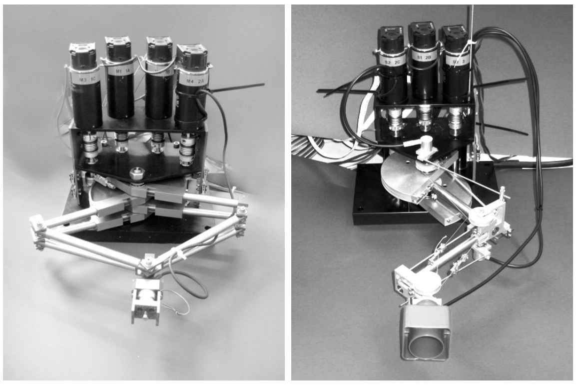

Figure 8.1: *Teleoperator: The master device (left) is connected via a bilateral controller to the slave (right).*

8.2 Method

A human subjects experiment was performed to quantify human operator performance, for four experimental conditions. Six subjects, four male, two female, without experience in from using haptic teleoperation participated with informed consent. They performed the trials after a brief introduction to the system and the experimental conditions. During the duration of the experiment the subjects had a clear direct view both of their own hands and of the slave device interacting with the remote environment.

8.2.1 Task Description

The task was a 3-dof planar assembly task where movement was restricted to motion in x-, y-, and rotation around the z-axis. One mechanical part with a hole (attached to the end-effector of the slave) was moved from a starting position, and docked on one of three fixed pegs, see Figure 8.2. The experiment was done with the task instruction to focus on *fast execution* but with *as low contact forces as possible*.

The pre-randomized order of the pegs to dock on was indicated with a led-light integrated in the pegs, which would turn on when the slave device was back in the starting position, a distance of 5 cm from the pegs. The *task completion time* was measured from the moment that the light was turned on until the mechanical parts were completely assembled, which was measured using a microswitch, and communicated to the subject with a sound signal. The accuracy of the time measurement is on the order of the sample time, which is 1 ms.

All subjects performed this assembly task 60 times for each of the four experimental conditions.

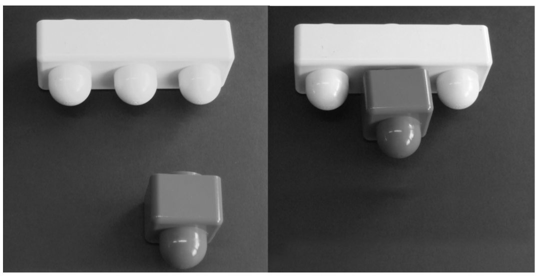

Figure 8.2: *Subject's view of the task: The dark part is moved to dock onto one of the three pegs of the fixed base. The order of which peg to dock onto is pre-randomized.*

8.2.2 Performance Metrics

For many teleoperated tasks the most relevant performance metrics are *task completion time* and *maximum contact force*. The balance between those two depends on the real task and how sensitive the environment is to excessive forces.

In this experiment the *task completion time* is measured only during the forwards motion, from a starting position (5 cm from the targets) to the complete docking of the two parts. The time to move back to the reference position is not included in the performance metric.

The maximum contact forces for each trial in this assembly task is separated in *low and high-frequency contact forces*, with a separation at around 10 Hz. The low-frequency forces represent the quasistatic interaction forces; how hard the operator is pushing on the pieces to ensure the docking of the piece on the peg. The force is measured at the slave device, as the norm of the force-vector in the x-y-plane. The high-frequency forces represent the impact forces at the moment of contact, which are due to the decelleration of the moving slave device end-effector inertia. The variation of the high-frequency forces in this experiment are due to variation of of impact velocity. Both aspects of the contact force are relevant for teleoperation tasks when working in a sensitive or brittle environment.

8.2.3 Experimental Apparatus

The *Planar Teleoperator* used in this experiment is a 3-dof master-slave system with haptic (kineasthetic) feedback, explained in detail in (Christiansson and v. d. Helm, 2007). The master device is a high-stiffness, high-bandwidth parallel robot, see Fig. 8.1, a design based on the force-redundant master device by Salcudean (Salcudean and Stocco, 2000).

The slave robot is a low-stiffness (soft) robot, where the end-effector inertia is decoupled from the motor inertia by the use of a series elastic element. The deflection is measured using two high-resolution encoders and gives an estimate for the low-frequency component of the interaction forces. At the tip of the slave device, an accellerometer is placed, which measure the effects of the high-frequency interaction forces. The peg-and-hole task is realized using Lego Primo™, a choice based on a suggestion by Yokokohji et al. (Yokokohji et al., 2003).

8.2.4 Experimental Conditions

The two main factors of the experiment are two different feedback cues: (F1) with/without classic force feedback, i.e. low-frequency contact information and (F2) with/without acceleration feedback for high-frequency contact information. These factors combine into four experimental conditions, see Table 8.1.

Table 8.1: *The four experimental conditions*

F1:	*Low-freq. off*	*Low-freq. on*
F2: High-freq. off	NONE	LF
High-freq. on	HF	LFHF

8.2.5 Statistical Analysis

To quantify the difference between the experimental conditions, the subjects' performance (task completion time, high/low-frequency contact forces) are compared using statistical tests that compare means of populations, based on the assumption of normality. Throughout the analysis, a p-level below 0.05 is considered significant.

The two main factors (*F1*: low-frequency force feedback, *F2*: high-frequency force feedback) in the four experimental conditions of Table 8.1, are the focus of the study. Considering that the variation between the subjects can be important, and may contain a large part of the measured variance, the subjects are treated as a separate factor (*F3*) in the analysis. The three main factors were compared using three-way Anova, (Analysis of variances with repeated measures, (Stevens, 1992)).

8.2.6 Subjective Task Load

In addition to the quantitative analysis of the human performance, a subjective workload assessment was performed using the NASA Task Load Index (TLX) (Hart and Staveland, 1988). The subjects quantify a percieved difficulty according to six dimensions of the workload: *Mental Demand, Physical Demand, Temporal Demand, Performance, Effort* and *Frustration Level*, on a scale from 0-100. The definition of these criteria were presented to the subjects using the standard definitions (Hart and Staveland, 1988).

One aspect of the subjective evaluation is that each subject has his own "reference level", so the average score of each person was subtracted from all data for each person to normalize the data. The scores shown in the diagrams in Section 8.3 are relative scores, after normalization. The scores of all the subjects are compared for each of the six task load dimensions separately.

8.3 Results

The performance, expressed in *task completion time*, *low-frequency contact force* and *high-frequency contact force* is measured for the two experimental factors (*F1 and F2*), with the subject variation as a third factor (*F3*) in a three-way Anova. The results of the analysis is shown in Table 8.2.

Table 8.2: *Anova results from the three factors on the three performance metrics. Significance is marked using* ***boldface***.

	F1 *Low Freq. Feedback*	*F2* *High Freq. Feedback*	*F3* *Subjects*
Tasktime	F[0.78]	F[2.67]	**F[143]**
	p=0.38	p=0.10	**$p < 0.001$**
LF force	F[2.56]	F[0.73]	**F[170]**
	p =0.11	p = 0.39	**$p < 0.001$**
HF force	**F[79.61]**	F[0.16]	**F[259]**
	$p < 0.001$	p = 0.69	**$p < 0.001$**

In the significance table, Table 8.2, the main results are shown. In the first column, representing factor *F1* (low-frequency feedback on/off), there is only one signficant value, the bottom one. This means that there is only a measurable influence from low-frequency feedback on the high-frequency impact forces, and no influence on neither task completion time nor low-frequency contact forces. The second column, representing factor *F2* (high-frequency feedback on/off), has no significant values. This factor does not influence task performance. The third column, representing factor *F3* (subjects) has highly significant values for all performance metrics. The variation in performance across the three factors is completely dominated by the difference between the different subjects.

To illustrate the small difference between the experimental conditions, the three performance metrics are plotted for all four conditions using boxplots showing the median value, the lower and upper quartile, and outliers. The *task completion time* is shown in Fig. 8.3, *low-frequency contact force* in Fig. 8.4 and the *high-frequency contact force* in Fig. 8.5.

To illustrate the large variation between subjects, one performance metric (task completion time) for all six subjects is shown in Fig.8.6. However, the subjects were allowed to make the trade-off between speed and impact force based on his/her judgement, which would suggest that each subject would choose a different speed/force level. To visualize this trade-off, the high-frequency impact forces (acceleration) is plotted against task completion rate (counted as correct assemblies per second, the inverse of task completion time) in Fig. 8.7. There is first of all a general tendency for higher impact forces for higher speeds, which is exactly what was expected. However, it is also clear that certain subjects are significantly better than others at this task. Comparing subjects 1 and 3 with subject 4 reveals that the latter person is consistently slower but generating impact forces that are twice as large.

For each of the six dimensions of the task load index, the four conditions are compared, using normalized scores (difference from mean value of each person). The relative scores are shown as boxplots in Fig. 8.8.

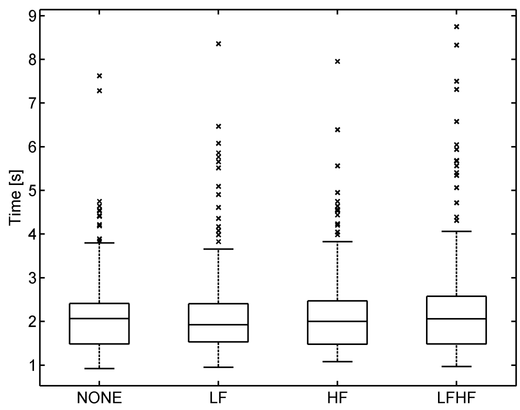

Figure 8.3: *Boxplot of task completion time for the four experimental conditions. There is no difference between the conditions.*

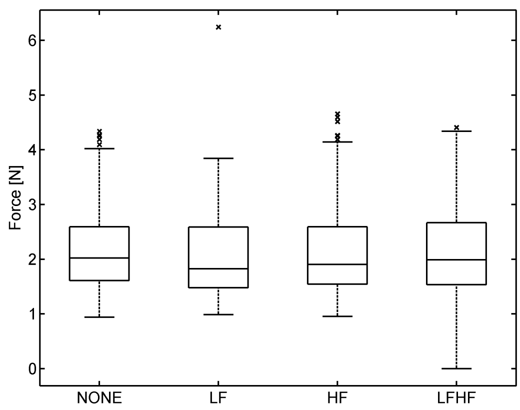

Figure 8.4: *Boxplot of low-frequency contact force for the four experimental conditions. There is no difference between the conditions.*

The *Mental Demand* shows no difference in mean, only in variation. For the *Physical Demand*, the LF and LFHF conditions are higher than the two others. The *Temporal Demand* is quite constant over the conditions, which reflects the nature of the task, since the subjects could choose the task rhythm themselves. The percieved *Performance* of the task, how well the subjects think they performed, is highest for the LFHF condition, even though there is no measureable improvement of objective improvement. The *Effort* is also constant over the conditions. Finally, the *Frustration Level* is lowest for the LFHF condition.

To investigate why there is a difference in physical demand between the conditions, the master device motion is plotted in Fig. 8.9. It seems that the movement is less smooth in conditions LF and also LFHF, where the low-frequency feedback is present.

8.4 Discussion

The main question of the experiment was the influence of the two factors (*F1*: low-frequency and *F2*: high-frequency feedback) on task performance. The results show that the haptic feedback influences the three task

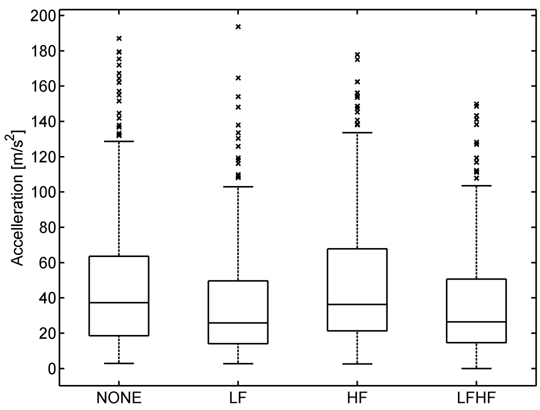

Figure 8.5: *Boxplot of slave acceleration (equivalent to maximum high-frequency force) for the four experimental conditions. Condition NONE and HF are significantly higher than conditions LF and HFLF.*

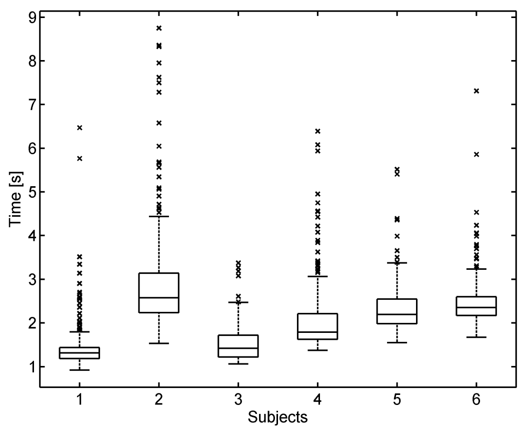

Figure 8.6: *Boxplot of task completion time for all subjects, to illustrate the large variation between the subjects.*

performance metrics differently.

The most dominating variation in the task performance consists of the difference between the different subjects, for all three performance metrics. However, between the four conditions, the differences are much smaller. There is no influence at all from the conditions on task completion time. The subjects perform the task with the same speed, independent of the feedback modality. This indicates that the subjects all chose a comfortable pace, which they could follow in all experimental conditions.

There is also no influence from the conditions on the low-frequency contact forces. The subjects press equally hard, regardless of feedback cues. More than 90% of the peg-in-hole trials are done with a low-frequency force of 1-3 N, which can be comfortably done with this teleoperator.

The only measureable influence from feedback condition on task performance is on the high-frequency contact forces, which describe the impact impulse. Here there is strong influence from the low-frequency force feedback (*F1*), but no influence from the high-frequency feedback (*F2*). It means that the low-frequency force feedback helps to reduce the contact impulse, which is equivalent to saying that the maximum impact velocity is lower. This is interesting, because there is no difference in total task completion time, so the average velocity during the motion cannot be lower, but still the velocity is lower at the moment of contact. This suggests that

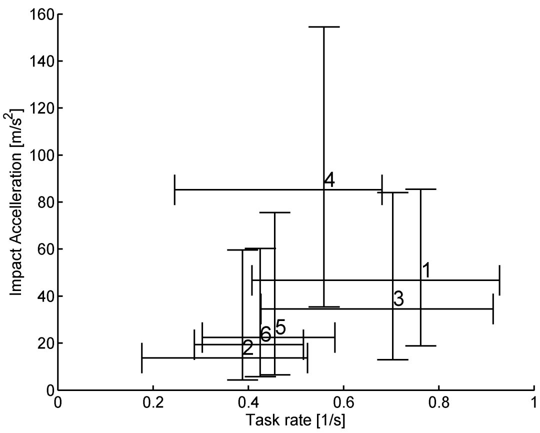

Figure 8.7: *Speed vs. impact force trade-off for the six subjects. The speed is shown as task completion rate (assemblies/second) and impulse force as acceleration.*

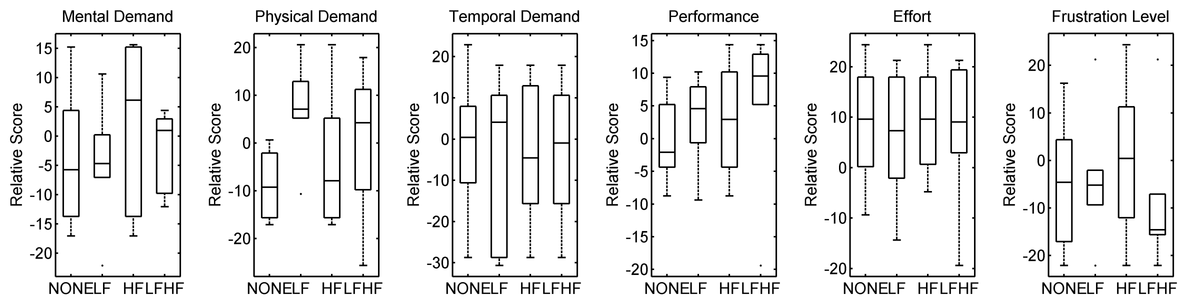

Figure 8.8: *Subjective workload for the six dimensions of NASA-TLX, comparing the four experimental conditions.*

the operator has better control over the motion of the slave.

Another important question is whether or not this improvement is relevant. The actual reduction of impact is from an average acceleration of $48m/s^2$ to $36m/s^2$, which is a reduction of 25%, but the variance is very large, as shown in Fig. 8.5. For certain applications, where the impact forces are critical, this improvement can justify the increased complexity and cost of adding low-frequency haptic feedback. The high frequency impact forces are not reduced by the addition of high-frequency haptic feedback cues, which can be explained by the fact that this information comes to the operator only after the first moment of impact.

One interesting phenomenon is that the addition of the low-frequency force feedback in conditions LF and LFHF influences the impedance felt at the master, both in contact with the environment and in free motion, as shown in Fig. 8.9. This is consistent with a negative subjective evaluation from the subjects regarding the NASA-TLX *Physical Demand*. The higher-order dynamics due to the feedback of low-frequency forces may also be the reason for the lower impact velocities for condition LF and LFHF, which was mentioned above. The challenge is to present the most useful cues to the operator without changing the dynamics in a detrimental way.

The variation among subjects is the single most important source of variation in this study. As was shown in Fig. 8.7, there is an important difference in skills at least among naive subjects. Task performance was more than twice as good for the best subjects compared with the worst, which is a much larger difference than was observed between the experimental conditions. This suggests that careful selection and training of operators may lead to larger task performance improvements than the addition of haptic feedback, at least in this task.

The subjective workload evaluation shows two contradictory patterns. First of all, the addition of low-

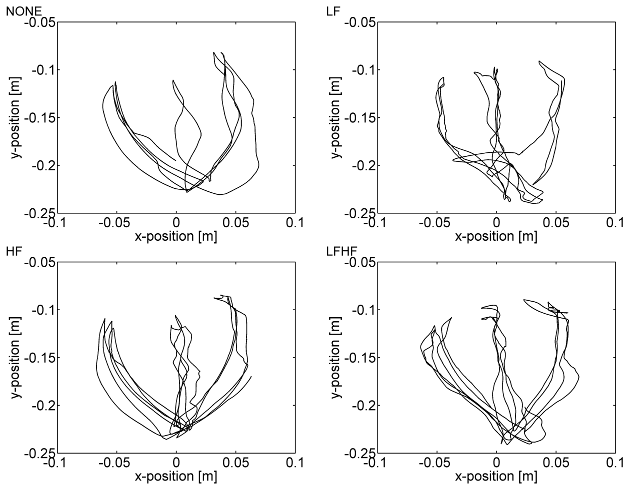

Figure 8.9: *Comparison of hand motion for the four conditions. The low-frequency haptic feedback (conditions LF, LFHF) introduces extra dynamics, which influences the human movement.*

frequency cues (condition LF and LFHF) increases the *Physical Demand*. Secondly, the combination of both low and high-frequency cues improve percieved *Performance* and reduces the *Frustration Level*. It is interesting that only the combination of the two cues is consistently percieved to improve work load.

A final important observation in this study is that the soft slave device itself seems to facilitate the peg-in-hole task, probably by its passive compliance. It has earlier been shown that low-frequency force-feedback to the operator can reduce contact forces in a peg-in-hole task with one order of magnitude (Hannaford et al., 1991), but that could not be seen in this study. The main difference between that study and the study presented in this paper is the slave compliance; the experiments in (Hannaford et al., 1991) were performed with a stiff slave teleoperator, and here a soft slave was used. To perform a peg-in-hole task successfully, it has been shown that the peg must be held with a certain minimal compliance (softness) (Hogan, 1985). This can be realized in different ways. One way is to include the compliance of the human operator in the loop, by creating a closed-loop feedback system, e.g. the force-feedback in the teleoperator of Hannaford. Another way to achieve the same thing is to include a passive compliance in the slave device, like in this study.

8.5 Conclusion

For this particular teleoperated assembly tasks using a hard-soft haptic teleoperator, the following conclusions could be drawn:

- Low-frequency haptic feedback reduces impact forces with the environment, at the cost of higher subjective *Physical Demand*, and worse dynamics in free air.
- High-frequency feedback improves the subjective perception of the teleoperation system, but does not improve the objective task performance.
- Careful selection or training of the operator allows more significant task improvement than the addition of haptic feedback.
- Using a soft slave device reduces the need for haptic feedback.

Part IV

Discussion and Conclusion

Chapter 9

Discussion

9.1 Recapitulation

The goal of this research, given in Section 1.5 was stated as:

The goal of this thesis is to quantify the advantages of hard-soft teleoperation considering human capabilities, remote environment characteristics and task requirements. This leads to design guidelines that allow teleoperator designers to achieve a better trade-off between task performance, stability and complexity.

The core of the research was performed to test the hypotheses posed in Section 1.6 on page 11. The individual experiments are described in Chapter 3-8, and this chapter relates the experiments to the hypotheses.

9.2 Human Performance

H1. *Reduced total teleoperator stiffness reduces human size and stiffness discrimination performance.*
H2. *Increased total teleoperator damping reduces human size discrimination performance.*

In the literature, it is often assumed that higher teleoperator stiffness and lower teleoperator damping is "better" (Lawrence, 1993; Hannaford, 1989b). This is based on an argument of "transparency", that the teleoperator should ideally present the environment impedance unaltered to the operator, which would be equivalent of direct manipulation. All distortions of the force- and velocity- signals would reduce performance. Therefore, optimization of these criteria would give the best teleoperator. This sounds logical, but is actually not always true.

In the human subject experiments in Chapter 7, the following results were unveiled: for the *size discrimination task*, the *teleoperator stiffness* does not influence task performance, in the wide range of 0.15-30 N/mm. There was also no difference between controlled stiffness and physical stiffness in the human task performance. For this task and these conditions, hypothesis **H1** has been proven false.

For the same *size discrimination task*, *teleoperator damping* does not influence task performance, in the range of 1-15 Ns/m. For this condition, hypothesis **H2** has been proven false.

For *stiffness discrimination* the often-claimed statement that "stiffer is better" could not be verified for all values of the teleoperator stiffness. For this task, hypothesis **H1** has been proven false. The total teleoperator *stiffness must be equal to or higher than the stiffness of the object itself* to allow accurate stiffness discrimination.

In short, the first set of hypotheses, which are often assumed to be true, was found to be false for many of the experimental conditions. The reason herefore is that the human sensory system is the limiting factor, and improving the teleoperator by increasing stiffness and reducing damping does not improve the task performance. The sensoric and perceptual mechanism by which the human perception is influenced by the device characteristics merits further research.

This means that for certain tasks, a teleoperator with lower stiffness and more damping is equally useful as one with higher stiffness and less damping. Allowing lower stiffness and more damping gives the designer more freedom in choosing low-cost components, which leads to cheaper teleoperators. However, there seems to be a break-point below which simplifications reduce performance, so it is adviceable to study the task in detail, preferably by prototyping, to find this critical level. Only then the teleoperator design can be optimally finalized.

9.3 The Haptic Sensory System

H3. *For size and stiffness discrimination tasks, a bracket or a loose thimble around the fingers gives worse performance compared with direct manipulation.*

In the current research, we could observe humans interacting with haptic teleoperators for in total hundreds of hours, which led to numerous quantitative and qualitative insights. One observation in the human task study from Chapter 7 was that the *brackets around the fingers did not influence performance*. It was expected that the loss of the multidimensional tactile information would reduce performance significantly, but this was not detectable. This, along with the fact that most people performed best when grasping with a force around 4 N suggests that people use the golgi tendon organs instead of skin sensors to detect the forces involved in the contact. For teleoperator design, it means that for *size and stiffness discrimination tasks*, a *bracket or a loose thimble is just as good as a multi-point-of-contact interface*. Hypothesis **H3** was found to be false.

Furthermore, we could observe that humans employ a dynamic measurement technique also to measure the static property of size of an object, c.f. Fig. 7.22. It seems that the high frequency information is used by the operator to switch control modes to change controlled stiffness, and that the low-frequency information is used in the closed-loop control of grasping force and position. This is consistent with the difference in signal propagation speed of the nerve fibres connecting these sensors with the central nervous system. The high-frequency information from the skin is connected via thin (slow) nerves, unsuitable for closed-loop control due to the time delay. The golgi tendon organs on the other hand have thicker (faster) nerves, which allows for low-latency feedback loops (Johansson, 1996).

It would be interesting to repeat the grasp task experiments together with a neurophysiologist, using anasthetics to block different sensoric pathways. Then the contribution from each sensoric system could be separated, which would lead to a deeper understanding of haptic feedback mechanisms, and ultimately to better teleoperator designs.

9.4 The Stability Improvement

H4. *A hard-soft teleoperator has better contact stability and lower contact forces compared with a hard-hard teleoperator.*

As was shown with great detail in Chapter 5, contact stability is improved for soft slave teleoperation, for all three control architectures investigated. This, in conjunction with the results from the grasping experiments in Chapter 7, makes it clear that the stability can be improved with equivalent task performance for certain tasks but not others. For the size discrimination task, the hard-soft teleoperator allows equal or better task performance for increased stability. For this task, hypothesis **H4** is true.

For the teleoperated assembly task in Chapter 8, it is clear that the task can be performed easily and quickly with the soft slave device. However, it was not possible to compare with hard-slave performance with the current experimental setup, an issue that warrants further investigation. It seems that for the soft slave, the compliant section facilitates the peg-in-hole task significantly. Stability could be guaranteed in contact with any environment.

However, the stability that was analyzed for the teleoperators in this research was for free air motion and contact tasks, two tasks that span the wide task- impedance continuum. However, there are certain other tasks, such as pick-and-place tasks, where the load at the tip of the teleoperator may vary. Increased mass at the tip can lead to lower controllability for a soft slave device, because the frequency of the first resonant mode is reduced, but this specific situation has not explicitly been quantified in this research.

In earlier research, the use of programmable softness (e.g. shared compliant control (Hannaford et al., 1991)), and software-based low-pass filters in the forward path (Qian, 1993; Tanner and Niemeyer, 2006) have been shown to improve stability. However, the use of a high-speed force-loop to transform a stiff robot into a virtual spring has a number of disadvantages compared with a mechanical spring: First, the cost of high quality force-sensors can be prohibitive, and second, the inertia of the stiff robot is difficult, to reduce by control. Third, the mechanical spring is faster than any controller, since these have a limited bandwidth. This is especially important at the moment of contact with a hard object, before the controller can compute any compensating force to reduce the forces. The advantage of the “programmed spring” is that the stiffness requirements may change during operation, and this can be adjusted by a simple gain change. A mechanical spring is generally more difficult to adjust on-line. Finally, the mechanical compliance in the soft slave decouples the inertia of the motor from the inertia of the tip. This reduction of which improves the high-frequency force-control and is one of the underlying reasons for the stability improvement.

9.5 Haptic Feedback Cues And Performance

H5. *Low-frequency and high-frequency haptic feedback improves (reduces) impact forces in hard-object assembly tasks.*
H6. *Low-frequency and high-frequency haptic feedback improves (reduces) task completion time in hard-object assembly tasks.*
H7. *Low-frequency and high-frequency haptic feedback improves (reduces) subjective workload in hard-object assembly tasks.*

It is often stated that the interaction information should be presented to the operator as "transparently" as possible (Lawrence, 1993), which means that the environment impedance should be as accurately reproduced as possible, over all frequencies. It is based on the assumption that all information is of equal value to the human operator, and that any additional feedback channel will lead to improved performance. However, there are reasons to assume that for a specific task, some information is more useful than other.

The assembly task experiment described in Chapter 8 provided valuable insight in how various haptic and visual cues are combined in a more complex task. The addition of low-frequency and high-frequency haptic feedback had very little impact on objective task performance metrics. The only measurable improvement was that *the high-frequency impact forces are reduced when low-frequency feedback is added*. This is in contrast to previous experiments in the literature, where addition of low-frequency force feedback improved task performance with one order of magnitude (Hannaford et al., 1991). Hypothesis **H5** is thus only true for the case of low-frequency feedback, and not for high-frequency feedback. Hypothesis **H6** is not true for any of the experimental conditions in this research.

It was noted by Hogan (Hogan, 1985) that peg-in-hole tasks are essentially impedance tasks, which means that the slave device stiffness must not be too large. In a classical teleoperator, the addition of low-frequency force feedback includes the human hand in the loop, which essentially acts as a passive spring in this part of the task, and reduces the impedance felt at the tip of the slave robot.

This is illustrated in Fig. 9.1, where four conditions of hard-object peg-in-hole assembly are compared, from the point of view of the peg. In the manual condition (a.), the hand provides the necessesary compliance (low stiffness). For the conditions b. and c. (the conditions compared by Hannaford in Hannaford et al. (1991)), the addition of haptic feedback includes the human hand in the loop, which then can act as the compliance. The condition without haptic feedback is in fact a position-controlled industrial robot, which is notoriously poor at this type of tasks. The final condition d. presents the two conditions of low-frequency haptic feedback in the assembly experiment presented in this thesis. Both with and without haptic feedback, there is a soft element in the slave device which ensures the necessary compliance. *A soft-slave teleoperator with visual feedback does not necessarily need haptic feedback for peg-in-hole tasks, thanks to the built-in compliance.*

However, there was a difference in subjective workload depending on the feedback cues. The addition of low-frequency haptic feedback changes the dynamics felt at the master device which is consistently reported as a negative change in "Physical Demand", as defined using NASA-TLX (Hart and Staveland, 1988). The addition of haptic feedback has thus both positive and negative effects, which is often neglected in the literature. The change of the master dynamics is strongest when using controllers where position-position control dominates. It is adviceable to take this into account when evaluating whether or not to add haptic feedback to teleoperators. The negative influence on subjective workload is probably one of the main reasons why haptic feedback is lacking from many commercial teleoperators today.

On the other hand, there were some positive effects of haptic cues in the assembly task. *A combination of high-frequency and low-frequency haptic feedback improves the subjective workload*, as defined by NASA-TLX Percieved Performance and Frustration Level. It is interesting to note that the subjects were more confident of their performance, even though the performance was almost identical to the no-haptic-feedback experimental condition. It is sometimes claimed that reduced subjective workload is better (Hart and Staveland, 1988), but in this case it may also give a false impression of the actual performance. It would be interesting to perform a study where each subject performs tasks of different difficulty to compare the correlation between percieved performance and actual performance.

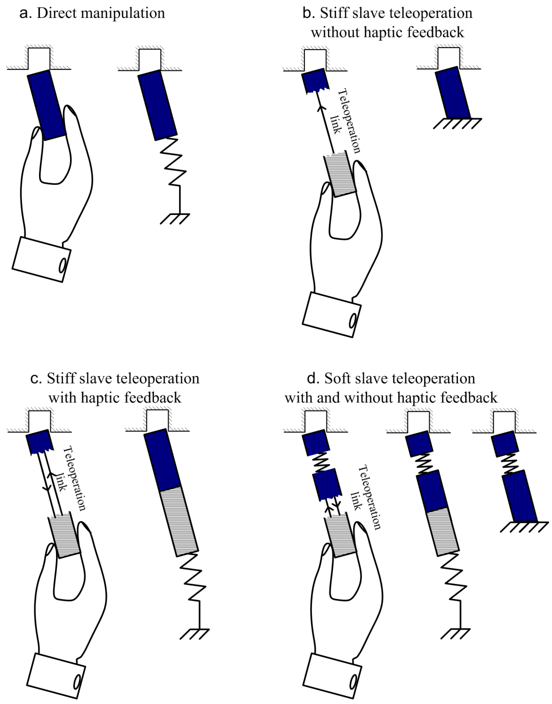

Figure 9.1: *Peg-in-hole task compliance: a. Direct manipulation (ok). b. Stiff slave teleoperation without haptic feedback (not ok). c. Stiff slave teleoperation with haptic feedback (ok). d. Soft slave teleoperation with/without haptic feedback (ok).*

Hypothesis **H7** is only true as a combination, where low- and high-frequency feedback cues together improves (reduced) subjective workload. Adding low-frequency feedback only actually increased the subjective workload.

An analogy from the audio world could illustrate why "perfect transparency" and an equal transmission of information over all frequencies is useful for some applications but not for others. In the hifi-audio world, the ideal system is a one-to-one perfect transmission of sound information from a remote artist to the ear of the beholder. Different components in the chain (amplifiers, speakers, connection cables) are characterized by the transmission characteristics, usually as functions of frequency. The more "transparent" the component, the higher the percieved performance for the specific task of "exquisite sound reproduction". However, a related audio-tool is a hearing aid, which also transmits and amplifies sound from a remote speaker to the ear of the beholder. In this case, the task is different; in general to distinguish human speech. Therefore, the sound is processed by frequency-selective filters to enhance certain parts of the sound information and attenuate others. This enlarges the differences between sounds with different meaning, which improves the capabilities of the listener to understand the spoken message. The selective filtering is based both on knowledge about the task at hand and on a deep insight in the sensoric system of the human hearing system.

Based on this research on haptic teleoperation, it seems that a similar methodology could be useful in this domain. For each different task, the contact information captured by the slave device can be processed to extract and amplify different cues, to support the operator optimally. To achieve this vision, more research is needed both regarding the haptic sensoric and perceptual system and on how to characterize task information. With this knowledge, more useful teleoperators can be designed for each task.

In both the grasp task experiments and the assembly task experiment, the variation between subjects constitute the largest difference in task performance. For novice users of teleoperators, as seen in the assembly experiment in Chapter 8, the best subjects are more than twice as good as the worst ones. This observation should be reconfirmed and quantified during training to measure if this difference would persist in the long term. In any case, is *careful selection and training of personnel as important as careful design of a teleoperator.*

A final note on the haptic feedback cues from the assembly task regards the implementation of the cues.

The cost of low-frequency feedback can be estimated to 100-1000 euro per degree of freedom, comprising a motor and an amplifier channel at the master side, and twice as much when measuring the forces using a force sensor. The cost of high-frequency feedback is in the order of 10-100 euro per degree of freedom, including an accellerometer and a vibrator. Furthermore, the human sensory system for high frequency information (pacinian corpuscles) is not direction dependent, so it is enough to actuate one degree-of-freedom (Johansson, 1996). The addition of the high-frequency feedback is a cost-efficient way of providing informative cues to the operator.

9.6 On Controller Synthesis

All modern control science techniques (H_∞ etc.) are based on optimization of a "performance measure" function (sometimes phrased as minimization of a "penalty function") (Skogestad and Postlethwaite, 1996). However, the underlying assumption is that this *performance measure function* is known and preferably that it is linear.

Contrary to the encouraging results indicated in literature, all of the commercially available haptic interfaces have controllers with hand tuned gains.

The core of the problem of using modern control methods and automated optimization, instead of using manual tuning, is that the *performance measure function is unknown*. The attempts that have been done in literature use simple linear performance measures like minimizing force error and velocity error equally over all frequencies (Lazeroms, 1999) or trying to achieve one specific master impedance (Fattouh and Sename, 2003). An experienced teleoperator designer uses a much more complex performance function, where he/she incorporates free-air inertia, transparency, stability, and all other aspects of the teleoperator while hand-tuning the gains. By moving the teleoperator in free air and in contact, while slowly adjusting the gains, the designer searches for an optimum of his/her integrated performance function.

If we could capture the internal model inside the head of the experienced teleoperator designer into a mathematical formula, the optimization could be greatly improved. One way to move forwards is to perform a black-box identification experiment to capture the integrated performance function inside the head of experienced teleoperator designers. This could be done by presenting a number of settings to an expert, who would classify the performance, e.g. in a pairwise forced-choice type of experiment. However, there is also the question of how good the internal model of the teleoperator designer actually is? Another way to proceed is to perform human factors experiments to quantify which information helps the operator the most, as has been done in this thesis, and to use this knowledge to optimize the teleoperator design. This thesis presents a first attempt to quantify the real human needs for two simple tasks (Part III) and one mechatronic attempt to improve the performance/stability trade-off by the concept of hard-soft design (Part II).

The important insight that the *requirements for a teleoperator are strongly task specific* gives a refreshing view on how optimize the mechanical and controller design. There will never be one perfect teleoperator design which is the best for everybody and for every task, but rather *different optimal designs for each specific task, operator and environment*.

Practical implementation of task-optimal teleoperation controllers meets two interesting hurdles - the formulation of the control problem, and how to ensure the usability of the teleoperator. In the framework of robust LPV control, the control problem could be expressed as a minimization of a standard performance function under a parameter variation in the input-output filters, see Fig. 9.2. Usually, the controller can handle variations of the plant, but in the case of a teleoperator used for different tasks, the mechanics of the plant remain constant but the performance filters ($W_1(s,\Theta)$, and especially $W_2(s,\Theta)$) vary. The controller synthesis problem can be formulated as the minimization of the following performance function:

$$\min_k \|W_1(s,\Theta)\,T(k,s)\,W_2(s,\Theta)\|_\infty \tag{9.1}$$

The shape of the W-filters are still an open issue, and it is also possible that the ∞-norm is not the most suitable one. However, (9.1) can be seen as a starting point for the application of modern control methods in the field of haptic teleoperation.

If it is possible to synthesize controllers for different tasks, the system must know which task the operator is performing (the external parameter Θ in the LPV methodology). One way of solving this is that the

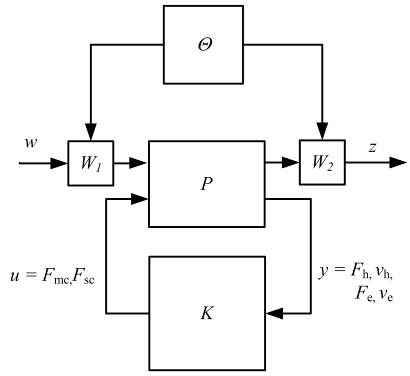

Figure 9.2: *Controller and plant structure for implementation of a LPV controller.*

operator indicates which task he/she is doing. Regarding the usability of such a system, there has been some interesting previous work on user-activated controller switching, where the operator has the choice of a discrete number of pre-synthesized controllers. One illustrating example is the chassis controller of the Volvo S60 Sports car, see Fig. 9.3. Three buttons allow the driver to choose between three controller gain settings appropriate for the task at hand ("Comfort Driving", "Sports Driving" or "Advanced Driving") (VOLVOCARS, 2006). The controllers that vary are related to engine control, anti-spin system and settings for the automatic transmission.

Figure 9.3: *Operator selection of task-optimal controller: Example from a Volvo S-60 car, where the "Active Chassis System" is a set of three pre-programmed controllers.*

Similar task-switching buttons could be useful for a teleoperator, where the operator would switch from e.g. "Manipulation" to "Sensing" and further to "Accurate positioning".

9.7 Contribution and Future Outlook

The field of haptic teleoperation is currently in a very dynamic phase. The last ten years has seen an explosion in publications and active projects, both in the Benelux area and on the global scale. This thesis contributes to the field in three important ways. First, the concept of hard-soft haptic teleoperation is presented in detail to the community. Second, the insight that teleoperator design requirements are strongly task specific is shared. Third, a number of general assumptions in the field are shown to be false, at least for the experimental conditions in this study. Of the hypotheses of this study, all generally assumed to be true, only one (**H4**) held for all tested conditions.

The main challenges in the coming years include:

- Standardization: Use a common notation for analysis and control. This field is surprisingly immature in this sense, even though people have built teleoperators for more than 50 years. One of the main problems is the lack of textbooks, and Chapter 2 of this thesis is a first attempt on a common textbook. A related, important development is the open standard for master-slave communication that Blake Hannaford at University of Washington, Seattle, is currently working on together with with SRI, Stanford.

- Modelling and Simulation Platform: There is a need for an easy-to-use modelling and simulation platform where teleoperators can be simulated and analyzed. In this project, a first attempt for a widespread open source analysis package was developed, but there is still a need for easy to use and accurate simulation tools. One of the problems with the current block-model representation is that causality may reverse during simulation; that the free air environment can be modelled as an impedance, but the stiff contact better is modelled as an admittance. This may be possible to solve using bond-graph based tools like Modelica or 20-Sim.

- Task-based information quantification: Create a notation and a method to specify real teleoperated manipulation tasks using quantified teleoperator requirements. There is information lacking both on the human haptic sensoric system, and how we process this information at a higher level. Task-based information quantification is the basis for computer-aided optimal control and mechatronic design. With well-formulated optimization criteria the important step can be taken from the 1950's control science (used in this thesis) to modern control science methods like robust control and LPV control.

- Integration of Multimodal Information: How can the haptic information best be combined with visual and auditive cues? Which part of the task information is best communicated via the haptic channel, and which through other channels? There is also a growing interest in presenting non-haptic information as haptic information, e.g. distances converted into force-fields (Abbink, 2006) or using task-information for augmented reality support cues. The question is how to combine the different information channels into consistent and helpful stimuli to the operator.

Chapter 10

Conclusions

The main conclusions of this research are:

- A hard-soft haptic teleoperator has better contact stability and lower contact forces, compared with a hard-hard teleoperator, mainly thanks to the decoupling of the tip mass from the motor inertia.
- Teleoperated manipulation allows for equal size discrimination performance, compared with direct manipulation.
- The total teleoperator stiffness does not influence human size discrimination performance.
- The total teleoperator damping does not influence human size discrimination performance.
- The total teleoperator stiffness does not influence human stiffness discrimination performance.
- For size and stiffness discrimination tasks, a bracket or a loose thimble is just as good as a multi-point-of-contact interface.
- Low-frequency haptic feedback reduces impact forces in hard-object assembly tasks.
- Low-frequency haptic feedback increases subjective workload (*NASA-TLX Physical Demand*) for hard-object assembly tasks.
- A combination of high-frequency and low-frequency haptic feedback reduces the subjective workload (*NASA-TLX Percieved Performance and Frustration Level*).
- A soft-slave teleoperator with visual feedback does not need haptic feedback for peg-in-hole tasks, thanks to the built-in compliance.
- Careful selection and training of personnel is as important as careful design of a teleoperator.
- Different tasks have different requirement on the teleoperator, so for each combination of task/human/environment, there is a different optimal controller and optimal mechanical design.

Appendix A

The MaximaHaptics Toolbox

G.A.V. Christiansson
Proceedings of IEEE WorldHaptics Conference 2005, Pisa, Italy

The Maxima Haptics Package is a free software package for symbolic analysis of linear models of haptic devices and teleoperators. From a mechanical model of the haptic device, the slave robot and a formulation of the controller, the package calculates the well known "hybrid matrix" representation of the whole system. From the acquired hybrid matrix, the linear performance measures and external device characteristics can be calculated, e.g. force bandwidth and free air inertia. The Maxima Haptics Package currently allows for linear analysis of single-degree-of-freedom haptic devices and teleoperators with kinesthetic feedback. The intention is to provide a common language for the haptic community for exchange of symbolic models and scientific publication of analytical results.

The Maxima Haptics Package is released to the public for the first time ever during the WorldHaptics Conference 2005.

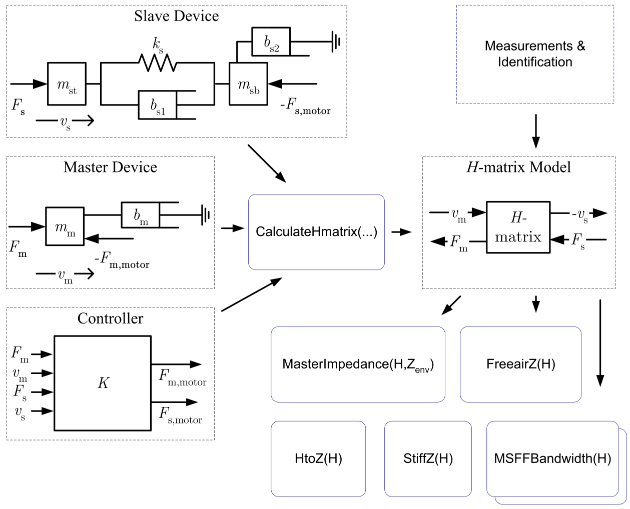

Figure A.1: *An overview of the Haptics package. You define your system using simple equations for the master, slave and the controller and the Haptics Package calculates the H-matrix. This matrix can be used to calculate various analysis characteristics, both symbolically and numerically*

A.1 Introduction

Mathematical analysis of haptic teleoperators and control schemes represent a substantial share of the haptic literature (Hannaford, 1989a), (Raju et al., 1989), (Lawrence, 1993), (Yokokohji and Yoshikawa, 1994) and a significant challenge for researchers new to the field, (Lazeroms et al., 1997), (Sherman et al., 2000). During the design process of a new teleoperator or when developing a new control scheme it is of great importance to be able to calculate the behaviour of the device.

The Maxima Haptics Package allows for linear analysis of single-degree-of-freedom teleoperators with kinesthetic feedback. The user defines a teleoperator hardware using mechanical model equations and controller equations, and the package calculates the linear transfer functions of the system in the hybrid matrix notation, introduced to haptics in (Hannaford, 1989a). (The two-port modelling theory was developed in early 1900's for electric networks, (Feldtkeller, 1937), but gained popularity in the teleoperation field only later.) This hybrid matrix model is used as a basis for all the linear performance measures, see Figure A.1 for a brief overview. The symbols and the notation are explained in section A.2 below. This paper explains the workings of the Maxima Haptics Package in a teleoperation setup, but the slave robot can just as well be the interaction with a virtual environment.

The goal for this package is to help researchers and developers to easily and accurately analyse teleoperators and haptic devices. You can also easily convert the model from the hybrid matrix notation to another, and all calculations and results are easily exported to LaTeX for beautiful typesetting. It is also possible to define numerical values of all components and to get numerical results.

The Maxima Haptics Package allows students to easily follow the calculations in articles in the haptics literature and the User's Guide contains some examples from major papers.

The Maxima Haptics Package is a free software package for the computer algebra system Maxima, which is also free software. Therefore all researchers and students all over the world can use this software at no cost (just like the VR Haptics library Chai3D (Conti et al., 2003)). Maxima runs on many platforms including Linux, Solaris, Microsoft Windows and Mac OS/X.

A.2 Symbols and Conventions

The Maxima Haptics Package uses the most common notations from the literature on haptics and teleoperation (Hannaford, 1989b), (Adams and Hannaford, 2002): impedances and admittances as transfer functions between forces and velocities. The positive direction is defined in Figure A.2: F_{m} is the force that the operator excerts on the master, F_{s} is the force that the slave. The velocities v_{m} and v_{s} are defined as positive when the operator is pushing the device into the environment.

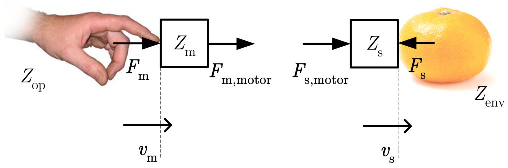

Figure A.2: *The direction of the forces and velocities are important. The Maxima Haptics Package works with the standard definitions from Hannaford (Hannaford, 1989a) and Lawrence (Lawrence, 1993)*

The standard linear model representation is the hybrid matrix form, see Figure A.3.

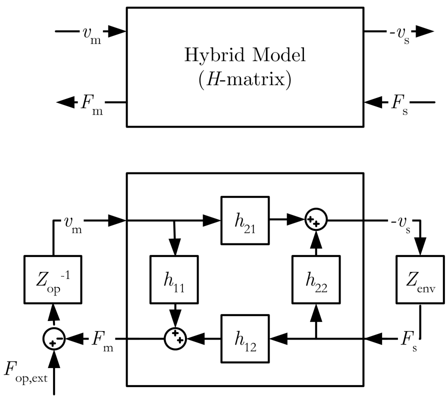

Figure A.3: *The Hybrid Matrix block model has v_{m} and F_{s} as inputs and F_{m} and -v_{s} as outputs. The environment is modelled as an impedance Z_{env} and the operator as $Z_{\mathrm{op}}^{-}1$*

The block model shown in Figure A.3 can also be written as an equation with the H-matrix:

$$\begin{bmatrix} F_{\mathrm{m}}(s) \\ -v_{\mathrm{s}}(s) \end{bmatrix} = \begin{bmatrix} h_{11}(s) & h_{12}(s) \\ h_{21}(s) & h_{22}(s) \end{bmatrix} \begin{bmatrix} v_{\mathrm{m}}(s) \\ F_{\mathrm{s}}(s) \end{bmatrix} \tag{A.1}$$

Please note that the velocity is positive into the device, both on the slave side and the master side, which causes the somewhat confusing convention to choose the negative v_{s} as output signal on the slave side. The H-matrix contains thus all information about how forces and velocities are transmitted through the teleoperation system. Therefore it can be used as a basis for all calculations of linear performance measures and stability margins.

The H-matrix components are calculated them from a component model of the teleoperator. Therefore, the H-matrix contains all information about the teleoperator, from the physical contact between the operator and the master interface to the physical contact between the slave robot and the remote environment.

A.2.1 Component Models

The component model of a device is based on the mechanical components of the device and the gains in the controller. In Figure A.4 an example model is shown to illustrate the concepts of the mechanical model. This model is also used in the section A.3 below. You can of course define any mechanical structure as master or slave device.

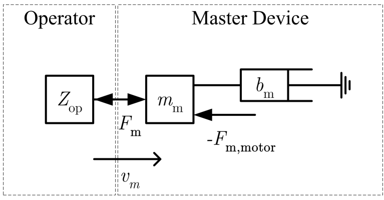

Figure A.4: *Example of a component model of the master device - here modelled as a mass and a damper*

The component models of the master and the slave are expressed using Newton's Laws of motion in Laplace form:

$$\begin{aligned} m_{\mathrm{m}}\, s\, v_{\mathrm{m}} + b_{\mathrm{m}}\, v_{\mathrm{m}} &= F_{\mathrm{m}} + F_{\mathrm{m,motor}} \\ m_{\mathrm{s}}\, s\, v_{\mathrm{s}} + b_{\mathrm{s}}\, v_{\mathrm{s}} &= -F_{\mathrm{s}} + F_{\mathrm{s,motor}} \end{aligned} \tag{A.2}$$

The controllers for the master and the slave device are described as linear transfer functions of the measured variables, see Figure A.5. (e.g. For a MIMO PD controller, the $K_{ij} = P_{ij} + s\, D_{ij}$.)

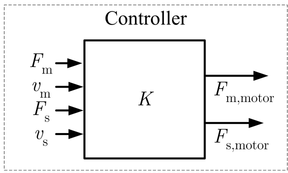

Figure A.5: *An general controller for a teleoperation system. It uses all sensor data to calculate the desired motor forces on the master side and the slave side*

Assuming that all signals (F_{m} ,v_{m} ,F_{s} ,v_{s}) are measured, the controller gains K_{ij} can be chosen arbitrarily according to the "4-Channel-architectures". By setting one or more of these gains to zero, the more traditional controller architectures "Position Error" or "Forward Flow" can be implemented - for a detailed account, see (Lawrence, 1993) or (Aliaga et al., 2004).

$$\begin{aligned} F_{\mathrm{m,motor}} &= k_{11}\, F_{\mathrm{m}} + k_{12}\, v_{\mathrm{m}} + k_{13}\, F_{\mathrm{s}} + k_{14}\, v_{\mathrm{s}} \\ F_{\mathrm{s,motor}} &= k_{21}\, F_{\mathrm{m}} + k_{22}\, v_{\mathrm{m}} + k_{23}\, F_{\mathrm{s}} + k_{24}\, v_{\mathrm{s}} \end{aligned} \tag{A.3}$$

The equations A.2 and A.3 contain all information of the model, and the Maxima Haptics Package calculates the H-matrix from these symbolic definitions.

A.3 Getting Started

This section gives some simple examples how to use the Maxima Haptics Package.

A.3.1 A Simple Setup

This section contains some examples on using the Haptics Package for a simple setup. The teleoperation setup chosen is the one presented by Zhu et al. in the interesting paper (Zhu et al., 1999). We will use his model and perform the same calculations as are done in that paper, and make sure that we get the same results. We can then proceed and calculate other interesting analytical or numerial measures that characterize that teleoperation setup.

First the Haptics Package functions must be loaded into the Maxima workspace. The package consists of different files, and all of them can be loaded using the following command:

```
(C1) load("haptics.mc")$
```

Now you can define your teleoperator components - the hardware devices and the controller. The architecture used is depicted in Figure A.6.

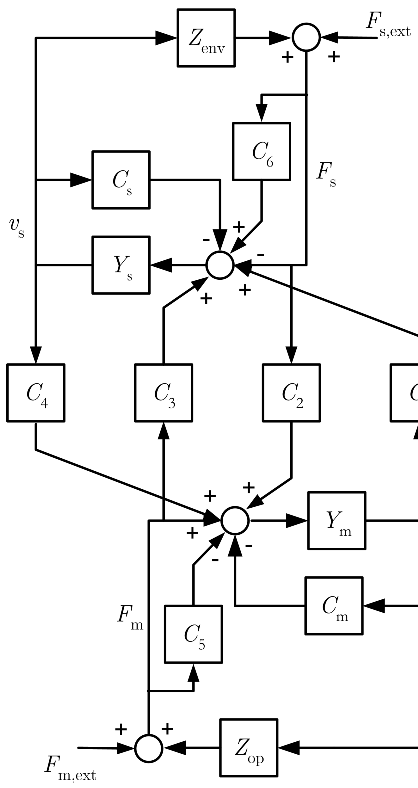

Figure A.6: *The component model of a teleoperation system used by Lawrence (Lawrence, 1993) and Zhu (Zhu et al., 1999). The C_i (sometimes called K_{ij}) blocks are part of the controllers.*

The devices can be expressed using Newton-equations for each involved mass - as a force balance. Zhu et al. chose to represent the master and slave devices as single masses: ($Z_{\text{m}} = m_{\text{m}}\, s$ and$Z_{\text{s}} = m_{\text{m}}\, s$)

```
(C2) masterEQ:Zm*vm=Fm+Fmmotor$
(C3) slaveEQ:Zs*vs=-Fs+Fsmotor$
```

The controller scheme used is expressed as controlled motor force as a function of the measured signals (e.g. F_{m}, v_{s} etc.). You define the controller, and then collect the equations using the following statements:

```
(C4) cEQ1:Fmmotor=-Cm*vm-CC2*Fs-CC4*vs$
(C5) cEQ2:Fsmotor=CC3*Fm+CC1*vm-Cs*vs$
(C6) device:[masterEQ,slaveEQ,cEQ1,cEQ2]$
(C7) redundant:[Fmmotor,Fsmotor]$
```

Now the complete system is defined, and the H-matrix can be calculated by the built-in function `CalculateHmatrix()` The command syntax is further explained in the Function Reference section.

```
(C8) H:CalculateHmatrix(device,redundant);
```

The variable `Hmatrix` now contains the complete H-matrix of the teleoperation system. We can use it to calculate various properties of the system, and we begin with the transmitted impedance. This is Equation (11) in (Zhu et al., 1999).

(C9) `Zeq11:GetMasterImpedanceH(H,-Ze);`
(D9)

$$\frac{(Z_m + C_m) Z_s + (Z_e + C_s) Z_m + (C_m + C_1 C_2) Z_e + C_m C_s + C_1 C_4}{Z_s + (1 - C_2 C_3) Z_e + C_s - C_3 C_4}$$

Note that the remote impedance is sent as negative, due to the sign conventions used in that particular paper.
Now we can define the device impedances and the controllers, according to Zhu (1)-(8):

(C10) `Zm: Mm*s$ Zs: Ms*s$`
(C11) `Cm:bm+km/s$ Cs:bs+ks/s$`
(C12) `CC1:Cs/G$ CC2:G$ CC3:1/G$ CC4:-Cm*G$`

And assumption Zhu (12) that the master and slave devices are the same. Note that we evaluate the slave impedance again (`ev(Zs)`) to propagate the updated variable value.

(C13) `Ms:Mm$ Zs:ev(Zs)$ H:ev(H)$`

Now we can calculate the transmitted impedance as function of controller parameters and device properties, as in Zhu (13):

(C14) `Zeq13:GetMasterImpedanceH(H,-Ze);`
(D14)

$$Z_e + m_m s$$

Finally we look how the H-matrix looks like, as in Zhu (14):

(C15) `Zeq14 : ratsimp(H);`
(D15)

$$\begin{bmatrix} m_m s & G \\ -\frac{1}{G} & 0 \end{bmatrix}$$

We have now used some of the functions of the Haptics Package, and two built-in functions from Maxima (`ev` and `ratsimp`).

A.3.2 A More Advanced Model

It is also possible to model more advanced systems, like a teleoperation system with a flexible slave robot (Fritz et al., 2004), (Christiansson, 2004), (Moschini and Fiorini, 2004). The mechanical model is shown in Figure A.7.

The addition to the code needed is another line in the definition of the slave device equation, because there are two moving masses. Optionally the controller can be extended to deal with the slave tip velocity v_s separate from the base velocity v_{sb}.

This way we can calculate the influence on any performance indicator, based on any model parameter. As an example, we can give numerical values to all parameters and vary one design parameter to understand the influence of this parameter on the performance. In Figure A.8 we plot how the slave compliance k_s influences the free air impedance, i.e. how the device feels when moving in free air.

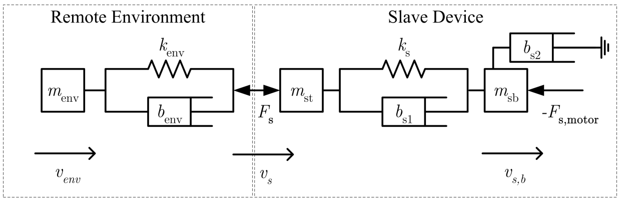

Figure A.7: *A flexible slave robot is an example of more advanced components that easily can be included in the analysis*

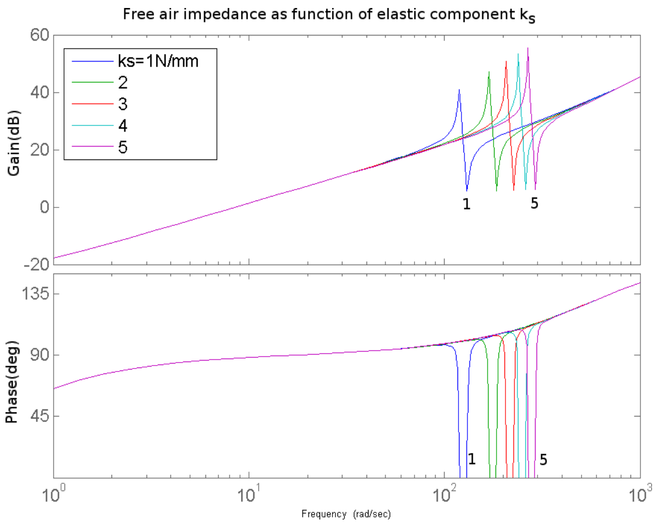

Figure A.8: *A combination of symbolic and numeric analysis allows us to calculate the device performance dependence on e.g. slave compliance k_s*

A.4 Conclusions and Future Work

The Maxima Haptics Package allows for symbolic and numerical analysis of all linear analysis of haptic teleoperators, independent of controller architecture. Using the straightforward commands of the Maxima Haptics Package, most of the characteristics of any teleoperator can easily be analyzed.

Future extensions of the software include improved export-functions to the Control Science Toolboxes of SciLab and Mathworks Matlab - to allow faster numerical manipulation with the results. Currently there are seven analysis functions implemented in the package and this can easily be extended to cover all the important performance measures in the haptics literature.

By using a standard notation and platform-independent free software, we hope to help the haptic community to converge to one notation for scientific publications, which will faciliate communication, teaching and understanding.

Installation

The Maxima Haptics Package is a package for Maxima (`http://maxima.sourceforge.net`), so first you must download and install Maxima (version 5.9.0 or later) for your operating system. The Maxima Haptics Package is available for download at the Delft Biorobotics Laboratory website: `http://dbl.tudelft.nl`

Function Reference

This section describes the most important functions in the Haptics Package; the H-matrix-calculation and some examples of the analysis tools.

CalculateHmatrix

This function calculates the H-matrix from the mechanical model equations of a system and the controller equations. The controller equations can be defined with great flexibility to accommodate for all linear architectures (including Position Error, Forward Flow, Lawrence 4-channel etc).

```
H:CalculateHmatrix(Eqns,redundantVars);

Input:  Device equations and a list of
        redundant variables
Output: H-matrix
```

For an example, see A.3.

AtoB-Functions

A given linear two-port can in principle be expressed using six different 2x2 transfer function matrices (H,G,Z,Y,C,B), depending on which signals are chosen as input and output. The standard notation used in this paper is the H-matrix. However, sometimes it is necessesary to convert to another notation, for comparison with other papers or old models. Therefore we include conversion formulae between all notations, as `AtoB`-functions, where `A` and `B` are names of the matrices. An example is the conversion from the hybrid matrix (H) to the impedance matrix (Z).

```
Zequivalent : HtoZ( Hmatrix );
Input:  Hmatrix - 2x2 matrix
Output: Zequivalent - 2x2 matrix
```

For a generic H-matrix the conversion to the impedance matrix is:

```
(C16) Hexample:matrix([h11,h12],[h21,h22]);
(C17) Zexample:HtoZ( Hexample );
(D17)
```

$$\begin{bmatrix} \frac{h_{11}\,h_{22}-h_{12}\,h_{21}}{h_{22}} & \frac{-h_{12}}{h_{22}} \\ \frac{-h_{21}}{h_{22}} & \frac{-1}{h_{22}} \end{bmatrix}$$

Analysis Tools

When we have calculated the H-matrix for a haptic device or a teleoperator, we can use the built-in functions for analysis of the device characteristics and calculate various performance measures. All of these functions can be performed either symbolically or numerically. At any time during the process, you may define numerical values on any of the symbols - and get numerical results.

Transmitted Impedance

One of the most importantv characteristics of a teleoperation system is how a certain remote environment (Z_{env}) feels at the master side. We can easily calculate how the remote impedance Z_{env} feels at the master side:

```
Zfelt: GetMasterImpedanceH(Hmatrix,Zenv);
Input:  Hmatrix (2x2), Zenv (impedance)
Output: The impedance felt at the master
    side for remote environment Zenv
```

Bandwidth Functions

As there are four different signals (forces and velocities), there are four different bandwidths. The first example is Master to Slave Force-Force bandwidth:

```
bw : MSFFBandwidthH( Hmatrix );
Input:  Hmatrix - hybrid matrix
Output: Master-Slave Force Bandwidth

bw : SMFFBandwidthH( Hmatrix );
Input:  Hmatrix - hybrid matrix
Output: Slave-Master Force Bandwidth
```

The velocity-velocity bandwidth is also interesting, because it describes how well movement is followed. In the literature most often the master-slave velocity bandwidth is mentioned, but also the slave-master bandwidth is valuable to compare.

```
bw : MSvvBandwidthH( Hmatrix );
Input:  Hmatrix - hybrid matrix
Output: Master-Slave Velocity Bandwidth

bw : SMvvBandwidthH( Hmatrix );
Input:  Hmatrix - hybrid matrix
Output: Slave-Master Velocity Bandwidth
```

Latex Export

The Maxima system has a nice built-in feature that allows the user to export mathematical formulae in LaTeXformat, the `tex(expression,filename)`-function. It can even convert Maxima-variables `Mm` to your LaTeXcode variable `\Mm`, using the `texput(Mm,"\\Mm")` function, which later will be interpreted as m_{m}. The Haptics Package includes two files that makes this automatic:

```
Hmaximalatex.mc, hapticssymbols.tex
```

The `Hmaximalatex.mc` file contains the `texput(maxima,latex)` declarations. This file is included automatically from `Haptics.mc`, so it is always active.

The `hapticssymbols.tex` file is a file full of symbol definitions, to turn `\Fs` into `\ensuremath{F_{\mathrm{s}}}` By including this file in your LaTeXdocuments, you can copy the output from Maxima directly into your source files.

Appendix B

Wave Variables and the Lawrence 4C-Framework

G.A.V. Christiansson
Submitted to EuroHaptics Conference 2008

Force-reflecting (haptic) teleoperation control is difficult. There have been numerous proposals for teleoperation architectures, using a variety of terminology and symbols. This paper expresses the "Wave variable" and the Lawrence/Salcudean "4-Channel" architectures in a unified MIMO framework in the frequency domain.

This allows better understanding of the strong and weak points of both architectures. Furthermore, it is illustrated that the information communicated between master and slave side is very similar in both cases. In fact the term "Control Effort" could be used instead of using the "word wave-variable", which may clarify the mechanism of the controller.

B.1 Introduction

Teleoperation control is difficult. It is relatively simple to formulate the problem, to coordinate the movements of two robots (master and slave device) to allow an operator to manipulate a remote enviroment and to feel how the interaction feels like (Yokokohji and Yoshikawa, 1994; Hannaford, 1989a). However, to implement a stable, accurate and enjoyable teleoperator controller remains a difficult problem. For each degree of freedom we typically measure or estimate a number of signals (forces, velocities, positions etc.) and usually control two forces (controlled force at master and slave side). The output from the controller is the *control effort* for the master and the slave device (F_{mc} and F_{sc}). The forces and velocities used in this paper are further explained in Fig. B.1.

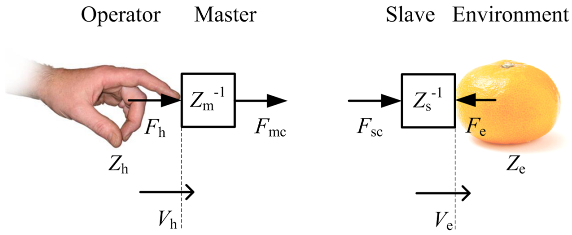

Figure B.1: *The main elements of a teleoperation system, here illustrated for a 1-dof system.*

Any linear controller can be expressed as a transfer function matrix (K):

$$\begin{bmatrix} F_{\mathrm{mc}} \\ F_{\mathrm{sc}} \end{bmatrix} = K \begin{bmatrix} F_{\mathrm{h}} \\ V_{\mathrm{h}} \\ F_{\mathrm{e}} \\ V_{\mathrm{e}} \end{bmatrix} \tag{B.1}$$

This is an intrinsic Multi-Input-Multi-Output (MIMO) control problem, for each degree of freedom, see Fig. B.2. The controller transfer function matrix (K) is a block-matrix consisting of transfer function submatrices for *local* and *communicated control effort*.

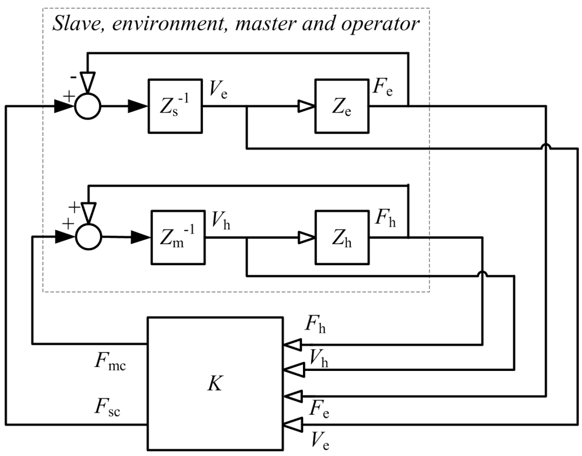

Figure B.2: *Analysis model of a generalized 1-dof teleoperation system, in the frequency domain. The controller (K) is defined as a matrix of transfer functions.*

It means that the controller has a large number of parameters that the teleoperation control engineer must wisely choose, and this is the kernel of the problem. People are not good at finding optima in multi-variable functions. Therefore, a number of procedures have been proposed to reduce the problem into a managable set of parameters: the "Transparency-Optimized 4-Channel method"(4C), (Lawrence, 1993) where the gains are selected according to a specified algorithm, or the "Wave variable architecture"(WAVE) (Niemeyer and Slotine, 2004), where certain constants are specified. Each of these controllers can be expressed in the generalized MIMO formalism, and this allows for easy comparison of the hidden similarities of the different schemes.

This paper describes how to express WAVE control in the 4C framework presented by Lawrence and Salcudean, to allow a deeper understanding of how these important control architectures are related. In particular the information communicated between the master and the slave is expressed in terms of communicated control effort, which is seen to be equivalent to the "wave variables".

B.2 Method

The two controller architectures (4C and WAVE) are presented as block schemes, drawn in the traditional way, as by Lawrence (Lawrence, 1993) and Niemeyer (Niemeyer, 1996). The WAVE scheme is redrawn using equivalent block scheme transformations into a form that is visually more similar to the way the classic 4C controller is usually drawn.

The basis of the analysis is the assumption of linearity. As long as the systems are linear, it does not matter if you add the force and velocity components of the control signal before or after you send it over the communication network. Linearity is generally regarded to be a valid assumption for any specific working point in the workspace. Therefore all models in this paper are expressed in the frequency domain, which allows for simple analysis of stability and traditional performance measures e.g. transparency and the master/slave force and velocity bandwidths.

B.2.1 Lawrence 4-Channel (4C) Control

The Lawrence/Salcudean model is presented as a block scheme in the frequency domain in Fig. B.3. The most important elements here are the summation points where the control efforts are added together. The total effort is the sum of *local control effort* and *communicated control effort*.

Lawrence suggested a method to choose the values for the C_i transfer functions, to ensure a high value of the "Transparency", (Lawrence, 1993), both for a specific time delay and without time delay. His choices are based on a local PI-controller for velocity (equivalent to a PD controller for position) and a P-controller for force, where the set points are the values from the other side (*for no time delay*):

$$\begin{cases} C_{\mathrm{m}} = K_{\mathrm{vm}} + \frac{K_{\mathrm{pm}}}{s} \\ C_4 = -\left(C_{\mathrm{m}} + Z_{\mathrm{m}}\right) = -K_{\mathrm{vm}} - \frac{K_{\mathrm{pm}}}{s} - Z_{\mathrm{m}} \\ C_{\mathrm{s}} = K_{\mathrm{vs}} + \frac{K_{\mathrm{ps}}}{s} \\ C_1 = \left(C_{\mathrm{s}} + Z_{\mathrm{s}}\right) = K_{\mathrm{vs}} + \frac{K_{\mathrm{ps}}}{s} + Z_{\mathrm{s}} \\ C_2 = 1 \\ C_3 = -1 \\ C_5 = 0 \\ C_6 = 0 \end{cases} \tag{B.2}$$

where K_{vm} and K_{pm} are velocity and position feedback gains on the master side, K_{vs} and K_{ps} on the slave side.

The inclusion of the master and slave impedance in the controller is an optional feed-forward action to improve the compensation of damping and inertia. Later, Hashtrudi-Zaad and Salcudean (Hashtrudi-Zaad and Salcudean, 2002) suggested other choices for C_5 and C_6, but the essence is similar. Based on the schematic the expressions for the communicated control effort can be expressed, see (B.3) below (where F_{msc} is the control effort communicated from master to slave, F_{smc} from slave to master):

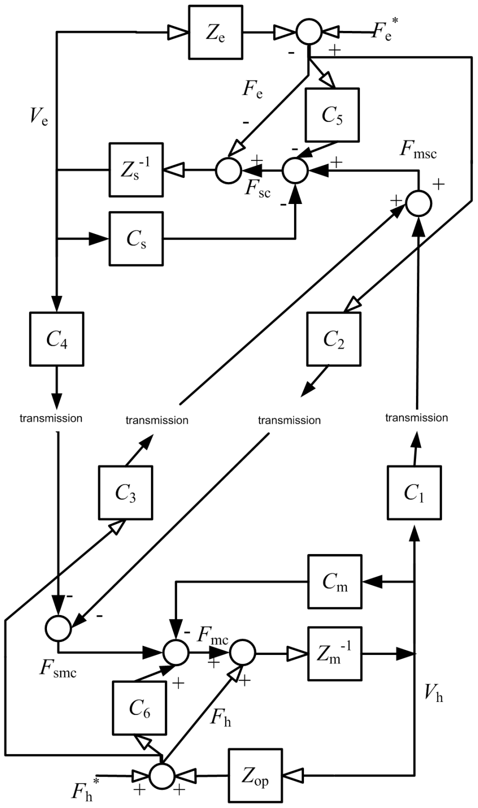

Figure B.3: *The Lawrence/Salcudean "4-Channel" teleoperator controller (4C), adapted from (Hashtrudi-Zaad and Salcudean, 2002). Note how the velocity and force information is transmitted and used.*

$$\begin{cases} F_{\mathrm{smc}} = -C_2\,F_{\mathrm{e}} - C_4\,V_{\mathrm{e}} = F_{\mathrm{e}} + (K_{\mathrm{vm}} + \frac{K_{\mathrm{pm}}}{s} + Z_{\mathrm{m}})\,V_{\mathrm{e}} \\ F_{\mathrm{msc}} = C_3\,F_{\mathrm{h}} + C_1\,V_{\mathrm{h}} = -F_{\mathrm{h}} + (K_{\mathrm{vs}} + \frac{K_{\mathrm{ps}}}{s} + Z_{\mathrm{s}})\,V_{\mathrm{h}} \end{cases} \tag{B.3}$$

The generalized MIMO controller can be expressed in the C_i-elements, based on the equations for the total control effort:

$$\begin{aligned} &\begin{cases} F_{\mathrm{mc}} = C_6\,F_{\mathrm{h}} - C_{\mathrm{m}}\,V_{\mathrm{h}} - C_2\,F_{\mathrm{e}} - C_4\,V_{\mathrm{e}} \\ F_{\mathrm{sc}} = C_3\,F_{\mathrm{h}} + C_1\,V_{\mathrm{h}} - C_5\,F_{\mathrm{e}} - C_{\mathrm{s}}\,V_{\mathrm{e}} \end{cases} \\ \Rightarrow K &= \begin{bmatrix} C_5 & -C_{\mathrm{m}} & -C_2 & -C_4 \\ C_3 & C_1 & -C_6 & -C_{\mathrm{s}} \end{bmatrix} \\ &= \begin{bmatrix} 0 & -K_{\mathrm{vm}} - \frac{K_{\mathrm{pm}}}{s} & 1 & K_{\mathrm{vm}} + \frac{K_{\mathrm{pm}}}{s} + Z_{\mathrm{m}} \\ 1 & K_{\mathrm{vs}} + \frac{K_{\mathrm{ps}}}{s} + Z_{\mathrm{s}} & 0 & -K_{\mathrm{vs}} - \frac{K_{\mathrm{pm}}}{s} \end{bmatrix} \end{aligned} \tag{B.4}$$

The controller is essentially a P-controller for forces combined with a PI controller with feedforward for velocities, similar at the master and the slave. The local velocity and position gains (C_{m}, C_{s}) can be chosen differently on master and slave side, to allow for different controlled impedance, which has proven to be advantageous for e.g. contact stability (Christiansson et al., 2006a).

Lawrence also showed how to select the filters (C_{m}, C_{s}, C_1-C_6) to ensure passivity of the controller also in presence of time delays (Lawrence, 1993).

B.2.2 Basic "Wave-variable" (WAVE) Control

In Fig. B.4, the basic elements of the WAVE controller is shown (adapted from (Niemeyer and Slotine, 2004)). In this paper the assumption is done that the master and slave velocities are chosen as measured input and the controlled forces as output. (Please note the potentially confusing choice of symbols for the "wave variables", the symbols v_s and v_m do not denote velocity!)

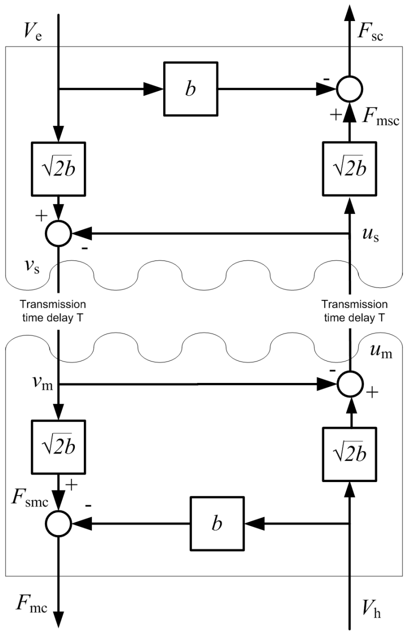

Figure B.4: *The basic "wave-variable" transformation elements, adapted from (Niemeyer and Slotine, 2004).*

The WAVE controller can be transformed using equivalent block-scheme transformations into a form where it is more easy to recognize which information is really communicated. First, the horizontal lines closest to the transmission is moved to the other side of the $\sqrt{2\,b}$ blocks (pure gains). The equivalent schematic is shown in Fig. B.5.

This schematic can be further transformed, by moving the same arrow further out, across the summation point. The consequence is that the signal is splitted in two parts, which are added together with the straight line from V_e and V_h. This way the interesting choice of the factor $2\,b$ becomes clear, because only half of it is sent to the other side. The equivalent schematic is shown in Fig. B.6.

The complete schematic of the basic wave controller architecture, with master and slave devices, and interconnecting operator and environment in shown in Fig. B.7, in a form that resembles the 4C controller. Note that the only measured quantity is the velocity, and that the force information is an estimate based on the commanded control force.

The communicated control effort for the WAVE controller reduces to (first slave to master, then master to slave):

$$\begin{cases} F_\mathrm{smc} = \sqrt{2\,b}\,v_\mathrm{m} = b\,V_\mathrm{e} - F_\mathrm{sc} \\ F_\mathrm{msc} = \sqrt{2\,b}\,u_\mathrm{s} = b\,V_\mathrm{h} - F_\mathrm{mc} \end{cases} \tag{B.5}$$

The communicated control effort contains velocity information and an estimate of the contact force based on the controlled force to the actuators. With a constant time delay, the communicated control effort can also be expressed in the measured velocities:

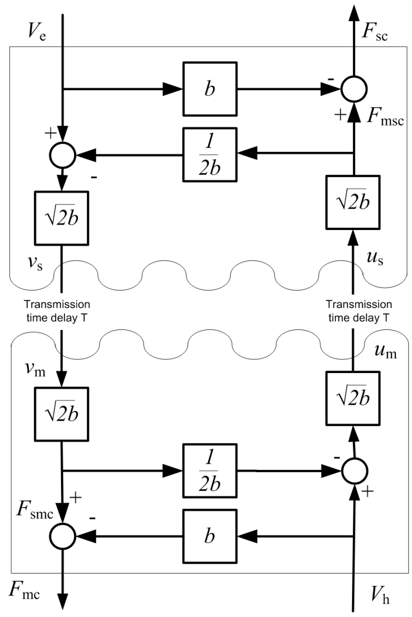

Figure B.5: *The basic "wave-variable" transformation, after equivalent block scheme transformation, to allow bundling of the $\sqrt{2\,b}$ blocks.*

$$\left\{\begin{array}{l} F_{\mathrm{smc}} = e^{-s\,T}\ (b\,V_{\mathrm{e}} - F_{\mathrm{sc}}) = \frac{2\,b\,V s\,e^{s\,T} - 2\,b\,V m}{e^{2\,s\,T}-1} \\ F_{\mathrm{msc}} = e^{-s\,T}\ (b\,V_{\mathrm{h}} - F_{\mathrm{mc}}) = \frac{2\,b\,V m\,e^{s\,T} - 2\,b\,V s}{e^{2\,s\,T}-1} \end{array}\right. \tag{B.6}$$

The WAVE controller can also be expressed in the generalized MIMO form: (*first without time delay*)

$$\begin{array}{l} \left\{\begin{array}{l} F_{\mathrm{mc}} = 0\,F_{\mathrm{h}} - b\,V_{\mathrm{h}} - \hat{F}_{\mathrm{e}} + b\,V_{\mathrm{e}} \\ F_{\mathrm{sc}} = \hat{F}_{\mathrm{h}} + b\,V_{\mathrm{h}} + 0\,F_{\mathrm{e}} - b\,V_{\mathrm{e}} \end{array}\right. \\ \Rightarrow K = \left[\begin{array}{cccc} 0 & -b & -1 & b \\ 1 & b & 0 & -b \end{array}\right] \end{array} \tag{B.7}$$

where $\hat{F}_{\mathrm{e}} = F_{\mathrm{sc}}$ and $\hat{F}_{\mathrm{h}} = -F_{\mathrm{mc}}$ With a constant known time delay, it is possible to express the controller purely using the measured velocities:

$$\begin{array}{l} \left\{\begin{array}{l} F_{\mathrm{mc}} = -b\,V_{\mathrm{h}} + F_{\mathrm{smc}} = -\left(\frac{b\,e^{2\,s\,T}+b}{e^{2\,s\,T}-1}\right)\,V_{\mathrm{h}} + \frac{2\,b\,e^{s\,T}}{e^{2\,s\,T}-1}\,V_{\mathrm{e}} \\ F_{\mathrm{sc}} = -b\,V_{\mathrm{e}} + F_{\mathrm{msc}} = \frac{2\,b\,e^{s\,T}}{e^{2\,s\,T}-1}\,V_{\mathrm{h}} - \left(\frac{b\,e^{2\,s\,T}+b}{e^{2\,s\,T}-1}\right)\,V_{\mathrm{e}} \end{array}\right. \\ \Rightarrow K = \left[\begin{array}{cccc} 0 & -\left(\frac{b\,e^{2\,s\,T}+b}{e^{2\,s\,T}-1}\right) & 0 & \frac{2\,b\,e^{s\,T}}{e^{2\,s\,T}-1} \\ 0 & \frac{2\,b\,e^{s\,T}}{e^{2\,s\,T}-1} & 0 & -\left(\frac{b\,e^{2\,s\,T}+b}{e^{2\,s\,T}-1}\right) \end{array}\right] \end{array} \tag{B.8}$$

B.3 Discussion

By studying the communicated control efforts for the two schemes we can understand the strengths and weaknesses of each method.

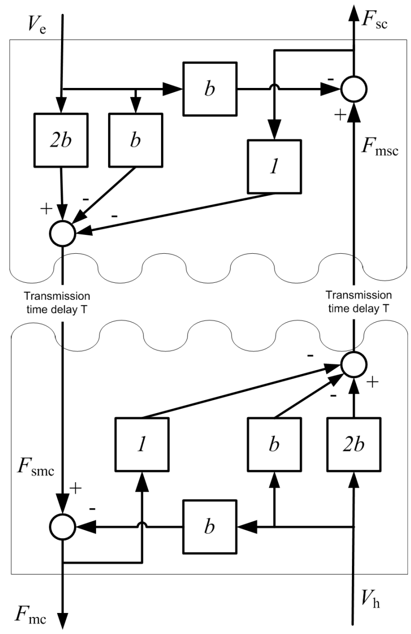

Figure B.6: *The basic "wave-variable" transformation, after equivalent block scheme transformation, on a form similar to 4C.*

For the wave controller, we see in (B.5) that the communicated control effort contains the velocity information and the total controlled force of the device as an estimate of the contact force. Therefore it is not surprising that the velocity error is small, but that there typically will be significant position drift, as reported by (Niemeyer, 1996). Furthermore, the use of controlled force to estimate contact force works only well at quasistatic conditions and where device friction is low, (Park and Khatib, 2006).

By only computing control effort based on velocity information, and ignoring position information, the local dynamics of both master and slave turns into a damped first order system, which always remains stable.

Another observation we can make is that the choice of the WAVE controller to have identical values for the velocity feedback gain (b) on master and slave side can be an important restriction, especially for asymmetric systems.

There have been suggestions to improve the performance of this scheme by adding additional channels for absolute position information (Chopra et al., 2006) and high frequency force information from an accellerometer or a force sensor (Tanner and Niemeyer, 2006). Each of these steps augments the WAVE controller until it almost becomes identical to the 4C controller presented by Lawrence (Lawrence, 1993).

Part of the confusion around WAVE controllers is due to the splitting of the pre-transmission and post-transmission gain blocks ($\sqrt{2\,b}$) which have no effect at all on the stability of the system. This turns the unit of the transmitted signal into an awkward $\sqrt{\mathrm{Watt}}$, when the communicated control effort is actually in Newtons. The reason herefore is easily seen by expressing the signals in SI units:

$$
\begin{aligned}
&[\mathbf{u}][\sqrt{b}] = \sqrt{\mathrm{Watt}}\,\sqrt{\mathrm{damping}} = \\
&\sqrt{\frac{kg\,m^2}{s^3}\,\frac{kg}{s}} = \sqrt{(\frac{kg\,m}{s^2})^2} = \mathrm{Newton}
\end{aligned}
\tag{B.9}
$$

Therefore the physical interpretation is much more straightforward than what has been suggested (Niemeyer, 1996). The information sent over the transmission line is essentially the communicated control effort.

The basic WAVE architecture has been shown to be a special case of the 4C controller, where the force information sent is estimated based on the control signal, and the local PI-velocity feedback controller is restricted to be a P-controller.

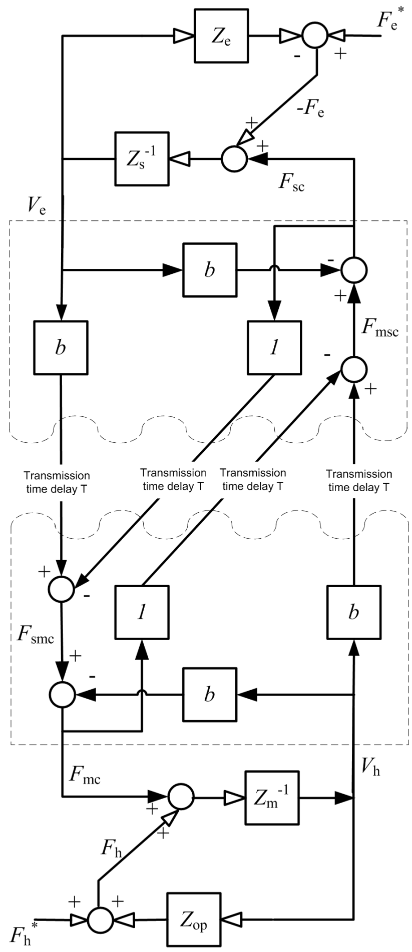

Figure B.7: *The basic WAVE teleoperator controller architecture, in a form similar to the classic 4C-controller schematic.*

It means that a WAVE controller just as easy can be expressed as a 4C controller, with strict restrictions on the gains. And on the other hand, it implies that any 4C controller can be implemented using only two information channels, just like the WAVE architecture, simply by adding the control effort before sending it over the communication link.

B.4 Conclusion

The "wave-variable" control architecture can easily be expressed in a general MIMO framework, which allows comparison with the successful Lawrence/Salcudean 4-Channel framework. The various augmentations to the basic wave variable architecture, by using separate additional paths for measured positions and high frequency forces have been shown to be additions within the 4-Channel framework.

This allows a better understanding of the typical characteristics of the "wave controller". In particular it has been shown that the information transmitted is equivalent to the *control effort*, which has the natural physical interpretation of force.

References

David Abbink. *Neuromuscular Analysis of Haptic Gas Pedal Feedback during Car Following*. Thesis/dissertation, Delft University of Technology, The Netherlands, 2006.

Richard J. Adams and Blake Hannaford. Control law design for haptic interfaces to virtual reality. *IEEE Transactions on Control Systems Technology*, 10(1):3–13, 2002.

Inaki Aliaga, Angel Rubio, and Emilio Sanchez. Experimental quantitative comparison of different control architectures for master-slave teleoperation. *IEEE Transactions on Control Systems Technology*, 12(1), 2004.

Chae H. An, Christopher G. Atkeson, and J. M. Hollerbach. *Model-Based Control of a Robotic Manipulator*. The MIT Press, Cambridge, MA, USA, 1988.

Robert J. Anderson and Mark W. Spong. Bilateral control of teleoperators with time delay. *IEEE Transactions on Automatic Control*, 34(4):494–501, 1989.

Paolo Arcara and Claudio Melchiorri. Control schemes for teleoperation with time delay: A comparative study. *Robotics and Autonomous Systems*, 38:49–64, 2002.

Ales Bardorfer. Connecting a haptic interface with a robot. 10th Mediterranean Electrotechnical Conference. IEEE, 2000.

Antonio Bicchi, Enzo P. Scilingo, and Danilo De Rossi. Haptic discriminiation of softness in teleoperation: The role of the Contact Area Spread Rate. *IEEE Transactions on Robotics and Automation*, 16(5):496–504, 2000.

W. BLUETHMANN, R. Ambrose, M. Diftler, S. Askew, E. Huber, F. Rehnmark, C. Lovchik, and D. Magruder. Robonaut: A robot designed to work with humans in space. *Autonomous Robots*, 14:179–197, 2003.

Grigore C. Burdea. *Force and Touch Feedback for Virtual Reality*. John Wiley & Sons, 1 edition, 1996.

Hyun c. Cho and Jong H. Park. Stable bilateral teleoperaton under a time delay using a robust impedance control. *Mechatronics*, 15:611–625, 2004.

Craig R. Carignan and Kevin C. Cleary. Closed-loop force control for haptic simulation of virtual environments. *Haptics-E*, 1(2):1–14, 2000.

Murat C. Cavusoglu, Alana Sherman, and Frank Tendick. Bilateral controller design for teleoperation in soft environments. International Conference on Robotics and Automation. IEEE, 2001.

Sok-Ho Chang, Jung-Tae Kim, In-Sup Kim, Jin-Hwan Borm, Chong-Won Lee, and Jong-Oh Park. Teleoperation system for humanoid robot. Proceedings of the 3rd International Workshop on Advanced Mechatronics, pages 395–400, 1999.

Nikhil Chopra, Mark W. Spong, Romeo Ortega, and Nikita E. Barbanov. On tracking performance in bilateral teleoperation. *IEEE Transactions on Robotics*, 22(4):861–867, 2006.

Goran A. V. Christiansson. Measuring asymmetric haptic teleoperation device properties. proc. Intl. Conf. on Systems, Man and Cybernetics, The Hague, Netherlands, pages 2454–2458. IEEE, Oct 2004.

Goran A. V. Christiansson. The Maxima Haptics Package - a tool for symbolic analysis of haptics and teleoperation. proc. Haptics Symposium and World Haptics Conference, pages 615–616. IEEE, Mar 2005.

Goran A. V. Christiansson and Erik C. Fritz. A novel 3-dof hard-soft haptic teleoperator. proc. of IEEE Haptics Symposium, World Haptics Conference. IEEE, 2007.

Goran A. V. Christiansson and Frans C. T. v. d. Helm. The low-stiffness teleoperator slave - a trade-off between performance and stability. *International Journal of Robotics Research*, 26(3):287–301, 2007.

Goran A. V. Christiansson, Matthias Mulder, and Frans C. T. van der Helm. Slave device stiffness and teleoperator stability. EuroHaptics Conference, Paris, France, 2006a.

Goran A. V. Christiansson, R. Q. van der Linde, and Ying Tang. Size discrimination in haptic teleoperation - influence of teleoperator stiffness. proc. International Conference on Robotics and Automation, Lake Buena Vista, FL, USA, pages 3263–3267. IEEE, May 2006b.

J. E. Colgate and J. M. Brown. Factors affecting the Z-width of a haptic display. International Conference on Robotics and Automation, San Diego, CA, USA, pages 3205–3210. IEEE, 1994.

J. E. Colgate and N. Hogan. An analysis of contact instability in terms of passive physical equivalents. International Conference on Robotics and Automation, pages 404–409. IEEE, May 1989.

J. E. Colgate and G. G. Schenkel. Passivity of a class of sampled data systems: Applicaton to haptic interfaces. *Journal of Robotic Systems*, 14(1):37–47, 1996.

J. E. Colgate, M. C. Stanley, and J. M. Brown. Issues in the haptic display of tool use. IEEE/RSJ International Conference on Intelligent Robots and Systems, pages 140–145, 1995.

F. Conti, F. Barbagli, R. Balaniuk, M. Halg, C. Lu, D. Morris, L. Sentis, E. Vileshin, J. Warren, O. Khatib, and K. Salisbury. The CHAI libraries. proc. EuroHaptics Conference, 2003.

R. W. Daniel and P. R. McAree. Fundamental limits of performance for force reflecting teleoperation. *International Journal of Robotics Research*, 17(8):811–830, 1998.

B. Dasgupta and T. S. Mruthyunjaya. Force redundancy in parallel manipulators: theoretical and practical issues. *Mechanical Machine Theory*, 33(6):727–742, 1998.

G. de Gersem. *Kinaesthetic feedback and enhanced sensitivity in robotic endoscopic telesurgery*. Thesis/dissertation, Katholieke Universiteit Leuven, Belgium, 2005.

J. Van de Vegte. *Feedback control systems*. Prentice-Hall Inc., Englewood Cliffs, New Jersey, 2 edition, 1990.

Erwin de Vlugt, Alfred C. Schouten, and Frans C. T. van der Helm. Adaptation of reflexive feedback during arm posture to different environments. *Journal of Biological Cybernetics*, 78:10–26, 2002.

Erwin de Vlugt, Alfred C. Schouten, and Frans C. T. van der Helm. Closed-loop multivariable system identification for the characterization of the dynamic arm compliance using continuous force disturbances: a model study. *Journal of Neuroscience Methods*, 122:123–140, 2003.

A. J. Van der Schaft. *$\mathcal{L}_2$-Gain and Passivity Techniques in Nonlinear Control*. Springer Verlag, 2000.

Alfred G. Dietze. Kinaesthetic discrimination: The difference limen for finger span. *The Journal of Psychology*, 51:165–168, 1961.

N Diolaiti, G. Niemeyer, F. Barbagli, J. K. Salisbury, and Claudio Melchiorri. The effect of quantization and coulomb friction on the stability of haptic rendering. Worldhaptics Conference. IEEE, 2005.

J.A. Doubler and D.S. Childress. An analysis of extended physiological proprioception as a prosthesis-control technique. *Journal of Rehabilitation Research and Development*, 21(1):5–18, 1984.

Anas Fattouh and Olivier Sename. h_∞-based impedance control of teleoperation systems with time delay. IFAC Workshop on Time-Delayed Systems. IEEE, 2003.

Richard Feldtkeller. *Einfuhrung in die Vierpoltheorie der elektrischen Nachrichtentechnik*. S. Hirzel, Leipzig, Germany, 1937.

Patrick Fischer, Ron Daniel, and K. V. Siva. Specification and design of input devices for teleoperation. International Conference on Robotics and Automation. IEEE, 1990.

K. Fite, Liang Shao, and M. Goldfarb. Loop shaping for transparency and stability robustness in bilateral telemanipulation. *IEEE Transactions on Robotics and Automation*, 20(3):620–624, 2004.

Kevin Fite, John E. Speich, and Michael Goldfarb. Transparency and stability robustness in two-channel bilateral telemanipulation. *ASME Journal of Dynamic Systems, Measurement and Control*, 123, 2001.

H. Flemmer, B. Eriksson, and J. Wikander. Control design and stability analysis of a surgical teleoperator. *Mechatronics*, 9:843–866, 1999.

ForceDimension. ForceDimension sa, http://www.forcedimension.com. Electronic Citation, 2006.

G. F. Franklin, J. D. Powell, and A. Emame-Naeini. *Feedback Control of Dynamic Systems*. Addison-Wesley, 1994.

Erik C. Fritz, Goran A. V. Christiansson, and Richard Q. v. d. Linde. Haptic gripper with adjustable inherent passive properties. proc. Eurohaptics Conference 2004, Munich, Germany, pages 324–329, Jun 2004.

Henry F. Gaydos. Sensitivity in the judgement of size by finger span. *American Journal of Psychology*, 71: 557–562, 1958.

Sebastien Grange, Francois Conti, Patrick Helmer, Patrice Rouiller, and Charles Baur. The Delta haptic device as a nanomanipulator. Microrobotics and Microassembly III. SPIE, 2001.

B. Hannaford. A design framework for teleoperators with kinesthetic feedback. *IEEE Transactions on Robotics and Automation*, 5(4):426–434, 1989a.

Blake Hannaford. Stability and performance tradeoffs in bilateral telemanipulation. International Conference on Robotics and Automation, Scottsdale, Arizona, pages 1764–1767. IEEE, 1989b.

Blake Hannaford, Laurie Wood, Douglas A. McAffee, and Haya Zak. Performance evaluation of a six-axis generalized force-reflecting teleoperator. *IEEE Transactions on Systems, Man and Cybernetics*, 21(3):620–633, 1991.

Blake Hannaford, Jack M. Winters, Ching-Ping Chou, and Pierre-Henry Marbot. The anthroform biorobotic arm: A system for the study of spinal circuits. *Annals of Biomedical Engineering*, 23:339–408, 1995.

Blake Hannaford, Jee-Hwan Ryu, Dong-Soo Kwon, Yoon S. Kim, and Se-Kyong Song. Testing time domain passivity control of haptic enabled systems. Report, 2002.

S. G. Hart and L. E. Staveland. Development of NASA-TLX (Task Load Index). In P. A. Hankock and N. Meshkati, editors, *Human Mental Workload*, pages 239–250. North Holland Press, 1988.

Keyvan Hashtrudi-Zaad and S. E. Salcudean. Analysis of control architectures for teleoperation systems with impedance/admittance master and slave manipulators. *International Journal of Robotics Research*, 20(6): 419–445, 2001.

Keyvan Hashtrudi-Zaad and Septimiu E. Salcudean. Transparency in time-delayed systems and the effect of local force feedback for transparent teleoperation. *IEEE Transactions on Robotics and Automation*, 18(1): 108–114, 2002.

S. S. Haykin. *Active Network Theory*. Addison-Wesley, 1970.

Vincent Hayward and Oliver R. Astley. Performance measures for haptic interfaces. In Robotics Research: 7th International Symposium, pages 195–207. Springer Verlag, 1996.

E. A. M. Heijnsdijk, A. Pasdeloup, J. Dankelman, and D. J. Gouma. The optimal mechanical efficiency of laparoscopic forceps. *Surgical Endoscopy*, 18(12):1766–1770, 2004.

N. Hogan. Impedance control: An approach to manipulation. *Journal of Dynamic Systems, Measurements and Control*, 107(11):1–24, 1985.

N. Hogan. On the stability of manipulators performing contact tasks. *IEEE Journal of Robotics and Automation*, 4(6):677–686, 1988.

Edward Holweg. *Autonomous Control in Dextrous Grasping*. Thesis/dissertation, TUDelft, 1996.

Robert D. Howe. A force-reflecting teleoperated hand system for the study of tactile sensing in precision manipulation. International Conference on Robotics and Automation, Nice, France, pages 1321–1326. IEEE, May 1992.

R. S. Johansson. Sensory and memory information in the control of dextrous manipulation. In F. Lacquaniti and P. Viviani, editors, *Neural Bases of Motor Behaviour*, NATO ASI Series. Kluwer, 1996.

Seul Jung, T. C. Hsiz, and R. G. Bonitz. Force tracking impedance control of robot manipulators under unknown environment. *IEEE Transactions on Control Systems Technology*, 12(3):474–483, 2004.

J. H. Kapaan, E. G. M. Holweg, and A. J. C. Vries. Steering device for a drive-by-wire vehicle - US7,017,704. Patent, 2001.

J. Karlsson. *World Robotics 2004*. United Nations Publications, Geneva, 2004.

K. Kato and S. Hirose. Proposition and basic experiments of shape feedback master-slave arm - on the application for the demining robots. International Conference on Robotics and Automation. IEEE, 2000.

Arif Kazi. Operator performance in telerobotic surgery. *Presence*, 10(5):495–510, 2001.

T. A. Kern, S. Klages, T. Meiss, and R. Werthschuetzky. Study of the influence of varying diameter and grasp-forces on mechanical impedance for the grasp of cylindrical objects. The EuroHaptics Conference, 2006.

K. J. Kuchenbecker, J. Fiene, and G. Niemeyer. Improving contact realism through event-based haptic feedback. *IEEE Transactions on Visualization and Computer Graphics*, 12(2):219–230, 2006.

Rajesh Kumar, Peter Berkelman, Peneet Gupta, Aaron Barnes, Patrick Jensen, Louis Whitcomb, and Russell Taylor. Preliminary experiments in cooperative human/robot force control for robot assisted microsurgical manipulation. International Conference on Robotics and Automation. IEEE, 2000.

W. J. Lam and L. de Vries. Flight simulator (virtual model control) US 4,398,889. Patent, 1981.

R. H. LaMotte. Tactual discrimination of softness. *Journal of Neurophysiology*, 83(1):1777–1786, 2000.

D. A. Lawrence. Designing teleoperator architectures for transparency. International Conference on Robotics and Automation, pages 1406–1411. IEEE, 1992.

Dale A. Lawrence. Stability and transparency in bilateral teleoperation. *IEEE Transactions on Robotics and Automation*, 9(5), 1993.

Dale A. Lawrence and Jim D. Chapel. Performance trade-offs for hand controller design. International Conference on Robotics and Automation. IEEE, 1994.

M. Lazeroms, W Jongkind, and G. Honderd. Telemanipulator design for minimally invasive surgery. American Control Conference. AACC, 1997.

M. C. L. Lazeroms. *Force reflection for telemanipulation : applied to minimally invasive surgery*. Thesis/dissertation, Delft University of Technology, The Netherlands, 1999.

Sukhan Lee and Hahk S. Lee. Modeling, design, and evaluation of advanced teleoperator control systems with short time delay. *IEEE Transactions on Robotics and Automation*, 9(5):607–623, 1993.

Peter Lindskog and Jonas Sjöberg. A comparison between semi-physical and black-box neural net modelling: A case study. International Conference: Engineering Applications of Artificial Neural Networks. IEEE, 1995.

L. J. Love and W. J. Book. Force reflecting teleoperation with adaptive impedance control. *IEEE Transactions on Systems, Man, and Cybernetics*, 34(1):159–165, 2004.

J. Marescaux, H. J. Marquez, J Leroy, M Gagner, F Rubino, D. Mutter, M. Vix, S. E. Butner, and M. K. Smith. Transatlantic robot-assisted telesurgery. *Nature*, 413:379–381, 2001.

Thomas H. Massie and J. K. Salisbury. The Phantom haptic interface: a device for probing virtual objects. Symposium on Haptic Interfaces for Virtual Environment and Teleoperator Systems. ASME, 1994.

Mathworks. Optimization toolbox manual 2.1. Report, 2003.

S McKnight, N. Melder, A. L. Barrow, W. S. Harwin, and J. P. Wann. Psychophysical size discrimination using multi-fingered haptic interfaces. volume 2004 of *Eurohaptics Conference*, 2004.

Davide Moschini and Paolo Fiorini. Performance of robotic teleoperation systems with flexible slave device. International Conference on Robotics and Automation. IEEE, 2004.

M. Mulder, W. J. Kaljouw, and M. M. van Paasen. Parameterized multi-loop model of pilot's use of central and peripheral visual motion cues. AIAA Modeling and Simulation Technologies Conference and Exhibit, pages 1–22. AIAA, 2005.

Andreas Muller. Internal preload control of redundantly actuated parallel manipulators - its application to backlash avoiding control -. *IEEE Transactions on Robotics*, 21(4):668–677, 2005.

Istvan Nagy, Hermann Mayer, and Alois Knoll. Application of force feedback in robot assisted minimally invasive surgery. Proc. of Eurohaptics Conference, 2004.

G. Niemeyer. *Using Wave Variables in Time Delayed Force Reflecting Teleoperation*. Thesis/dissertation, Massachusetts Institute of Technology, 1996.

G. Niemeyer and J-J. E. Slotine. Telemanipulation with time delays. *International Journal of Robotics Research*, 23(9):873–890, 2004.

Marcia K. O'Malley and Michael Goldfarb. The effect of virtual surface stiffness on the haptic perception of detail. *IEEE/ASME Transactions on Mechatronics*, 9(2):448–454, 2004.

Ya-Jun Pan, Carlos Canudas de Wit, and Olivier Sename. A new predictive approach to teleoperation with application to drive-by-wire systems. *IEEE Transactions on Robotics*, 22(6):1146–1162, 2006.

Jaeheung Park and Oussama Khatib. A haptic teleoperation approach based on contact force control. *International Journal of Robotics Research*, 25(5-6):575–591, 2006.

D. T. Pawluk and R. E. Ellis. Dynamics identification and control of a teleoperational system. International Conference for Robotics and Automation. IEEE, 1991.

R. Pintelon and J. Schoukens. *System Identification, a frequency domain approach*. IEEE Press, New York, 2001.

Jerry Pratt, Ben Krupp, and Chris Morse. Series elastic actuators for high fidelity force control. *Industrial Robot*, 29(3):234–241, 2002.

Haipeng Qian. *Stable Robot Force Control in Case of Hard Contact*. Thesis/dissertation, KU Leuven, dept. Mechanical Engineering, 1993.

G. J. Raju, George C. Verghese, and Thomas B. Sheridan. Design issues in 2-port network models of bilateral remote manipulation. International Conference on Robotics and Automation, pages 1316–1321. IEEE, 1989.

ABB Robotics. Irb260 datasheet. Electronic Citation, Aug 2006.

Schilling Robotics. Schilling robotics titan 4 underwater manipulator for teleoperation. Electronic Citation, 2007.

Jee-Hwan Ryu and Dong-Soo Kwon. A novel adaptive bilateral control scheme using similar closed-loop dynamic characteristics of master/slave manipulators. *Journal of Robotic Systems*, 18(9):533–543, 2001.

Jee-Hwan Ryu, Dong-Soo Kwon, and Blake Hannaford. Stable teleoperation with time-domain passivity control. *IEEE Transactions on Robotics and Automation*, 20(2):365–373, 2004.

S. E. Salcudean and L. Stocco. Isotropy and actuator optimization in haptic interface design. International Conference on Robotics and Automation. IEEE, 2000.

Craig Sayers, Dana Yoerger, Richard Paul, and John Lisiewicz. A manipulator work package for teleoperation from unmanned untethered vehicles - current feasibility and future applications. International Advanced Robotics Program Workshop on Subsea Robotics, 1996.

Wagahta Semere, Masaya Kitagawa, and Allison M. Okamura. Teleoperation with sensor/actuator asymmetry: Task performance with partial force feedback. IEEE Symposium on Haptic Interfaces for Virtual Environment and Teleoperator Systems. IEEE, 2004.

SensAble. SensAble Technologies Inc website: http://www.sensable.com/products/. Electronic Citation, 2006.

Alan Sherman, Murat C. Cavosoglu, and Frank Tendick. Comparison of teleoperator control architectures for palpation tasks. Symposium on Haptic Interfaces for Virtual Environments and Teleoperator Systems. ASME, 2000.

M. R. Sirouspour, S. P. DiMaio, S. E. Salcudean, P Abolmaesumi, and C. Jones. Haptic interface control - design issues and experiments with a planar device. International Conference on Robotics and Automation, pages 789–794. IEEE, 2000.

Jonas Sjoberg. A nonlinear grey-box example using a stepwise system identification approach. 11th Symposium on Identification. IEEE, 2000.

S. Skogestad and I. Postlethwaite. *Multivariable Feedback Control*. John Wiley & Sons, 1996.

James Stevens. Repeated measures analysis. In *Applied Multivariate Statistics for the Social Sciences*, book chapter 13, pages 438–488. Lawrence Erlbaum Ass. Inc. Publishers, 2 edition, 1992.

Stefano Stramigioli. *From differentiable manifolds to interactive robot control*. Thesis/dissertation, Delft University of Technology, 1998.

S. Tafazoli, S. E. Salcudean, K. Hashtrudi-Zaad, and P. D. Lawrence. Impedance control of a teleoperated excavator. *IEEE Transactions on Control Systems Technology*, 10(3):355–367, 2002.

H. Z. Tan, M. A. Srinivasan, B. Eberman, and B. Cheng. Human factors for the design of force-reflecting haptic interfaces. ASME Conference on Dynamics Systems and Control, 1994.

Hong Z. Tan, Nathaniel I. Durlach, G. L. Beauregard, and Mandayam A. Srinivasan. Manual discrimination of compliance using active pinch grasp: The roles of force and work cues. *Perception and Psychophysics*, 57 (4):495–510, 1995.

Neal A. Tanner and G. Niemeyer. High-frequency accelleration feedback in wave variable telerobotics. *IEEE/ASME Transactions on Mechatronics*, 11(2):119–127, 2006.

Richard Q. v. d. Linde and Piet Lammertse. Hapticmaster - a generic force controlled robot for human interaction. *Industrial Robot*, 30(6):515–524, 2003.

Andr van der Ham. *A Dextrous Teleoperator for Hazardous Environments*. Thesis/dissertation, Delft University of Technology, The Netherlands, 1997.

VOLVOCARS. Volvo s60r active chassis control buttons. Electronic Citation, 2006.

Christopher R. Wagner, Nicholas Stylopoulos, and Robert D. Howe. The role of force feedback in surgery: Analysis of blunt dissection. 10th Symposium on Haptic interfaces for virtual reality and teleoperation. ASME, 2002.

D. E. Whitney. Historical perspective and state of the art in robot force control. International Conference on Robotics and Automation, pages 262–228. IEEE, 1985.

Chi-Haur Wu and Shih-Lang Chang. Implementation of a neuromuscular-like control for compliance of a puma 560 robot. Conference on Decision and Control. IEEE, 1995.

Y Yokokohji and T Yoshikawa. Bilateral control for master-slave manipulators for ideal kinesthetic coupling - formulation and experiment. *IEEE Transactions on Robotics and Automation*, 10(5):605–620, 1994.

Y Yokokohji, Y. Iida, and T Yoshikawa. 'toy problem' as the benchmark test for teleoperation systems. *Advanced Robotics*, 17(3):253–273, 2003.

N. Zemiti, T. Ortmaier, and G. Morel. A new robot for force control in minimally invasive surgery. proceedings of the International Conference on Intelligent Systems and Robotics IROS, pages 3643–3648. IEEE, 2004.

M. Zhu and S. E. Salcudean. Achieving transparency for teleoperator systems under position and rate control. International Conference on Intelligent Robots and Systems. IEEE, 1995.

Wen-Hong Zhu, S. E. Salcudean, and Ming Zhu. Experiments with transparent teleoperation under position and rate control. International Conference on Robotics and Automation, pages 1870–1875. IEEE, 1999.

M. Zinn, O Khatib, B. Roth, and J. K. Salisbury. Actuation methods for human-centered robotics and associated control challenges. Second Joint CSS/RAS International Workshop on Control Problems in Robotics and Automation,, 2002.

Summary

This thesis introduces a novel concept in haptic teleoperation, the hard-master soft-slave teleoperator. The "hard master" is a high-bandwidth, stiff device which can represent rigid objects accurately, both regarding stiffness and the high frequency transient forces during initial contact. The "soft slave" is a low-bandwidth, intrinsically compliant device, which is a representation of the operator's own hand. The idea is to create similar dynamics in the interactions between operator/master and slave/environment, to improve stability and enhance the information transfer to the human operator.

This research quantifies the advantages of soft-slave teleoperation considering human capabilities, remote environment characteristics and task requirements. Two novel hard-soft teleoperators are designed and realized, on which a series of experiments are performed to quantify the human information needs in a series of tasks and the stiffness-stability trade-off. Along with the experimental study, a thorough theoretical analysis of the device performance and stability characteristics is performed.

The main conclusions from this research are that the human needs differ between tasks and that for each combination of task and environment, a different teleoperator is optimal. This is true both for the mechanical solution and the choice of controller architecture and control gains. For some of the tasks studied in this research, size discrimination and teleoperated assembly of stiff objects, the hard-master soft-slave teleoperator has distinct advantages to a hard-hard teleoperator: Contact forces are lower and there is a better stability robustness. For stiffness discrimination, the only restriction of the hard-soft concept is that the total teleoperator stiffness should be higher than the stiffness of the objects to discriminate. It was seen that for grasping tasks, the use of a bracket around the fingers, instead of manipulation with the bare hands, did not influence size and stiffness discrimination performance. Furthermore, for teleoperated assembly tasks using a hard-soft teleoperator, the added value of haptic feedback is statistically significant, but very small. Contrary to most claims in the literature, low-frequency haptic feedback can increase certain aspects of the subjective workload, instead of reducing it. Only in combination with high-frequency haptic feedback there is any improvement at all of subjective mental workload.

This research shows that hard-master soft-slave haptic teleoperation is superior to current hard-hard implementations for tasks like size discrimination and manipulation in brittle environments.

Samenvatting

Harde Meester en Zachte Slaaf voor Haptische Teleoperatie

Dit onderzoek kwantificeert de voor- en nadelen van de harde meester, zachte slaaf teleoperatie, waarbij de menselijke capaciteiten, de omgevingsfactoren en de taakvereisten in acht worden genomen. Twee innovatieve "hard-zacht" teleoperateurs zijn ontworpen en gerealiseerd. Met gebruik hiervan hebben een aantal experimenten plaats gevonden om de menselijke informatiebehoeften te kwantificeren voor verschillende taken en de stijfheid-stabiliteit afweging in kaart te brengen. Naast het experimentele onderzoek is er een grondige theoretische analyse gedaan van de uitvoering van de apparaten en de stabiliteitsfactoren.

De belangrijkste conclusies van dit onderzoek zijn dat de menselijke behoeften verschillen tussen de verschillende taken en dat voor elke combinatie van taak en omgeving, een andere teleoperateur optimaal is. Dit geldt zowel voor de mechanische oplossing, als voor de keuze van regelaararchitectuur en regelinstellingen. Voor sommige taken die zijn bestudeerd in dit onderzoek, grootte discriminatie en het door middel van teleoperatie assembleren van harde objecten, heeft de harde meester, zachte slaaf teleoperateur onderscheidende voordelen ten opzichte van een harde-harde teleoperateur: de contactkrachten zijn kleiner en er is een betere stabiliteit. Voor stijfheid discriminatie is de enige beperking van het "hard-zacht" concept dat de totale teleoperateur stijfheid hoger moet zijn dan de stijfheid van de objecten, om een goed onderscheid te kunnen maken. Bij de grijptaken is naar voren gekomen dat het gebruik van een beugel rond de vingers, in plaats van manipulatie met blote handen, de uitvoering van de grootte discriminatie en de stijfheid discriminatie niet benvloedt.

De toegevoegde waarde van haptische feedback bij teleoperatie assemblage met gebruik van een "hard-zacht" teleoperateur is statistisch significant, maar klein. In tegenstelling tot de meeste beweringen in de literatuur, kan laag-frequente haptische feedback bepaalde aspecten van de subjectieve werkbelasting verhogen, in plaats van het te verminderen. Slechts in combinatie met de hoog-frequente haptische feedback is er enige verbetering in de subjectieve mentale werkbelasting.

Dit onderzoek toont dat harde meester, zachte slaaf haptische teleoperatie superieur is aan de hedendaagse "hard-hard" uitvoering, voor taken zoals grootte discriminatie en manipulatie in brosse omgevingen.

Dankwoord

This has been an exciting, intense and satisfying project. During the last four years, I have had the opportunity to work together with some brilliant people who have graciously shared their precious time to introduce me to Science and to the world of haptic teleoperation.

The spiritual father of the project is Richard van der Linde, who initiated the Biorobotics and the Haptics research in Delft. Richard was awarded with the NWO Veni-grant, which he skillfully managed to employ the excellent mechatronic designer Erik Fritz and me, while partly financing his own activities. Without Richard's enthousiastic encouragement, interesting advice and critical supervision this project would not have attained it's current success. Erik made this project physical. He designed and assembled the experimental teleoperation setups *Hugin* and *Munin*, which have been key to understanding the true mechanisms of why some teleoperation systems do work and some don't. Like me, Erik learned a lot about haptics and teleoperation during the project, and we had many a good discussion regarding controller architectures, mechatronic design, sensors and estimation. I am also grateful for many a good advice on managing children.

Frans van der Helm, my promotor, gave me deep insights into what Science really is about: what you can claim and what not. Frans' deep passion for biomechanics and the human sensomotoric system gave this project a strong human orientation, which is somewhat unique and which proved valuable in the field of haptic teleoperation. Maarten Steinbuch, co-promotor from TU Eindhoven, shared his experiences from mechatronic design and analysis, and inspired me again and again to focus and persist in times of struggle.

I am also grateful to all my M.Sc. students: Jasper, Ying, Yan, Karlijne, Matthias, Luke and Marc. Thanks for allowing me to practice coaching on you, and thanks for asking all your questions about haptics, grasping and teleoperation. Your curiosity and confusion helped me to think and think again until I could explain to you (and myself) the true meaning of the hammering effect or the GK-form. Also Ruben, David and John, co-founders of the Delft Haptics Lab, helped fill my days with interesting inquiries and startling remarks, as did Patrice and Ilhan in my last few months. I am proud of you, and feel confident to leave the Lab and my favourite robots in your caring hands. All of you in the department; Martijn, Daan, Jan, David, Peter, Sander, Tetsuo, and all the others: I am glad to have spent four excellent years of my prime in your company.

Another part of the story is the outside world and the international research community. I am grateful for the long discussions I have had with you; Vincent Hayward, Blake Hannaford, Sebastien Grange, Paolo Fiorini, Antal Bejczy, John Hollerbach, Gabriel Robles-de-la-Torre, Gunter Niemeyer, Tim Salcudean and Dale Lawrence, and all the others. Thanks for helping me and for sharing your experience with us in Delft!

During this research project I also benefited from excellent support from an unusual source. Anna-Karin, PhD in Control Science, and also my mother, proof-read all my papers with unmatched diligience and helped me to focus the narrative on the main story. Thanks for teaching me teaching.

This book would not have been written if I had not met Marijke. I am infinitely grateful for your inspiration, support and love.

Curriculum Vitae

Göran Christiansson was born in Norrköping, Sweden in 1974, as one of three brothers. Both his parents and both his brothers followed the path of science and engineering, almost all at the Chalmers University of Technology in Gothenburg, Sweden. During the studies, he managed an equilibrium between the analytic depth of mathematics at Engineering Physics and the artistic expression at the Chalmersspexet, the University comedy musical.

With a few years of experience from industry (*Ericsson, Moscow, Russia and Mecel/Delphi, Gothenburg, Sweden*), Göran decided to re-enter the doors of the academia and pursue a PhD project at the Delft Biorobotics Laboratory. The fruits of this research project is partly the book you hold in your hands and partly the experimental infrastructure of haptic hardware and open source software at the lab.

During the last four years, Göran worked actively to promote the spread of knowledge about haptics and teleoperation to society; to other universities, institutes and industry, through the Dutch-Belgian Haptics Network, which he co-founded in 2003. In 2006, Göran co-founded the Delft Haptics Laboratory, which now is the most renowned haptics laboratory in the Benelux area.

Parallel with this research project, Göran has passed a number of milestones of man, including buying a house and a car, entering wedlock with Marijke, and seeing the birth of Erik and Jonatan.

Göran looks forwards to returning to industry to continue working on high-tech product development and applied research, now with the experience and skills of a real scientist.